

THE DEVELOPMENT OF INSTRUMENTATION FOR
THE DIRECT MEASUREMENT OF HEAT LOSS FROM
MAN IN A NORMAL WORKING MODE

by

T. HODGSON

The development of instrumentation for
the direct measurement of heat loss
from man in a normal working mode

by

T. Hodgson



A thesis submitted to the University of Natal for the degree of
Doctor of Philosophy in the Department of Mechanical Engineering

PRETORIA, SOUTH AFRICA, SEPTEMBER, 1974

THE DEVELOPMENT OF INSTRUMENTATION FOR THE
DIRECT MEASUREMENT OF HEAT LOSS FROM MAN
IN A NORMAL WORKING MODE

SUMMARY

Based on a theoretical analysis of the heat transfer process between the human body and its environment, graphs are presented for determining the theoretical skin surface temperatures and sweat rates as a function of the physiological conductance, under certain assumed environmental conditions with regard to air temperature, relative humidity and wind speed.

In addition, the development of unique measuring techniques for the direct measurement of the evaporative and radiative heat transfer rates between a human body in a natural working position and its environment as well as the development of a low-cost radiometer for the measurement of the emissivity and temperature of human skin are described.

The heat loss measuring equipment was installed in the horizontal test section of the climatic chamber of the Human Sciences Laboratory of the Chamber of Mines.

Basically the evaporative heat loss measuring system consists of two air-sampling probes, for sampling the air on the upstream and downstream

sides of the body, a double circuit heat exchanger, for equalising the dry-bulb temperatures of the two air samples and a differential humidity-measuring system incorporating electrical resistance hygrometers, for measuring the difference in specific humidity between the two air samples. In addition, a steam generator is provided for introducing a known amount of steam at a predetermined rate into the wake of the body.

Since the output of the humidity-measuring system is linearly related to the evaporative heat loss rate, the unknown rate of evaporation of moisture from the human body can be determined relatively easily from a knowledge of the respective outputs of the humidity-measuring system due to the moisture evaporation rate of the human body and the known vapour production rate by the steam generator.

The direct-measuring instrument for determining the radiation energy exchange rate of a working subject is in the form of a rotating hoop. The inside and outside surfaces of the hoop are lined with thermal radiation-sensing elements, so connected as to measure the net radiation energy exchange between the subject and the surroundings.

The hoop integrates over the circular strip formed by the elements and upon rotation, integrates the radiation over the total 4π surface enveloping the subject. While the interposition of a surface between

the body and its surroundings must of necessity influence the radiation exchange, the method introduces a small surface only.

The significance of the evaporative and radiative heat loss measuring techniques which were successfully used in animate studies, is reflected in the, hitherto unknown, accuracy regarding partial calorimetric studies.

The low-cost radiometer for measuring the skin temperature and emissivity is equipped with two non-selective thermal radiation detectors in the form of semi-conductor thermocouples. The one radiation-sensing element faces a built-in reference black body. The other detector, which can be temperature controlled, is used to detect the incoming radiation from the target.

The output of the radiation-sensing elements which is sufficiently high to be measured on a recorder without the use of a chopper-amplifier system, can either be measured differentially or the output of the radiation-sensing element facing the target can be measured separately; for the purpose of temperature and emissivity measurements, respectively.

The unique facility of being able to vary the temperature of the radiation detector enabled a new method of determining the emissivity

of a surface to be developed. As a result, accurate measurements of the emissivities of samples of excised skin could be carried out. An improvement in the response of the radiometer would, however, be necessary for the rapid determination of the emissivity of living skin by this means.

The accuracy with which surface temperatures could be determined by means of the radiometer compared favourably with more sophisticated radiometers.

TABLE OF CONTENTS

	Page
Summary	1
List of Tables	11
List of Figures	15
Nomenclature	30
Acknowledgements	36
Preface	38
1. INTRODUCTION	42
2. DESCRIPTION OF THE CLIMATIC CHAMBER	49
2.1 Horizontal test chamber	51
2.2 Humidity control system	52
2.2.1 Humidity-sensing system	53
2.2.2 Method of humidity control	55
2.3 Air temperature control system	55
2.4 Wall temperature control system	56
2.5 Range and stability of environmental control	57
3. THERMOPHYSIOLOGICAL CONSIDERATIONS	58
3.1 Physiological conductance	60
3.2 Sweating	63
3.3 Moisture evaporation rate from the skin of a human subject : theoretical considerations	64
3.3.1 Mass transfer rate neglecting radiation	72
3.3.2 Mass transfer rate taking thermal radiation into account	79
3.3.3 Maximum mass transfer rate value	88

	Page
3.4 Radiation heat loss from a human subject : theoretical considerations	94
3.4.1 Maximum radiative heat flux	95
3.5 Influence of air velocity, thermal radiation and air temperature on the skin temperature	98
3.5.1 Influence of air velocity on the surface temperature, t_s	99
3.5.2 Effect of thermal radiation on the surface temperature, t_s	100
3.5.3 Effect of air temperature, t_g , on the surface temperature, t_s	100
4. MEASUREMENT OF THE EVAPORATIVE HEAT LOSS RATE FROM A HUMAN BODY	104
4.1 Possible methods of measuring the evaporative heat loss rate from a subject in the horizontal test section of the climatic chamber	106
4.2 Required sensitivity of the humidity-sensing device	113
4.3 Methods of sensing the humidity increase in the wake of a human body	119
4.3.1 Differential wet- and dry-bulb psychrometer	120
4.3.2 Differential hair hygrometer	125
4.3.3 Spectroscopic hygrometer	126
4.3.4 Electrical resistance hygrometer	130
4.4 Choice of humidity-sensing system	142
4.5 Proposed method of measuring the evaporative heat loss rate from a human body	145
4.5.1 Analogy method	147
4.5.2 Comparative method	163
4.5.3 Choice of evaporative heat loss measuring system	180
4.6 Details of the evaporative heat loss measuring instrument	181

	Page
4.6.1 Design considerations	183
4.6.2 Air-sampling rate	185
4.6.3 Air-sampling probes	186
4.6.4 Double circuit heat exchanger	193
4.6.5 Steam generator	209
4.7 Performance tests	212
4.7.1 Double circuit heat exchanger	212
4.7.2 Preliminary full-scale inanimate tests	213
4.7.3 Animate studies	219
4.8 Discussion of the evaporative heat loss measuring system	221
5. <u>MEASUREMENT OF THE RADIATIVE HEAT LOSS RATE FROM A HUMAN BODY</u>	224
5.1 Proposed method of measuring the radiative heat loss rate from a human body	226
5.1.1 Radiometer layers	226
5.1.2 Spherical integrating grid around the body	228
5.1.3 Rotating 4π radiometer	228
5.2 Choice of thermal radiation-sensing elements	230
5.2.1 Thermal detectors	235
5.2.2 Photon-counter detectors	236
5.2.3 Proposed thermal radiation-sensing elements	238
5.3 Preliminary performance tests	241
5.3.1 Description of the test apparatus	242
5.3.2 Test procedure	245
5.3.3 Test results	247
5.3.4 Preliminary performance tests on a full-scale prototype model of the radiometer arm in the form of a semi-circular hoop	249

	Page
5.4 Constructional details of the 4π radiometer	253
5.4.1 General description	253
5.4.2 Radiation-sensing elements	257
5.4.3 Wind-shield for protecting the radiation-sensing elements from forced convective influences due to air movement	261
5.4.4 Radiometer arm drive	268
5.4.5 Electrical connections	271
5.4.6 Lower support for the radiometer arm	272
5.5 Method of recording the radiometer output	275
5.5.1 Theoretical considerations	275
5.5.2 Temperature variations with time of the radiation-sensing elements incorporated in the vertical sections of the radiometer arm	297
5.5.3 Required sensitivity of the 4π radiometer	307
5.5.4 Proposed method of measuring the radiometer output	308
5.6 Full-scale inanimate tests	313
5.6.1 Test results	315
5.7 Animate studies	317
5.8 Discussion of the 4π radiometer	321
6. <u>DEVELOPMENT OF A LOW-COST RADIOMETER FOR SKIN TEMPERATURE AND EMISSIVITY MEASUREMENTS</u>	323
6.1 Skin temperature measuring techniques	324
6.1.1 Contact thermometers	325
6.1.2 Radiometric temperature-measuring devices	327

	Page
6.2 Radiometer for human skin temperature and emissivity measurements : design considerations	331
6.2.1 Choice of thermal radiation-sensing elements	332
6.3 Constructional details of the low-cost radiometer	338
6.3.1 Spectral response	343
6.3.2 View angle	348
6.4 Calibration tests	348
6.4.1 Temperature measurement	348
6.4.2 Emissivity measurement	353
6.5 Discussion	356
7. DISCUSSION AND CONCLUSIONS	358
8. BIBLIOGRAPHY	362
APPENDIX A : METHOD OF CALCULATING THE MOISTURE EVAPORATION RATE FROM A HEATED SURFACE SUCH AS THE HUMAN BODY	385
APPENDIX B : NET THERMAL RADIATIVE FLUX BETWEEN A HUMAN SUBJECT IN THE HORIZONTAL TEST CHAMBER OF THE CLIMATIC CHAMBER AND THE SURROUNDING TEST CHAMBER WALLS	404
APPENDIX C : METHODS OF MEASURING HUMIDITY	413
APPENDIX D : TESTS ON AN ELECTROLYTIC CONDENSATION HYGROMETER	437
APPENDIX E : CALCULATIONS TO DETERMINE THE MAXIMUM DIFFERENCE BETWEEN THE RESPECTIVE AIR FLOW RATES THROUGH THE VARIOUS SAMPLING HOLES IN THE DOWNSTREAM AIR-SAMPLING PROBE OF THE EVAPORATIVE HEAT LOSS MEASURING INSTRUMENT	447

	Page
APPENDIX F : CALCULATIONS TO DETERMINE THE EFFECTIVE- NESS OF THE DOUBLE CIRCUIT HEAT EXCHANGER INCORPORATED IN THE EVAPORATIVE HEAT LOSS MEASURING SYSTEM	452
APPENDIX G : DETERMINATION OF THE CONFIGURATION FACTORS BETWEEN THE RADIATION-SENSING ELEMENTS, THE BODY AND VARIOUS SECTIONS OF THE SURROUNDING WALLS OF THE HORIZONTAL TEST CHAMBER OF THE CLIMATIC CHAMBER	462
APPENDIX H : COMPARISON OF ALTERNATIVE SYSTEMS OF MEASURING THE OUTPUT OF THE 4π RADIOMETER	471

LIST OF TABLES

	Page
Table 1 : Assumed environmental conditions for calculating the mass transfer rate from a human body	68
Table 2 : Determination of the mass driving force : Values of the term $(f_G - f_s)/(f_s - f_l)$ where f_G and f_s are the respective mass concentrations of moisture in the air stream and adjacent to the body surface, respectively	70
Table 3 : Calculated values for the mass transfer rate and surface temperature of a nude resting man, neglecting radiative effects and assuming the physiological conductance, K'' , to remain constant at $20 \times 10^{-3} \text{ kW/m}^2 \text{ }^\circ\text{C}$	77
Table 4 : Calculated values for the mass transfer rate and surface temperature of a nude resting man in the spreadeagle position, assuming the surrounding wall temperature to be equal to the air temperature	89
Table 5 : Calculated values for the radiative heat flux per unit area of body surface of a nude man in the spreadeagle position, assuming the surrounding wall temperature to be equal to the air temperature	96

	Page
Table 6 : Measurement of the humidity increase in the wake of a human body : accuracies of various humidity-measuring devices	143
Table 7 : Model evaporative heat loss studies : determination of the evaporative heat loss rate by analogy : comparison between the calculated and actual values of the evaporation heat loss rate	157
Table 8 : Differential hygrometer for measuring the evaporative heat loss rate from a human body : positioning of the air-sampling holes along the length of each of the four arms of the rotating air-sampling probe	189
Table 9 : Assumed surface temperature values for the purpose of calculating the net radiation energy exchange rates and hence the radiation heat transfer coefficients for the radiation-sensing elements located in one of the vertical sections of the 4π radiometer arm	289
Table 10 : Theoretical radiation energy exchange rates of the "inner" and "outer" radiation-sensing elements located in one of the vertical sections of the 4π radiometer, based on the assumed surface temperature values given in Table 9	293

	Page
Table 11 : Radiation heat transfer coefficients of the "inner" and "outer" radiation-sensing elements located in one of the vertical sections of the 4π radiometer arm	295
Table 12 : Theoretical temperatures of the "inner" and "outer" radiation-sensing elements incorporated in the vertical sections of the 4π radiometer arm for various temperature conditions and radiometer positions within the horizontal test chamber of the climatic chamber	300
Table 13 : Calibration of the low cost radiometer as a surface temperature-measuring instrument : test results.	351

APPENDICES

Table G1 : Radiation energy exchange : calculation of the configuration factor between the surfaces depicted in Figure G1 : range of Z co-ordinates for the elemental areas of surface A	463
Table G2 : Radiation energy exchange : calculation of the configuration factor between the surfaces depicted in Figure G1 : symmetry repetition coefficients for the various Z co-ordinates	465

	Page
Table G3 : Radiation energy exchange : calculation of the configuration factor between the surfaces depicted in Figure G1 : geometric factors for the elemental areas having similar Z co-ordinates.	467

LIST OF FIGURES

	Page
Figure 1 : Layout of tunnel and test chambers of climatic chamber	50
Figure 2 : The effect of variations in the ratio of physiological conductance, K'' , to the film coefficient of transfer, $h_c = c_g g_h$, on the surface temperature, t_s ; neglecting thermal radiation	74
Figure 3 : Influence of the ratio of the film coefficient of heat transfer, $h_c = c_g g_h$, to the physiological conductance, K'' , on the term, $\dot{m}'' c_g / K''$, and the surface temperature, t_s ; neglecting thermal radiation	78
Figure 4 : The effect of variations in the ratio of the physiological conductance, K'' , to the film coefficient of heat transfer, $h_c = c_g g_h$, on the surface temperature, t_s , for an air velocity of 0,5 m/s; taking thermal radiation into account	83
Figure 5 : The effect of variations in the ratio of the physiological conductance, K'' , to the film coefficient of heat transfer, $h_c = c_g g_h$, on the surface temperature, t_s , for an air velocity of 5,0 m/s; taking thermal radiation into account	84

	Page
Figure 6 : Influence of the ratio of the film coefficient of heat transfer, $h_c = c_G g_h$, to the physiological conductance, K , on the term, $\dot{m}'' c_G / K$, and the surface temperature, t_s , for an air velocity of 0,5 m/s; taking radiation into account	85
Figure 7 : Influence of the ratio of the film coefficient of heat transfer, $h_c = c_G g_h$, to the physiological conductance, K , on the term, $\dot{m}'' c_G / K$, and the surface temperature, t_s , for an air velocity of 5,0 m/s; taking thermal radiation into account	86
Figure 8 : Moisture evaporation rate : theoretical considerations : flow diagram of the computer programme for the calculation of the mass driving force, B_f , versus the surface temperature, t_s	87
Figure 9 : Theoretical surface temperature, t_s , and mass transfer rate, \dot{m}'' , versus the physiological conductance, K , for different environmental conditions assuming the surface to be completely wet	93

	Page
Figure 10 : Spatial distribution of the axial components of air velocity in the wake of a human body	117
Figure 11 : Average value for the axial components of velocity in the wake of a human body as a function of the distance from the body on the downstream side	118
Figure 12 : Psychrometer tube with the wet-bulb element and cotton sock removed from the tube	122
Figure 13 : Schematic layout of differential infra-red hygrometry system for measuring the humidity increase in the wake of a human body	128
Figure 14 : Air flow through the crystal holder of the electrolytic condensation hygrometer	134
Figure 15 : Components of the electrolytic condensation hygrometer	135
Figure 16 : Diagrammatic layout of the test arrangement for the determination of the total evaporation rate from a wetted body by analogy	148
Figure 17 : Model evaporative heat loss tests : recorder deflections due to the temperature increase in the wake of the test body	154
Figure 18 : Model evaporative heat loss tests : recorder deflections due to the humidity increase in the wake of the test body	155

	Page
Figure 19 : Model evaporative heat loss tests : specific humidity distribution in the wake of the test body	156
Figure 20 : Model evaporative heat loss studies : the influence of the free air stream velocity on the ratios $\dot{q}_c/c_G\Delta t_{G,w}$ and $\dot{q}_{e,act}/h\Delta w_w$	159
Figure 21 : Diagrammatic layout of the test arrangement for the determination of the total evaporation rate from a body by the comparative method	164
Figure 22 : Model evaporative heat loss tests : 50 mm dia by 220 mm long body constructed from "Mhoglass"	166
Figure 23 : Mini flow-meter for the accurate measurement of the mass flow rates of water supplied to the steam generator	169
Figure 24 : Output of the mini flow-meter as a function of the rate of flow of water	172
Figure 25 : Section of the recorder chart showing the rate of response of the mini flow-meter	173
Figure 26 : Model evaporative heat loss tests : investigations into the comparative method of determining the evaporative heat loss rate from a test body : recorder deflections due to the humidity increase in the wake of the test body	174

	Page
Figure 27 : Model evaporative heat loss tests : recorder deflection as a function of the steam input rate by the auxiliary steam generator	176
Figure 28 : Model evaporative heat loss studies : steam input rate to the main body versus the water vapour loss rate from the main body as determined by the comparative method	179
Figure 29 : Schematic layout of the differential hygrometer for measuring the evaporative heat loss rate from a human subject	182
Figure 30 : Evaporative heat loss measuring instrument : details of the rotating air-sampling probe in the wake of the subject	187
Figure 31 : Evaporative heat loss measuring instrument : view of the central housing and drive unit of the rotating air-sampling probe in the wake of the subject	191
Figure 32 : Differential hygrometer for the measurement of the evaporative heat loss rate from a human body : details of the double circuit heat exchanger	196

	Page
Figure 33 .: Differential hygrometer for the measurement of the evaporative heat loss rate from a human body : exploded view of the double circuit heat exchanger for the differential hygrometer	197
Figure 34 : Differential hygrometer for the measurement of the evaporative heat loss rate from a human body : views of the lithium chloride humidity sensors	203
Figure 35 : Differential hygrometer for the measurement of the evaporative heat loss rate from a human body : views of the top cover of the double circuit heat exchanger showing the relative positions of the various control and measuring elements	204
Figure 36 : Measurement of the evaporative and radiative heat loss rates from a human body : test rig showing the heated cylinder that was used during preliminary full-scale investigations	215
Figure 37 : Direct measurement of the evaporative heat loss rate : full-scale tests : recorder deflection as a function of the steam input rate by the auxiliary steam generator	217

	Page
Figure 38 : Measurement of the radiative heat loss rate from a human body : schematic diagram of the 4π integrating radiometer	229
Figure 39 : Radiation intensity of a black body as a function of wave-length at various black body temperatures	233
Figure 40 : The spectral sensitivity of photo-electric cells and thermistor bolometers	237
Figure 41 : Sectional views of the thermopile and electrical resistance elements that were investigated as thermal radiation sensors for the 4π radiometer arm	
Figure 42 : Direct measurement of the radiative heat loss rate from a human body : view of the apparatus for determining the response time of the nickel resistance wire thermal radiation-sensing elements of the proposed 4π radiometer arm	243
Figure 43 : Direct measurement of the radiative heat loss rate from a human body : view of a section of the 4π radiometer arm being inserted into the radiant heat source that was used to determine the response time of a test section of the radiometer arm	246

	Page
Figure 44 : Direct measurement of the radiative heat loss rate from a human body : variations in the output of a section of the 4π radiometer arm with time, during studies to determine the response time of the 4π radiometer	248
Figure 45 : Direct measurement of the radiative heat loss rate from a human body : calibration curve for a test section of the prototype radiometer arm using the test rig shown in Figure 42	250
Figure 46 : Direct measurement of the radiative heat loss rate from a human body : view of the test rig in the horizontal test chamber of the climatic chamber during preliminary tests on a prototype model of the 4π radiometer arm	251
Figure 47 : Measurement of the radiative heat loss rate from a human body : schematic layout of the radiometer arm	254
Figure 48 : Measurement of the radiative heat loss rate from a human body : assembly of the extruded aluminium sections which form the basic framework of the radiometer arm	256

	Page
Figure 49 : Spectral emissivity of different materials	258
Figure 50 : Direct measurement of the radiative heat loss rate from a human body : details of the supporting brackets for the radiation-sensing elements of the radiometer arm	262
Figure 51 : Direct measurement of the radiative heat loss rate from a human body : view of one end of a section of the 4π radiometer arm showing the method of mounting the nickel resistance wire thermal radiation-sensing elements	263
Figure 52 : Measurement of the radiative heat loss rate from a human body by means of the 4π radiometer arm : mounting of the thermal radiation-sensing elements in one of the sections of the radiometer arm	264
Figure 53 : Transmission of polythene (Lupolen-H), 0,1 mm thick	266
Figure 54 : Direct measurement of the radiative heat loss rate from a human body : outside view of the main drive unit for the 4π radiometer arm	269

	Page
Figure 55 : Direct measurement of the radiative heat loss rate from a human body : outside view of the supporting yoke and clutch assembly of the 4π radiometer arm	270
Figure 56 : Direct measurement of the radiative heat loss rate from a human body : "Slip ring" contacts for the electrical leads connected to the thermal radiation-sensing elements in the 4π radiometer arm	273
Figure 57 : Direct measurement of the radiative heat loss rate from a human body : details of the lower roller support for the rotating 4π radiometer arm	274
Figure 58 : Configuration factors between the radiation-sensing elements located in one of the vertical sections of the 4π radiometer arm, the body and various sections of the surrounding walls of the test section of the climatic chamber with and without the body in position	290
Figure 59 : Flow diagram of the computer programme for calculating the net radiation energy exchange rate between the radiation-sensing elements in the radiometer arm, the body	292

and various sections of the surrounding
walls of the test chamber

- Figure 60 : Theoretical temperature variations with 304
time of the "inner" and "outer" radiation-
sensing elements of the 4π radiometer arm
during a typical revolution of the radiometer
with the body temperature higher than the
surrounding wall temperatures
- Figure 61 : Theoretical temperature variations with 305
time of the "inner" and "outer" radiation-
sensing elements of the 4π radiometer arm
during a typical revolution of the radiometer
with the body temperature lower than the
surrounding wall temperatures
- Figure 62 : Direct measurement of the radiative heat 311
loss rate from a human body by means of the
 4π radiometer arm : circuit diagram for the
electrical resistance thermal radiation-
sensing elements
- Figure 63 : Direct measurement of the radiative heat 316
loss rate from a human body : calibration
curve for the 4π radiometer
- Figure 64 : Direct measurement of the heat loss rate 318
from a human body : test rig for animate
studies. (Photograph : D. Rabe)

	Page
Figure 65 : Direct measurements of the various components of the heat loss rate from a human body : typical test results showing, <u>inter alia</u> , variations in the radiant heat loss rate with time of a subject in the horizontal test chamber of the climatic chamber of the Human Sciences Laboratory.	320
Figure 66 : Exploded view of the low-cost portable radiometer for surface temperature and emissivity measurements	339
Figure 67 : View of components of the low-cost portable radiometer for surface temperature and emissivity measurements	344
Figure 68 : Portable low-cost radiometer for surface temperature and emissivity measurements : block diagram and inter-connections	345
Figure 69 : Portable low-cost radiometer for surface temperature and emissivity measurements : power supply units	346
Figure 70 : Portable low-cost radiometer for surface temperature and emissivity measurements : amplifiers, polarity discriminators and relays	347

	Page
Figure 71 : Measurement of surface temperature : calibration curve for low-cost radiometer	352

APPENDIX A

Figure A1 : Reynolds flow in the air and water vapour mixture adjacent to an interface	388
Figure A2 : Mass transfer and heat fluxes across an interface	
Figure A3 : An illustration of the processes which occur adjacent to the interface of a "sweating" body exposed to relatively dry air	393

APPENDIX B

Figure B1 : Geometrical data referring to thermal radiation from a body in an enclosure	405
--------------------------------------------------------------------------------------------	-----

APPENDIX C

Figure C1 : Schematic layout of manually operated dewpoint hygrometer	415
Figure C2 : Monochromatic absorptivity for water vapour and carbon dioxide	424

	Page
Figure C3 : Schematic layout of infra-red hygrometer by Wood	426
Figure C4 : Schematic diagram of the Wylie electrolytic condensation hygrometer	433
 <u>APPENDIX D</u>	
Figure D1 : The measured equilibrium resistance of a NaCl crystal in the electrolytic hygrometer as a function of the relative humidity of the surrounding air	440
Figure D2 : The surface resistance of a KCl crystal as a function of the relative humidity of the surrounding air	442
Figure D3 : Ventilation rate through the component parts of the modified Wylie hygrometer as a function of the pressure drop across the instrument	443
Figure D4 : The modified Wylie electrolytic conden= sation hygrometer : time taken to indicate 66 and 90% of a step change in temperature, for various pressure drop values across the instrument	446

APPENDIX G

Figure G1 : Radiation energy exchange : isometric view 464
showing the layout of surfaces referred to
in an example to demonstrate the method
of calculating the configuration factor
between surfaces.

NOMENCLATUREUpper case symbols

A	area	m^2
A	constant	dimensionless
A	psychrometric constant	dimensionless
A	recorder deflection	mm
B	mass driving force	dimensionless
B	recorder deflection	mm
C	characteristic constant of radiometer	dimensionless
C	constant	dimensionless
C	temperature coefficient of resistance	$^{\circ}C^{-1}$
C_{air}	air capacity rate	$W/^{\circ}C$
D	diameter	m
D	diffusion coefficient	dimensionless
E	heat exchanger effectiveness	dimensionless
E	radiant intensity	kW
F	configuration factor	dimensionless
\dot{G}	mass flow rate of bulk of stream of fluid	kg/s
\dot{G}''	mass flow rate of bulk of stream of fluid per unit cross-sectional area	$kg/m^2 s$
H	specific enthalpy	kJ/kg
\dot{H}'	heat input rate per unit length	W/m
\dot{H}''	heat input rate per unit area	W/m^2
I	current	A

K''	physiological conductance or overall heat transfer conductance between the core of the body and the skin surface per unit area of body surface	$\text{kW/m}^2 \text{ } ^\circ\text{C}$
L	length	m
M	slope of line	dimensionless
\dot{M}	metabolic heat production rate	kW
\dot{M}''	metabolic heat production rate per unit area of body surface	kW/m^2
N_{Le}	Lewis number	dimensionless
N_{Nu}	Nusselt number	dimensionless
N_{Pr}	Prandtl number	dimensionless
N_{Re}	Reynolds number	dimensionless
N_{Sc}	Schmidt number	dimensionless
N_{St}	Stanton number	dimensionless
N_{tu}	heat transfer units	dimensionless
P	atmospheric pressure	kPa
\dot{Q}	air flow rate	m^3/s
R	resistance	Ω
\dot{S}	heat storage rate	kW
\dot{S}''	heat storage rate per unit area of body surface	kW/m^2
S	geometric factor	dimensionless
S	length of line	m
T	absolute temperature	$^\circ\text{K}$
U	overall coefficient of heat transfer	$\text{W/m}^2 \text{ } ^\circ\text{C}$

V	voltage	v
\dot{W}	work rate of subject	kW
\dot{W}''	work rate of subject per unit area of body surface	kW/m ²

Lower case symbols

a, b, c	constants	dimensionless
c	specific heat	kJ/kg °C
d	distance between surfaces	mm
e	emissive power	dimensionless
f	friction factor	dimensionless
f	mass concentration of moisture in the air	dimensionless
g	acceleration due to gravity	m/s ²
g	Reynolds flux per unit area	kg/m ² s
h	coefficient of heat transfer	kW/m ² °C
j	mass transfer coefficient	kg/kPa m ² s
k	coefficient of discharge	dimensionless
k	thermal conductivity	W/m °C
ℓ	latent heat of evaporation of sweat	kJ/kg
\dot{m}	mass transfer rate	kg/s
\dot{m}''	mass transfer rate across unit area of the interface into the air stream	kg/m ² s
n	number off	
p	pressure	kPa
q̇	heat transfer rate	kW

\dot{q}''	heat transfer rate per unit area of body surface	kW/m^2
r	radius	m
t	temperature	$^{\circ}\text{C}$
\dot{v}	velocity	m/s
w	specific humidity	kg/kg of dry air

Greek symbols

∞	radiometer output	
β	correction factor	dimensionless
ϵ	emissivity	dimensionless
λ	wave-length	μm
μ	dynamic viscosity of fluid	kg/ms
ρ	density	kg/m^3
σ	Stefan-Boltzman constant	$\text{kW/m}^2 \text{K}^4$
ϕ	angle	radians
θ	length of exposure	s
ω	solid angle	radians

Subscripts

A	enclosing body surface
a	atmospheric
ax	axial
aux	auxiliary

act	actual
B	enclosed body surface
b	black body
bg	bar-grid panel
c	coil
c	convective
e	entering
e	evaporative
f	based on the mass concentration of water in a mixture
f	water film, sweat film
G	air-vapour mixture
g	galvanometer
ht	heater tape
h	based on enthalpy
i	inside
i	mixture component
ise	inner radiation-sensing element
ℓ	leaving
L	through the L surface
lu	through pulmonary ventilation
ose	outer radiation-sensing element
o	outside
or	orifice
r	core
r	at point r

rad	radiative, radiometer, radiation detector
s	adjacent to the interface on the air side
s	surface, skin
se	sensing element
so	solid panel
sp	spiral tube
t	target
t	tube
T	total
TL	water crossing L surface
TS	water crossing S surface
w	wake
w	water
wb	wet-bulb
wv	water vapour
x	section of arm

ACKNOWLEDGEMENTS

I am indebted to:

Dr J.P. Bindon and
Professor M. Reed

my supervisors, for their encourage=
ment, support and guidance.

Chamber of Mines of
South Africa

on whose behalf the work was carried
out, for permission to use the data
for a thesis.

Dr H.G. Denkhaus and my
colleagues at the National
Mechanical Engineering Research
Institute of the Council for
Scientific and Industrial
Research of South Africa

for their continual support.

Professor C.H. Wyndham and
Dr N.B. Strydom

for their help and interest

Dr D. Mitchell and his
colleagues at the Human
Sciences Laboratory

for their assistance in carrying
out certain calibration studies.

Professor C.J. Rallis

for his guidance and encouragement.

Mrs M. Kotzé

for her assistance in the typing
of the thesis.

The Technical Services

for the construction of the

Department of the Council

apparatus and printing of the

for Scientific and Industrial

thesis.

Research of South Africa

PREFACE

At the request of the Human Sciences Laboratory of the Chamber of Mines, the National Mechanical Engineering Research Institute of the Council for Scientific and Industrial Research of South Africa, undertook the design and development of the following items of equipment:

- (i) a climatic chamber in which any particular set of environmental conditions prevailing underground in the deep level gold mines could be reproduced and accurately maintained,
- (ii) a human calorimeter for the measurement of body heat storage, and
- (iii) instrumentation for measuring the convective, evaporative and radiative heat loss components of a working subject in the test section of the climatic chamber.

Work on the climatic chamber was completed in 1955 and in 1962 the human calorimeter was commissioned.

I assisted Prof. J. Visser with the design of the human calorimeter and was subsequently responsible for the development of the instrumentation for measuring the evaporative and radiative heat exchange rates of a working subject as well as the final commissioning of all the heat loss measuring equipment.

In addition, I carried out theoretical studies to assess, inter alia, the relative magnitudes of the evaporative and radiative heat loss rates from a human body under certain assumed conditions with regard to air temperature, relative humidity and air velocity. During these studies, Mr T. Bartlett assisted with the compilation of programmes for carrying out certain calculations with the aid of a computer.

The development of the radiation heat loss measuring instrument was based on a basic principle of measurement proposed by Prof. J. Visser. Messrs T. Boelema and R. Haar assisted with the mounting of the radiation-sensing elements in the radiometer and Dr A.J. Vermeulen assisted with the full-scale calibration tests on the radiative heat loss measuring instrument.

During the development of the evaporative heat loss measuring equipment, I was assisted by Dr J. Wentzel who carried out certain of the model studies and calibration tests under my direction.

The actual construction of the radiative and evaporative heat loss measuring equipment was carried out by the Technical Services Department of the CSIR.

Work on the development of the heat loss measuring equipment was completed in 1971.

During the development and commissioning of the heat loss measuring equipment, certain modifications to the climatic chamber were carried out under my guidance to ensure the satisfactory operation of the heat loss measuring equipment. These modifications included:

- (i) the installation of graphite impregnated fibre glass heating pads on the floor panels of the diffuser-contraction section of the climatic chamber, to overcome the problem of zero instability of the convective heat loss measuring instrument; due to certain uncontrolled temperature variations with time which occurred in the boundary layer of the air stream in the horizontal test chamber of the climatic chamber,
- (ii) alterations to certain non-return valves in the temperature control system for the test chamber walls,
- (iii) the installation of wire mesh screens on the upstream and downstream sides of the test chamber, to minimise the adverse effect which uncontrolled surface temperature variations had on the measurement of the radiation heat exchange rate of a subject, and
- (iv) modifications to the humidity control system which included the installation of a unique humidity-sensing system with an output which is only dependent on the absolute humidity.

During the final commissioning of the heat loss measuring equipment, I developed a low temperature radiometer for the measurement of skin

temperature and emissivity. The calibration of the latter instrument was carried out with the assistance of Dr D. Mitchell of the Human Sciences Laboratory.

The development of the evaporative and radiative heat loss measuring equipment and the low temperature radiometer as well as the theoretical studies, are described in this dissertation.

CHAPTER 1

INTRODUCTION

Recognition has long been given to the fact that the human body is a generator of heat in a state of energy exchange with its surroundings. The implications of this and the influence on the well-being and productivity of man have been studied by many workers since the crude investigations of Lavoisier (1777). The net picture today is one of a complicated combination of physical, physiological and psychological phenomena governing the reactions of the body to a given stress condition^{1)*}.

Generally, the heat produced within the human body due to metabolic processes is dissipated to the surroundings, principally by radiation, convection and evaporation. Under normal body temperature conditions a state of equilibrium exists and a feeling of comfort is induced. Whenever the heat dissipation rate is curbed or accelerated, however, the body is subjected to a strain as the mean body temperature and heart rate changes and the body's thermo-regulatory system attempts to maintain the status quo ante. Under such conditions, the rate of heat transfer between the human body and its surroundings has a profound influence on the mean temperature level or strain of the body.

* The numbers in parenthesis refer to the bibliography at the end of the dissertation.

A knowledge of heat transfer is thus essential for the study of human reactions in environments that cannot be moulded to suit the requirements of the body and the resultant strain is high.

In South Africa, deep level mining operations are characterised by hot air and rock temperatures and humid conditions imposing high heat stresses on workers. Great efforts have been made to improve the environmental conditions by ventilation engineers, but nevertheless a high degree of thermal stress still obtains. Thus, data on working efficiency, acclimatisation and endurance limits of men under conditions prevailing are necessary in order to plan shifts intelligently to ensure maximum production with the least hazard to human life.

Considerable research in this direction is being undertaken by the Chamber of Mines through its Human Sciences Laboratory. The National Mechanical Engineering Research Institute of the Council for Scientific and Industrial Research of South Africa has actively assisted in this research by, inter alia, designing a climatic chamber with test sections of adequate size to accommodate subjects in normal working positions,^{2,3,4)} for this laboratory. In addition, a human calorimeter⁵⁾, which is in the form of a relatively small enclosure in which the human body is placed, was designed for the measurement of heat storage and unique direct-measuring techniques for determining the convective, evaporative and radiative heat loss rates of a working subject in the climatic chamber were developed.

In the past the usefulness of climatic chambers has been severely limited by the lack of suitable instrumentation capable of the direct measurement of heat loss from a working subject in the chamber; the heat loss from the subject in such a chamber being determined indirectly from his oxygen consumption rate and his carbon dioxide output rate^{6,7)}. One of the restrictions on such indirect methods of measurement is that the body must be given sufficient time to attain thermal equilibrium with its environment.

Previously the more direct methods of measurement were carried out in "calorimeters". Some of the earliest direct measurements were made by observation of the heat given to insulated water baths in which the body was immersed⁸⁾. Apart from unduly long thermal lags, the water bath calorimeter is unsuitable as the heat exchange system is totally different from natural exposure to air. Furthermore, separation between modes of heat transfer is impossible with this technique.

Another type of calorimeter was constructed by C.E.A. Winslow et al⁹⁾ with particular emphasis on the complete analysis of the process of heat exchange, namely, convection, radiation and evaporation. The convective and radiant heat loss components were calculated indirectly from measurements of the air velocity and surface temperatures, while the evaporative heat loss was deduced from the change in mass of the subject.

The indirect calculation of the heat loss from a human body is of little value. The accuracy with which the losses can be determined is poor and the cumulative error in the summation exceedingly large due, mainly, to the irregular shape of the body, the non-uniform temperature distribution across the body surface and the difficulty of determining by the integration of single measurements, the average temperature of the skin. Such techniques are also entirely unsuitable for the determination of the heat loss rate under transient conditions since the calculation procedures are cumbersome and do not lend themselves to continuous recording.

An improved calorimeter was subsequently developed by Benzinger et al¹⁰⁾. However, due to the limited size of the calorimeter (800 mm x 800 mm x 2 000 mm), the system of measurement was subject to the major physiological disadvantage of all calorimeters in which the subject must be in a supine or sitting position; apart from restricting normal working movement, the position of the body may lead to an alteration in peripheral circulation or respiration^{11,12)}.

The disadvantages of previously developed methods of measuring the heat loss from a human body are eliminated in the newly developed unique direct measuring techniques which enable the various heat loss components from a subject in a natural working position to be measured directly.

The instrumentation was specifically designed for use in the horizontal test chamber of the climatic chamber of the Human Sciences Laboratory.

The development of part of the heat loss measuring equipment is described in this dissertation. In particular reference is made to the development of instrumentation for measuring the evaporative and radiative heat loss rates as well as the development of a unique low-temperature radiometer for measuring the emissivity and surface temperature of human skin.

In Chapter 2, following the Introduction, the climatic chamber is described in some detail. In particular, attention is paid to the temperature and humidity control facilities of the climatic chamber in view of the stringent requirements of the direct heat loss measuring equipment in this regard.

In Chapter 3, entitled "Thermophysiological considerations", the mechanism of heat transportation from deep inside the body to the periphery is referred to and the modes of heat transfer involved in the resultant energy exchange process between the skin of the body and its environment are discussed. A method of determining the moisture evaporation rate from the skin from a knowledge of the physiological conductance of the body and the surrounding environmental conditions

is developed and values of the mass transfer and radiation energy exchange rates are calculated for the purpose of assessing the required sensitivities of the evaporative and radiative heat loss measuring instruments.

The development of the direct-measuring technique for determining the evaporative heat loss from a human body, including the design of a highly sensitive humidity-sensing system, is described in Chapter 4. Since the air flows through the test chamber of the climatic chamber in a horizontal direction, the moisture evaporated and hence the evaporative heat loss from the subject in the test section all appears in the wake of the body. The problem of evaporative heat loss measurement thus resolves to the development of a technique of accurately assessing the moisture evaporation rate from measurements of, inter alia, the specific humidity increase of the air flowing over the body.

Chapter 5 deals with the design, construction and calibration of the direct-measuring instrument for determining the radiation heat loss from a working subject. Factors affecting the choice of a suitable thermal radiation detector are discussed and reference is made to certain preliminary studies that were carried out to determine the response characteristics of the thermal radiation detection system incorporated in the radiometer.

Finally, in Chapter 6 the development of the low temperature radiometer for measuring the surface temperature and emissivity of human skin is described.

The dissertation ends with a discussion of the subsequent successful application of the direct heat loss measuring equipment to heat transfer studies in the climatic chamber.

CHAPTER 2

DESCRIPTION OF THE CLIMATIC CHAMBER

The climatic chamber was designed and commissioned by Grant^{2,3,4}). It is built in the form of a return flow wind tunnel having two working sections or test chambers, one for horizontal and the other for vertical air flow.

Figure 1 presents a general layout of the tunnel and test chambers.

The air flows through the humidity and temperature control sections of the tunnel in turn, before entering the horizontal and vertical test chambers through gaps between bar-grid panels which comprise the opposite walls of the chambers. Diffuser-contraction sections are provided on the upstream sides of the test chambers to provide satisfactory air inflow conditions to the test chambers. Air speeds within the test chamber are controlled by means of the main variable speed axial flow fan. Fresh air is introduced into the system by means of a fresh air fan installed on the upstream side of the main fan.

All the tunnel walls are thermally insulated to reduce the influence of ambient air temperatures on air temperatures in the tunnel.

The floor panel of the diffuser-contraction section of the tunnel,

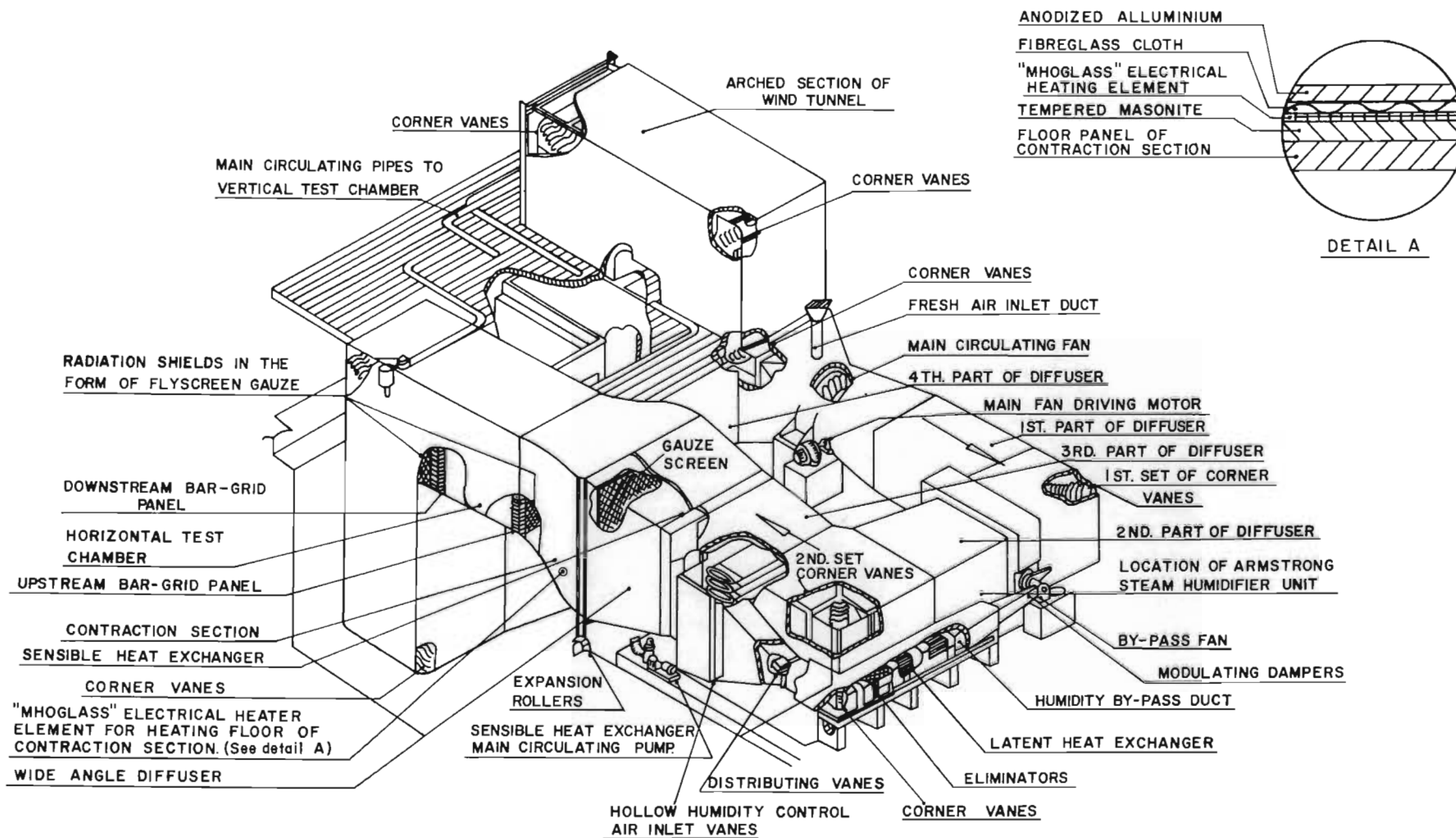


FIGURE 1

Layout of tunnel and test chambers of climatic chamber.

between the heat exchanger in the temperature control section and the horizontal test chamber, is equipped with graphite impregnated fibre glass heater elements to enable the entire floor area of this section of the tunnel to be uniformly heated to a temperature equal to the air temperature in the tunnel. In this manner temperature gradients which tend to be set up in the boundary layer adjacent to the floor whenever the tunnel is operated at air temperatures above the ambient air temperature could be effectively eliminated. The latter requirement is a major prerequisite for the satisfactory operation of the convective heat loss measuring instrument.

Wire mesh screens of the fly screen gauze type are installed across the full cross-section of the tunnel on the upstream and downstream sides of the inlet and outlet bar-grid panels of the horizontal test chamber. The gauze screens act as thermal radiation screens between a subject in the horizontal test chamber and the surfaces of the tunnel which are not temperature controlled and which would normally be "seen" by a subject in the chamber, through the gaps between the bar-grid panels of the horizontal test chamber.

2.1 Horizontal test chamber

The horizontal test chamber which is similar to the vertical test section in construction, is 3 m x 3 m x 3 m in size.

The air enters and leaves the chamber through 25 mm gaps between horizontal bar-grid panels comprising opposite walls. The bar-grids are 25 mm wide by 150 mm deep in the direction of air flow and extend across the full width of the test chamber. Water is circulated through the bar-grid panels for the purpose of temperature control; each bar-grid panel being provided with a separate temperature control system. Similar facilities are provided for the independent temperature control of the floor, roof and each of the side wall panels of the test chamber.

Access to the horizontal test chamber is provided by a door in the one wall. The door is of hollow construction and part of the fluid circulating through the adjoining panel is circulated through the door for the purpose of temperature control.

2.2 Humidity control system

The humidity control system basically consists of a humidity-sensing system, a finned tube de-humidifying coil installed in a bypass duct, modulating dampers for controlling the flow rate of air through the bypass duct and an Armstrong steam humidifier unit.

The steam nozzles of the humidifier unit are located in the main air stream on the upstream side of the second set of corner

vanes after the main fan of the climatic chamber.

A water-ethylene glycol mixture is continuously re-circulated between the de-humidifying coil and a temperature-controlled storage tank; the temperature of the fluid being automatically controlled at a fixed temperature of 1°C, by means of a refrigeration plant.

2.2.1 Humidity-sensing system

An Aminco electrical resistance hygrometer incorporating a narrow range lithium-chloride sensor was used as the humidity-sensing device for the purpose of humidity control. In view of the narrow range of the sensor - about 12 per cent relative humidity - the particular sensor used is selected to suit the required humidity control value.

A narrow range sensor was selected in preference to the wide range type in view of the increased sensitivity of such a sensor.

The hygrometer-indicating unit contains a built-in bridge network which provides a signal of 0 to 25 mV d.c. for a 12 per cent change in relative humidity.

The output voltage from the hygrometer is biased against a regulated 10 mV supply and the resulting signal applied to a Bristol dynamaster electro-pneumatic recorder-controller.

For the purpose of detecting the humidity conditions in the test chamber a sample of air is withdrawn from the test chamber (near the air-inlet bar-grid panel) at a flow rate of 12 l/s and passed through a heat exchanger, to fix the dry-bulb temperature. The sample of air is then fed through the hygrometer tube containing the lithium chloride sensor.

The heat exchanger, which is in the form of a spirally wound copper tube immersed in a temperature controlled water bath, enabled the dry-bulb temperature of the sample air to be controlled to within 0,1°C. The sampling tube on the upstream side of the heat exchanger was heated and the heat exchanger maintained at a sufficiently high temperature to prevent condensation.

Since the dry-bulb temperature of the air sample is controlled at a fixed temperature, the output of the hygrometer is independent of air temperature variations

within the test chamber and is only a function of the absolute humidity.

2.2.2 Method of humidity control

Humidity conditions within the test chamber are controlled by introducing steam into the tunnel at a fixed pre-determined rate and varying the rate of air flow through the bypass duct by means of modulating dampers in accordance with the humidity requirements.

The modulating dampers are automatically controlled by the humidity-sensing device through an electro-pneumatic controller unit. On humidity rise within the chamber the dampers are opened. On humidity fall the reverse action takes place.

2.3 Air temperature control system

Air temperatures within the horizontal test chambers are automatically controlled by means of a temperature-sensing element of the resistance type installed in the tunnel on the upstream side of the horizontal test chamber, a sensible heat exchanger installed in the tunnel on the downstream side of the bypass duct of the humidity control system and modulation valves in the water supply system to the heat exchanger.

The heat exchanger is supplied with a mixture of water from a cold and a hot tank, each with a capacity of 22 500 litres. The one tank is equipped with a cooling coil coupled to a refrigeration plant and the other with 48 kW electrical heater elements.

The respective temperatures of the tanks are set according to the conditions required in the tunnel. Valves actuated from the temperature controller inject either hot or cold fluid into the heat exchanger circuit as required to give the required air temperature within the test chamber.

2.4 Wall temperature control system

The respective temperatures of surrounding side wall, bar-grid, roof and floor panels of the horizontal and vertical test chambers are individually controlled by means of systems similar to the air temperature control system.

Water at a controlled temperature is circulated through each of the hollow panels surrounding the test chambers, the temperature of each panel being controlled by means of a temperature-sensing element of the resistance type located in a pocket in the water supply line to the particular panel.

2.5 Range and stability of environmental control

Temperature and relative humidity conditions within the horizontal test chamber can be controlled within the following limits:

- Air temperature : Within $0,2^{\circ}\text{C}$ and $0,1^{\circ}\text{C}$ at air velocities below and above 1 m/s , respectively, over the temperature range of 10°C to 50°C .
- Wall temperature : Within $0,1^{\circ}\text{C}$ over the temperature range of 10°C to 50°C
- Relative humidity : Within $0,5\%$ and $0,05\%$ at air velocities below and above 1 m/s , respectively, over the vapour pressure range of $0,5$ to 5 kPa .

In general, the environmental conditions within the horizontal test chamber could be controlled within sufficiently close limits to ensure the satisfactory operation of the heat loss measuring equipment.

CHAPTER 3

THERMOPHYSIOLOGICAL CONSIDERATIONS

Heat is continuously being generated within the human body as a result of the chemical processes associated with breathing, digestion and physical effort, all these processes being grouped under the term metabolism. Apart from a small portion of the metabolic heat which is lost through the pulmonary system and a part which may be converted into physical work, most of the heat which is produced is transported to the skin and dissipated to the environment.

The human body constantly endeavours to maintain a state of balance between the heat generated in it and that rejected from it.

Inasmuch as the body is a generator of heat and is free to exchange energy with its surroundings, it can be regarded as a thermodynamic system.

On the basis of the first law of thermodynamics the following equation may be applied to the human body:

$$\dot{M} + \dot{S} = \dot{q}_c + \dot{q}_{rad} + \dot{q}_e + \dot{q}_{lu} + \dot{W} \quad \dots\dots\dots (1)$$

where \dot{M} = rate of metabolic heat production

\dot{S} = rate of heat storage (rate of gain or loss in the
heat content of the body)

and \dot{q}_c = rate of thermal exchange by convection

\dot{q}_{rad} = rate of thermal exchange by radiation

\dot{q}_e = rate of evaporative heat loss

\dot{q}_{lu} = rate of evaporative and sensible heat loss through
pulmonary ventilation

\dot{W} = work rate of the subject

In high temperatures or during great physical exertion the transfer of heat from the site of production to the skin and the secretion of sweat and its evaporation, are the main physiological mechanisms involved to assist in the dissipation of heat from the body.

Sweating is a powerful mechanism which man and some higher primates have for controlling body temperatures under high heat stress conditions¹³⁾.

Under these conditions, the transfer of heat from deep inside the body to the periphery is primarily a function of the cardio-vascular system which must deliver an adequate quantity of blood not only to the working muscles but also the skin for cooling and for supplying the active sweat glands. Heat conduction through the tissues of the body on the other hand, accounts for only about 20 per cent of the necessary heat transmission from the core to the skin surface in the case of a nude resting man and a negligible percentage of that necessary in a working man¹⁴⁾.

In low and moderate air temperatures, the evaporative loss of heat from the skin is practically independent of air temperature and wind speed and the only controllable modes of dissipation of body heat are due to radiation and convection.

The relative importance of heat conduction through the body tissues is increased at low ambient temperatures due to the blood flow to large areas of the body, particularly the limbs, being restricted under these conditions.

Any changes to the metabolic rate of heat production and rate of blood circulation to the skin will, in general, result in a change in skin temperature. Nielson¹⁵⁾ and Pederson¹⁶⁾ pointed out that, if the skin temperature remains constant under these conditions, the extra metabolic heat production is being compensated exactly by extra sweating.

3.1 Physiological conductance

Physiological conductance is a concept originally proposed by Burton and Bazett⁸⁾ to express the rate of heat flow from the core of the body to the skin, quantitatively. The actual value of the physiological conductance, which takes the heat flow due to the circulatory system as well as the heat flow due to thermal conduction through the body tissues into account, depends on a great many factors in addition to blood flow; including body

dimensions, thickness of subcutaneous fat, the proximity of patent blood vessels to the surface and the direction of local spatial temperature gradients near the surface. Physiological conductance may be described quantitatively by the net rate of heat transfer divided by the temperature difference driving the heat flow. See equation (1) on page 58.

$$\text{Thus, } K'' = (\dot{M}'' \pm \dot{S}'' - \dot{q}''_{lu} - \dot{W}'') / (t_r - t_s) \quad \dots\dots\dots (2)$$

where K'' = physiological conductance, per unit area of body surface, $\text{kW/m}^2 \text{ } ^\circ\text{C}$

and \dot{M}'' = metabolic heat production rate, per unit area of body surface, kW/m^2

\dot{S}'' = rate of heat storage, per unit area of body surface, kW/m^2

\dot{q}''_{lu} = heat loss rate through the pulmonary system, per unit area of body surface, kW/m^2

\dot{W}'' = work rate, per unit area of body surface, kW/m^2

t_s, t_r = skin and core temperature of the body, respectively, $^\circ\text{C}$.

According to Cooper and Kenyon¹⁷⁾ and Nielson and Nielson¹⁸⁾, the core temperature, t_r , may be taken as the temperature of the oesophagus which approximates to the temperature of the arterial blood. However, core temperature is also related

quite well to the rectal temperature in the steady state condition¹⁹⁾.

Mitchell et al²⁰⁾ found that in hot dry environments with dry-bulb temperatures between 35°C and 50°C, the physiological conductance, K'' , attained a constant value of the order of $20 \text{ W/m}^2 \text{ }^\circ\text{C}$ in the case of nude resting men, which is in good agreement with the measurements of Robinson²¹⁾. The constancy of the conductance value apparently arises from the "saturation" of the mechanism of vasometer control²²⁾. In this case the thermoregulatory system of the body attempts to increase the physiological conductance by increasing the blood flow rate to the periphery, in order to facilitate heat dissipation from the body core. However, this improvement cannot be unlimited, and eventually the vasometer mechanism saturates and the conductance adopts a constant value.

Higher physiological conductance values can be reached in working men^{23,24)}. The conductance value in this case increases as the air temperature is increased mainly as a result of (a) the re-direction of blood flow to the periphery, by dilation of the peripheral blood vessels and constriction of the non-peripheral vessels and (b) the increase in the cardiac output rate.

There is evidence that the increase in metabolic rate due to physical work is a more important stimulus to the heart to increase its output than vasodilation of peripheral blood vessels due to heat stress^{25,26}). Consequently, conductance can appear to saturate with increasing thermal stress in resting men at values much lower than those attained in working men.

3.2 Sweating

In man thermally induced sweat originates from eccrine glands which consist of convoluted bulbs situated in the dermal region of the skin. The bulbs, which are well supplied with blood, are connected to the skin surface through minute ducts located in the skin. The sweat glands are capable of producing copious amounts of sweat over the whole body; of the order of 0,8 to 1,0 g/s for short periods up to 0,5 hr and 0,17 g/s for periods of 24 hr²⁷).

There is also a loss of water which is not dependent on the secretion of sweat. This was confirmed by Richardson²⁸) during observations on human subjects congenitally devoid of sweat glands. It appears that this loss represents the passive diffusion of water vapour through the epidermis as was assumed by Taylor and Buettner²⁹). At low sweat rates in dry environments the sweat may evaporate in the duct of the gland without

"wetting" the skin.

3.3 Moisture evaporation rate from the skin of a human subject: theoretical considerations

The evaporative heat loss rate from a human body is given by the following equation:

$$\dot{q}''_e = \ell \dot{m}'' \quad \text{..... (3)}$$

where \dot{q}''_e = evaporative heat loss rate, per unit
area of body surface, kW/m²

and ℓ = latent heat of evaporation of sweat, kJ/kg

\dot{m}'' = mass transfer rate across unit area of the
interface into the air stream, kg/m² s.

A knowledge of the moisture evaporation rate or mass transfer rate, \dot{m}'' , from a human subject in the horizontal test chamber of the climatic chamber is necessary to determine the required sensitivity of the evaporative heat loss measuring instrument.

Physically, the rate of evaporation from a heated wet surface varies with the area and shape of the surface, the vapour pressure or mass concentration gradients in the air stream adjacent to the body, the velocity of the air and the rate at which heat is conducted to the surface from the heated body.

Equations expressing the moisture evaporation rate from a human body are usually expressed in the form^{30,31)}:

$$\dot{m}'' = jC(p_{wv,s} - p_{wv,G}) \quad \dots\dots\dots (4)$$

where \dot{m}'' = moisture evaporation rate per unit area of body surface, $\text{kg/m}^2 \text{ s}$

and j = mass transfer coefficient, $\text{kg/m}^2 \text{ s kPa}$

C = constant

$p_{wv,s}, p_{wv,G}$ = partial water vapour pressures of moisture on the surface of the skin and the water vapour in the air stream, respectively, kPa.

Calculation of the moisture evaporation rate from a human body by means of equation (4), is complicated by the fact that the skin or interface temperature is unknown. The latter temperature, apart from being influenced by the environmental conditions, is also affected by the physiological conductance value.

An alternative method based on the hypothetical model originally proposed by Reynolds³²⁾, was, therefore, used for calculating the moisture evaporation rate or mass transfer flux, \dot{m}'' , assuming various values for the physiological conductance, K'' . This method of calculation was used by Spalding³³⁾ in preference

to the method based on the Stefan flow model or "stagnant film" theory used by Sherwood and Agford³⁴⁾.

The theoretical analysis, which is described in some detail in Appendix A, led to the following equation for calculating the mass transfer rate (see equation (21) on page 395 of Appendix A):

$$\begin{aligned}\dot{m}''/g_f &= g_h/g_f \left\{ \frac{c_G [\{t_G + (K''/g_h c_G)t_r\} - t_s \{1 + K''(g_h c_G)\} - \dot{q}''_{\text{rad}}/g_h c_G]}{\ell + c_f(t_s - t_f)} \right\} \\ &= (f_G - f_s)(f_s - 1) \quad \dots\dots\dots (5)\end{aligned}$$

where \dot{m}'' = mass transfer rate across unit area of the interface into the air stream, $\text{kg/m}^2 \text{s}$

g_f = $\dot{m}''(f_s - 1)/(f_G - f_s)$ = Reynolds flux based on mass concentration values in a mixture, per unit area of body surface, $\text{kg/m}^2 \text{s}$

and c_G, c_f = specific heats at constant pressure of the air and the water film on the surface of the body, respectively, $\text{kJ/kg } ^\circ\text{C}$

t_r, t_G, t_s, t_f = temperature of the core of the body, air temperature, body surface temperature and water film surface temperature, respectively, $^\circ\text{C}$

K'' = physiological conductance per unit area of body surface, $\text{kW/m}^2 \text{ } ^\circ\text{C}$

\dot{q}''_{rad} = net radiant heat flux per unit area of body surface, kW/m^2

ℓ = latent heat of change of phase of sweat, kJ/kg

g_h/g_f = 0,901; based on the analogy between heat and mass transfer. See equation (25) on page 398 of Appendix A

g_h = Reynolds flux based on enthalpy values per unit area of body surface, $\text{kg/m}^2 \text{s}$

f_G, f_s = mass concentration of moisture in the air stream and adjacent to the body, respectively, kg/kg

The value of g_h in equation (5) is deduced from the convective film coefficient of heat transfer, h_c , by means of the following relation (see equation (22) on page 396 of Appendix A):

$$g_h = h_c / c_G \quad \dots\dots (6)$$

For the purpose of calculating the mass transfer rate by means of equation (5), the alternative environmental conditions set out in Table 1 were assumed.

As far as the radiative influence on the mass transfer rate was concerned two conditions were considered, namely (a) neglecting radiation and (b) taking radiation into account. In the latter case the test chamber walls were assumed to be equal to the air temperature.

TABLE 1 : ASSUMED ENVIRONMENTAL CONDITIONS FOR CALCULATING
THE MASS TRANSFER RATE FROM A HUMAN BODY

TEMPERATURE °C			RELATIVE HUMIDITY, %	AIR VELOCITY, m/s	DESCRIPTION OF CONDITION
DRY-BULB	WET-BULB	DEW POINT			
15	11,8	10	72	0,5	Cold
15	11,8	10	72	5,0	Cold, windy
25	15,4	10	39	0,5	Warm
25	15,4	10	39	5,0	Warm, windy
35	18,4	10	22	0,5	Hot, dry
35	18,4	10	22	5,0	Hot, dry, windy
35	30,4	29,4	72	0,5	Hot, humid
35	30,4	29,4	72	5,0	Hot, humid, windy

It was furthermore assumed that the core temperature of the body, corresponding to the oesophagus or rectal temperature of the body, remained constant at 37°C over all ranges of environmental conditions, and the skin was completely wetted with moisture.

As a first step in the calculations to determine the moisture evaporation or mass transfer rate, \dot{m}'' , the term $(f_G - f_s)/(f_s - 1)$ in equation (5) was calculated for various assumed body surface temperature conditions. (The term $(f_G - f_s)/(f_s - 1)$ is the mass transfer driving force, $B = \dot{m}''/g_f$. (See equation (1) on page 387 in Appendix A).

Values of $(f_G - f_s)/(f_s - 1)$ are given in Table 2 for the dew-point temperature conditions assumed in Table 1.

Graphs of $(f_G - f_s)/(f_s - 1)$ versus the body surface temperature, t_s , were then plotted together with the family of straight lines representing the middle term of equation (5), assuming nominal values for the ratio $K''/g_h c_G$ ranging from 0 to 100. Based on certain approximations referred to in Appendix A, the straight lines all pass through the point with abscissa t_r and ordinate $(g_h/g_f)(c_G/\ell)(t_G - t_r - q''_{\text{rad}}/g_h c_G)$.

Neglecting radiation, the ordinate is $(g_h/g_f)(c_G/\ell)(t_G - t_r)$.

TABLE 2 : DETERMINATION OF THE MASS DRIVING FORCE : VALUES OF THE TERM $(f_G - f_s)/(f_s - 1)$ WHERE f_G AND f_s ARE THE RESPECTIVE MASS CONCENTRATIONS OF MOISTURE IN THE AIR STREAM AND ADJACENT TO THE BODY SURFACE, RESPECTIVELY

1. Dew point temperature : 10°C (See Table 1 on page 66)

$t_s, ^\circ\text{C}$	15	20	25	30	35	40
f_s^*	0,01280	0,01768	0,02420	0,03287	0,04433	0,05949
f_G^*	0,00916	0,00916	0,00916	0,00916	0,00916	0,00916
$f_G - f_s$	-0,00364	-0,00852	-0,01504	-0,02371	-0,03517	0,05033
$f_s - 1$	-0,98720	-0,098232	-0,97580	-0,96713	-0,95567	0,94051
$(f_G - f_s)/(f_s - 1)$	0,003687	0,0086733	0,015413	0,024516	0,036801	0,053514

2. Dew point temperature : 29,4°C (See Table 1 on page 66)

$t_s, ^\circ\text{C}$		30	35	40
f_s^*		0,03287	0,04433	0,05949
f_G^*		0,03178	0,03178	0,03178
$f_G - f_s$		-0,00109	-0,01255	-0,02771
$f_s - 1$		-0,96713	-0,95567	-0,94051
$(f_G - f_s)/(f_s - 1)$		0,001127	0,013132	0,029463

* Values for f_G and f_s were obtained from Table 6 in reference (144) for an atmospheric pressure of 837 kPa

The mass transfer rate was then determined as follows:

The value of $\dot{m}'' c_G / K''$ was calculated from the equation

$$\dot{m}'' c_G / K'' = (\dot{m}'' / g_f) (g_f / g_h) (g_h c_G / K'') \quad \text{..... (7)}$$

where \dot{m}'' = mass transfer rate across unit area of the interface into the air stream, $\text{kg/m}^2 \text{ s}$

c_G = specific heat at constant pressure of the air,
1,01 kJ/kg °C

K'' = physiological conductance per unit area of body surface, $\text{kW/m}^2 \text{ °C}$

g_f / g_h = 1/0,901, dimensionless (see Appendix A on page 399)

$g_h c_G / K''$ = ratio of the convective film coefficient of heat transfer to the physiological conductance, dimensionless.

The values for \dot{m}'' / g_f and $g_h c_G / K''$ in equation (7) are obtained from the intersection points of the $(f_G - f_s) / (f_s - 1)$ curve with the family straight lines representing the middle term in equation (5).

Graphs of the surface temperature, t_s , and the ratio $\dot{m}'' c_G / K''$ versus the ratio $g_h c_G / K''$ permit the mass transfer rate to be obtained for various values of the physiological conductance, K'' , and the film coefficient of heat transfer, $h_c = g_h c_G$.

According to the animate studies that were carried out³⁵⁾, using the convective heat loss measuring instrument that had previously been developed³⁶⁾, the following equation for the convective heat transfer from man was obtained:

$$h_c = 8,28 \times 10^{-3} (P/101,3)^{0,6} \dot{v}^{0,6} \quad \dots\dots (8)$$

where h_c = film coefficient of heat transfer,
kW/m² °C

and P = atmospheric pressure, kPa

\dot{v} = air velocity, m/s.

From equation (8), h_c was calculated to be $4,886 \times 10^{-3}$ kW/m² °C and $19,45 \times 10^{-3}$ kW/m² °C, for air velocities of 0,5 and 5,0 m/s respectively, and an atmospheric pressure of 83,7 kPa.

Assuming a value for the physiological conductance, K'' , of 20×10^{-3} kW/m² °C for nude resting men (see Section 3.1 on page 62), the following values of $K''/g_{h,c_G}$ are obtained for the two air velocity conditions listed in Table 1:

For an air velocity of 0,5 m/s, $K''/g_{h,c_G} = 20/4,886 = 4,09$

For an air velocity of 5,0 m/s, $K''/g_{h,c_G} = 20/19,45 = 1,03.$

3.3.1 Mass transfer rate neglecting radiation

Graphs of $(f_G - f_s)/(f_s - 1)$ versus the body surface temperature, together with the family of straight lines for the middle term of equation (5) on page 66, albeit

neglecting the radiation parameter $\dot{q}''_{\text{rad}}/g_h c_G$ in the middle term, are plotted in Figure 2 for the various assumed sets of environmental conditions with regard to air temperature and relative humidity that are listed in Table 1. Since the radiation term was neglected, the test chamber walls were assumed in this particular case to have no influence on the surface temperature of the body, t_s .

The intersections of the $(f_G - f_s)/(f_s - 1)$ curve with the various straight lines give the values of the driving force \dot{m}''/g_f and skin temperature, t_s , that can be expected for the various assumed values of $K''/g_h c_G$.

The dimensionless expression $K''/g_h c_G$ measures the ratio of the physiological conductance per unit area of body surface to the conductance on the air side of the liquid-gas interface.

Inspection of Figure 2 shows that the intersection of the $(f_G - f_s)/(f_s - 1)$ curve with the family of straight lines lies higher and farther to the right, the greater is the value of $K''/g_h c_G$. Thus, when the physiological conductance, K'' , is increased relative to that for the liquid-gas interface, the temperature

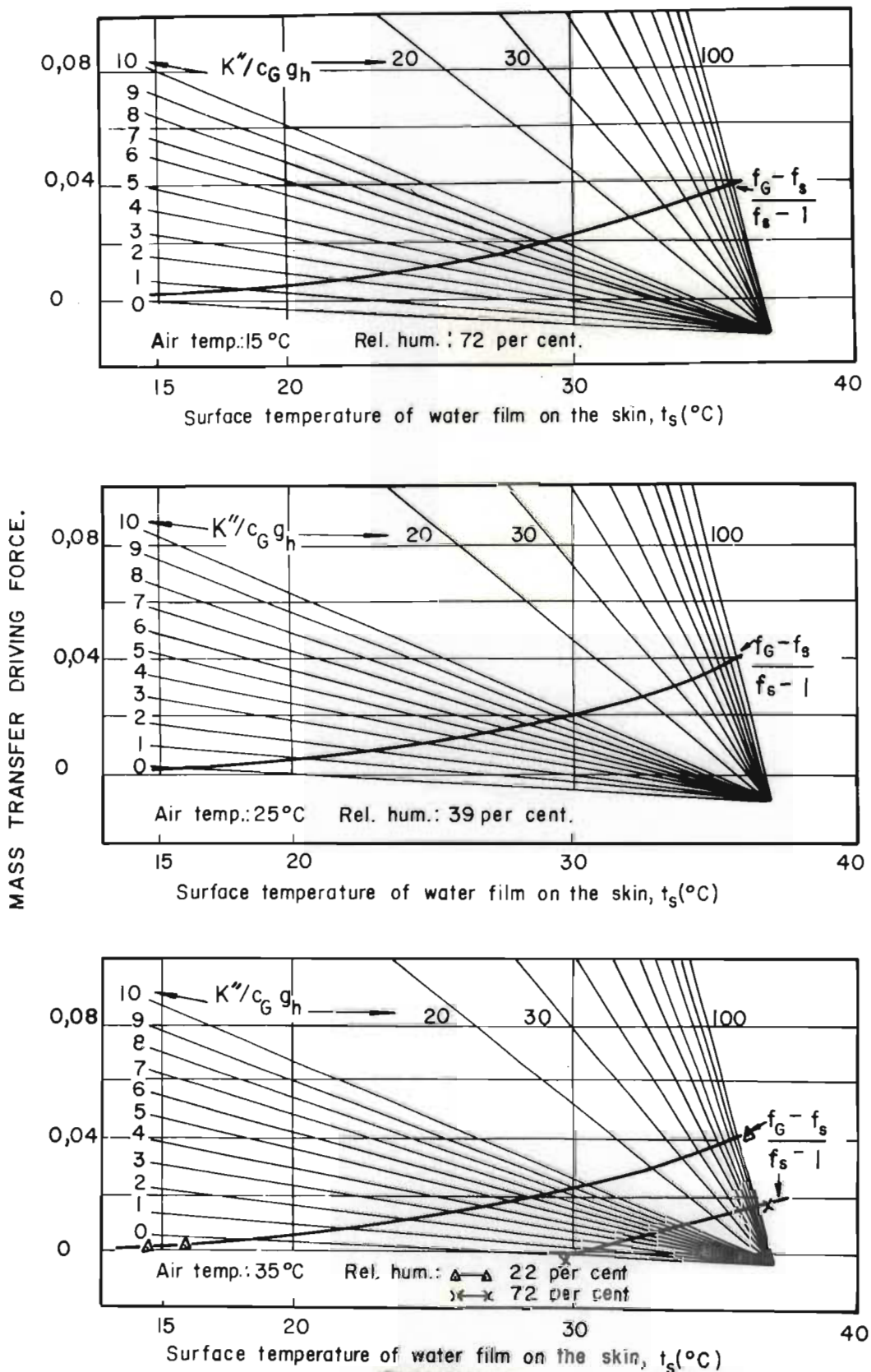


FIGURE 2

The effect of variations in the ratio of physiological conductance, K'' , to the film coefficient of heat transfer, $h_c = c_G g_h$, on the surface temperature, t_s ; neglecting thermal radiation

of the interface or skin temperature approaches the core temperature of the body and the mass-transfer driving force is increased. Decreasing values of $K''/g_h c_G$, on the other hand, tend to lower the interface temperature and mass transfer driving force over the range of air temperature conditions that were considered.

Thus, for example, if the ratio $K''/g_h c_G$ were to be reduced from 4,09 to 1,03 due to an increase in the air velocity from 0,5 m/s to 5,0 m/s and a corresponding increase in the convective film coefficient of heat transfer, say, the skin temperature would be reduced from 27,7°C to 21,6°C and from 32,9°C to 31,3°C under air temperature and relative humidity conditions of 35°C and 22 per cent and 35°C and 72 per cent, respectively. An increase in relative humidity condition albeit at constant dry-bulb temperature thus tends to reduce the influence of air velocity on skin temperature.

From the bottom set of graphs in Figure 2, (this applies to an air temperature of 35°C), it is also seen that the driving force is reduced considerably when the relative humidity is increased from 22 per cent to 72 per cent.

Figure 3 presents graphs of the surface temperature, t_s , and the ratio $\dot{m}''c_G/K''$ versus the ratio $g_h c_G/K''$.

Body surface temperatures, t_s , and the corresponding mass transfer rates across unit area of the human body surface, \dot{m}'' , were determined from Figure 3 for the values of 0,2443 and 0,972 for the ratio $g_h c_G/K''$; the latter values apply when the physiological conductance, K'' , is $20 \times 10^{-3} \text{ kW/m}^2 \text{ }^\circ\text{C}$ and the convective film coefficients, $h_c = g_h c_G$, are $4,886 \times 10^{-3} \text{ kW/m}^2 \text{ }^\circ\text{C}$ and $19,45 \times 10^{-3} \text{ kW/m}^2 \text{ }^\circ\text{C}$ for air velocities across the body of 0,5 m/s and 5,0 m/s, respectively (see Section 3.3 on page 72).

The results are presented in Table 3.

It is of interest to note from a comparison of the wet-bulb temperature values in Table 1 on page 68 and the intersections of the $K''/c_G g_h$ family of straight lines and the $(f_G - f_s)/(f_s - 1)$ curves in Figure 2 that, when radiation is neglected, the surface temperature of the body, t_s , approaches the wet-bulb temperature of the air as the ratio $K''/c_G g_h$ approaches zero. This occurs when the physiological conductance approaches zero and/or the convective film coefficient of heat transfer $h_c = c_G g_h$ becomes infinitely large. Under these conditions the body

TABLE 3 : CALCULATED VALUES FOR THE MASS TRANSFER RATE AND SURFACE TEMPERATURE OF A NUDE RESTING MAN, NEGLECTING RADIATIVE EFFECTS AND ASSUMING THE PHYSIOLOGICAL CONDUCTANCE, K'' , TO REMAIN CONSTANT AT $20 \times 10^{-3} \text{ kW/m}^2 \text{ } ^\circ\text{C}$

ENVIRONMENTAL CONDITIONS			SKIN TEMPERATURE, t_s ($^\circ\text{C}$)	$g_h c_G / K''$	$\dot{m}'' c_G / K''$	c_G / K''	MASS TRANSFER RATE PER UNIT AREA OF BODY SURFACE. \dot{m}'' ($10^{-3} \text{ kg/m}^2 \text{ s}$)
AIR TEMPERATURE ($^\circ\text{C}$)	RELATIVE HUMIDITY (%)	WIND SPEED (m/s)					
15	72	0,5	24,6	0,2443	0,00400	50,5	0,0792
15	72	5,0	17,8	0,97275	0,00695	50,5	0,0138
25	39	0,5	26,4	0,2443	0,00442	50,5	0,0876
25	39	5,0	20,0	0,97275	0,00875	50,5	0,1733
35	22	0,5	27,7	0,2443	0,00487	50,5	0,0970
35	22	5,0	21,6	0,97275	0,01090	50,5	0,2158
35	72	0,5	32,9	0,2443	0,00228	50,5	0,0400
35	72	5,0	31,3	0,97275	0,00433	50,5	0,0850

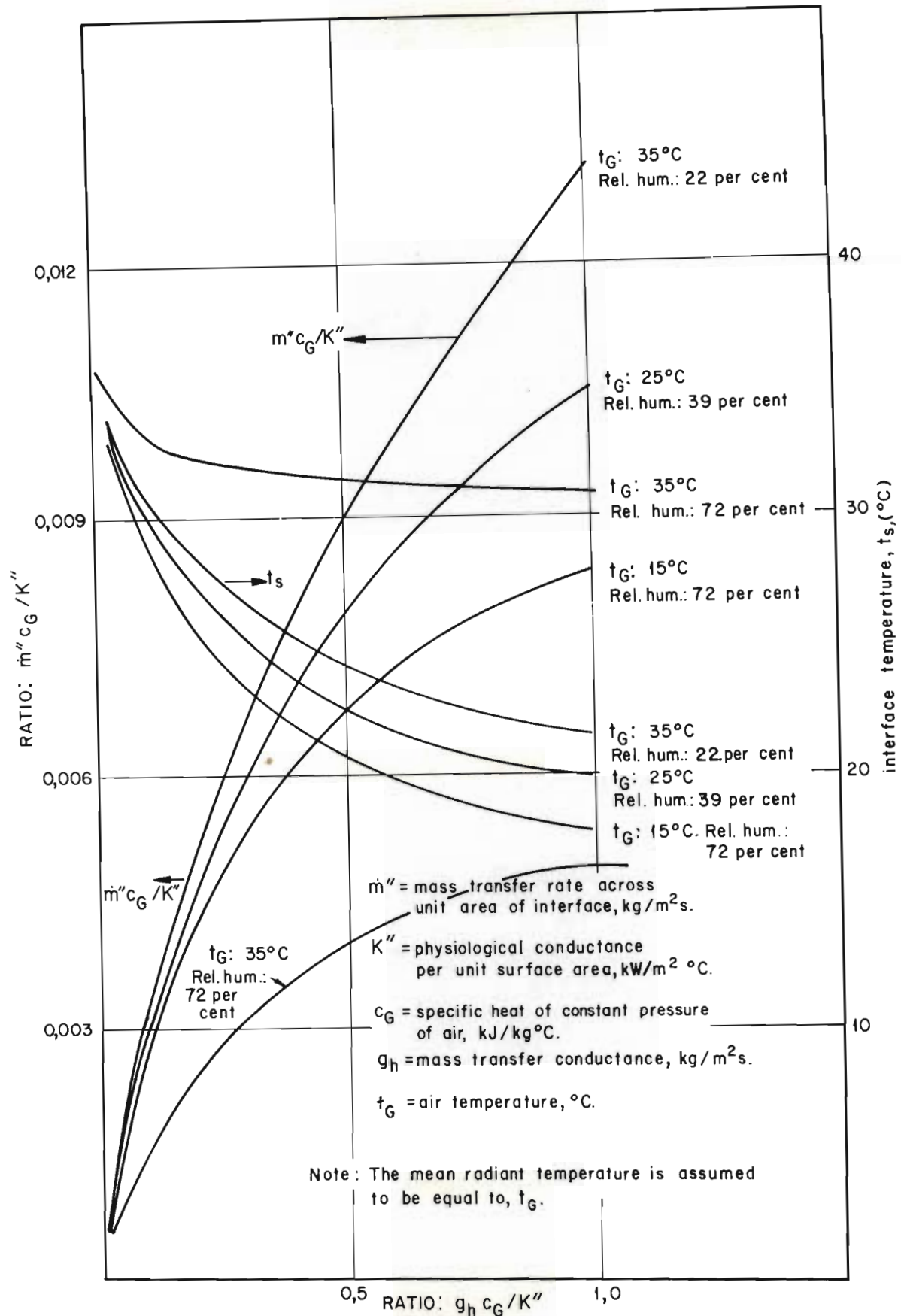


FIGURE 3

Influence of the ratio of the film coefficient of heat transfer, $h_c = c_G g_h$, to the physiological conductance, K'' , on the term, $m''c_G/K''$, and the surface temperature, t_s , neglecting thermal radiation.

behaves as a wet-bulb thermometer.

In general, increasing air temperatures and/or air velocity conditions tend to increase the mass transfer rate. The effect of air velocity on the mass transfer rate is reduced as the relative humidity at a particular dry-bulb temperature is increased. This is evident from a consideration of the mass transfer rate values in Table 3 on page 77. Thus, for example, at an air temperature of 35°C and relative humidity conditions of 22 per cent and 72 per cent, an increase in air velocity from 0,5 m/s to 5,0 m/s can be expected to increase the mass transfer rate by $0,2158 - 0,0970 = 0,1188 \times 10^{-3} \text{ kg/m}^2 \text{ s}$ and $0,08 - 0,04 = 0,04 \times 10^{-3} \text{ kg/m}^2 \text{ s}$, respectively; the mass transfer rate value at 72 per cent relative humidity being considerably lower than the mass transfer rate value at a relative humidity of 22 per cent.

3.3.2 Mass transfer rate taking thermal radiation into account

The calculation procedure to determine the mass transfer rate taking thermal radiation into account, was similar to the method described in the preceding section; albeit taking the radiation term, $\dot{q}_{\text{rad}}''/g_h c_G$ in equation (5) on page 66 into consideration.

Using the method of calculation described in Appendix B, the following expression for the net radiative flux, \dot{q}''_{rad} , was obtained (see Appendix B on page 412)

$$\dot{q}_{\text{rad}} = 6,28 \times 10^{-3} A_{\text{rad},B} / A_{B,T} (t_A - t_B) \dots (9)$$

where \dot{q}''_{rad} = net radiative flux per unit area of body surface, kW/m²

and $A_{B,\text{rad}}, A_{B,T}$ = radiant surface area and total surface area of the enclosed body, respectively, m²

t_A, t_B = surface temperatures of the enclosing and enclosed bodies, respectively, °C.

Using the photodermoplanimeter developed by the National Physical Research Laboratory of the Council for Scientific and Industrial Research of South Africa³⁷⁾, van Graan³⁸⁾ found that the total body surface area, $A_{B,T}$, could be obtained by adding 4,1 per cent to the radiant area, $A_{\text{rad},B}$, measured in the spreadeagle posture. The area thus obtained is somewhat higher than the du Bois surface area predicted from the height and weight of the subject³⁹⁾.

Assuming for the purpose of the present analysis that the subject is in the spreadeagle position and that the total body surface area, $A_{B,T}$, is 4,1 per cent higher

than the radiant area, $A_{\text{rad}, B}$, the ratio $A_{\text{rad}, B} / A_{B, T}$ becomes $1/(1+0,04) = 0,961$ and equation (9) can be re-written as:

$$\dot{q}''_{\text{rad}} = (6,28)(0,961)(t_A - t_B) \times 10^{-3} \quad \text{..... (10)}$$

Assuming further that the surrounding wall temperature is equal to the air temperature, t_G , and re-writing the body surface temperature t_B as t_s , equation (10) becomes:

$$\dot{q}''_{\text{rad}} = 6,035(t_G - t_s) \times 10^{-3} \quad \text{..... (11)}$$

where \dot{q}''_{rad} = radiative heat flux per unit area of body surface, kW/m^2

and t_G, t_s = air temperature and temperature of the body surface, respectively, $^{\circ}\text{C}$.

The above-mentioned expression for \dot{q}''_{rad} was substituted in equation (5) on page 66, and the mass transfer rate was determined in general accordance with the calculation procedure outlined in Appendix A on page 385).

Graphs of the mass-driving force, $(f_G - f_s) / (f_s - 1)$ versus the body surface temperature, t_s , and the family of straight lines representing the middle term of equation (5) were plotted, assuming nominal values for the ratio $K'' / g_h c_G$ ranging from 0 to 100 and the environmental

conditions set out in Table 1 on page 68.

Figures 4 and 5 present two sets of graphs for air velocities of 0,5 m/s and 5,0 m/s, respectively.

Graphs of the ratio $\dot{m}''c_g/K''$ and the surface temperature, t_s , versus the ratio $c_{g,h}/K''$ were then compiled to enable the mass transfer rate, \dot{m}'' , to be determined. The results are presented in Figures 6 and 7 for air velocities of 0,5 m/s and 5,0 m/s, respectively.

The analysis was carried out with the aid of a digital computer. The computer flow diagram is shown in Figure 8.

Values for the surface temperature, t_s , and the mass transfer rate, \dot{m}'' , were determined from the data contained in Figures 6 and 7 for various values of the physiological conductance, K'' , ranging from $5 \times 10^{-3} \text{ kW/m}^2 \text{ }^\circ\text{C}$ to $40 \times 10^{-3} \text{ kW/m}^2 \text{ }^\circ\text{C}$ and from $20 \times 10^{-3} \text{ kW/m}^2 \text{ }^\circ\text{C}$ to $160 \text{ kW/m}^2 \text{ }^\circ\text{C}$ for the air velocity conditions of 0,5 m/s and 5,0 m/s, respectively.

Note: The mean radiant temperature is assumed to be equal to the air temperature.

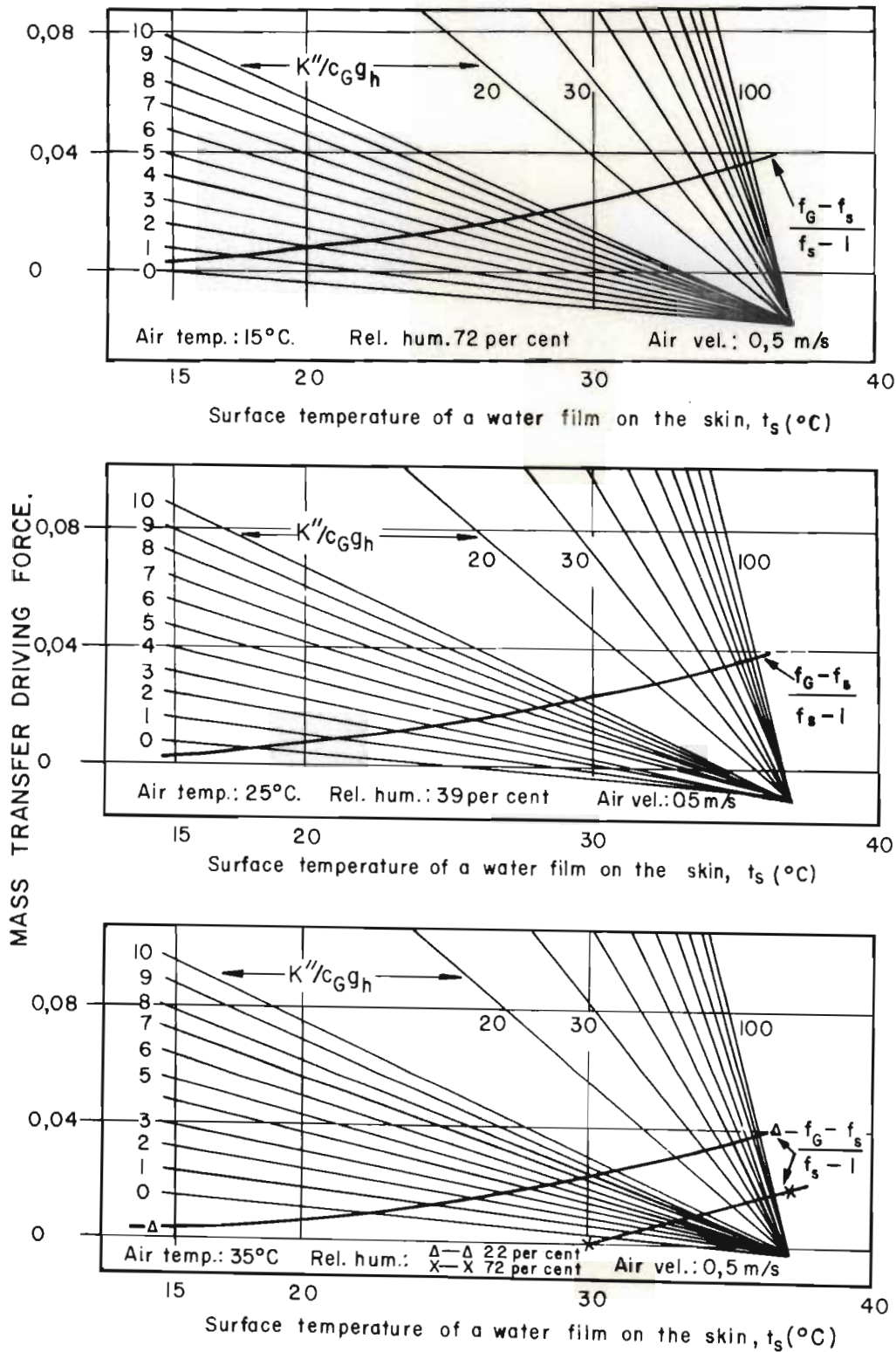


FIGURE 4

The effect of variations in the ratio of physiological conductance, K'' , to the film coefficient of heat transfer, $h_c = c_G g_h$, on the surface temperature, t_s , for an air velocity of 0,5 m/s; taking thermal radiation into account

Note: The mean radiant temperature is assumed to be equal to the air temperature.

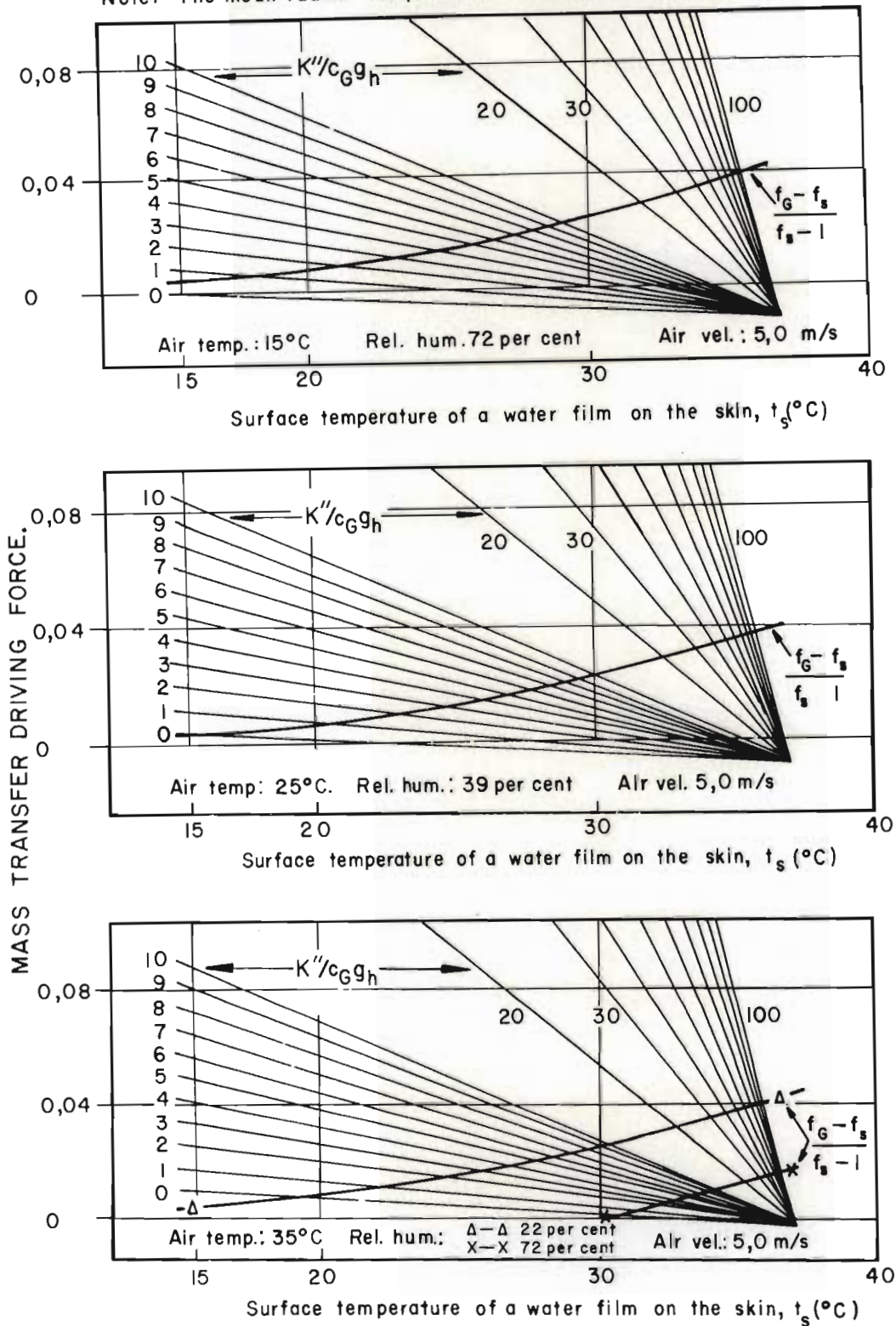


FIGURE 5

The effect of variations in the ratio of physiological conductance, K'' , to the film coefficient of heat transfer, $h_c = c_G g_h$, on the surface temperature, t_s , for an air velocity of 5.0 m/s; taking thermal radiation into account

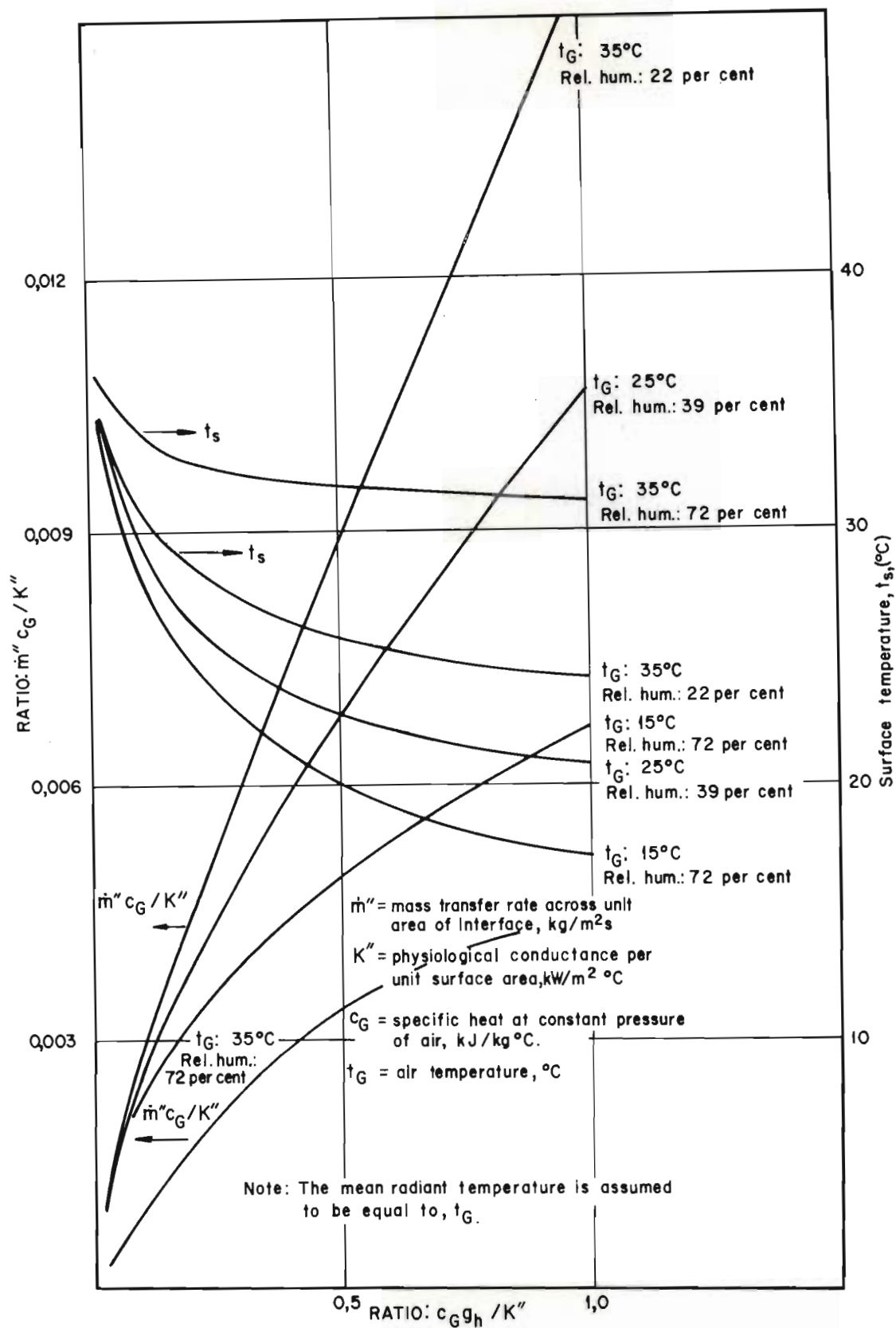


FIGURE 6

Influence of the ratio of the film coefficient of heat transfer, $h_c = c_6 g_h$, to the physiological conductance, K^ , on the term, $m^* c_6 / K^*$, and the surface temperature, t_s , for an air velocity of 0,5 m/s; taking thermal radiation into account.*

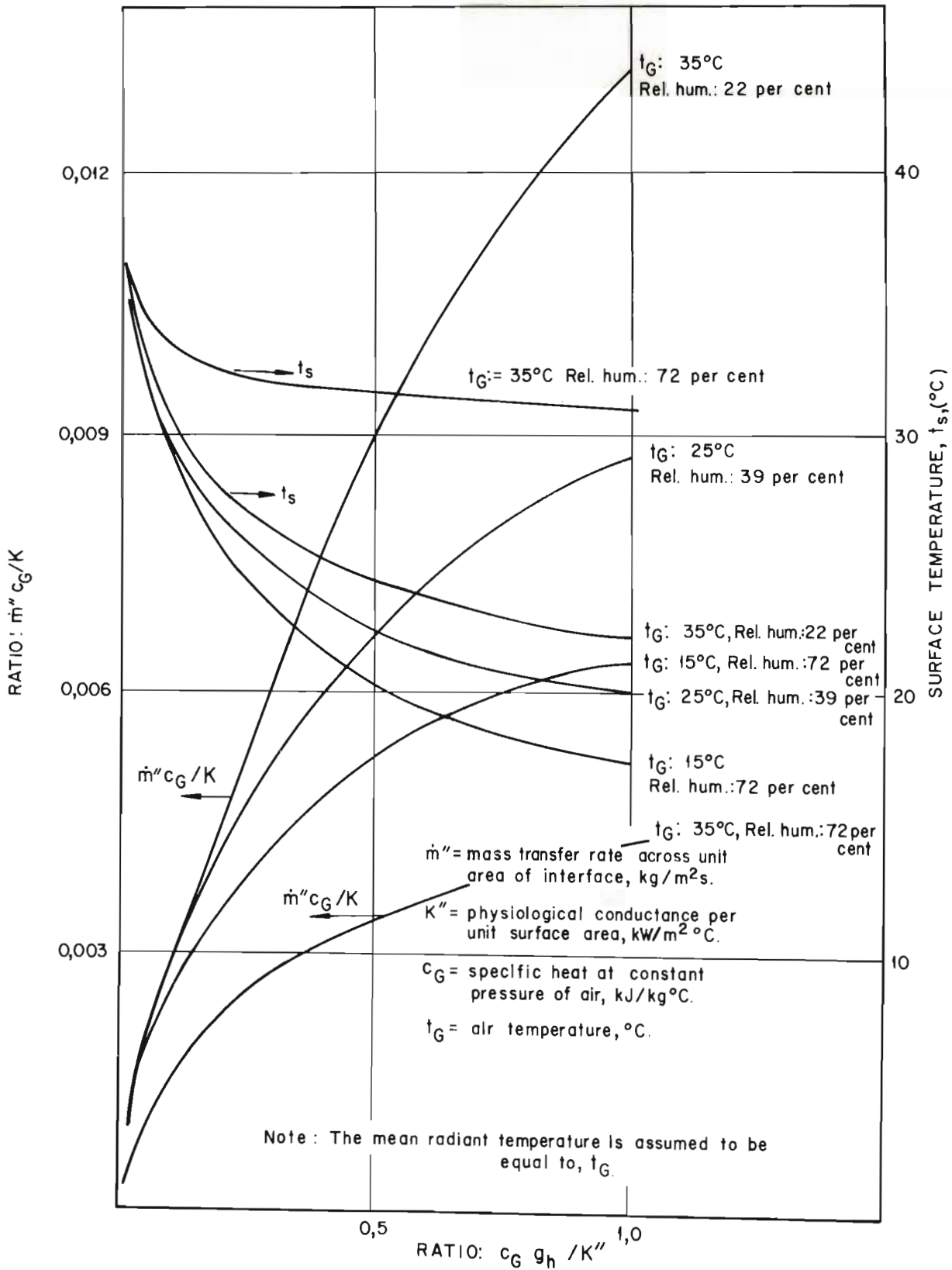


FIGURE 7

Influence of the ratio of the film coefficient of heat transfer, $h_c = c_G g_h$, to the physiological conductance, K'' , on the term, $\dot{m}'' c_G / K''$, and the surface temperature, t_s , for an air velocity of 5.0 m/s; taking thermal radiation into account.

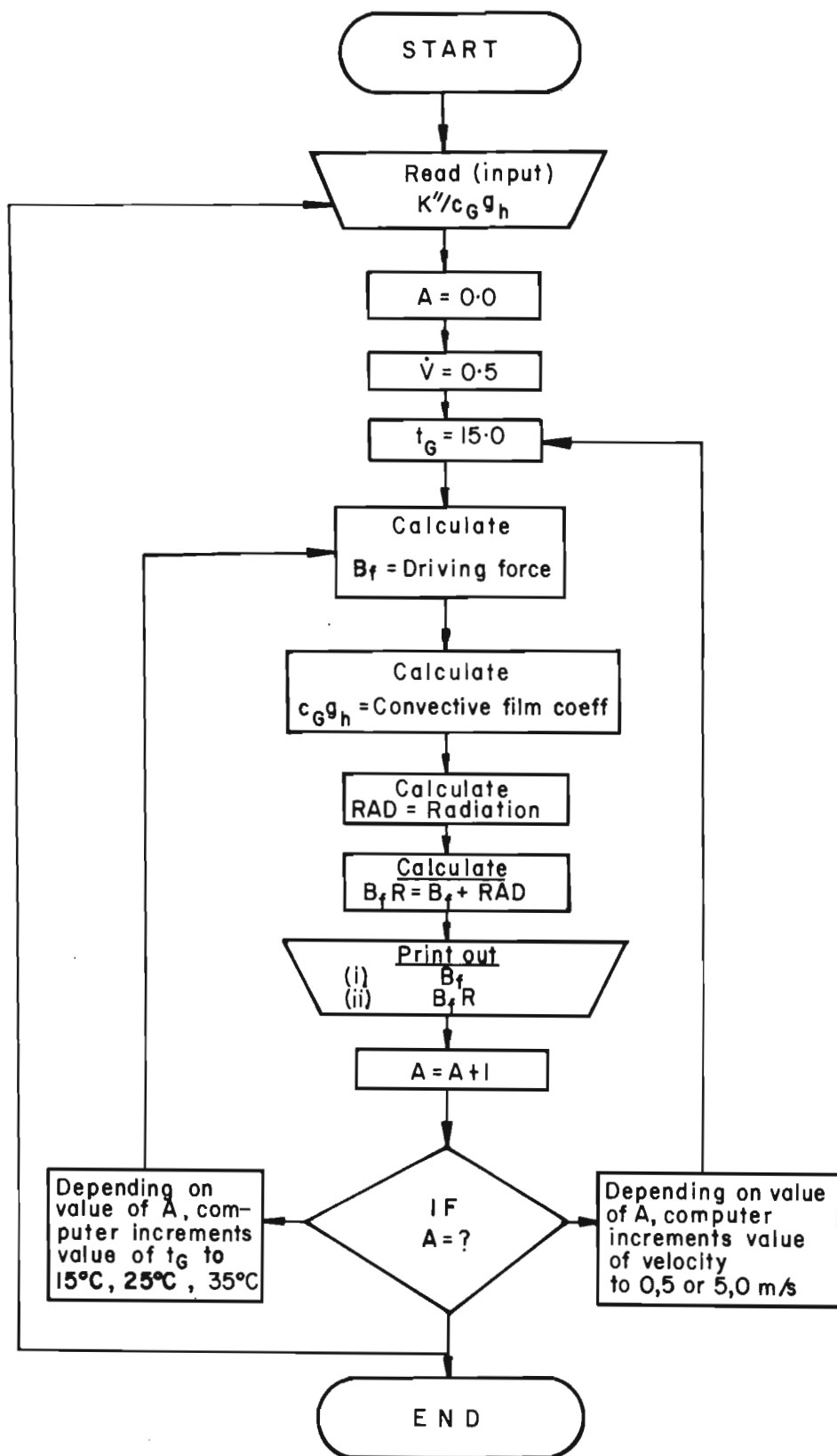


FIGURE 8
Moisture evaporation rate: theoretical considerations:
flow diagram of the computer programme for the calculation
of the mass driving force, B_f , versus the surface
temperature, t_s

Values for the surface temperature, t_s , and the mass transfer rate, \dot{m}'' for various physiological conductance values, K'' , when radiation is taken into account, are presented in Table 4. Values for the surface temperature and mass transfer rate for a physiological conductance, K'' , of $20 \times 10^{-3} \text{ kW/m}^2 \text{ }^\circ\text{C}$, albeit neglecting radiation, are included in the table for the sake of comparison.

3.3.3 Maximum mass transfer rate value

Figure 9 presents graphs of the surface temperature, t_s , and the mass transfer rate, \dot{m}'' , versus the physiological conductance, K'' .

At an air temperature of 35°C , a relative humidity of 72 per cent, an air velocity of $0,5 \text{ m/s}$ and a physiological conductance of $60 \times 10^{-3} \text{ kW/m}^2 \text{ }^\circ\text{C}$, the moisture evaporation rate and the skin temperature were found to be $0,074 \times 10^{-3} \text{ kg/m}^2 \text{ s}$ and $32,2^\circ\text{C}$, respectively. (See Figure 9 and Table 4). These results compare favourably with the results given by Wyndham²⁷⁾. Wyndham reported a moisture evaporation rate of $0,1 \times 10^{-3} \text{ kg/s}$ (400 ml/hr) at an air temperature of 34°C , with the air saturated with water vapour and a physiological conductance of $57 \times 10^{-3} \text{ kW/m}^2 \text{ }^\circ\text{C}$.

TABLE 4 : CALCULATED VALUES FOR THE MASS TRANSFER RATE AND SURFACE TEMPERATURE OF A NUDE RESTING MAN IN THE SPREAD EAGLE POSITION, ASSUMING THE SURROUNDING WALL TEMPERATURE TO BE EQUAL TO THE AIR TEMPERATURE.

AIR VELOCITY : 0,5 m/s

PHYSIOLOGICAL CONDUCTANCE, K" (kW/m ² °C)	ENVIRONMENTAL CONDITIONS		$\xi_h c_G / K''$	SURFACE TEMP. (°C)	$\dot{m}'' c_G / K''$	c_G / K''	MASS TRANSFER RATE PER UNIT AREA OF BODY SURFACE, \dot{m}'' (10 ⁻³ kg/m ² s)	REMARKS *
	Air Temp. (°C)	Rel. Hum. (%)						
40x10 ⁻³	15	72	0,1222	27,3	0,00276	25,3	0,1090	Neglecting radiation
20x10 ⁻³	15	72	0,2443	23,8	0,00356	50,5	0,0700	
20x10 ⁻³	15	72	0,2443	24,6	0,00400	50,5	0,0792	
10x10 ⁻³	15	72	0,4886	20,2	0,00486	101,0	0,0480	
5x10 ⁻³	15	72	0,9727	17,4	0,00660	202,0	0,0330	
40x10 ⁻³	25	39	0,1222	28,7	0,00300	25,25	0,1190	Neglecting radiation
20x10 ⁻³	25	39	0,2443	25,6	0,00436	50,5	0,0860	
20x10 ⁻³	25	39	0,2443	26,4	0,00442	50,5	0,0876	
10x10 ⁻³	25	39	0,4886	22,9	0,00672	101,0	0,0670	
5x10 ⁻³	25	39	0,9727	20,8	0,01045	202,0	0,0520	

* Unless specified otherwise, radiation was taken into account

TABLE 4 : Continued

AIR VELOCITY : 0,5 m/s

PHYSIOLOGICAL CONDUCTANCE, K" (kW/m ² °C)	ENVIRONMENTAL CONDITIONS		$\xi_h c_G / K''$	SURFACE TEMP. (°C)	$\dot{m}'' c_G / K''$	c_G / K''	MASS TRANSFER RATE PER UNIT AREA OF BODY SURFACE, \dot{m}'' (10 ⁻³ kg/m ² s)	REMARKS *
	Air Temp. (°C)	Rel. Hum. (%)						
40x10 ⁻³	35	22	0,1222	30,3	0,00324	25,3	0,128	Neglecting radiation
20x10 ⁻³	35	22	0,2443	28,0	0,00576	50,5	0,114	
20x10 ⁻³	35	22	0,2443	27,7	0,00487	50,5	0,097	
10x10 ⁻³	35	22	0,4886	25,9	0,00870	101,0	0,086	
5x10 ⁻³	35	22	0,9700	24,2	0,01524	202,0	0,075	
40x10 ⁻³	35	72	0,1222	33,8	0,00167	25,3	0,066	Neglecting radiation
20x10 ⁻³	35	72	0,2443	32,8	0,00200	50,5	0,045	
20x10 ⁻³	35	72	0,2443	32,9	0,00228	50,5	0,040	
10x10 ⁻³	35	72	0,4886	32,2	0,00320	101,0	0,032	
5x10 ⁻³	35	72	0,9700	31,6	0,00438	202,0	0,022	

* Unless specified otherwise, radiation was taken into account

TABLE 4 : Continued

AIR VELOCITY : 5,0 m/s

PHYSIOLOGICAL CONDUCTANCE, K" (kW/m ² °C)	ENVIRONMENTAL CONDITIONS		$g_h c_G / K''$	SURFACE TEMP. (°C)	$\dot{m}'' c_G / K''$	c_G / K''	MASS TRANSFER RATE PER UNIT AREA OF BODY SURFACE, \dot{m}'' (10 ⁻³ kg/m ² s)	REMARKS *
	Air Temp. (°C)	Rel. Hum. (%)						
160x10 ⁻³	15	72	0,1222	28,2	0,00264	6,3	0,420	Neglecting radiation
80x10 ⁻³	15	72	0,2443	24,5	0,00454	12,6	0,360	
40x10 ⁻³	15	72	0,4886	19,8	0,00632	25,3	0,252	
20x10 ⁻³	15	72	0,9727	17,4	0,00696	50,5	0,138	
20x10 ⁻³	15	72	0,9727	17,8	0,00696	50,5	0,138	
160x10 ⁻³	25	39	0,1222	28,8	0,00302	6,3	0,480	Neglecting radiation
80x10 ⁻³	25	39	0,2443	25,9	0,00529	12,6	0,420	
40x10 ⁻³	25	39	0,4886	22,6	0,00750	25,3	0,300	
20x10 ⁻³	25	39	0,9727	20,0	0,00936	50,5	0,185	
20x10 ⁻³	25	39	0,9727	20,0	0,00875	50,5	0,173	

* Unless otherwise specified, radiation was taken into account

TABLE 4 : Continued

AIR VELOCITY : 5,0 m/s

PHYSIOLOGICAL CONDUCTANCE, K" (kW/m ² °C)	ENVIRONMENTAL CONDITIONS		$\varepsilon_h c_G / K''$	SURFACE TEMP. (°C)	$\dot{m}'' c_G / K''$	c_G / K''	MASS TRANSFER RATE PER UNIT AREA OF BODY SURFACE, \dot{m}'' (10 ⁻³ kg/m ² s)	REMARKS *
	Air Temp. (°C)	Rel. Hum. (%)						
160x10 ⁻³	35	22	0,1222	29,8	0,00332	6,3	0,527	Neglecting radiation
80x10 ⁻³	35	22	0,2443	27,2	0,00592	12,6	0,470	
40x10 ⁻³	35	22	0,4886	24,2	0,00885	25,3	0,350	
20x10 ⁻³	35	22	0,9727	22,0	0,01302	50,5	0,258	
20x10 ⁻³	35	22	0,9727	21,6	0,01090	50,5	0,215	
160x10 ⁻³	35	72	0,1222	34,8	0,00180	6,3	0,286	Neglecting radiation
80x10 ⁻³	35	72	0,2443	32,6	0,00270	12,4	0,214	
40x10 ⁻³	35	72	0,4886	31,8	0,00348	25,3	0,138	
20x10 ⁻³	35	72	0,9727	31,6	0,00430	50,5	0,086	
20x10 ⁻³	35	72	0,9727	31,3	0,00433	50,5	0,085	

* Unless otherwise specified, radiation was taken into account

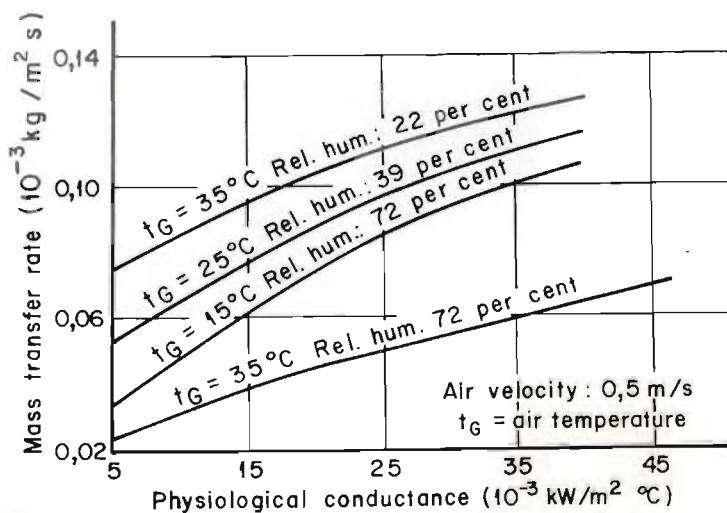
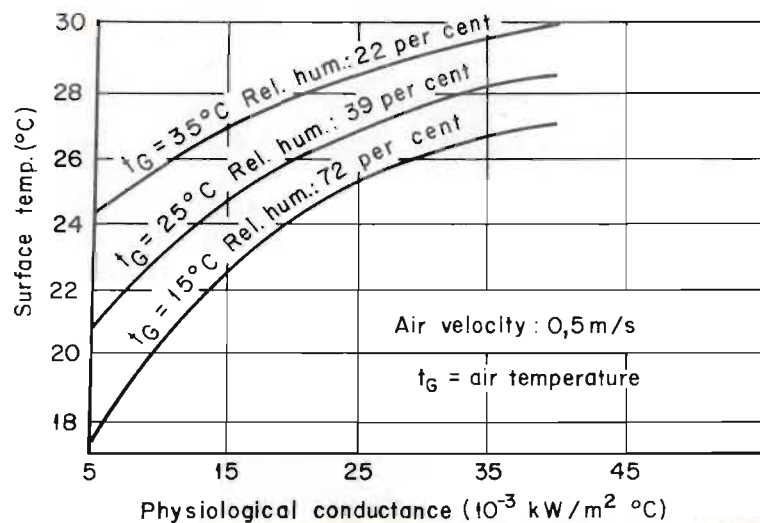
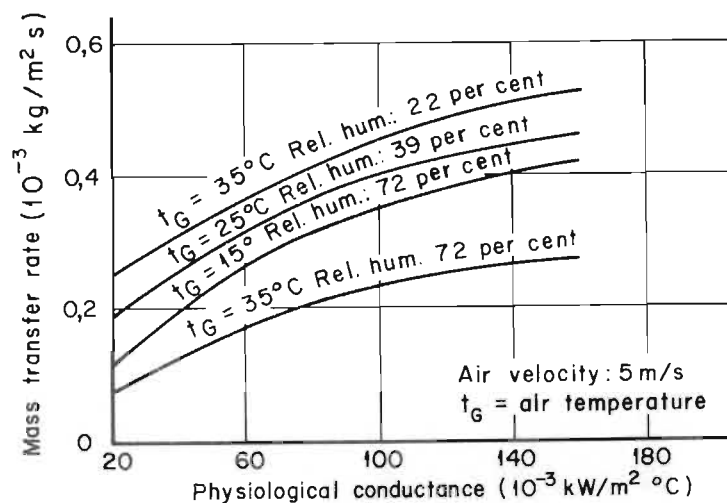
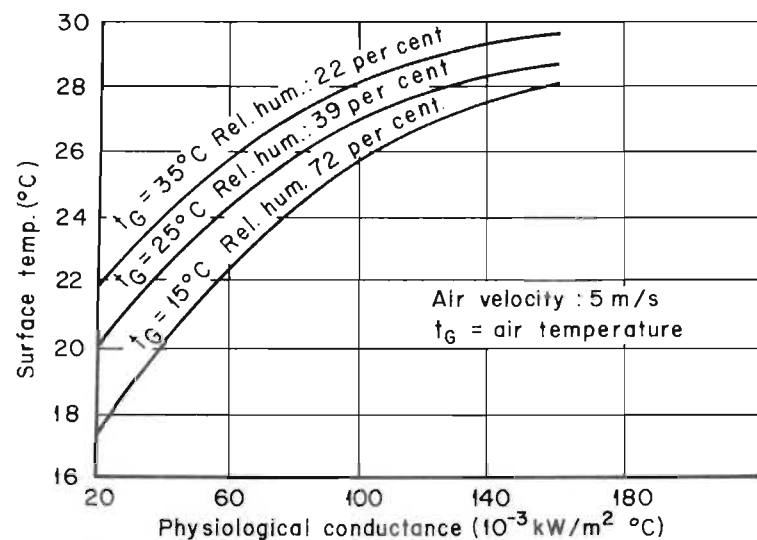


FIGURE 9

Theoretical surface temperature, t_s , and mass transfer rate, \dot{m}'' , versus the physiological conductance, K'' , for different environmental conditions, assuming the surface to be completely wet

Assuming the physiological conductance to be increased to $80 \times 10^{-3} \text{ kW/m}^2 \text{ }^\circ\text{C}$ (this could occur during exercise), the relative humidity to be reduced to 22 per cent and the wind speed to be increased to 5,0 m/s, the mass transfer rate could be expected to increase to $0,470 \times 10^{-3} \text{ kg/m}^2 \text{ s}$ or $1,69 \text{ kg/m}^2 \text{ h}$.

At a physiological conductance value of $20 \times 10^{-3} \text{ kW/m}^2 \text{ }^\circ\text{C}$ under the above-mentioned environmental conditions, the mass transfer rate can be expected to be $0,258 \times 10^{-3} \text{ kg/m}^2 \text{ s}$ or $0,929 \text{ kg/m}^2 \text{ h}$.

The latter value for the mass transfer rate, which corresponds to the highest mass transfer rate for the various environmental conditions listed in Table 1 on page 68 if a physiological conductance of $20 \times 10^{-3} \text{ kW/m}^2 \text{ }^\circ\text{C}$ is assumed, was used to determine the required sensitivity of the proposed evaporative heat loss measuring instrument.

3.4 Radiation heat loss from a human subject : theoretical considerations

A knowledge of the net radiative heat flux of a subject in the test chamber of the climatic chamber is necessary to determine

the required sensitivity of the radiation heat loss measuring instrument.

The net radiant heat exchange rate between a subject in the test chamber of the climatic chamber and the surrounding walls, \dot{q}''_{rad} , was calculated by means of equation (11) on page 81, assuming the surrounding wall temperature to be equal to the air temperature. The calculations were carried out assuming the air temperature, t_G , and the body surface temperatures, t_s , that are given in Table 4 on pages 89 to 92 for the physiological conductance values of 10×10^{-3} , 20×10^{-3} , 40×10^{-3} and $80 \times 10^{-3} \text{ kW/m}^2 \text{ }^\circ\text{C}$.

The results are summarised in Table 5.

3.4.1 Maximum radiative heat flux

From the results in Table 5 it is seen that the highest values for the radiative heat flux, \dot{q}''_{rad} , between a body in the test chamber and the surrounding test chamber walls under the assumed environmental conditions, could be expected to occur when the air temperature and hence the surrounding wall temperature, the relative humidity and the air velocity is 35°C , 22 per cent and 5,0 m/s, respectively.

TABLE 5 : CALCULATED VALUES FOR THE RADIATIVE HEAT FLUX PER UNIT AREA OF BODY SURFACE OF A NUDE MAN IN THE SPREADEAGLE POSITION, ASSUMING THE SURROUNDING WALL TEMPERATURE TO BE EQUAL TO THE AIR TEMPERATURE

PHYSIOLOGICAL CONDUCTANCE, K" (kW/m ² °C)	ENVIRONMENTAL CONDITIONS			SURFACE TEMPERATURE, * t _s (°C)	t _G -t _s	RADIATIVE HEAT FLUX, PER UNIT AREA OF BODY SURFACE, q" rad (10 ⁻³ kW/m ²)
	Air Temp., t _G (°C)	Rel. Hum. (%)	Air Velocity (m/s)			
10 x 10 ⁻³	15	72	0,5	20,2	-5,2	-31,38
10 x 10 ⁻³	25	39	0,5	22,9	2,1	12,67
10 x 10 ⁻³	35	22	0,5	25,9	9,1	54,92
10 x 10 ⁻³	35	72	0,5	32,2	2,8	16,90
20 x 10 ⁻³	15	72	0,5	23,8	-8,8	-53,1
20 x 10 ⁻³	25	39	0,5	25,6	-0,6	- 3,62
20 x 10 ⁻³	35	22	0,5	28,0	7,0	42,25
20 x 10 ⁻³	35	72	0,5	32,8	2,2	12,28
20 x 10 ⁻³	15	72	5,0	17,4	-2,4	-14,48
20 x 10 ⁻³	25	39	5,0	20,0	5,0	30,18
20 x 10 ⁻³	35	22	5,0	22,0	13,0	78,46
20 x 10 ⁻³	35	72	5,0	31,6	3,4	20,52
40 x 10 ⁻³	15	72	0,5	27,3	-12,3	-74,23
40 x 10 ⁻³	25	39	0,5	28,7	- 3,7	-22,33
40 x 10 ⁻³	35	22	0,5	30,8	4,8	28,97
40 x 10 ⁻³	35	72	0,5	33,8	1,2	7,24

* See Table 4 on pages 89 to 92.

TABLE 5 : Continued

PHYSIOLOGICAL CONDUCTANCE, K" (kW/m ² °C)	ENVIRONMENTAL CONDITIONS			SURFACE TEMPERATURE, * t _s (°C)	t _G -t _s	RADIATIVE HEAT FLUX, PER UNIT AREA OF BODY SURFACE. q̇" rad (10 ⁻³ kW/m ²)
	Air Temp., t _G (°C)	Rel. Hum. (%)	Air Velocity (m/s)			
40 x 10 ⁻³	15	72	5,0	19,8	-4,8	-28,97
40 x 10 ⁻³	25	39	5,0	22,6	2,4	14,48
40 x 10 ⁻³	35	22	5,0	24,2	10,8	65,18
40 x 10 ⁻³	35	72	5,0	31,8	3,2	19,31
80 x 10 ⁻³	15	72	5,0	24,5	-9,5	-57,30
80 x 10 ⁻³	25	39	5,0	25,9	0,9	5,43
80 x 10 ⁻³	35	22	5,0	27,2	7,8	47,07
80 x 10 ⁻³	35	72	5,0	32,6	2,4	14,48

* See Table 4 on pages 89 to 92

The following values for \dot{q}''_{rad} were obtained for an air temperature of 35°C, a relative humidity of 22 per cent and an air velocity of 5 m/s:

PHYSIOLOGICAL CONDUCTANCE $\text{kW/m}^2 \text{ } ^\circ\text{C}$	RADIATIVE HEAT FLUX PER UNIT AREA OF BODY SURFACE kW/m^2
20×10^{-3}	$78,46 \times 10^{-3}$
40×10^{-3}	$65,18 \times 10^{-3}$
80×10^{-3}	$47,07 \times 10^{-3}$

The radiative heat flux thus attained the maximum value of $78,46 \text{ kW/m}^2 \times 10^{-3}$ at the relatively low physiological conductance value of $20 \times 10^{-3} \text{ kW/m}^2 \text{ } ^\circ\text{C}$. The latter value for the radiative heat flux per unit area of body surface was used to determine the required sensitivity of the radiometer for measuring the radiation heat exchange rate of a subject in the horizontal test section of the climatic chamber.

3.5 Influence of air velocity, thermal radiation and air temperature on the skin temperature

The relative effects of air velocity, thermal radiation and air temperature on the skin temperature, t_s , under the environmental conditions referred to in Table 1 on page 68 can be assessed from a consideration of Figures 2 to 7 and the information contained in Table 4 on pages 89 to 92.

3.5.1 Influence of air velocity on the surface temperature, t_s

From a comparison of Figure 2 with Figures 4 and 5 it is noted that, whereas the air velocity has no effect on the ordinate and slope of the family of straight lines when radiation is neglected, the air velocity affects both the ordinate and slope of the lines when radiation is present; the effect of air velocity being most pronounced at the lower air temperature values. As the air velocity is increased the ordinate is raised and the slope of the lines are reduced.

The net effect of increased velocities is to reduce the influence of radiation on the surface temperature, t_s .

The effect of air velocity on surface temperatures in the presence of thermal radiation is also evident from the results contained in Table 4. For example, at an air temperature of 15°C , an air velocity of $0,5 \text{ m/s}$ and a physiological conductance value of $20 \times 10^{-3} \text{ kW/m}^2 \text{ }^{\circ}\text{C}$, radiation reduces the surface temperature, t_s , from $24,6^{\circ}\text{C}$ to $23,8^{\circ}\text{C}$, a drop of $0,8^{\circ}\text{C}$. At an air velocity of $5,0 \text{ m/s}$, on the other hand, the corresponding drop of the surface temperature, t_s is only $0,4^{\circ}\text{C}$.

In general, the effect of air velocity is to lower the surface temperature, t_s , due mainly to the evaporative cooling effect of the air on a wet surface. In spite of the lower surface temperatures, however, the moisture evaporation rate from the body increases as the air velocity is increased.

3.5.2 Effect of thermal radiation on the surface temperature, t_s

From a comparison of the surface temperatures, t_s , that are given in Table 4 for a physiological conductance of $20 \times 10^{-3} \text{ kW/m}^2 \text{ } ^\circ\text{C}$ it is evident that thermal radiation tends to reduce the surface temperature, t_s , when the air temperature and hence the radiation temperature is below t_s . The surface temperature, t_s , is increased on the other hand when the radiant temperature is higher than t_s .

3.5.3 Effect of air temperature, t_a , on the surface temperature, t_s

Mitchell et al²⁰⁾ found the mean skin temperature to be linearly dependent on the ambient temperature at air temperatures below 35°C . At air temperatures above this critical temperature the mean skin temperature remained practically constant and was virtually

independent of both ambient temperature and wind speed.

Neuroth⁴⁰⁾, who made a systematic study of environments between 5°C and 50°C, found that skin temperature increased with air temperature. Stolwijk and Hardy⁴¹⁾ also came to that conclusion.

Phelps and Vold²³⁾ claimed that the mean skin temperature increased 0,25°C per degree Centigrade rise in air temperature.

According to the present analysis the skin temperature, t_s , can be expected to change from 23,8°C to 25,6°C for an air temperature rise from 15°C to 25°C, assuming the physiological conductance, K'' , and air velocity to be $20 \times 10^{-3} \text{ kW/m}^2 \text{ } ^\circ\text{C}$ and 0,5 m/s, respectively. (See Table 4 on pages 89 to 92). The change in skin temperature is thus $(25,6 - 23,8)/(25 - 15) = 0,18^\circ\text{C}$ per degree Centigrade change in air temperature. At an air velocity of 5 m/s the corresponding change in skin temperature is $20,4^\circ\text{C} - 17,4^\circ\text{C} = 2,6^\circ\text{C}$ or $0,26^\circ\text{C}$ per degree Centigrade change in air temperature; relatively close to the value claimed by Phelps and Vold²³⁾.

The values obtained by Mitchell et al²⁰⁾ which are in good agreement with the findings of Iampietro⁴²⁾, were somewhat higher; 0,4°C and 0,5°C at air velocities of 0,67 m/s and 4,9 m/s, respectively.

Iampietro⁴²⁾ deduced that, for air temperatures below 31°C, the change in mean skin temperature per degree Centigrade change in air temperature could be obtained from the following equation:

$$dt_s/dt_G = \frac{0,0177\theta + 57,1}{0,60 + 70,7} - \frac{4,10}{\dot{v}_G + 6,79} \dots\dots (12)$$

dt_s, dt_G = incremental changes in skin and air temperature, respectively, °C

and θ = length of exposure, s

\dot{v}_G = air velocity, m/s.

The comparatively large effect which air temperature has on the skin temperature at low skin temperatures, compared to the small effect predicted in the present theoretical analysis, is probably due to the fact that the skin is only partially wet under these conditions. (In the theoretical analysis the skin was assumed to be completely wet).

For this reason too, actual skin temperature at low ambient temperatures are somewhat higher than the theoretical values; Mitchell et al²⁰⁾ found skin temperatures to be of the order of 28°C and 23,5°C at an air temperature of 15°C and air velocities of 0,67 m/s and 4,94 m/s respectively. According to Table 4, the predicted skin temperatures at an air temperature of 15°C and air velocities of 0,5 m/s and 5 m/s, respectively, are 23,8°C and 17,4°C.

CHAPTER 4

MEASUREMENT OF THE EVAPORATIVE HEAT LOSS RATE FROM A HUMAN BODY

The problem involves the direct measurement of the evaporative heat loss from a subject in the horizontal test chamber of the climatic chamber.

In the past the moisture evaporation rate and hence the evaporative heat loss rate from human subjects in relatively large climatic chambers capable of accommodating subjects in normal working positions have generally been assessed from measurements of the mass variations of the subject with time, caused by, inter alia, the loss of moisture through the skin of the subject^{9,43,44}).

Such a system of measurement is, however, subject to a number of disadvantages: high accuracies are generally difficult to attain in view of the relatively small magnitude of the mass variation compared to the total body mass and the various corrections that have to be made for the changes in body mass caused by factors other than the evaporation of moisture from the skin of the subject. For example, corrections have to be made for the mass of oxygen absorbed and carbon dioxide and water vapour eliminated through the lungs of the subject and, under high heat stress conditions, for the sweat which drips from the body without evaporating on the body surface and hence contributing to the evaporative cooling effect.

Another disadvantage of the weighing technique is that continuous mass measurements, particularly during exercise are generally not feasible. As a result, the moisture evaporation rate is generally obtained as an average value over a predetermined period of time by means of this technique.

The more direct methods of assessing the amount of moisture actually evaporated from the skin surface involved the use of "calorimeters". In this case, the human subject was placed in a calorimeter of relatively small size and the rate of moisture evaporated was measured by either absorbing the liberated vapour in a desiccant and weighing⁴⁵⁾ or by measuring the change in vapour pressure or moisture content of the air flowing over the subject^{46,47,48)}.

However, due to the limited space available in the "calorimeter" the normal working movement of the subject is restricted. The latter system of measurement is thus generally unsuitable for assessing the moisture evaporation rate from a subject performing work in a natural posture.

Considerable improvement over existing methods of measurement would be possible if a technique for the direct measurement of the moisture evaporation rate from a subject in a normal working mode could be developed.

4.1 Possible methods of measuring the evaporative heat loss rate from a subject in the horizontal test section of the climatic chamber

Since the air flow through the horizontal test chamber of the climatic chamber is in a horizontal direction, the evaporative heat loss from the subject all appears in the wake. By integrating the insensible heat gain of the air in a plane of the wake perpendicular to the air stream, therefore, the evaporative heat loss can be determined.

However, uneven velocity and humidity distributions exist in a plane of the wake perpendicular to the air stream due to the nature of air flow in the wake. Thus, in order to determine the insensible heat gain of the air, it is required that the plane of the wake be divided into a grid of elements of equal area ΔA . The mean specific humidity increase and the mean axial velocity should then be measured for each elemental area and the insensible heat gain found by summation.

Thus, for a total number, n , of elemental areas ΔA , the evaporative heat loss rate from a human subject is given by the following equation:

$$\dot{q}_e = \rho_G \ell \Delta A \sum_{r=1}^n \Delta w_r \dot{v}_{ax,r} \quad \dots\dots\dots (13)$$

where \dot{q}_e = evaporative heat loss rate from a subject, kW

and ρ_G = density of the air, kg/m³

ℓ = latent heat of evaporation of sweat, kJ/kg

Δw_r = specific humidity increase, kg/kg

$\dot{v}_{ax,r}$ = axial component of the velocity, m/s

ΔA = A/n

where A = total area perpendicular to wake, m².

The main practical problem associated with this method is that

Δw_r and $\dot{v}_{ax,r}$ have to be determined for each point r .

The summation $\sum_{r=1}^n \Delta w_r \dot{v}_{ax,r}$ in the above equation may, however be replaced by the summation $\beta \dot{v} \sum_{r=1}^n \Delta w_r$ where β is an empirical correction factor dependent on the geometry of the body and the distance of the measuring plane downstream of the body and \dot{v} is the free stream velocity.

Equation (13) may, therefore, be written as:

$$\dot{q}_e = \rho_G \ell \Delta A \beta \dot{v} \sum_{r=1}^n \Delta w_r \quad \dots\dots\dots (14)$$

$$\text{or } \dot{q}_e = \rho_G \ell A \beta \dot{v} \overline{\Delta w}_w \quad \dots\dots\dots (15)$$

where $\overline{\Delta w}_w$ is the mean specific humidity increase for the whole wake, kg/kg.

The important advantage of this method is that if a grid of humidity sensing elements be placed in the wake and coupled differentially to a similar grid upstream a single reading will give the value of $\Delta \bar{w}_w$.

It is, however, important that the grid should cover the whole wake. If the grid is larger than the wake, $\Delta \bar{w}_w = 0$ and the grid will have no numerical integration. With this method the value of β has to be determined experimentally.

In view of problems associated with the experimental determination of β , the following alternative methods of measurement were considered:

(a) By analogy to the convective heat loss

Use is made of the analogy between heat and mass transfer^{49,50)} to determine the evaporative heat loss from the human body. Because of the analogy it is assumed that the respective profiles of the spatial specific humidity and air temperature distributions in the same plane in the wake of the body are similar.

In equation (15) the evaporative heat loss rate \dot{q}_e is expressed as

$$\dot{q}_e = \rho_G \ell A \beta \dot{V} \Delta \bar{w}_w$$

Similarly, the convective heat loss rate, \dot{q}_c , from a body in the horizontal test section of the climatic chamber can be expressed by the following equation:

$$\dot{q}_c = \rho_G c_G A \beta \dot{v} \overline{\Delta t}_w \quad \text{..... (16)}$$

where \dot{q}_c = convective heat loss rate from a subject, kW

and ρ_G = density of the air, kg/m³

c_G = specific heat at constant pressure of the air,
1,01 kJ/kg °C

A = area perpendicular to wake, m²

\dot{v} = axial component of the velocity, m/s

$\overline{\Delta t}_w$ = mean temperature increase between a plane on the upstream side of the body and a plane which extends across the whole wake; both planes being perpendicular to the air stream, °C

β = empirical correction factor dependent on the geometry of the body and the distance of the measuring plane downstream of the body (assumed to be equal to β in equation (15) if $\overline{\Delta t}$ is measured in the same plane as $\overline{\Delta w}$).

Division of equation (15) by equation (16) leads to:

$$\dot{q}_e / \dot{q}_c = \ell \overline{\Delta w}_w / c_G \overline{\Delta t}_w \quad \text{..... (17)}$$

Based on the assumption that the profiles of the spatial temperature and specific humidity distributions in the wake of the body are similar, the ratio of the mean specific humidity increase to the mean temperature increase, $\overline{\Delta w_w} / \overline{\Delta t_w}$, in equation (17) can be replaced by the ratio of the specific humidity increase, Δw_w , to the air temperature increase, Δt_G , between two fixed points on the upstream and downstream side of the subject to give

$$\dot{q}_e / \dot{q}_c = \ell \Delta w_w / c_G \Delta t_w \quad \dots\dots\dots (18)$$

In the proposed method, both the temperature and specific humidity increase between two fixed points on the upstream and downstream side of the body as well as the convective heat loss rate are measured simultaneously; the convective heat loss rate being determined by means of the convective heat loss measuring instrument that had previously been developed³⁶⁾.

The evaporative heat loss rate of the body may then be calculated by means of equation (18).

- (b) By introducing a known quantity of water vapour into the wake of the body

This method of determining the evaporative heat loss rate from a body is based on the following assumption:

If the mean specific humidity increase due to an evaporating body is measured between two fixed planes; one on the upstream side and the other on the downstream side of the body across the full wake and water vapour is introduced into the wake of the body by means of an auxiliary evaporating body positioned on the downstream side of the main evaporating body, relatively close to it, the ratio of the mean specific humidity increase due to the main body to the mean specific humidity increase due to the auxiliary body, is equal to the ratio of the moisture evaporation rate of the main body to the moisture evaporation rate of the auxiliary body; provided the auxiliary supply of water vapour is introduced into the wake of the main body in such a way that it does not disturb the general flow pattern of air in the wake of the main body.

In this case the β value in equation (15) would be the same for the main body and the auxiliary body.

Thus, the evaporative heat loss from the main body would be

$$\dot{q}_e = \rho_G \lambda \beta \dot{V}_{aw} \quad (\text{see equation (15) on page 107})$$

and the evaporative heat loss from the auxiliary body would be

$$\dot{q}_{e,aux} = \rho_G \ell A \beta \dot{v} \overline{\Delta w}_{w,aux} \quad \dots\dots\dots (19)$$

where $\dot{q}_e, \dot{q}_{e,aux}$ = evaporative heat loss rates from the main and auxiliary bodies, respectively, kW

and ρ_G = density of the air, kg/m³

ℓ = latent heat of evaporation of water, kJ/kg

A = area perpendicular to wake, m²

β = empirical correction factor dependent on the geometry of the main body and the distance of the measuring plane downstream of the body

\dot{v} = free stream velocity, m/s

$\overline{\Delta w}_w, \overline{\Delta w}_{w,aux}$ = mean specific humidity increases in the wake due to the main and auxiliary evaporating bodies, respectively, °C.

Division of equation (15) by equation (19), leads to

$$\dot{q}_e / \dot{q}_{e,aux} = \overline{\Delta w}_w / \overline{\Delta w}_{w,aux} \quad \dots\dots\dots (20)$$

Measurements of the rate of water vapour addition by the auxiliary body and hence its evaporative heat loss rate, $\dot{q}_{e,aux}$, and the mean specific humidity increases in the wake due to the main body and auxiliary body, are thus necessary to determine the evaporative heat loss

rate from the main body by means of this method.

In both the above-mentioned methods of determining the evaporative heat loss rate, accurate measurements of the specific humidity increase of the air flowing over the body is necessary.

Initial investigations were, therefore, aimed at the development of a suitable humidity-measuring instrument.

4.2 Required sensitivity of the humidity-sensing device

It is required to measure the evaporative heat loss rate from a human body, under high evaporative conditions, with an accuracy of 15%.

In accordance with the theoretical analysis described in Section 3.3.3 on page 94, the rate of water loss per unit area from the skin of a nude resting man by the evaporation of sweat can be expected to be of the order of $0,258 \times 10^{-3} \text{ kg/m}^2 \text{ s}$ when the physiological conductance of the body is $20 \times 10^{-3} \text{ kW/m}^2 \text{ }^\circ\text{C}$ and the environmental conditions with regard to dry-bulb temperature, relative humidity and wind speed are 35°C , 22 per cent and 5,0 m/s respectively.

Assuming the total surface area of the body to be $1,85 \text{ m}^2$ (38), the moisture evaporation rate from the body would thus be $0,258 \times 10^{-3} \times 1,85 = 0,47 \times 10^{-3} \text{ kg/s}$ or $1,69 \text{ kg/h}$.

During exercise the physiological conductance would increase and a higher evaporation rate could be expected. For example, for a physiological conductance value of $80 \times 10^{-3} \text{ kW/m}^2 \text{ } ^\circ\text{C}$, the mass transfer rate could attain the relatively high value of $0,47 \times 10^{-3} \text{ kg/m}^2 \text{ s}$ or $0,87 \times 10^{-3} \text{ kg/s}$. (See Section 3.3.3 on page 94).

However, for the purpose of the present analysis, it is proposed that the $0,47 \times 10^{-3} \text{ kg/s}$ evaporation rate value which applies to a nude resting man, should be used to assess the required sensitivity of the humidity-measuring device for measuring the humidity increase in the wake of the human body.

The resultant mean specific humidity increase of the air flowing through the horizontal test chamber of the climatic chamber can be calculated by means of the following equation:

$$\dot{m} = \rho A \bar{v} \Delta w \quad \dots\dots\dots (21)$$

where \dot{m} = total moisture evaporation rate from the subject, kg/s

and ρ = density of the air, $1,056 \text{ kg/m}^3$

- A = area of test chamber in a plane at right angles
 to the direction of air flow, $3 \text{ m} \times 3 \text{ m} = 9 \text{ m}^2$
 \dot{v} = free stream air velocity, 5 m/s
 $\overline{\Delta w}$ = mean specific humidity increase, kg/kg of dry air.

Substitution of the calculated values of $0,47 \times 10^{-3} \text{ kg/s}$
 for \dot{m} in equation (21) leads to a value of $0,00000989 \text{ kg/kg}$
 of dry air for the mean specific humidity increase $\overline{\Delta w}$. This
 corresponds to a dew-point temperature change of $0,015^\circ\text{C}$.

The mean specific humidity increase and hence change in
 dew-point temperature is thus extremely small.

The increase in specific humidity will be somewhat higher if
 measured in the wake of the body; the exact value being
 dependent on the area of the wake in the plane of measurement
 and the corresponding average value of the axial velocity
 component.

Preliminary investigations were carried out in the 3 m diameter
 low speed wind tunnel of the National Mechanical Engineering
 Research Institute's Aeronautics Research Unit to establish
 the extent of the wake and the spatial distribution of the axial
 velocity components within the wake. The results of the air

velocity measurements, which were carried out by means of an electrical vane anemometer, are shown in Figure 10 for a free stream air velocity of 5 m/s.

In Figure 11 the average value for the axial components of the velocity in the wake is plotted as a function of the distance from the body on the downstream side. From the latter figure it is seen that the average air velocity at a distance of 1,3 m from the body is 2 m/s. The area of the wake in a plane at right angles to the general direction of air flow at this point was found to be of the order of $1,5 \text{ m}^2$; approximately 2,5 times the projected area of the body.

The corresponding mean specific humidity increase of the air was calculated from the following equation:

$$\dot{m} = \rho A_w \bar{v}_{ax} \bar{\Delta w}_w \quad \text{..... (22)}$$

where \dot{m} = total moisture evaporation rate from the subject,
kg/s

and ρ = density of the air, $1,056 \text{ kg/m}^3$

\bar{v}_{ax} = average value for the axial components of velocity
in the wake in a plane at right angles to the
direction of the free stream air velocity, 2 m/s

$\bar{\Delta w}_w$ = average specific humidity increase in the wake of the
body, kg/kg of dry air

A_w = wake area, $1,5 \text{ m}^2$

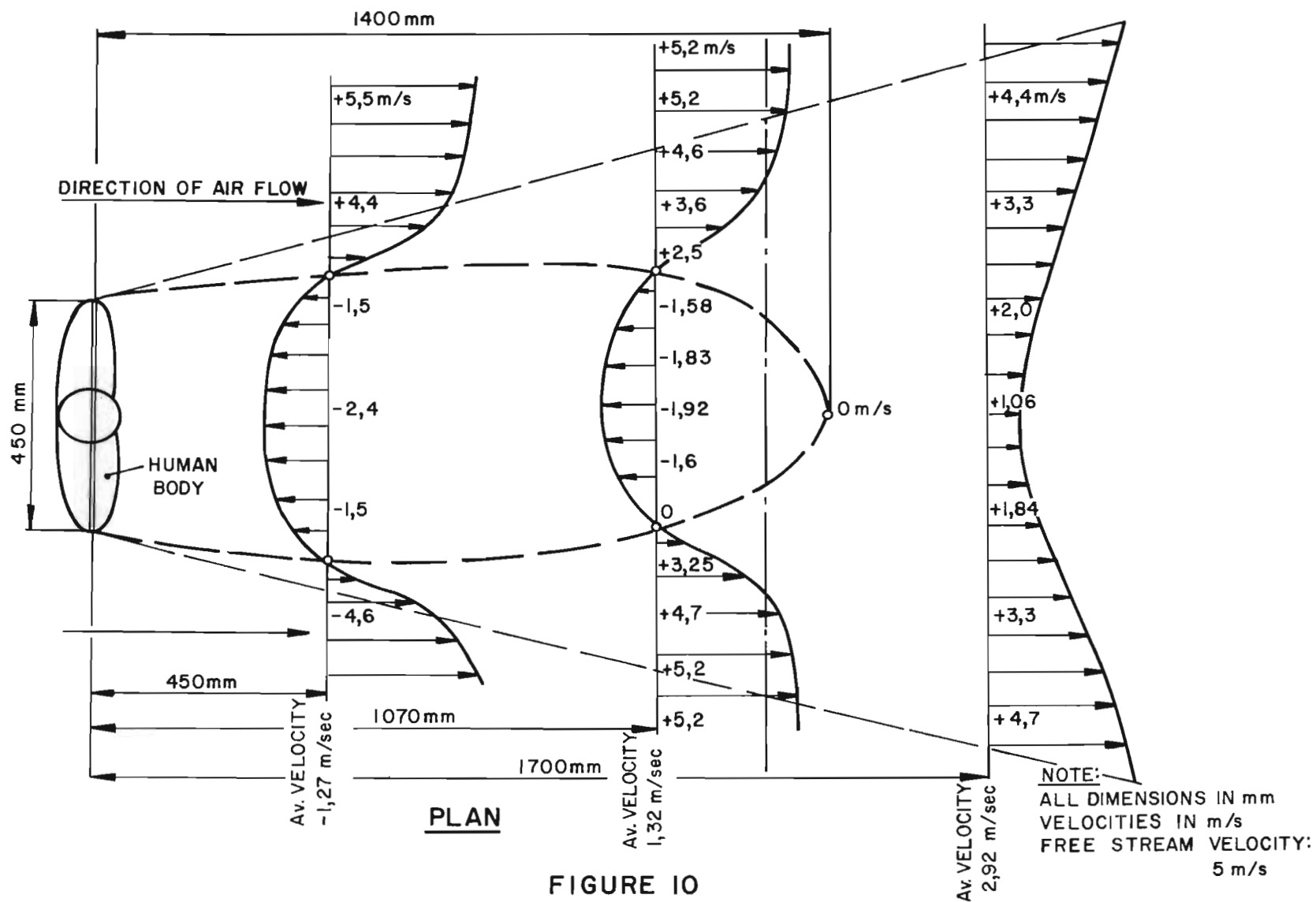


FIGURE 10
*Spatial distribution of the axial components
 of air velocity in the wake of a human body*

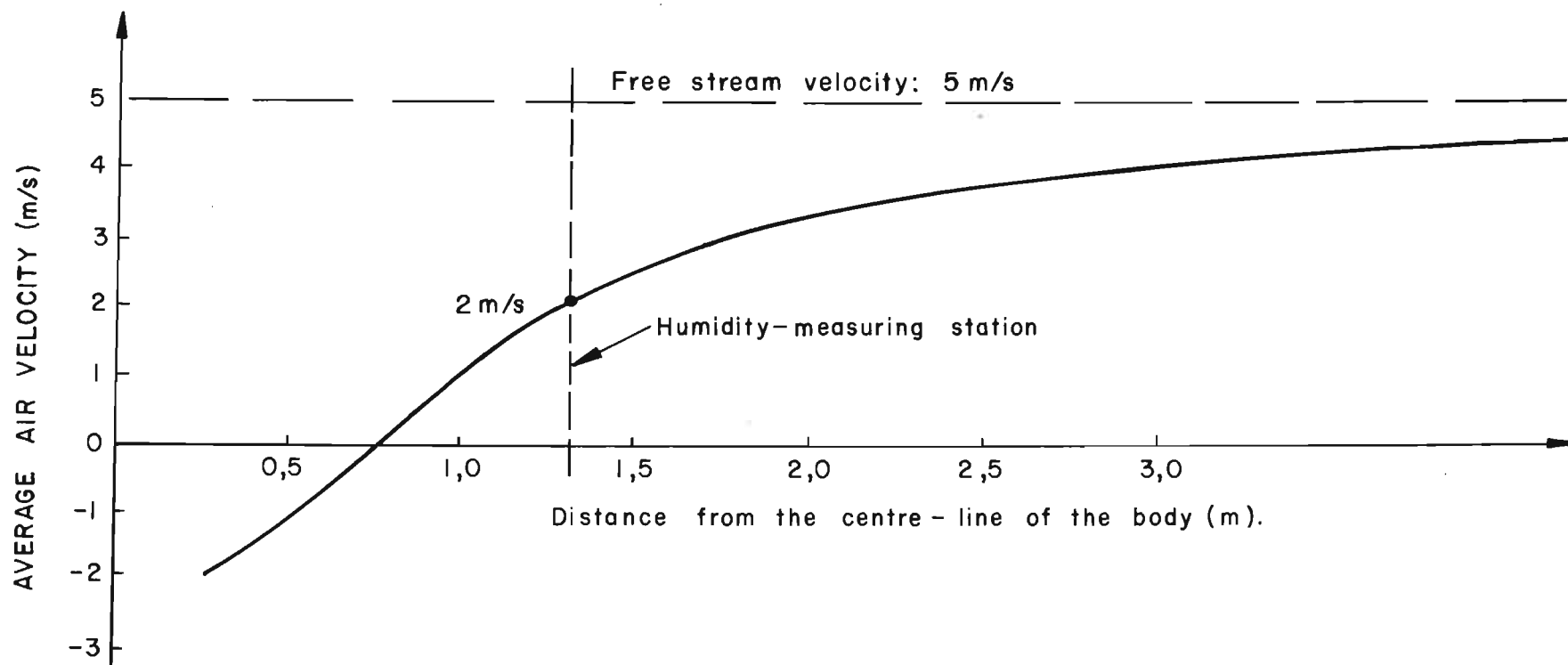


FIGURE II
Average value for the axial components of velocity in the wake of a human body as a function of the distance from the body on the downstream side. (see figure 10)

Substitution of the calculated value of $0,47 \times 10^{-3} \text{ kg/s}$ for \dot{m} in equation (22) leads to a value of $0,000148 \text{ kg/kg}$ of dry air for $\Delta \bar{w}_w$. This corresponds to a dew-point temperature increase of $0,24^\circ\text{C}$.

Thus, if the evaporative heat loss rate from a human body is to be determined from measurements of the specific humidity increase in the wake of the body, with an accuracy of 15%, an instrument that can measure the specific humidity increase to within $0,000148 \times 0,15 = 0,000022 \text{ kg/kg}$ of dry air, or the dew-point temperature increase to within $0,24 \times 0,15 = 0,036^\circ\text{C}$ is required.

Various types of humidity-sensing devices were subsequently investigated to determine whether the required sensitivity could be obtained.

4.3 Methods of sensing the humidity increase in the wake of a human body

Appendix C on page 413 contains brief descriptions of various devices that have been developed for the detection and/or measurement of humidity⁵¹⁾.

The following possible methods of detecting the humidity increase in the wake of a human body in the horizontal test chamber of the climatic chamber were subsequently investigated.

4.3.1 Differential wet- and dry-bulb psychrometer

Basically the wet- and dry-bulb psychrometer^{52,53,54)} comprises two thermometers one of which, the wet-bulb, is covered with a cotton sheath which is maintained moist.

To determine the water vapour pressure of an air sample from ventilated wet- and dry-bulb measurements, the following psychrometric equation is generally used.

(See Section 2 of Appendix C on page 417):

$$p_{wv,G} = p_{wv,wb} - AP(t_G - t_{wb}) \quad \dots\dots\dots (23)$$

where $p_{wv,G}, p_{wv,wb}$ = partial vapour pressure and saturated partial vapour pressure at the wet-bulb temperature, respectively, kPa

and A = psychrometric constant. (A , as well as being dependent on the Reynolds number, is slightly dependent on t_{wb} and to a lesser extent on t_G)

P = total atmospheric pressure, kPa

t_G, t_{wb} = dry- and wet-bulb temperatures, respectively, °C.

In the measurement of the evaporative heat loss from a human body, the difference between the respective specific humidity values on the upstream and downstream sides of the body must be determined. Thus, if two similar instruments are used to measure the upstream and downstream humidities and the instruments are connected differentially to give a direct reading of the difference between the two humidity values, instrument errors will be cancelled out to a large extent and a higher degree of accuracy should be possible.

The possible use of the differential psychrometer developed by Visser and Hodgson⁵⁾ was, therefore, investigated.

In this method, the samples of air of which the difference in specific humidity is to be determined are passed through a double circuit heat exchanger to equalize their dry-bulb temperatures at some temperature above the highest dew-point temperature. The samples are then fed through two separate psychrometer tubes, where the difference in wet-bulb temperature is measured. One such tube is shown in Figure 12.

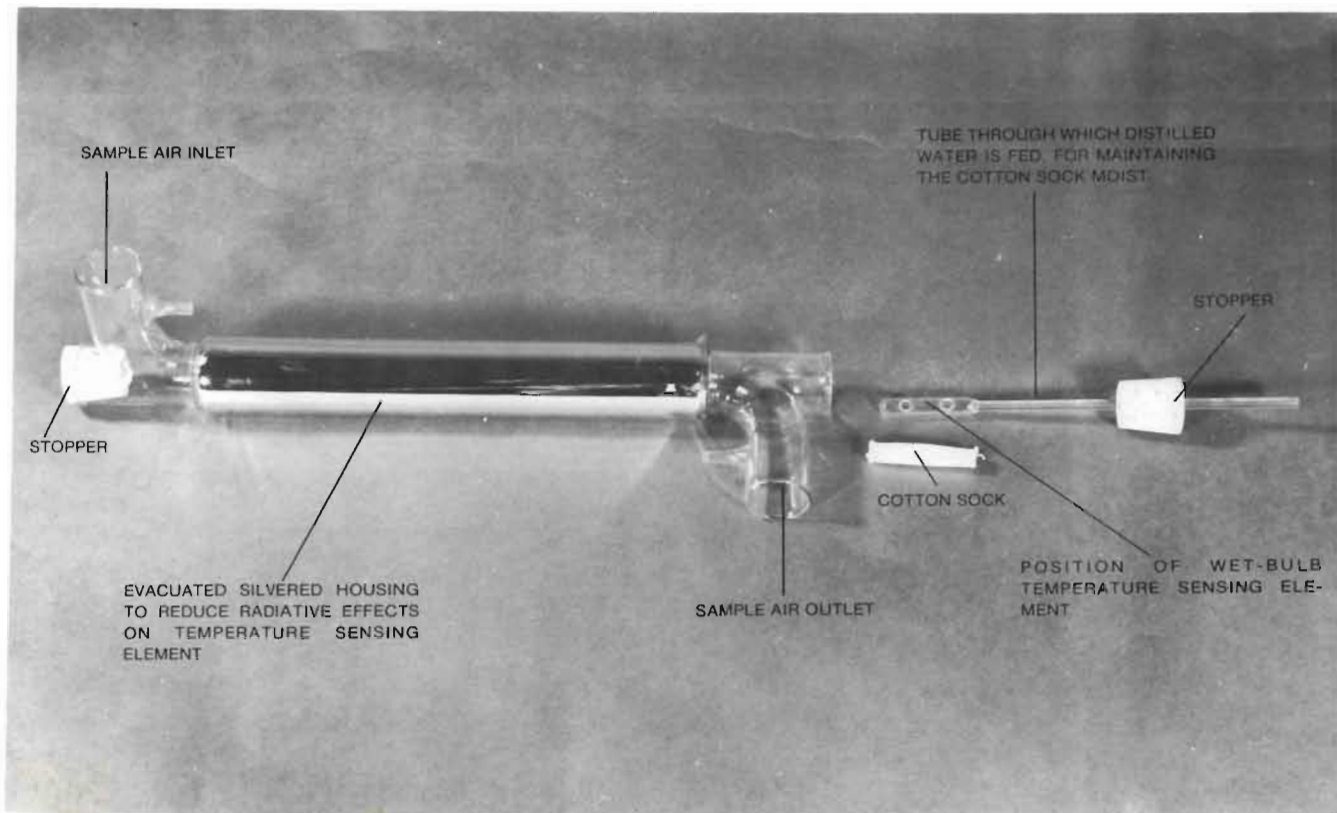


FIGURE 12

Psychrometer tube with the wet-bulb element and cotton sock removed from the tube

In the differential psychrometer air speeds over both pairs of wet-bulb temperature-sensing elements as well as the dry-bulb temperatures and absolute air pressures in each psychrometric tube are the same. The exact value of AP in equation (23) is thus not important in this case, since a knowledge of the absolute value of humidities is not required and the psychrometer will be calibrated before use.

Since the dry-bulb temperatures of both samples are the same, the difference in wet-bulb temperatures is proportional to the difference in specific humidity.

In the initial design, two pairs of temperature sensitive strain gauges, Baldwin type 14, were mounted in the two psychrometer tubes. Each pair was covered with cotton wicks of small size which could be kept moist. The resistance elements were then connected in a Wheatstone bridge; each pair being connected in opposite arms of the bridge to enable the difference between the wet-bulb temperatures to be measured directly.

However, as a result of the migration of moisture through the electrical insulation around the nickel wire temperature-sensing elements, the gauge had to be replaced frequently.

The use of thermocouples as an alternative method of temperature measurement was, therefore, investigated. For this purpose eight 30 SWG copper-constantan thermocouples, covered with flannelette which could be kept moist, were mounted in each tube and connected differentially.

By coupling the differential output of the thermocouples to a Kipp Micrograph BD-597 recorder and using the 100 micro-volt scale, dew-point temperature differences down to $0,03^{\circ}\text{C}$ could be measured by this means. The corresponding difference in specific humidity at a dew-point temperature of 10°C was $0,000018 \text{ kg/kg}$ of dry air.

The degree of accuracy is thus sufficiently high for the measurement of the specific humidity increase in the wake of a human body. (See Section 4.2 on page 119).

However, in view of certain problems related to the operation of wet- and dry-bulb psychrometers of the continuous recording type, in particular, the problem of ensuring that the sock over the wet-bulb element is always clean and sufficiently moist, other alternative methods of measuring the humidity increase in the wake of a human body were investigated.

4.3.2 Differential hair hygrometer

The most commonly used type of mechanical hygrometer is the so-called hair hygrometer. This hygrometer is based on the principle that animal hairs which have been carefully cleaned and freed from grease, change their length when they absorb or part with moisture. In particular, the length generally increases as the moisture content of the surrounding gas increases. (See Section 8 of Appendix C on page 421).

The principle of operation of the hair hygrometer was investigated as a possible means of measuring the humidity increase in the wake of a human body in the test chamber of the climatic chamber.

In the proposed system, a length of fine nylon thread (held taut by means of a spring or weight) would be strung across the wake of the body in the test chamber. Either the change in length or tension could then be taken as a measure of the humidity value.

Absolute calibration would not be necessary if a similar grid were to be installed on the upstream side of the subject and both grids (on the downstream and upstream sides of the body), were coupled differentially to give

a direct reading of the humidity increase.

However, preliminary investigations indicated that there was a marked hysteresis effect which rendered the method unsuitable for this particular application.

4.3.3 Spectroscopic hygrometer

The principle of operation of the spectroscopic hygrometer is derived from the fact that infra-red radiation is attenuated by water vapour⁵⁵⁻⁵⁸). (See Section 9 of Appendix C on page 423).

Since the output of the infra-red hygrometer is a function of the total amount of water molecules in the optical path, the method is ideally suited to the determination of humidity in the outer atmosphere where long path lengths and hence relatively large signals can be obtained.

The main advantages of the spectroscopic type of hygrometer are:

- (i) Short time response,
- (ii) the method in no way alters the humidity content of the air sample and
- (iii) since the sensing element is a beam of radiation, an integrated reading of humidity in the

radiation path is obtained.

In view of the above-mentioned factors, the method appeared to be ideally suited for carrying out humidity measurements in the wake of a human body.

In the proposed system which is illustrated diagrammatically in Figure 13, a filtered light beam of selected wavelength is split in two, such that one half of the light beam traverses the front or upstream side of the body and the other the downstream side. Both light beams are then focussed on a photocell; the beams on the upstream and downstream sides of the body being alternatively cut off by means of a rotating sector disc.

In such a system the ratio of the respective transmitted energies of each of the two light beams would be proportional to the humidity increase in the wake of the body.

Initial investigations, aimed at determining whether the required sensitivity could be obtained with such a system, were conducted using a germanium multilayer narrow band-pass transmission filter with a transmission peak at a wave-length of 2,56 micron. A wave-length of 2,56

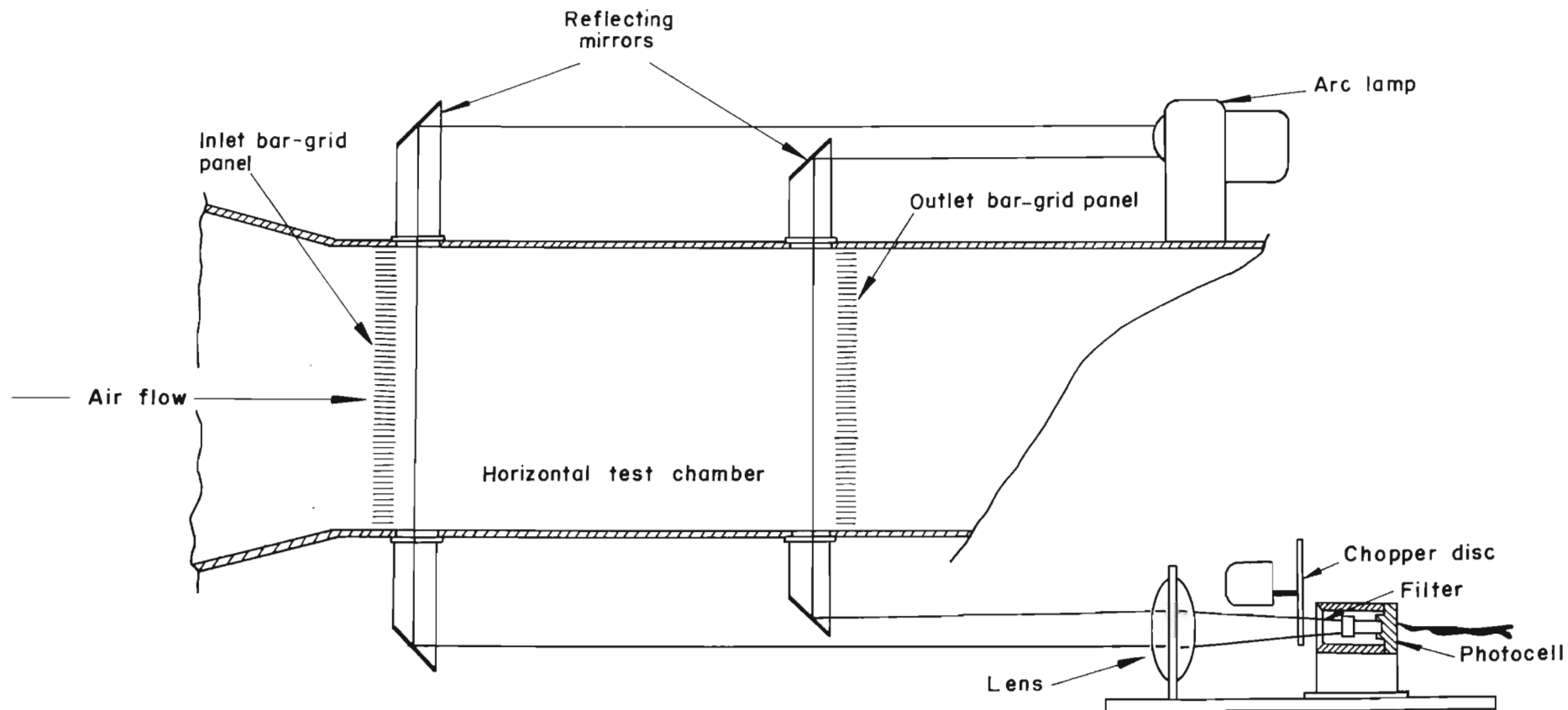


FIGURE 13

Schematic layout of differential infra-red hygrometry system for measuring the humidity increase in the wake of a human body.

microns was selected in view of the relatively strong attenuating effect of water vapour and the negligible effect of carbon dioxide (which may also be present in the wake of the subject) have on the radiant transmission at this wave-length. See Figure C2 on page 424 in Appendix C.

The major problem experienced with the technique was the lack of sensitivity due mainly to insufficient active path length to provide sufficient absorption. Problems were also experienced in producing parallel rays of light which would be of sufficient intensity at the end of the path length to activate the photo detector at its most efficient level; it appeared that a radiant path length of at least 6,5 m would be required to achieve a sensitivity of 0,000022 kg/kg of dry air, specific humidity.

In view of the problem of attaining a sufficiently long effective path length of sufficient intensity, other alternative methods of humidity measurement were investigated.

4.3.4 Electrical resistance hygrometer

The humidity-sensing elements incorporated in electrical resistance hygrometers generally consist of hygroscopic materials which change in moisture content and hence electrical resistance whenever the relative humidity of the surrounding air changes.

In general, electrical resistance hygrometers are very sensitive to small changes of humidity and have a rapid response.

In the past, the chief defect of electrical resistance hygrometers has been the instability of calibration. However, this problem appears to have been overcome in certain commercial models of the instrument. (See Section 10 of Appendix C on page 429).

Consideration was given to the use of various types of electrical resistance hygrometers for the measurement of the evaporative heat loss from a human body in the horizontal test chamber of the climatic chamber. In particular, the use of the Wylie⁵⁹⁾ hygrometer and other humidity-measuring systems which depend on the change in electrical resistance of a salt film for their

operation, were investigated.

Wylie electrolytic condensation hygrometer

The principle of operation of the Wylie hygrometer⁵⁹⁾ is derived from the fact that water vapour is taken up by the surface of a water-soluble crystal if the water vapour pressure is greater than the vapour pressure of a saturated solution of the crystalline substance at the temperature of the crystal surface.

The temperature of the crystal is determined at which a thin layer of the saturated solution, formed on the surface of the crystal and observed by virtue of its electrical properties, is in equilibrium with the gas which is the subject of measurement. The conducting layer of saturated solution is maintained in thermal equilibrium with the gas by controlling the crystal temperature at a temperature which, according to Wylie⁵⁹⁾, is related to the dew-point temperature of the gas.

The instrument is usually operated automatically. For automatic operation, the temperature of the metal enclosure is controlled by the electrical resistance of the crystal through an electronic controller. The temperature of the enclosure, corresponding to the

equilibrium temperature, at which the crystal moisture content is constant at a predetermined value, is continuously recorded.

According to Wylie, the hygrometer is capable of measuring the absolute dew-point temperature to within $0,01^{\circ}\text{C}$. At a dew-point temperature of 10°C , this corresponds to a specific humidity value of $0,000006 \text{ kg/kg}$ of dry air.

In view of the high degree of accuracy claimed by Wylie, the use of the Wylie hygrometer was investigated for measuring the humidity increase in the wake of a human body.

In the proposed system, individual samples of air from the upstream and downstream sides of the human body are circulated through two separate electrolytic hygrometers; the principle of operation of each hygrometer being based on the system originally proposed by Wylie⁵⁹⁾. The temperature of each enclosure is thus controlled at a value corresponding to the humidity of the particular air sample being circulated through the enclosure by means of the electrical resistance of the crystal within the enclosure.

By mounting a resistance thermometer in each of the crystal enclosures and connecting them differentially in the form of a Wheatstone bridge network, the temperature difference between the two enclosures and hence the differences in humidity between the two air samples could be measured directly.

One of the major prerequisites for the accurate measurement of the humidity increase by this means is that the respective temperatures of each crystal enclosure should be controlled within close limits. It is important too that the response time of each hygrometer should be sufficiently short to enable changes in humidity to be followed relatively quickly. In view of the latter requirement, each enclosure should preferably be of minimum mass and the ventilation rate through the enclosure should be relatively high.

Particular attention was given to these aspects in the design of the prototype hygrometer which is shown in Figures 14 and 15.

The crystal enclosure consisted essentially of three light concentric tubes, 0,1 mm thick. A potassium

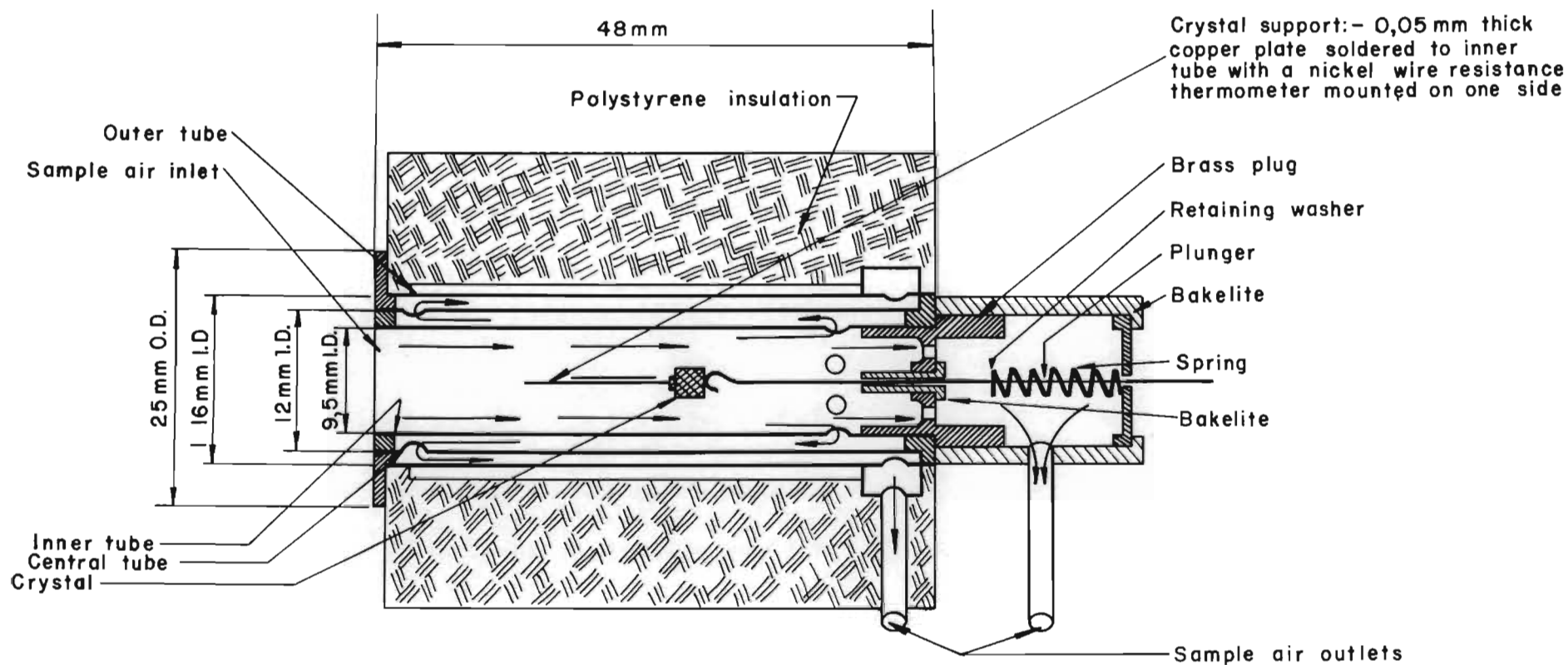
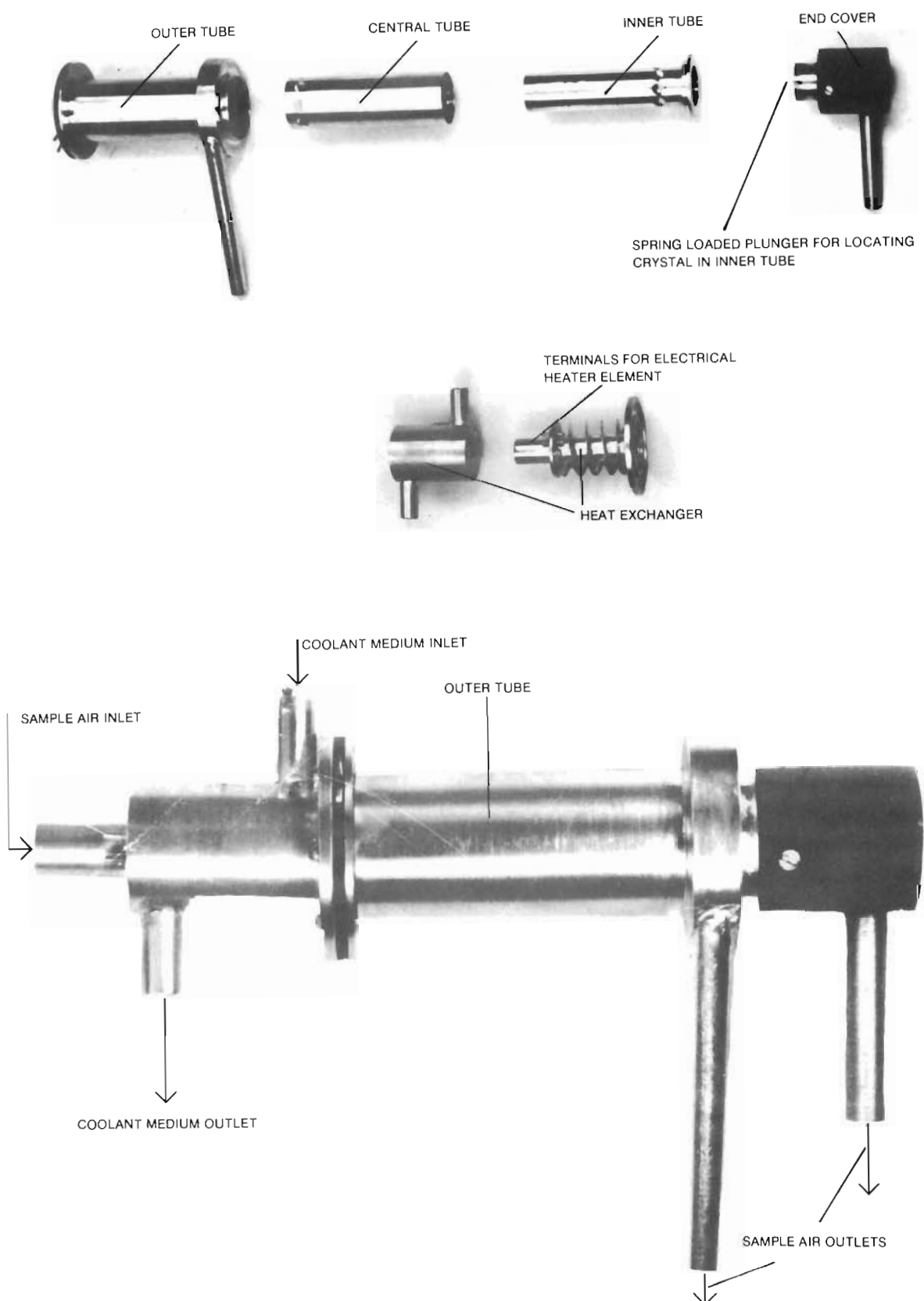


FIGURE 14
*Air flow through the crystal holder of the
 electrolytic condensation hygrometer.*

**FIGURE 15**

Components of the electrolytic condensation hygrometer

chloride crystal, in the form of a cube 2 mm in size, was supported on a thin copper plate, 0,05 mm thick, soldered to the inner tube; the crystal being held in position by means of a light spring-loaded plunger.

A nickel wire resistance thermometer for measuring the temperature of the air passing over the crystal and hence the crystal temperature, was mounted on one side of the copper plate, adjacent to the crystal.

In order to maintain ~~iso-thermal~~ conditions within the crystal enclosure ~~and hence~~ minimize the thermal radiative influences of the surrounding walls on the temperature of the thermometer and crystal, the air flow system shown in Figure 14 was adopted; ~~after~~ flowing over the thermometer and crystal, the air ~~passed~~ through the annular spaces between the concentric tubes. In addition, the entire enclosure was thermally insulated.

The temperature of the air flowing through the enclosure was controlled by means of a heat exchanger, installed on the air inlet side of the enclosure. (See Figure 15).

The main object of the air temperature control system was

to maintain the crystal resistance constant at a predetermined value. For the purpose of temperature control, an electrical heater element was mounted along the helical passages of the heat exchanger through which carbon dioxide (expanded from cylinder pressure to atmospheric pressure), could be circulated at a predetermined rate).

The temperature of the air circulating through the enclosure and hence the crystal temperature was controlled by maintaining a constant flow rate of the expanded carbon dioxide through the helical passages of the heat exchanger (to provide the necessary cooling) and automatically controlling the heat input to the heater element by means of the electrical resistance of the crystal (through a suitable temperature controller).

The heat exchanger which was of low thermal capacity, was secured to the inlet flange of the crystal enclosure with a fibre washer between the two components to reduce heat conduction. Both the heat exchanger and crystal enclosure were cadmium plated to eliminate the possibility of crystal contamination by the enclosure material.

The calibration tests that were carried out on the hygrometer are described in some detail in Appendix D on page 437 .

Initial calibration studies indicated that the proposed system of humidity measurement would be capable of measuring the humidity increase in the wake of the human body to within a dew-point temperature of $0,04^{\circ}\text{C}$ or a specific humidity of $0,000024 \text{ kg/kg}$ of dry air.

The limited degree of accuracy attainable with the system was mainly due to the problem of controlling the temperature of the air circulating through the enclosure and hence the crystal temperature, to within sufficiently close limits.

In order to reduce the influence of the temperature control system on the accuracy of measurement an alternative system of measurement was proposed.

In the alternative system the samples of air from the upstream and downstream (in the wake) sides of the human body are circulated over two separate salt crystals, mounted in a single enclosure; the air from the upstream side of the body being discharged onto the one crystal and the air from the downstream side of the body being discharged onto the other crystal. Suitable heat exchanger equipment is built into the system to ensure

that both streams of air as well as the crystal enclosure are maintained at the same temperature.

In such a system the difference in electrical resistance between the two crystals is a measure of the humidity increase in the wake of the human body. By connecting the two crystals in a Wheatstone bridge, variations in the resistance between the two crystals could be measured directly.

However, preliminary investigations showed that, due to certain uncontrolled variations in the electrical resistance of each crystal, the instrument would be subject to extensive zero drift and for this reason would be unsuitable for measuring the humidity increase in the wake of a human body.

Electric grid hygrometer

In this method, a long length of cotton covered platinum wire was twisted together and impregnated with a lithium chloride solution. The twisted wire was mounted on an insulated frame to form a grid.

Two similar grids were constructed to investigate the possibility of measuring the integrated humidity rise in the wake of the body; the two grids being connected in

a Wheatstone bridge with two other fixed resistances. The difference in resistance was measured by means of a strain gauge recorder.

Tests with this type of hygrometer were disappointing in view of certain uncontrolled changes in the resistance of the salt that took place resulting in a zero shift. In addition, the desired sensitivity could not be attained.

Use of commercially available electrical resistance hygrometers

Investigations were carried out to determine the suitability or otherwise of a commercially available electrical resistance hygrometer for measuring the humidity increase in the wake of the body.

It was found that commercial lithium chloride sensors, the resistance of which is a function of the relative humidity of the surrounding air, were comparatively stable and extremely sensitive to variations in relative humidity.

The absolute accuracy to which these elements can be calibrated is of the order of 0,1% relative humidity.

At dry-bulb and dew-point temperatures of 35°C and 10°C , respectively, this corresponds to a specific humidity difference of $0,00004 \text{ kg/kg}$ of dry air or a dew-point temperature change of $0,065^{\circ}\text{C}$.

The particular commercial hygrometer that was investigated for measuring the specific humidity increase in the wake of a human body was an Aminco electrical resistance hygrometer manufactured by the Hydrodynamics Inc., incorporating narrow range lithium chloride sensors. Each sensor has a range of about 12 per cent. Narrow range sensors were selected in preference to the wide range type in view of the increased sensitivity of such a sensor.

The hygrometer indicating unit contains a built-in bridge network which provides a signal of 0 to 25 millivolts for a change in relative humidity of about 12 per cent.

By adopting the differential hygrometry system of measurement outlined in Section 4.3.1 on page 121 albeit incorporating two separate Aminco electrical resistance hygrometers, a high degree of accuracy could be attained.

In the system that was investigated samples of air from the upstream and downstream sides of the human body were circulated through a double heat exchanger to equalise their dry-bulb temperatures. The respective humidities of the two air samples were then measured with two separate hygrometer indicating systems. By coupling the respective outputs of the two indicators to a Kipp Micrograph type BD-597 recorder in such a way that the recorder measures the difference in output between the two systems, differences in relative humidity as small as 0,01 per cent could be recorded. At dry-bulb and dew-point temperatures of 35°C and 10°C, respectively, the above-mentioned relative humidity value corresponds to a specific humidity difference of 0,000004 kg/kg of dry air or a dew-point temperature change of 0,007°C.

The accuracy of such a system is thus sufficient to measure the specific humidity increase in the wake of the human body; the required measurement accuracy being 0,000022 kg/kg of dry air specific humidity or 0,035°C dew-point temperature. (See Section 4.2 on page 119).

4.4 Choice of humidity-sensing system

The respective accuracies attainable with various humidity-measuring systems are summarised in Table 6.

**TABLE 6 : MEASUREMENT OF THE HUMIDITY INCREASE IN THE WAKE OF
A HUMAN BODY : ACCURACIES OF VARIOUS HUMIDITY-MEASURING
DEVICES**

Required accuracy : 0,000022 kg/kg of dry air or 0,036°C dew-point
temperature (See Section 4.2 on page 119)

TYPE OF HUMIDITY- MEASURING DEVICE	ACCURACY		REMARKS
	SPECIFIC HUMIDITY*, kg/kg OF DRY AIR	DEW-POINT TEMPERATURE °C	
Dew-point hygrometer	0,000185	0,300	
Wet- and dry-bulb psychrometer	0,000460	0,750	
Differential wet- and dry-bulb psychrometer	0,000018	0,030	
Hair hygrometer	0,001700	2,530	
Differential infra- red hygrometer	0,000022	0,036	Based on a path length of 6,5 m
Wylie electrolytic hygrometer	0,000006	0,010	The design was based on the Wylie hygro- meter Using a lithium chloride sensor Using two of the commercial resis- tance hygrometers coupled differen- tially
Differential elec- trolytic hygrometer	0,000024	0,040	
Commercial electrical resistance hygrometer	0,000040	0,065	
Differential electri- cal resistance hygro- meter	0,000004	0,007	

* At a dew-point temperature of 10°C

It is seen that the required accuracy for measuring the humidity increase in the wake of a human body can be attained with the wet- and dry-bulb psychrometer, as well as the infra-red, electrolytic and electrical resistance hygrometers, providing the differential system of measurement is employed. (In such a system the hygrometers which measure the respective humidities on the upstream and downstream sides of the body are coupled differentially and the humidity increase in the wake of the body is given as a direct reading).

Of the above-mentioned methods of measuring the humidity increase in the wake of the body, the differential electrical resistance hygrometer was preferred in view of the following considerations:

The humidity sensors which are commercially available, are stable and do not suffer from the following problems associated with the other systems of measurement:

- (i) The maintenance problems of the wet- and dry-bulb psychrometer. (When used as a continuous measuring system, problems are generally experienced in ensuring that the

- wet-bulb element is moist and that the cotton sock over the element is free of contaminants),
- (ii) the problem of zero drift due to uncontrolled electrical resistance variations which were found to occur in salt crystals incorporated in the electrolytic hygrometer, and
 - (iii) the problem of obtaining a parallel beam of light of sufficient length and intensity in the case of the infra-red hygrometer.

4.5 Proposed method of measuring the evaporative heat loss rate from a human body

The following two alternative methods of measuring the evaporative heat loss rate from a human body referred to in Section 4.1 on page 106, were investigated:

(a) Analogy method

In this method both the temperature and the specific humidity increase between two fixed points (the one on the upstream side of the body and the other in the wake of the body), are measured simultaneously. In addition, the convective heat loss rate is measured by means of the convective heat loss measuring instrument that had previously been developed⁷⁾.

The evaporative heat loss rate is then determined by analogy, assuming the ratio of the evaporative heat loss rate to the convective heat loss rate to be proportional to the ratio of the product of the latent heat of evaporation of water and the specific humidity increase in the wake of the body to the product of the specific heat of air at constant pressure and the temperature increase in the wake of the body. See equation (18) on page 110.

(b) Comparative method

In this method a known quantity of water vapour (produced by an auxiliary steam generator), is introduced into the wake of the body at a predetermined rate. The steam is introduced in such a way that the output of the humidity-measuring device (for measuring the humidity increase in the wake of the body), is the same for the same vapour release from the human body or auxiliary steam generator.

Assuming the output of the humidity-measuring device or recorder deflection to be linearly related to the evaporative heat loss rate, the unknown moisture evaporation rate from the human body producing a given recorder deflection may be calculated relatively easily if the recorder deflection due to the known vapour

production rate by the steam generator is known.

See equation (20) on page 112.

Model studies were carried out in the 0,7 m x 0,7 m temperature and humidity controlled wind tunnel of the CSIR's National Mechanical Engineering Research Institute to determine the most suitable method of measuring the evaporative heat loss rate from a human body.

4.5.1 Analogy method

Figure 16 presents a diagrammatic layout of the experimental apparatus that was used to investigate the analogy method of determining the evaporative heat loss from a human body.

A wetted body, ϕ 50 mm diameter by 220 mm long, was suspended from the top of the wind tunnel by means of a thin wire. The body which was supplied with water at a constant rate, was constructed from a fine wire mesh screen covered with a layer of tissue paper and a silk cloth to ensure an even distribution of water over the surface of the body.

To increase the rate of evaporation, heat was supplied

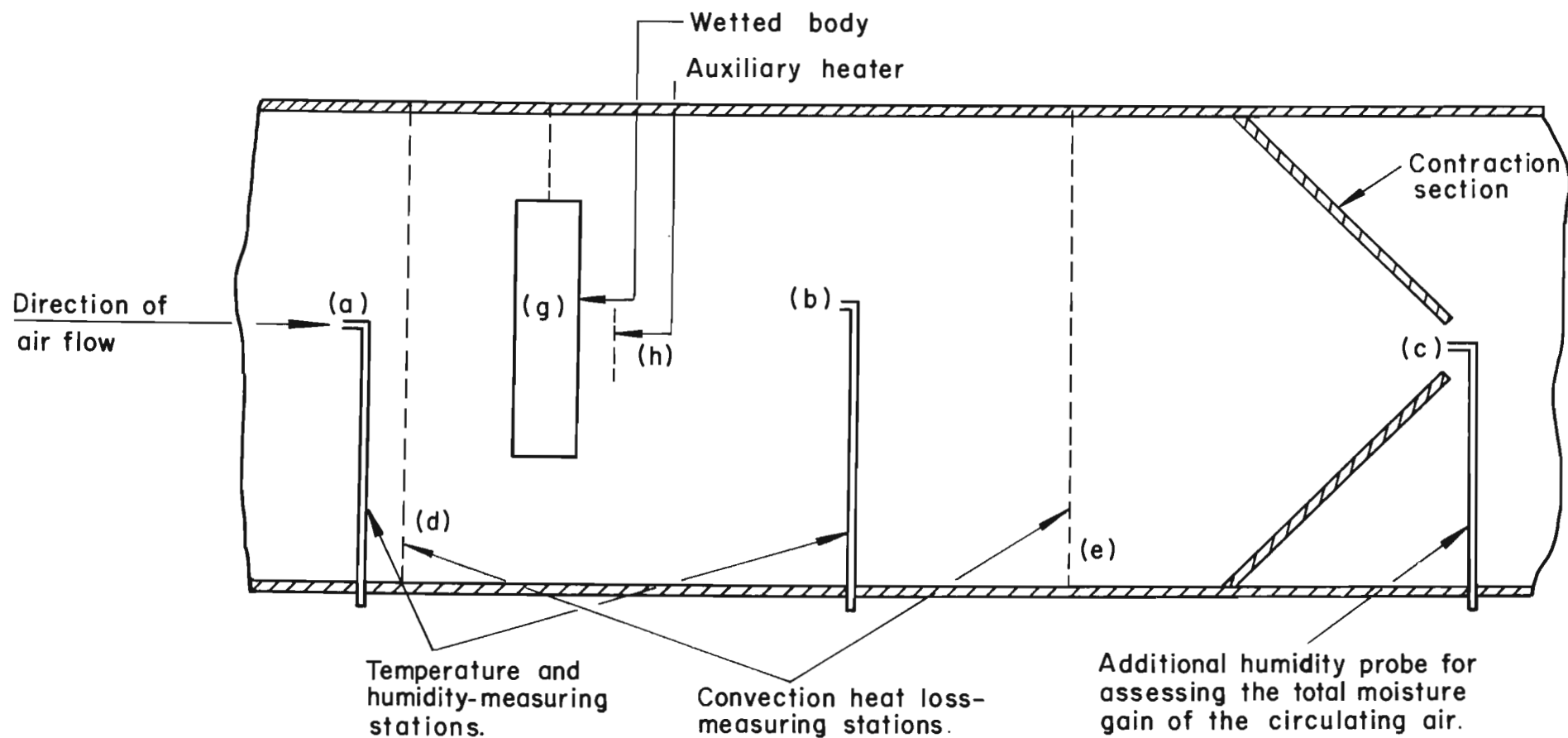


FIGURE 16
Diagrammatic layout of the test arrangement for the determination of the total evaporation rate from a wetted body by analogy

to the body at a constant rate by means of an electrical heater coil wound around the body.

The evaporative heat loss rate from the body was maintained at a sufficiently high value to enable the actual moisture evaporation rate and hence evaporative heat loss rate from the body to be assessed by means of equations (3) and (21) on pages 64 and 114, respectively from the overall specific humidity increase and mass flow rate of the air flowing over the body (as a check on the evaporative heat loss rate values determined by the analogy method).

This method was preferred to the alternative method of assessing the actual evaporation heat loss rate from measurements of the water supply rate to the wetted body, in view of the difficulty in maintaining the moisture content of the body constant: unknown variations in the rate of water absorption by the body tended to occur and as a result, the measured water supply rate to the body differed from the moisture evaporation rate at certain times.

For the purpose of assessing the overall specific humidity

increase, a contraction section was installed in the wind tunnel on the downstream side of the body and air-sampling probes (required for the humidity measurements), were installed at the measuring stations a and c shown in Figure 16. (The contraction section obviated the need for carrying out a large number of humidity readings on the downstream side of the body to obtain an average value for the humidity increase).

Air samples were drawn off through the air-sampling probes at a and c. The specific humidities at these points were determined from readings of the dry-bulb temperature of the air, as measured with 30 SWG copper-constantan thermocouples and the corresponding relative humidity values as measured with the electrical resistance hygrometer referred to in Section 4.3.4 on page 141.

The convective heat loss rate from the body was measured by means of the two resistance wire grids, d and e, and a small auxiliary heater, h, mounted immediately downstream of the body; the measurements being carried out in accordance with the method described by Carroll and Visser³⁶).

At the same time relative humidity and temperature measurements were carried out at the measuring stations, a and b; one on the upstream side and the other in the wake of the evaporating body. The air-sampling probe b was also used to determine the spatial specific humidity distribution in the wake of the body.

The temperature measurements were carried out by means of 30 SWG copper-constantan thermocouples and a Kipp Micrograph type BD-597 recorder.

The relative humidity measurements were carried out by means of an Aminco electrical resistance hygrometer coupled to a Kipp Micrograph type BD-597 recorder.

The evaporative heat loss rate, \dot{q}_e , from the evaporating body was then determined from equation (18) on page 110.

$$\begin{aligned}\dot{q}_e / \dot{q}_c &= l \Delta w_w / c_G \Delta t_{G,w} \\ \therefore \dot{q}_e &= \dot{q}_c l \Delta w_w / c_G \Delta t_{G,w} \quad \dots\dots\dots (24)\end{aligned}$$

where \dot{q}_e = evaporative heat loss rate from the body, kW

and \dot{q}_c = convective heat loss rate from the body, kW

l = latent heat of evaporation of water, kJ/kg

$\Delta w_w, \Delta t_{G,w}$ = respective increases in specific humidity, kg/kg and temperature, °C between two fixed points on the upstream and downstream side (in the wake) of the subject

c_G = specific heat at constant pressure of the air, 1,01 kJ/kg °C.

The above-mentioned value for the evaporative heat loss rate, \dot{q}_e , was compared to the actual evaporative heat loss rate, $\dot{q}_{e,act}$ as determined by means of the following equation from the measurements of the mean increase in specific humidity between points, a and c, shown in Figure 16 and the mass flow rate of air flowing through the tunnel:

$$\dot{q}_{e,act} = \ell \Delta w_{c-a} \dot{G}_G \quad \text{..... (25)}$$

where $\dot{q}_{e,act}$ = actual evaporative heat loss rate from the body, kW

and ℓ = latent heat of evaporation of water, kJ/kg

Δw_{c-a} = increase in specific humidity of the air between points c and a, shown in Figure 16, respectively, kg/kg

\dot{G}_G = mass flow rate of the air, kg/s

The mass flow rate of the air was determined from measurements of the air velocity on the upstream side of the body in the plane at d, shown in Figure 16, the cross-sectional area of the test section at this point and the density of the air.

$$\dot{G}_G = \dot{v}_G A \rho_G \quad \text{..... (26)}$$

where \dot{G}_G = mass flow rate of the air, kg/s

and \dot{v}_G = mean air velocity in the test section of the wind tunnel, m/s

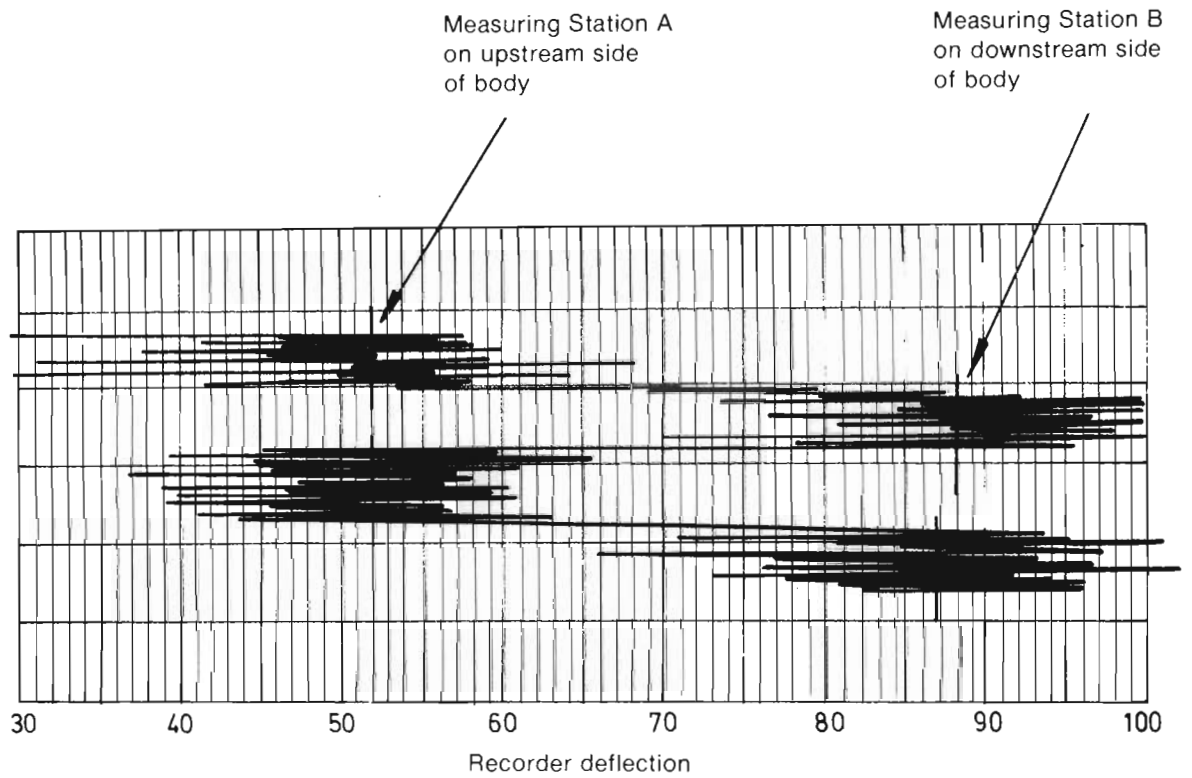
A = cross-sectional area of wind tunnel, m²

ρ_G = air density, kg/m³

Test results

Figures 17 and 18 present typical graphs of the variations in recorder output with time during a series of temperature and humidity measurements, respectively. The spatial specific humidity distribution in the wake of the test body during a typical test is presented in Figure 19.

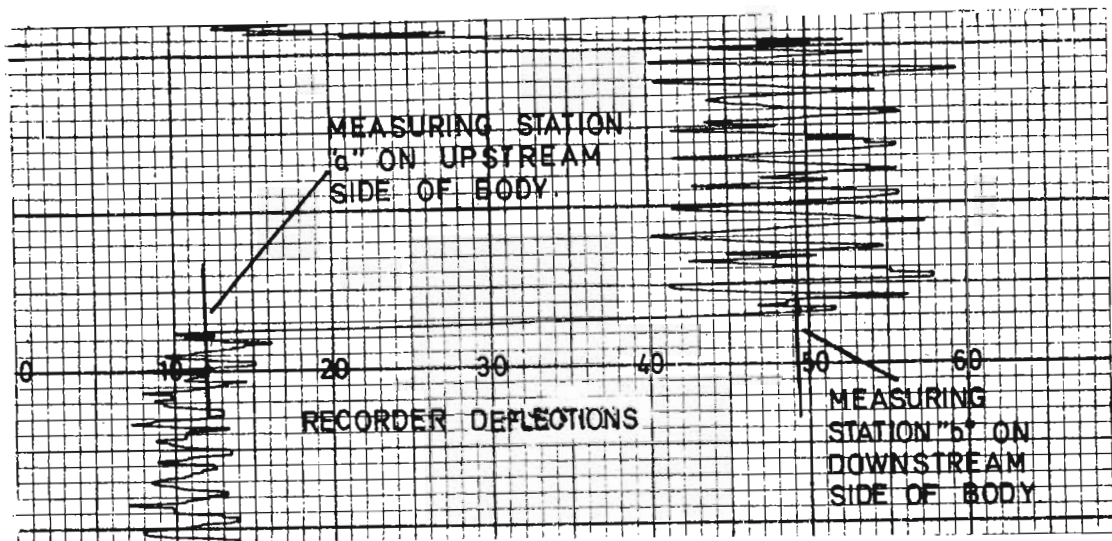
The results of the tests to determine the evaporative heat loss rate from the test body are summarised in Table 7.



1. See figure 16 for positions of measuring stations in the wind tunnel.
2. Test conditions:
 - (i) Air velocity: 0,5 m/s
 - (ii) Evaporation rate from body: 0,007 g/s
 - (iii) Heat input rate to evaporating body: 0,033 kW.
3. Recorder sensitivity: 1,0 mV

FIGURE 17

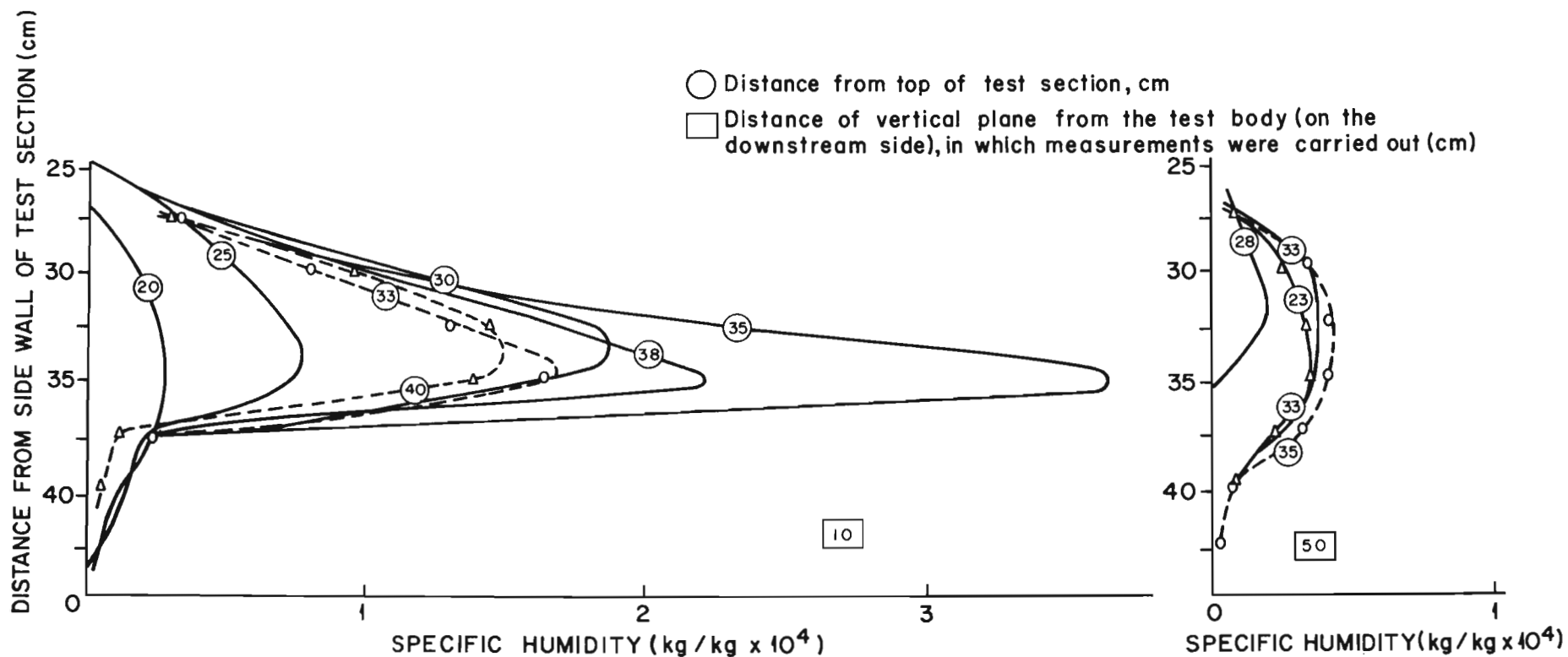
Model evaporative heat loss tests: recorder deflections due to the temperature increase in the wake of the test body



1. See figure 16 for position of measuring stations in the wind tunnel
2. Test Conditions:
 - (i) Air velocity: 0,5 m/s
 - (ii) Evaporation rate from test body: 0,007 g/s
 - (iii) Heat input rate to evaporating body: 0,033 kW.
3. Recorder sensitivity: 1.0 mV

FIGURE 18

Model evaporative heat loss tests: recorder deflections due to the humidity increase in the wake of the test body.



Test conditions: Size of test body : 50mm dia x 220mm long
 Evaporation rate from test body : 0,006 g/s
 Air velocity : 0,5 m/s
 Air temperature : 23°C

FIGURE 19
*Model evaporative heat loss tests: specific humidity distribution
 in the wake of the test body.*

TABLE 7 : MODEL EVAPORATIVE HEAT LOSS STUDIES : DETERMINATION OF THE EVAPORATIVE HEAT LOSS RATE BY ANALOGY : COMPARISON BETWEEN THE CALCULATED AND ACTUAL VALUES OF THE EVAPORATIVE HEAT LOSS RATE

(1)	(2)	(3)	(4)	(5)	(6)	(7)	(8)
Specific humidity increase in wake of body, Δw_w (kg/kg)	Overall specific humidity increase*, Δw_{c-a} (kg/kg)	Air velocity, \dot{v}_G (m/s)	Mass flow rate of air $\dot{G}_G = \dot{v}_G A_G^{**}$ (kg/s)	Actual evaporation heat loss rate, $\dot{q}_{e,act}$ (10^{-3} kW)	Evaporation*** rate calculated by analogy method, \dot{q}_e (10^{-3} kW)	$\dot{q}_{e,act}$ $h \Delta w_w$ (10^{-3} kg/s)	\dot{q}_c $c_G \Delta t_{G,w}$ (10^{-3} kg/s)
0,000715	0,0000614	0,395	0,140	19,20	17,70	11,0	10,4
0,000705	0,0000791	0,396	0,141	24,82	15,70	14,4	8,9
0,000684	0,0000681	0,396	0,141	21,47	17,75	12,6	10,4
0,000762	0,0000911	0,380	0,135	27,42	23,60	14,7	12,4
0,000865	0,0000776	0,380	0,135	23,86	28,93	10,3	13,4
0,000922	0,0001045	0,380	0,135	32,14	31,06	14,3	13,5
			Average :	24,80	22,45	12,9	11,5

* Specific humidity increase between points c and a shown in Figure 16. on page 148

** Cross-sectional area of tunnel, $A = 0,37 \text{ m}^2$, air density, $\rho_{air} = 0,96 \text{ kg/m}^3$

*** See equation (24) on page 151.

The evaporative heat loss rate values, \dot{q}_e , as calculated from equation 24 on page 151, in accordance with the analogy method, are given in column 6 of Table 7. A comparison of these values with the actual evaporative heat loss rate values, $\dot{q}_{e,act}$, listed in column 5 shows that the calculated evaporative heat loss rate values, \dot{q}_e , were generally on the low side.

By substituting the values of the actual evaporative heat loss rate, $\dot{q}_{e,act}$ in equation (24) on page 151 two ratios are obtained which should be equal for the same test conditions, namely:

$$\dot{q}_{e,act}/\ell\Delta w_w \text{ and } \dot{q}_c/c_G\Delta t_{G,w}$$

The values of these two ratios for a particular test are given in columns 7 and 8 of Table 7.

Although the two ratios are of the same order of magnitude, a mean difference of about 10% is evident.

In Figure 20 the values of the ratios $\dot{q}_{e,act}/\ell\Delta w_w$ and $\dot{q}_c/c_G\Delta t_{G,w}$ are shown as functions of the free air stream velocity in the tunnel, for velocities within the range 0,18 m/s to 0,65 m/s.

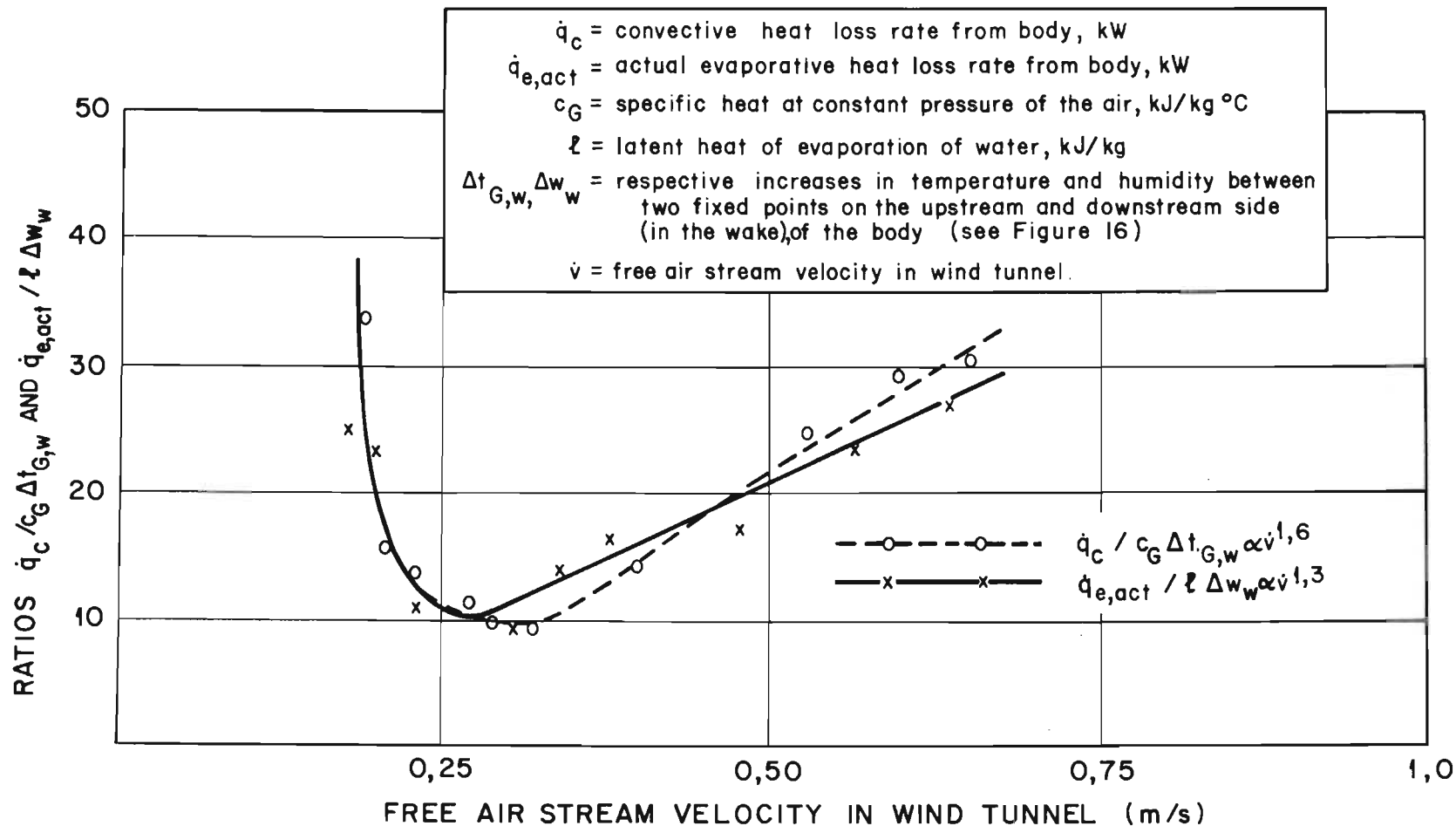


FIGURE 20
Model evaporative heat loss studies: the influence of the free air stream velocity on the ratios, $\dot{q}_c / c_G \Delta t_{G,w}$ and $\dot{q}_{e,act} / \ell \Delta w_w$

It is seen that both ratios attain a minimum value at an air velocity of the order of 0,3 m/s.

The sharp increase in the values of $\dot{q}_{e,act}/\ell \Delta w_w$ and $\dot{q}_c/c_G \Delta t_{G,w}$ at air velocities below 0,3 m/s is probably due to natural convection or buoyancy effects. As a result of the latter influence the wake tends to rise above the measuring station, b, and relatively low values for Δt_G and Δw_w are obtained.

Above air velocities of 0,3 m/s, straight lines drawn through the plotted points of each ratio appear to have different slopes; the ratios $\dot{q}_{e,act}/\ell \Delta w_w$ and $\dot{q}_c/c_G \Delta t_{G,w}$ appear to be proportional to $\dot{v}_G^{1,3}$ and $\dot{v}_G^{1,6}$ respectively, where \dot{v}_G is the air velocity.

As a result, the values of the ratio, $\dot{q}_{e,act}/\ell \Delta w_w$ is higher than the ratio, $\dot{q}_c/c_G \Delta t_{G,w}$ at air velocities below 0,47 m/s. At air velocities above 0,47 m/s, on the other hand, the ratio $\dot{q}_c/c_G \Delta t_{G,w}$ generally exceeds the ratio $\dot{q}_{e,act}/\ell \Delta w_w$.

In view of the difference between the slopes of the $\dot{q}_{e,act}/\ell \Delta w_w$ and $\dot{q}_c/c_G \Delta t_{G,w}$ versus velocity lines, the

analogy method of calculating the evaporative heat loss rate would tend to give evaporative heat loss values which would be on the low and high side at velocities below and above 0,47 m/s, respectively.

However, it should be noted that the scatter of the plotted points in Figure 20 could be due to experimental error, particularly with regard to the measurements of, inter alia, the temperature and relative humidity and hence the specific humidity increase of the air flowing over the body.

An idea of the influence of slight errors in the measurement of temperature and relative humidity on the overall accuracy of measurement is evident from the following considerations:

Assume a dry-bulb temperature of 20°C and a relative humidity of 50 per cent. Furthermore, assume that the increase in relative humidity due to evaporation is 0,3%. This represents an increase in the specific humidity of the air of 0,000053 kg/kg of dry air.

Error due to the measurement of relative humidity

In Table 6 on page 143, the accuracy of the commercial

electrical resistance hygrometers used in the model studies is given as 0,000040 kg/kg of dry air. For an overall increase in relative humidity of 0,000053 kg/kg of dry air, errors in the measurement of relative humidity may thus cause errors in the final results of almost 100 per cent.

Error due to the measurement of temperature

An error of 0,01°C in the measurement of the dry-bulb temperature can result in the following variations in the calculated specific humidity values:

Temperature (°C)	Relative humidity (per cent)	Specific humidity (kg/kg)	Calculated change in specific humidity (kg/kg)
20,01	50,3	0,006769	-
19,99	50,0	0,008706	0,000063
19,99	50,3	0,008759	-
20,01	50,0	0,008716	0,000043

Thus reasonably small errors in temperature measurement can cause errors in the final result of $\pm 20\%$ (based on an overall specific humidity increase of 0,000053 kg/kg of dry air). By controlling the temperature of the air sample before its moisture content is being measured, the possible error involved during the temperature measurement may be limited.

In view of the above-mentioned considerations, further experimental data would be necessary in order to establish with any degree of certainty whether the respective slopes of the two lines representing the ratios $\dot{q}_{e,act}/h\Delta w_w$ and $\dot{q}_c/c_G \Delta t_G$ versus velocity are in fact different to each other (at air velocities above 0,3 m/s).

In general, the evaporative heat loss from a wetted body could be determined to within 15% by means of the analogy technique.

4.5.2 Comparative method

Figure 21 presents a diagrammatic layout of the experimental apparatus that was used to investigate the comparative method of determining the evaporative heat loss from a human body.

The apparatus, which was installed in the 0,7 m x 0,7 m temperature and humidity controlled wind tunnel of the CSIR's National Mechanical Engineering Research Institute, basically consisted of an "evaporating" body, an auxiliary steam generator and air sampling probes for the purpose of the humidity measurements.

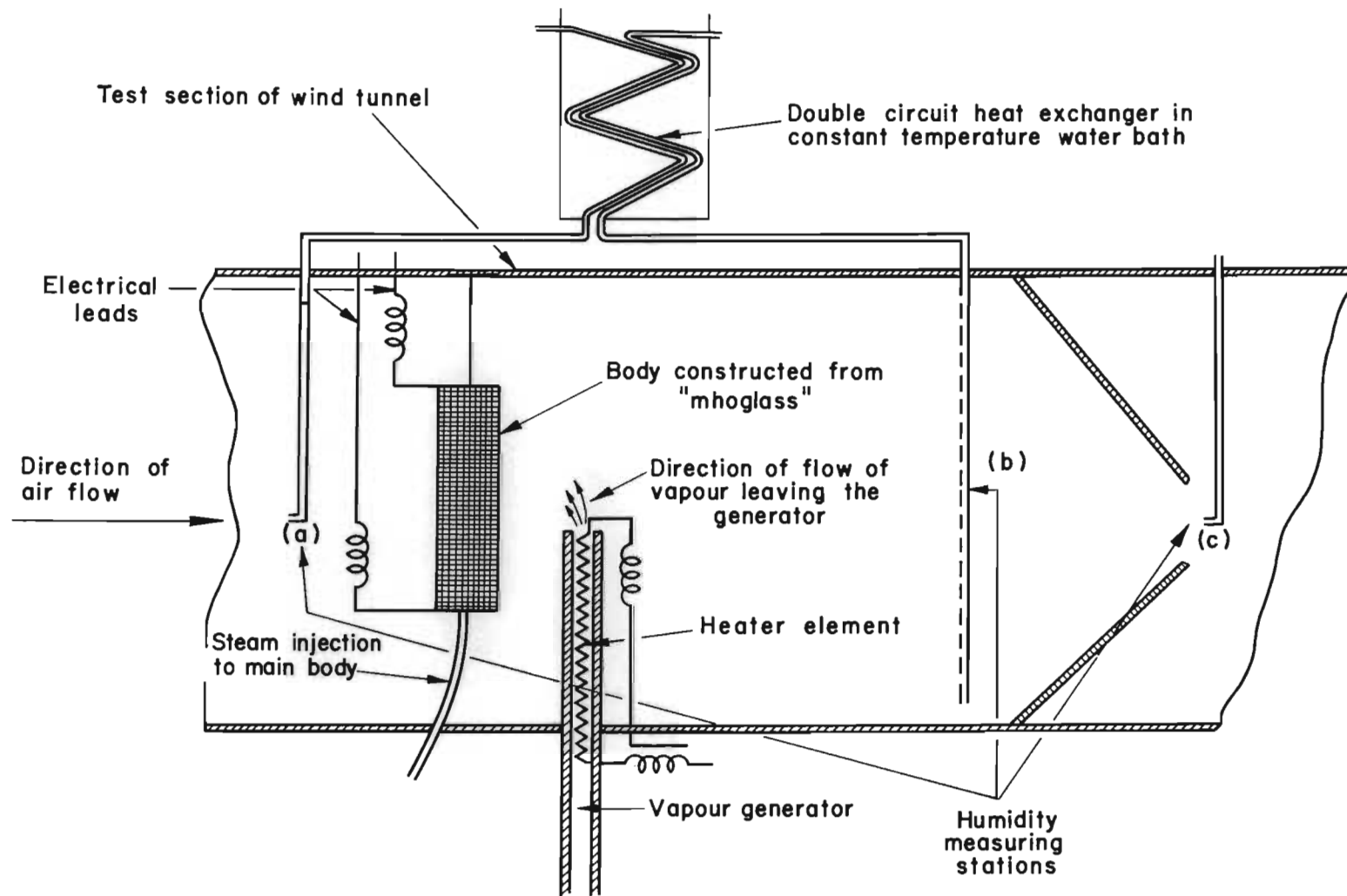


FIGURE 21

Diagrammatic layout of the test arrangement for the determination of the total evaporation rate from a body by the comparative method.

"Evaporating" body

The "evaporating" body which was of similar size to the wetted body that was used for the investigations into the analogy method of measuring evaporative heat loss, was constructed from "Mhoglass"* and suspended in the tunnel. See Figure 22. Electrical terminals were fitted to each end of the body and connected to a variable voltage supply unit to permit the heat input to the body to be regulated.

Water was evaporated in a steam generator and injected into the body at a controlled rate.

The above-mentioned construction for the "evaporating" body was adopted in preference to the type of construction used for the wetted body in the analogy tests in view of the tendency of the vapour produced by the auxiliary steam generator in the wake of the body to condense on the surface of the original wetted body.

In the case of the "Mhoglass" body, the "Mhoglass" itself

* "Mhoglass" is a graphite impregnated fibre glass heating element which is similar in appearance to a fine gauze screen.

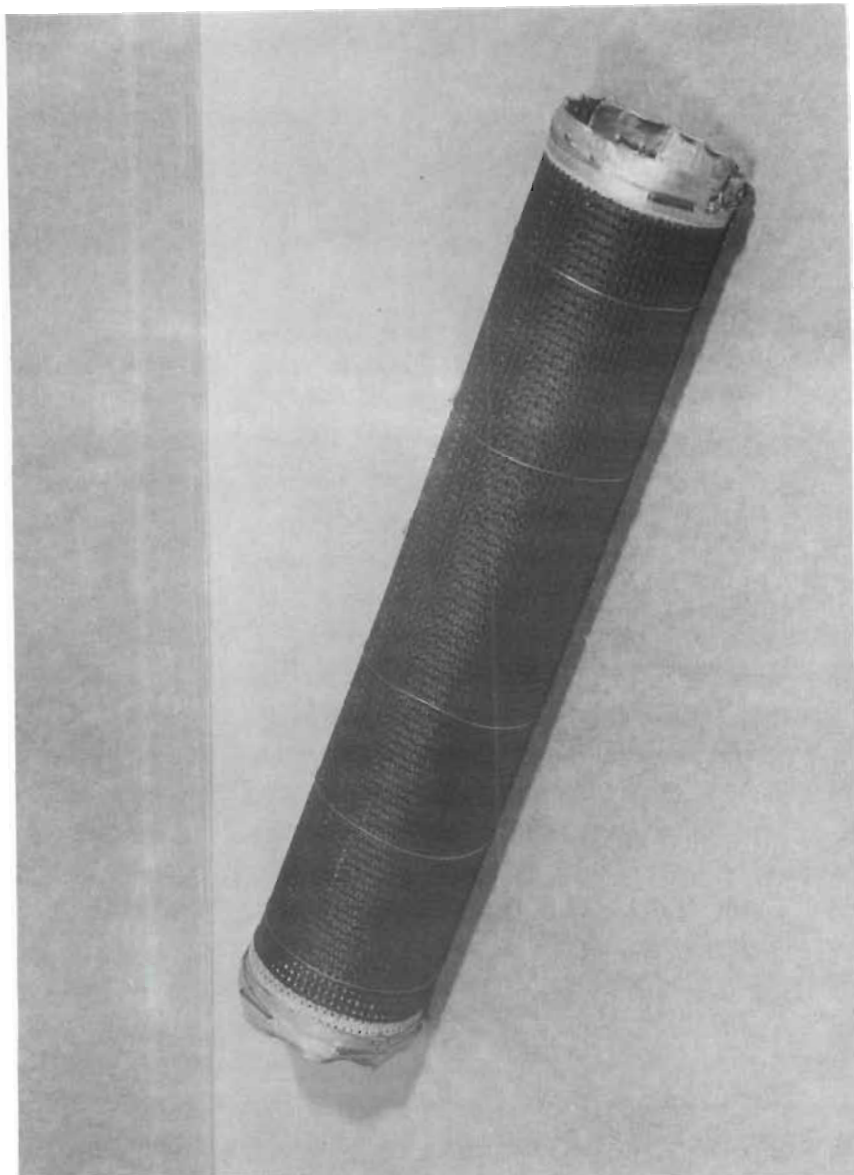


FIGURE 22

Model evaporative heat loss tests: 50 mm dia. x 220 m.
long body constructed from 'Mhoglass'

forms the heater element and the temperature of the entire body could thus be uniformly controlled at a value above the dew-point temperature of the surrounding air, thereby minimising the tendency for water vapour to condense on the body.

The rate at which steam is supplied to the body could thus be assumed to be equal to the rate of steam dissipation through the "Mhoglass" body to the surrounding air. The rate of water vapour "loss" from the "evaporating" body could, therefore, be determined directly by measuring the rate at which steam is supplied to the body.

Auxiliary water vapour generator

A predetermined quantity of steam was introduced into the wake of the body by means of the auxiliary water vapour generator shown in Figure 21 on page 164.

The auxiliary water vapour generator basically consisted of a thick-walled glass capillary tube and an electrical heater element. Water was passed through the tube at a controlled rate and vapourised by means of a heater element of 0,035 kW capacity, constructed from fine

Nichrome wire and installed within the capillary tube. The generator was capable of producing steam at the rate of 0,01 g/s.

The rate at which water was supplied to the generator was measured by means of a mini flow-meter that had previously been developed by Heyman and Hodgson⁶⁰⁾.

Mini flow meter

Figure 23 presents a cross-sectional view through the mini flow-meter.

Basically the flow-meter consists of an electrical heater element constructed from 40 SWG constantan wire and two copper-constantan thermocouples mounted in a glass tube. The entire assembly is mounted in an evacuated silvered glass housing to minimise heat losses.

During the operation of the flow-meter, the heat input rate by the electrical heater element incorporated in the flow-meter is maintained constant and the flow rate is determined from measurements of the temperature increase of the water passing over the heating coil.

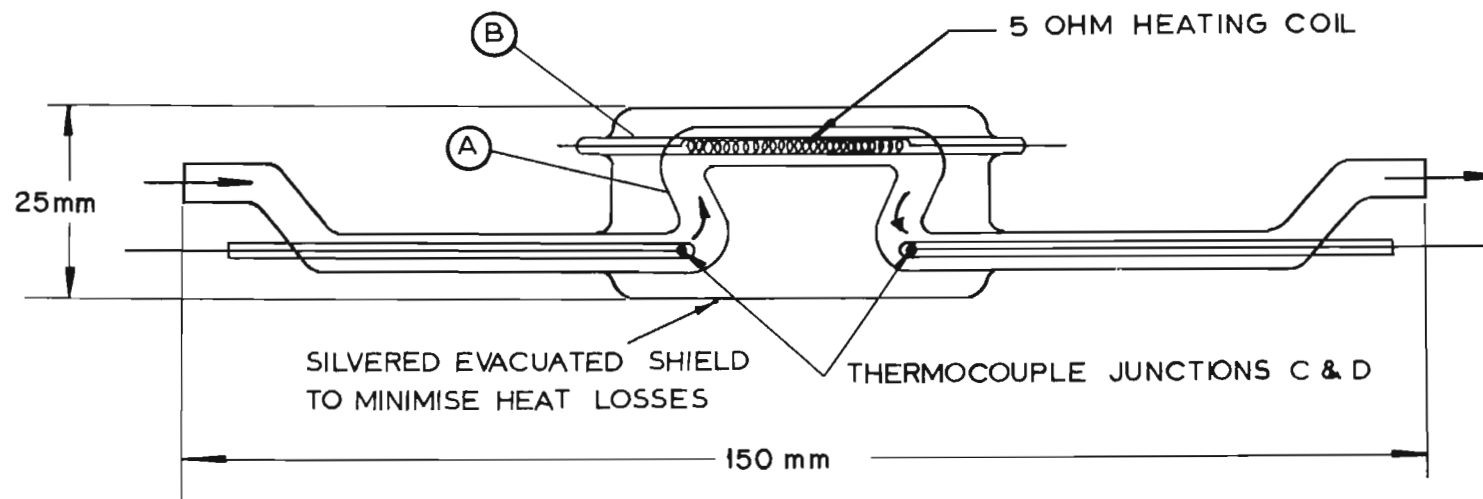


FIGURE 23

Mini flow-meter for the accurate measurement of the mass flow rate of water supplied to the steam generator

With the aid of the mini flow-meter and the vapour generator, a known amount of water vapour could be introduced into the wake of the body at a predetermined rate.

A similar flow-meter and vapour generator was used for introducing measured rates of steam into the main "evaporating" body.

Air-sampling probes and humidity-sensing system

Air-sampling probes were installed at the positions marked a and b in Figure 21 to enable the humidity increase in the wake of the body to be measured by means of the differential electrical resistance hygrometry system of measurement outlined in Section 4.3.4 on page 142.

The air samples were drawn through a double circuit heat exchanger (to equalize their dry-bulb temperatures at a value above the dew-point temperature of the air) and over the two Aminco electrical resistance hygrometers in turn, with the aid of a vacuum pump. By connecting the two hygrometers to a suitable bridge network and recording

the differential output on a Kipp Micrograph type BD-597 recorder a direct reading of the difference in specific humidity between the two air samples could be obtained.

The values of water vapour loss rate thus obtained were compared to the water flow rate to the main body's steam generator as measured with the mini flow-meter.

The air-sampling probe, b, was in the form of a tube with a series of fine sampling holes along the length of the tube. The tube was mounted in a similar manner to a pendulum to permit sampling of the entire wake area by swinging the tube through the wake.

Test results

Figures 24 and 25 present calibration and response time curves for the mini flow-meter.

Figure 26 presents the response of the differential hygrometer during a typical test. In this particular test, steam at the rate of 0,006 g/s, was injected into the wake of the "evaporating" body for a period of 180 s.

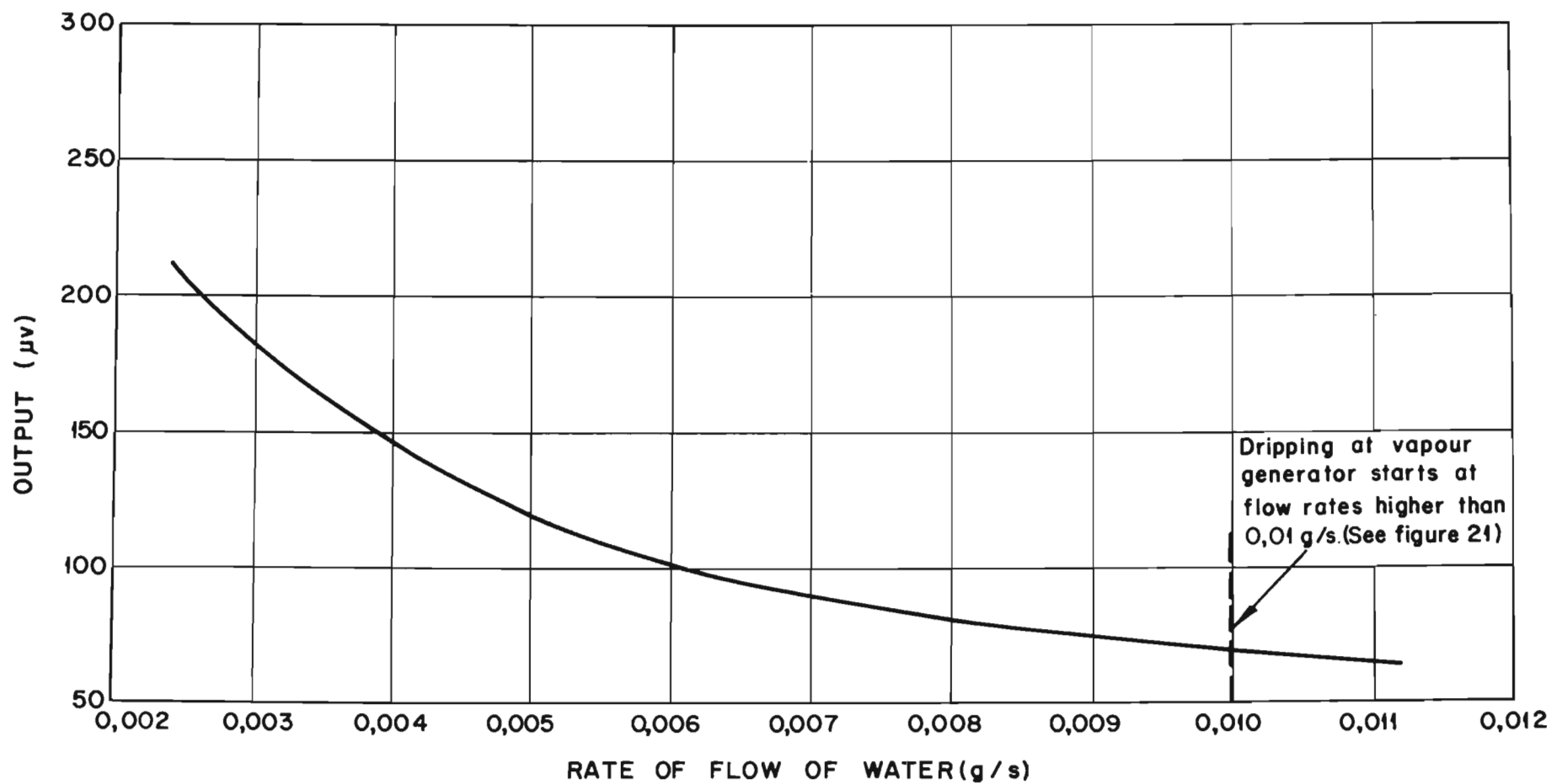


FIGURE 24

Output of the mini flow-meter as a function of the rate of flow of water.

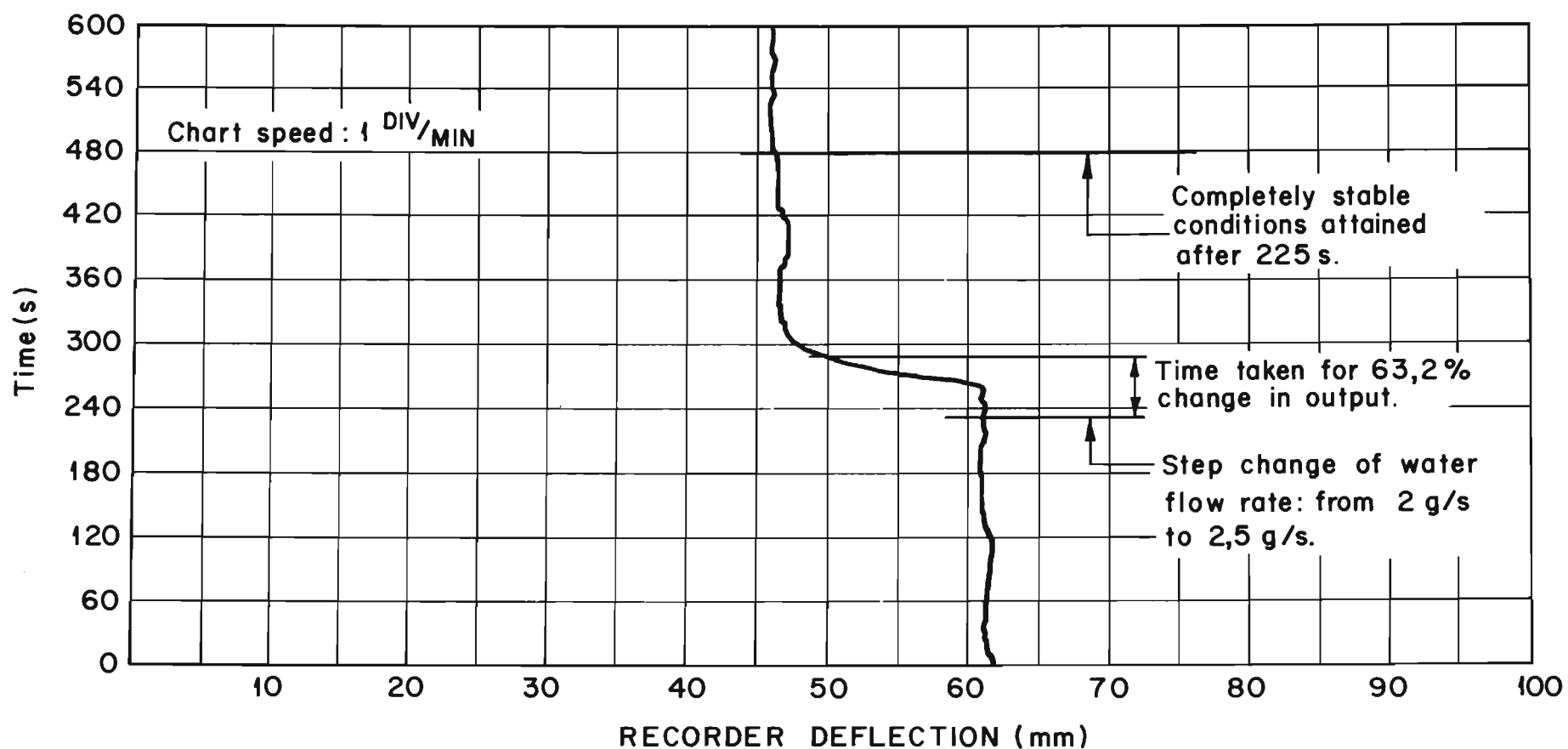
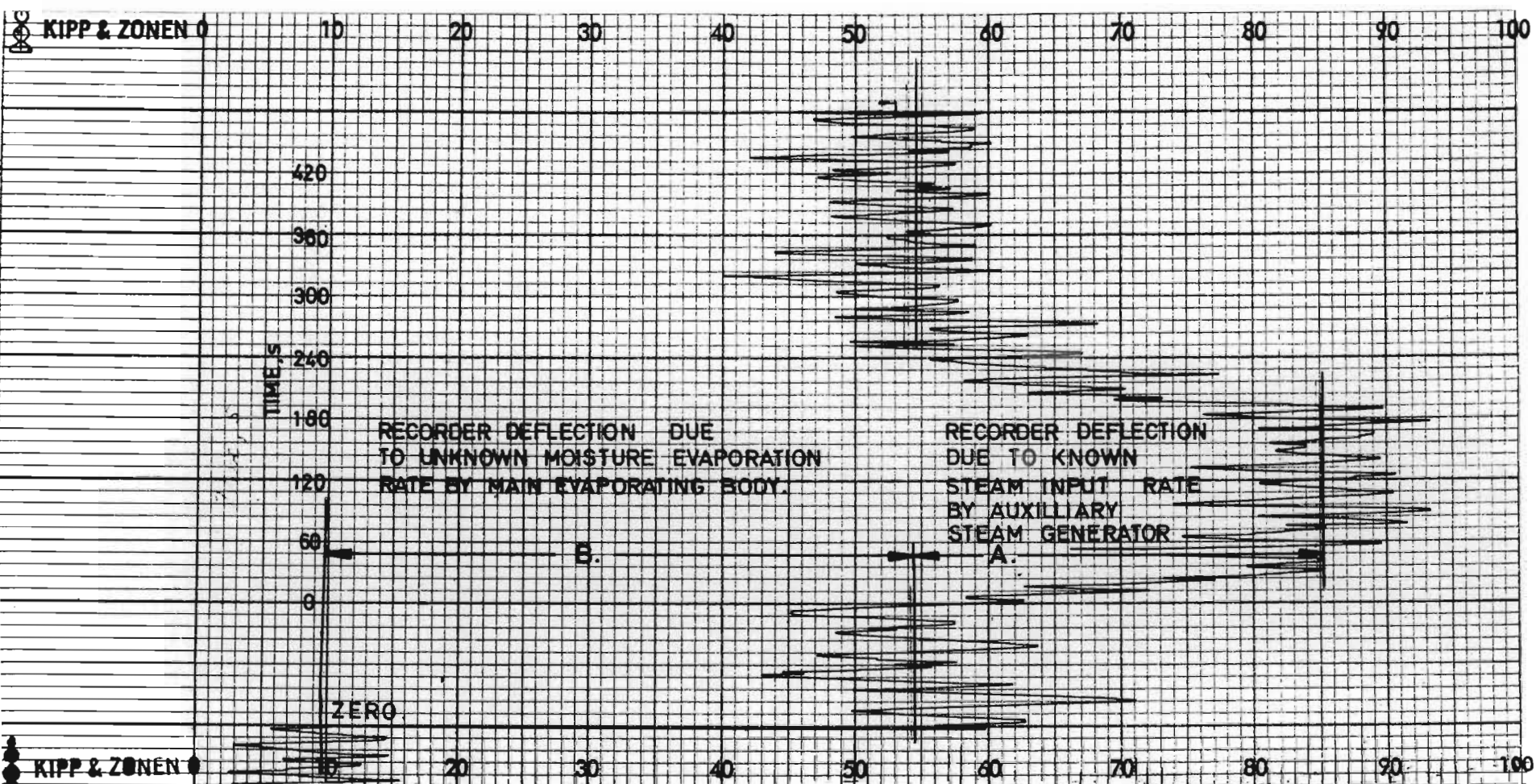


FIGURE 25
Section of the recorder chart showing the rate of response of the mini flow-meter.



- NOTE: 1. Test conditions: (i) Air velocity: 0,5 m/s
(ii) Steam input rate by steam generator; 0,006 g/s.
2. Recorder sensitivity: 1,0 mV

FIGURE 26

Model evaporative heat loss tests: investigations into the comparative method of determining the evaporative heat loss rate from a test body; recorder deflections due to the humidity increase in the wake of the test body.

In Figure 27 the output of the differential hygrometer is plotted as a function of the steam input rate to the main body in the test section of the wind tunnel. From the data it is evident that the output of the differential hygrometer is linearly related to variations in the steam input rate to the "evaporating" body.

In the comparative system of measurement the evaporative heat loss rate from the body is calculated from equation (20) on page 112.

$$\dot{q}_e / \dot{q}_{e,aux} = \overline{\Delta w}_w / \overline{\Delta w}_{w,aux}$$

where \dot{q}_e = evaporative heat loss rate from the body, kW

$\dot{q}_{e,aux}$ = known latent heat input rate by the auxiliary steam generator, kW

and $\overline{\Delta w}_w, \overline{\Delta w}_{w,aux}$ = mean increases in specific humidity due to the unknown water vapour "loss" rate from the "evaporating" body and the known steam input rate by the auxiliary steam generator, respectively, kg/kg

Assuming the latent heat of evaporation, l , to be the same for the water evaporated by the main body's water

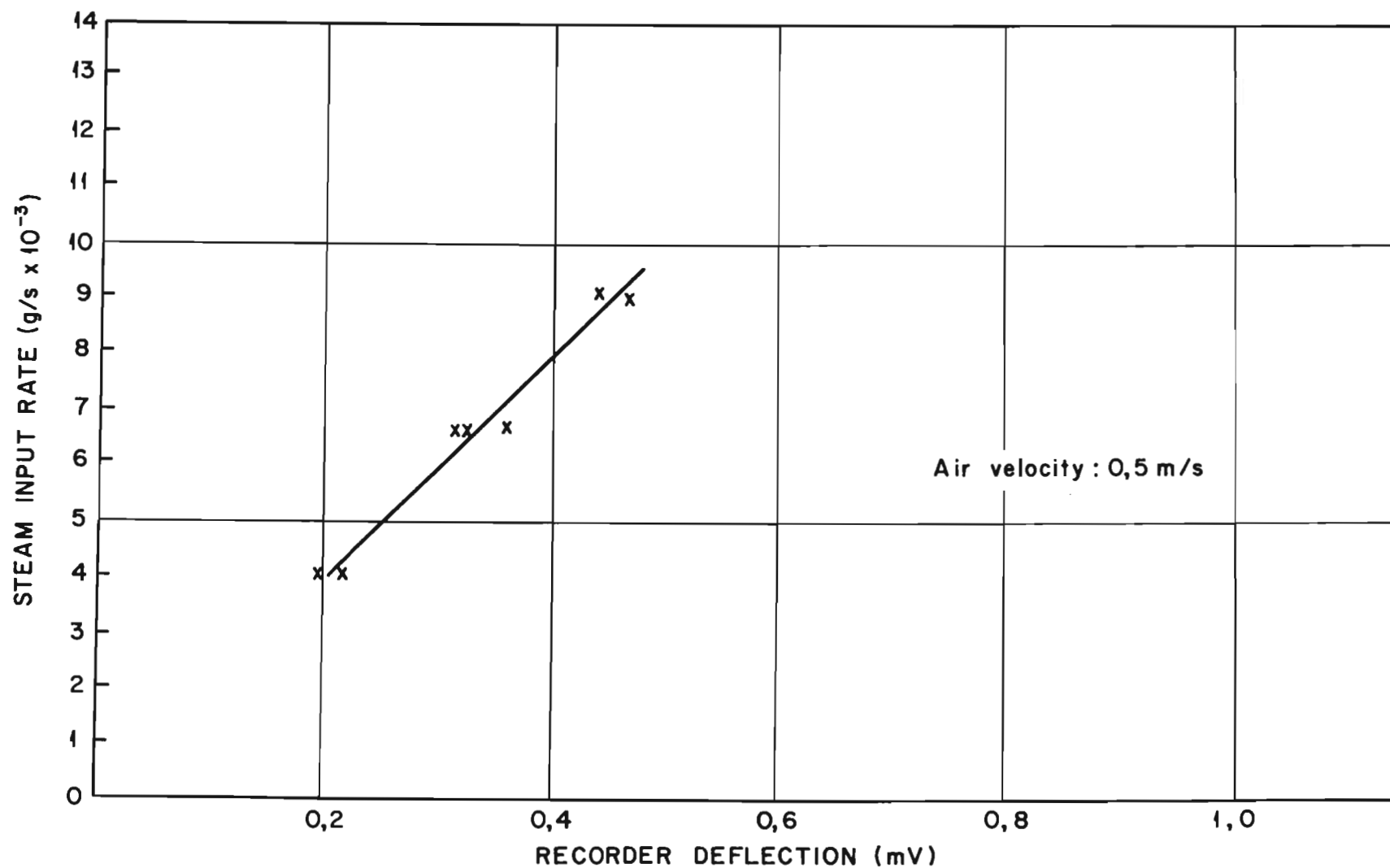


FIGURE 27

Model evaporative heat loss tests: recorder deflection as a function of the steam input rate by the auxiliary steam generator. (see figure 21)

vapour generator and the auxiliary vapour generator,
the above-mentioned equation can be written
as:

$$\begin{aligned}\dot{q}_e / \dot{q}_{e,aux} &= \dot{m} \ell / \dot{m}_{aux} \ell \\ &= \dot{m} / \dot{m}_{aux} \quad \dots\dots\dots (27)\end{aligned}$$

where \dot{m}, \dot{m}_{aux} = mass transfer rates for the main and
auxiliary bodies, respectively, kg/s

From a comparison of equations (18) and (27) it is evident
that, for a constant mass flow rate of air through the
test section, ΔW_w and $\Delta W_{w,aux}$ are directly proportional
to the vapour "loss" rate from the "evaporating" body and
the steam input rate by the auxiliary water vapour
generator, respectively.

Since the output of the differential hygrometer is
linearly related to the steam "input" rate to the test section
and hence ΔW_w and $\Delta W_{w,aux}$ (for a given air velocity)
equation (28) may be rewritten as:

$$\dot{m} / \dot{m}_{aux} = B/A \quad \dots\dots\dots (28)$$

where B and A are the recorder deflections due to the
"moisture evaporation" rate from the main body and the
known steam input rate by the auxiliary steam generator,
respectively.

In the test results presented in Figure 26, the recorder deflections B and A were found to be $(55 - 10) = 45$ and $(95 - 55) = 40$, respectively. Substitution of the values for the recorder deflections in equation (28) leads to:

$$\begin{aligned}\dot{m} &= \dot{m}_{\text{aux}} \times (55 - 10)/(95 - 55) \\ &= 1,28 \dot{m}_{\text{aux}}\end{aligned}$$

Since $\dot{m}_{\text{aux}} = 0,006 \text{ g/s}$ for this particular test,

$$\begin{aligned}\dot{m} &= 1,28 \times 0,006 \\ &= 0,00768 \text{ g/s}.\end{aligned}$$

Values for the vapour "loss" rate from the main body under other test conditions were calculated in a similar manner.

Figure 28 presents a graph of the vapour "loss" rate from the main body (as determined by means of the comparative method) versus the actual steam injection rates to the main body for air velocities of 0,5 m/s and 1 m/s.

In general, the vapour "loss" rate could be determined within 10% by means of the comparative technique. The accuracy of measurement appeared to be unaffected by velocity.

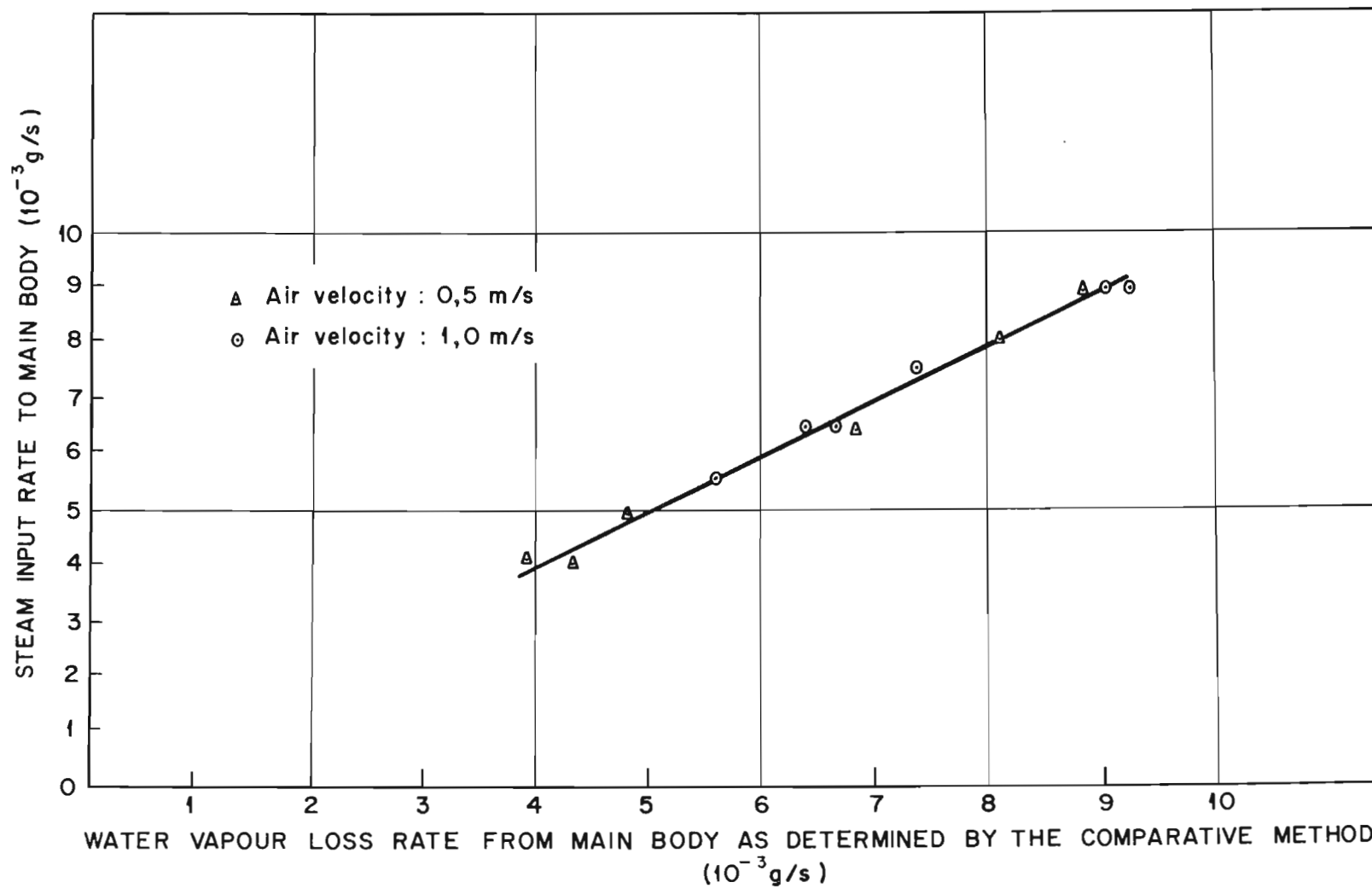


FIGURE 28

Model evaporative heat loss studies : steam input rate to the main body versus the water vapour loss rate from the main body as determined by the comparative method.

4.5.3 Choice of evaporative heat loss measuring system

As mentioned in Section 4.2 on page 113, the required accuracy for the evaporative heat loss measuring instrument is 15%.

During model evaporative heat loss studies it was found that the evaporative heat loss rate from a cylindrically shaped body could be measured to within 15% and 10% by means of the analogy and comparative techniques, respectively. (See the last paragraphs of Sections 4.5.1 and 4.5.2 on pages 163 and 178).

The required accuracy can thus be obtained with both systems of measurement.

However, the comparative method of measurement is preferred in view of (i) the higher accuracy attainable with such a system compared with the analogy system of measurement and (ii) the fact that the evaporative heat loss rate from a body can be determined without the need for measuring the convective heat loss rate by this means.

4.6 Details of the evaporative heat loss measuring instrument

The evaporative heat loss measuring instrument is to be used for measuring the evaporative heat loss rate from a working subject in the 3 m x 3 m x 3 m horizontal test chamber of the climatic chamber of the Human Sciences Laboratory.

For the purpose of providing a suitable work load on the subject a bicycle ergometer is mounted in the centre of the test chamber. The subject performs various rates of work by pedalling the bicycle ergometer which is suitably designed to enable the work rate of the subject to be measured relatively easily. Additional facilities are provided to enable physiologists to investigate the effect of exercise on the physiological response of the subject.

The evaporative heat loss measuring instrument must, therefore be suitable for measuring the evaporative heat loss from a subject positioned on the bicycle.

Figure 29 presents a diagrammatic layout of the proposed evaporative heat loss measuring system.

Basically the system consists of two air-sampling probes for sampling the air on the upstream and downstream sides of the body, a double circuit heat exchanger for equalising the dry-bulb temperatures of the two air samples and a differential humidity-

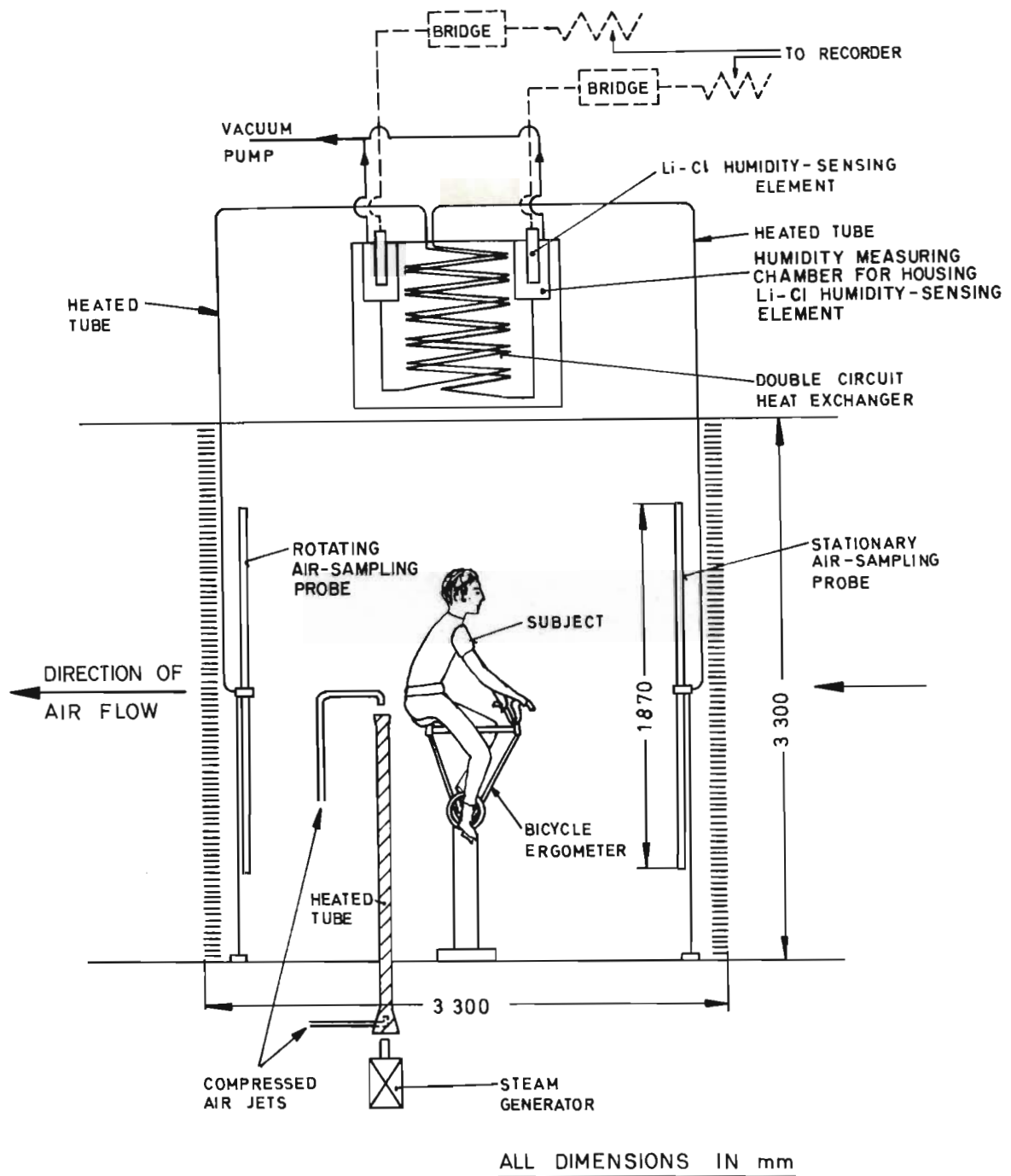


FIGURE 29
*Schematic layout of the differential hygrometer
 for measuring the evaporative heat loss rate
 from a human subject*

measuring system for measuring the difference in humidity between the two air samples. In addition, a steam generator is provided for introducing a known amount of steam into the wake of the body at a predetermined rate.

4.6.1 Design considerations

One of the major prerequisites for the air-sampling probe on the downstream side of the body (which traverses the wake in a plane at right angles to the general direction of air flow), is that it should sample the full cross-sectional area of the wake.

During the tests referred to in Section 4.2 on page 116, it was found that the wake of a standing man in the centre of the chamber would have an area of $1,5 \text{ m}^2$ in the plane of measurement. Although the wake area of a subject on the bicycle ergometer would be somewhat less, due to the subject being in a slightly crouched position, it was, nevertheless, decided that the downstream probe should be capable of traversing a wake area of at least $1,5 \text{ m}^2$.

In the proposed method of measuring the humidity increase in the wake of the body, the air samples from the upstream and downstream sides of the body are drawn through a double

circuit heat exchanger (to equalise their dry-bulb temperatures) and over two electrical resistance hygrometers in turn. By connecting the two hygrometers to a suitable bridge network and recording the differential output on a Kipp Micrograph recorder, a direct reading of the difference in specific humidity between the two air samples is obtained.

In such a system the accuracy depends, inter alia, on the extent to which the dry-bulb temperatures of the two air samples are equalised.

It was shown in Section 4.5.1 on page 162 that, if the specific humidity is determined from measurements of the dry-bulb temperature and relative humidity of the air, an error in the measurement of the dry-bulb temperature of $0,01^{\circ}\text{C}$ can cause an error in the determination of specific humidity of $\pm 20\%$. Similarly, in the proposed method of measurement, a temperature difference of $0,01^{\circ}\text{C}$ between the two air samples could result in an error in the measurement of the humidity increase of $\pm 20\%$. This would be unacceptable since the required overall accuracy of measurement is 15% .

In order to reduce the errors of measurement that are caused by uncontrolled temperature differences between the two samples of air to 1%, say, under normal operating conditions, the double circuit heat exchanger must be capable of reducing the temperature difference between the two air samples to less than $0,01/20 = 0,0005^{\circ}\text{C}$.

4.6.2 Air-sampling rate

The air-sampling rate affects, inter alia, the response time of the humidity-measuring system as well as the basic design of the air-sampling probes and double circuit heat exchanger. Thus, one of the first steps in the design of the various components of the evaporative heat loss measuring instrument, in particular, the double circuit heat exchanger and the air-sampling probes, is the selection of a suitable air-sampling rate for the upstream and downstream air-sampling probes.

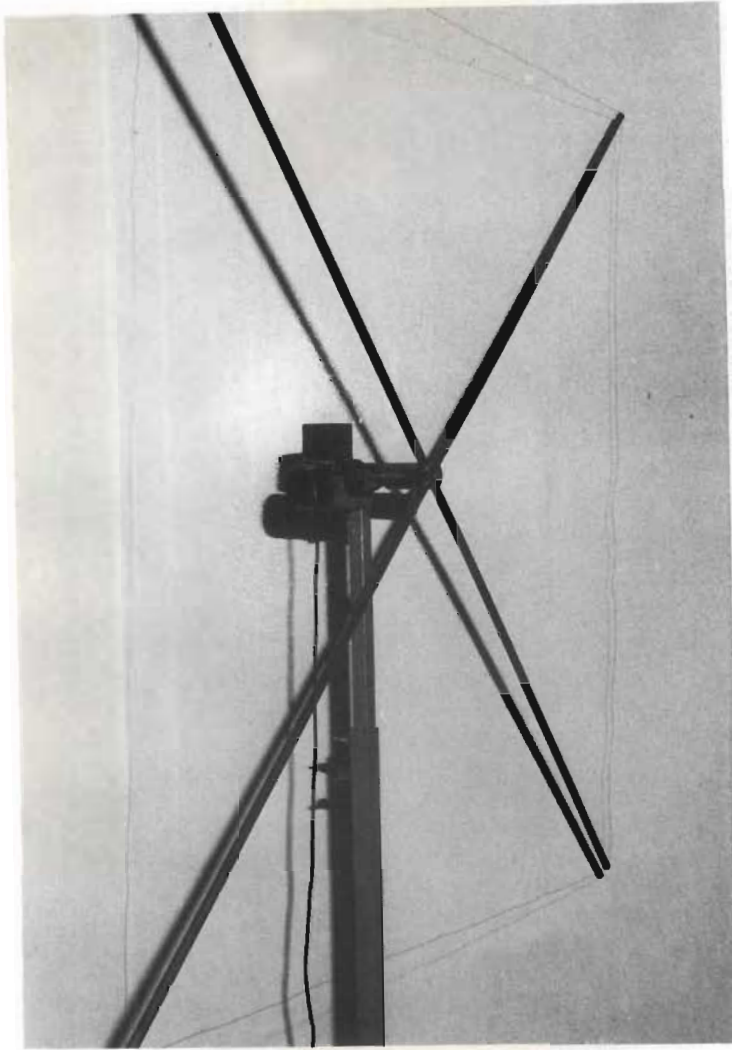
From a consideration of the response time of the instrument as well as the available capacity of the existing vacuum pump at the Human Sciences Laboratory, it was decided that the air should be sampled at the rate of $0,2 \times 10^{-3} \text{ m}^3/\text{s}$.

4.6.3 Air-sampling probes

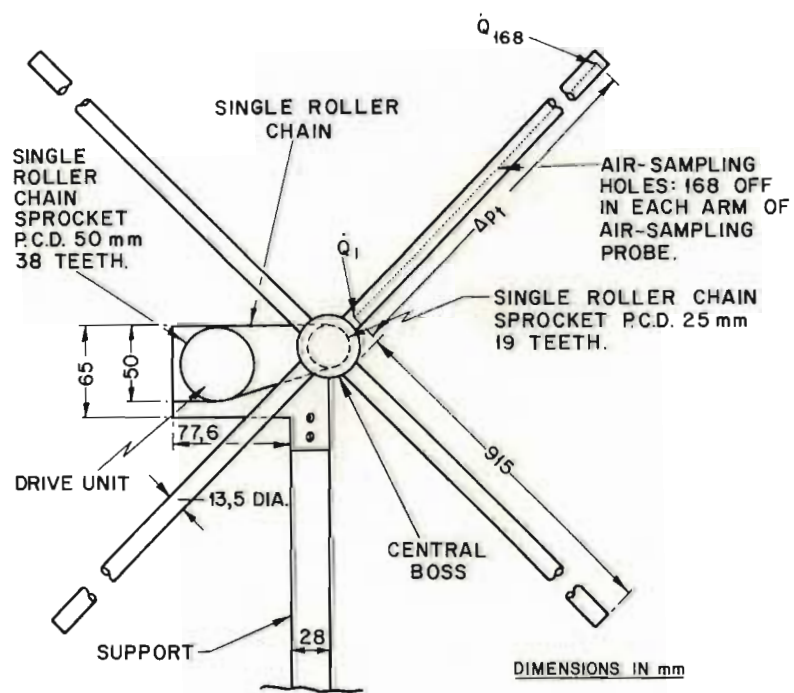
(a) Air-sampling probe on the downstream side of the body

In order to meet with the requirement that the air-sampling probe on the downstream side of the body should be capable of sampling a wake area of at least $1,5 \text{ m}^2$ to ensure that the full cross-sectional area of the wake is sampled, it was decided to construct the air-sampling probe on the downstream side of the body in the form of a cross which would rotate through the wake in a plane at right angles to the direction of the free air stream velocity and which would sample the air along the full length of each arm of the cross. Details of the air-sampling probe are presented in Figure 30.

The four arms of the probe were constructed from 13,5 mm diameter brass tubing with a tip-to-tip length of 1,87 m. The sampling "area" is thus $\pi/4(1,87)^2 = 2,75 \text{ m}^2$ which is adequate. The tubes forming the four arms of the probe were mounted at right angles to each other on a central boss and a series of relatively small holes, 0,343 mm diameter, were drilled along the length of each tube for the purpose of sampling the air; the total number of holes being selected to give a reasonable velocity of between 3 and 4 m/s through the holes.



a) View of the rotating air-sampling probe.



b) Dimensional details of rotating air-sampling probe

FIGURE 30

The mean air velocity through the holes is given by the following equation:

$$\dot{v} = \dot{Q}/nA \quad \text{..... (29)}$$

where \dot{v} = air velocity through each hole, m/s

and \dot{Q} = total air flow rate, $0,2 \times 10^{-3}$, m³/s

n = total number of sampling holes

A = cross-sectional area of each sampling hole

$$= \pi(0,343 \times 10^{-3})^2/4 = 0,0924 \times 10^{-6} \text{ m}^2$$

Assuming the total number of holes to be 672, say, the average air velocity through each hole is

$$\begin{aligned} \dot{v} &= 0,2 \times 10^{-3} / 672 \times 0,0924 \times 10^{-6} \\ &= 3,24 \text{ m/s, which is reasonable.} \end{aligned}$$

Since the air-sampling probe has four arms, the total number of holes in each arm of the probe is $672/4 = 168$.

The holes were distributed along the length of each arm of the probe in such a manner that the number of holes in each section of the arm was proportional to the radius of the circular path the section of the probe traverses and the length of the particular section of the probe.

$$\text{Thus } n_x \propto r_x L_x$$

where n_x = number of holes in a particular section x
of one of the arms of the probe

and r_x = mean radius of the path each section x of the arm
would traverse as the arm rotates, and

L_x = length of the section x of the arm.

The position of the holes along the length of each of
the four arms is given in Table 8.

TABLE 8 : DIFFERENTIAL HYGROMETER FOR MEASURING THE EVAPORATIVE HEAT
LOSS FROM A HUMAN BODY : POSITIONING OF THE AIR-SAMPLING
HOLES ALONG THE LENGTH OF EACH OF THE FOUR ARMS OF THE
ROTATING AIR-SAMPLING PROBE

Note : Total number of holes in each arm is 168

Diameter of each sampling hole : 0,343 mm

LENGTH OF SECTION OF PROBE (mm)	MEAN RADIUS OF THE AREA WHICH THE SECTION OF THE PROBE TRAVERSES (mm)	NUMBER OF HOLES IN EACH SECTION	CENTRE DISTANCE OF HOLES (mm)
140	90	5	28,0
70	195	5	14,0
70	265	7	10,0
70	335	9	7,8
70	405	11	6,3
70	475	13	5,0
70	545	15	4,4
355	750	103	3,5
TOTAL :		168	

Based on the assumption that the air flow rate through each of the air-sampling holes is the same, the proposed distribution of holes along the length of each of the arms of the rotating air-sampling probe would ensure that the total air-sampling rate through each section of the probe is proportional to the area traversed by the particular section of the probe.

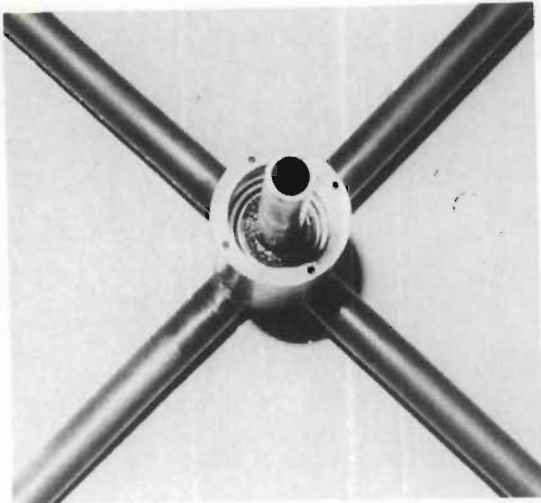
Calculations were subsequently carried out to determine to what extent the air flow rate through each of the air-sampling holes can be expected to vary from each other.

The analysis is described in Appendix E. It was shown that, under the assumed conditions of air flow, the respective air flow rates through each of the air-sampling holes can be expected to be within 4.9% of each other, which is acceptable.

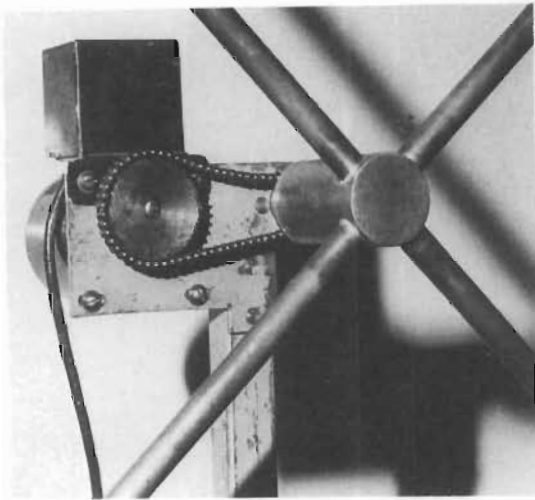
Constructional details of the rotating air-sampling probe on the downstream side of the body

Figure 31 presents views of the central boss of the rotating air-sampling probe.

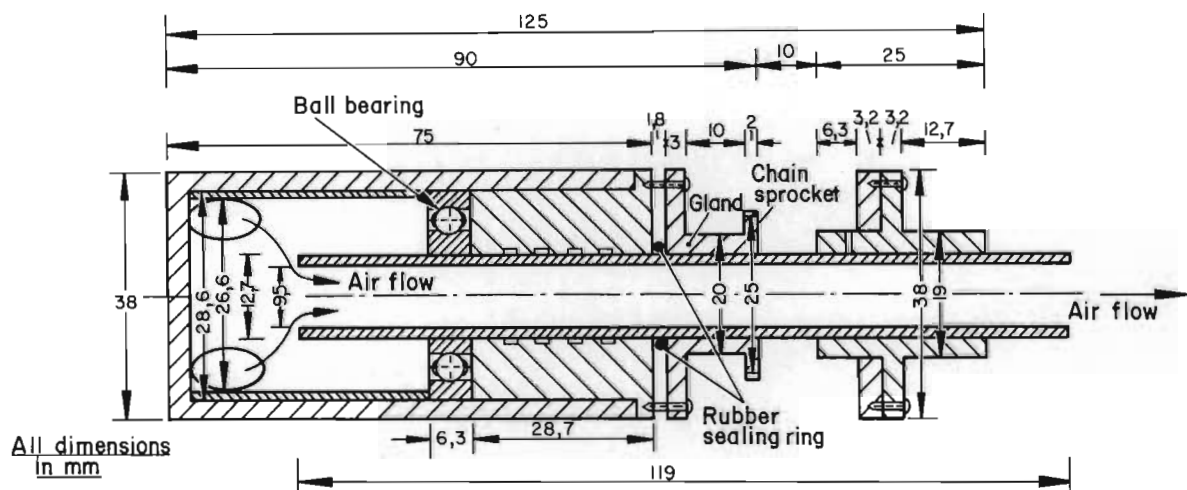
It is seen that the four arms of the probe are connected to a hollow housing which rotates around a central suction



(a) View of housing with the gland removed (see the cross-sectional view through the central boss).



(b) View of the drive unit



(c) Cross-sectional view through the central boss of the air-sampling probe

FIGURE 31

Evaporative heat loss measuring instrument: view of the central housing and drive unit of the rotating air-sampling probe in the wake of the subject

tube which is stationary; the housing being mounted on a ball bearing which is fixed to the suction tube. A gland and O-ring sealing arrangement is provided to minimise the leakage of air into the housing along the outer surface of the stationary suction tube.

The sample air from the four sampling tubes thus flows through the central housing and into the stationary tube which in turn is connected to one of the copper coils in the double circuit exchanger.

The arm is rotated at the rate of 0,07 Hz, by means of a Berger type RSM 64 NG, 220v 50 Hz electric motor which runs at a speed of 0,035 Hz. The drive unit consists of a single roller chain drive together with suitable sprockets on the motor and sampling probe (see Figure 31b).

(b) Air-sampling probe on the upstream side of the body

The construction of the arms of the air-sampling probe on the upstream side of the body is similar to the arms of the downstream probe. However, the upstream probe is mounted in a fixed position and does not rotate. The four arms of the upstream air-sampling probe are thus connected directly to the central suction tube.

4.6.4 Double circuit heat exchanger

The major function of the double circuit heat exchanger is to ensure that the respective dry-bulb temperatures of the two air samples which are drawn through the air-sampling probes on the upstream and downstream side of the body, are equalised at a temperature which is higher than the maximum dew-point temperature (to prevent the condensation of moisture within the heat exchanger).

Basically, the double circuit heat exchanger consists of two helical copper coils mounted in a constant temperature water bath; the one coil being connected to the air-sampling probe on the downstream side of the body and the other to the probe on the upstream side of the body as shown in Figure 29 on page 182.

After circulating through the copper coils, the air samples enter the two cylindrically shaped humidity-measuring chambers in which the lithium chloride humidity-sensing elements are housed.

As a first step in the design of the double circuit heat exchanger, calculations were carried out to determine the lengths of the coils that would be required in order to

reduce the initial temperature difference between the two air samples to less than $0,0005^{\circ}\text{C}$. (See Section 4.6.1 on page 185).

The maximum temperature increase in the wake of a human body in the horizontal test section of the climatic chamber can be expected to be of the order of 2°C^{61}).

The heat exchanger must thus be capable of reducing the temperature difference between the two air samples from 2°C to $0,0005^{\circ}\text{C}$. From a preliminary analysis of the problem it appeared that this requirement could be met if each coil were to be constructed from copper tubing with an inside diameter of 7,5 mm say, and a nominal length of 16 m.

Based on the following assumptions, check calculations were then carried out to determine whether such a heat exchanger would, in fact, be satisfactory:

- (i) Water temperature in the constant temperature bath : 40°C
- (ii) Air flow rate through each copper coil : $0,2 \text{ m/s}$

(iii) Coil data

Material	: Copper
Tube diameter	: 9,52 mm outside
	: 7,5 mm inside
Mean coil diameter	: 355 mm
Number of coils	: 14

(iv) Velocity of water across

the coils : 0,5 m/s

The calculations which are described in Appendix E, indicated that the double circuit heat exchanger would be capable of reducing an initial temperature difference between two air samples of 2°C to 0,0001°C which is well below the required value of 0,0005°C.

The heat exchanger is thus highly effective in equalising the temperatures of the two air samples on the upstream and downstream side of the body.

Figures 32 and 33 present exploded views of the double circuit heat exchanger.

The helical copper coils, through which the two air samples from the upstream and downstream side of the test subject in the test chamber are circulated, are fixed to

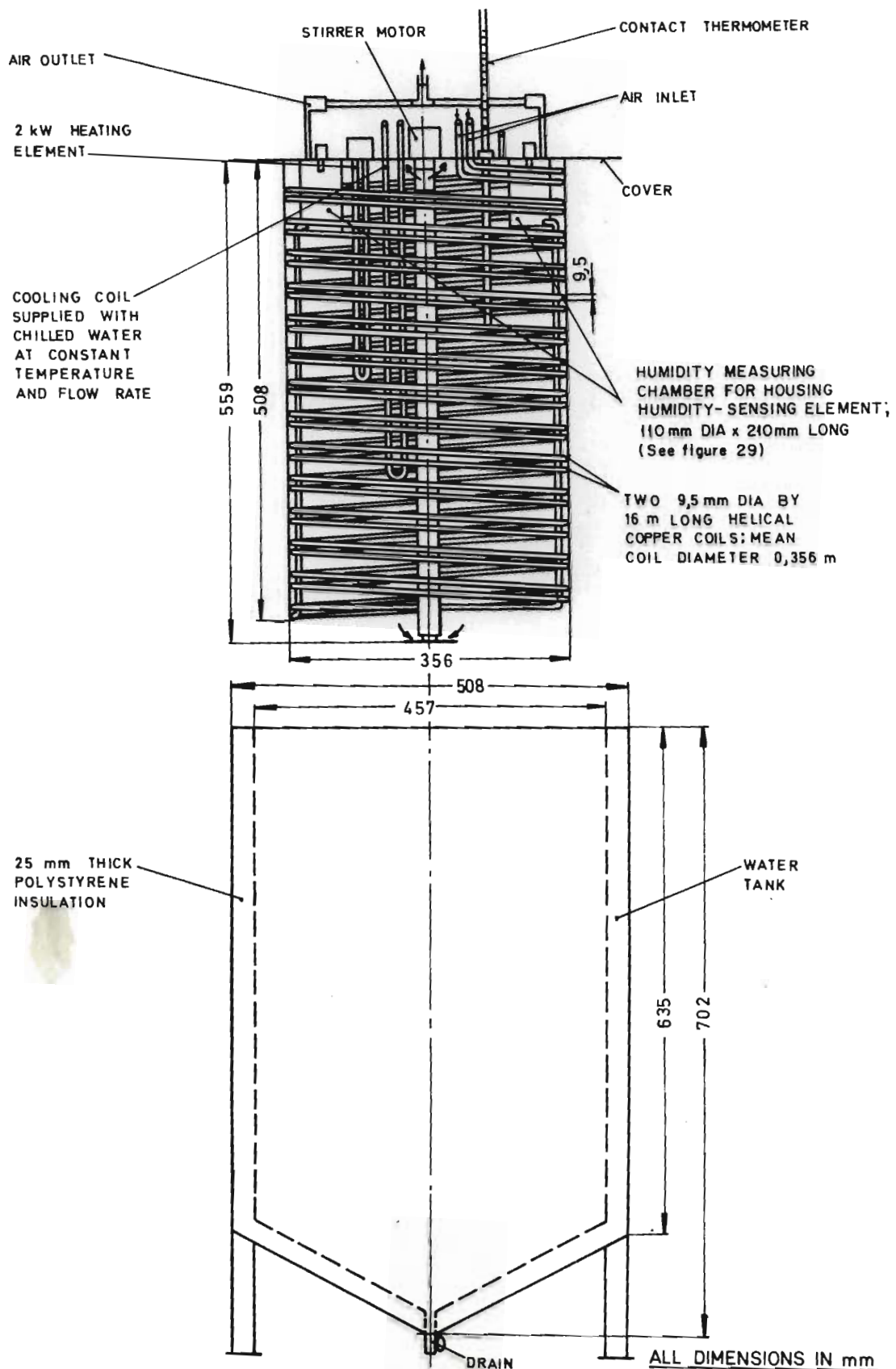


FIGURE 32

Differential hygrometer for the measurement of the evaporative heat loss rate from a human body: details of the double circuit heat exchanger.

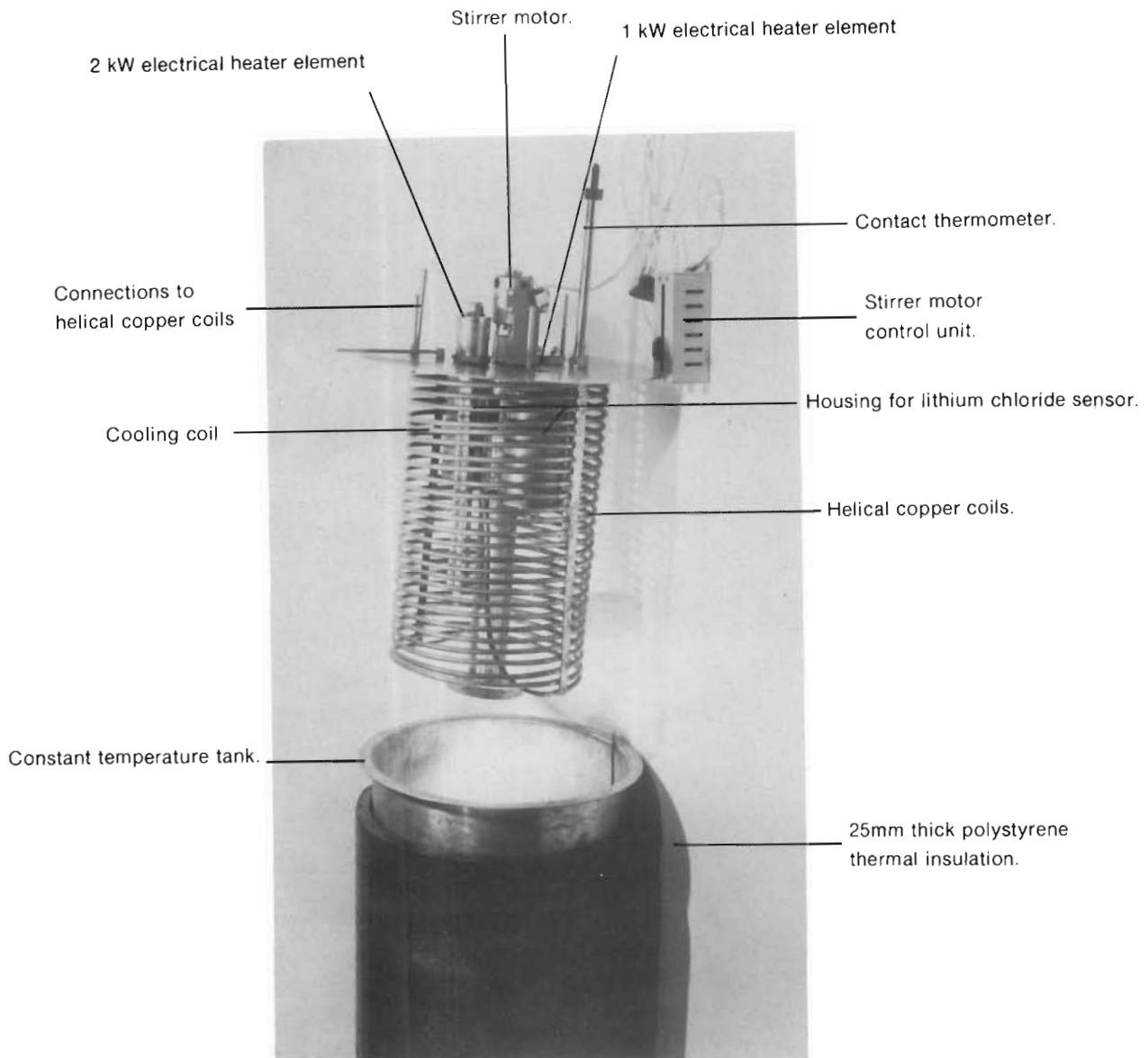


FIGURE 33

Differential hygrometer for the measurement of the evaporative heat loss rate from a human body: exploded view of the double circuit heat exchanger for the differential hygrometer.

the underside of the top cover of the constant temperature water bath.

The air samples enter the helical copper coils through tubes located in the top cover. After circulating through the copper coils, the air samples enter the two cylindrically shaped humidity-measuring chambers in which the lithium chloride humidity-sensing elements are housed. The humidity-measuring chambers are attached to the underside of the top cover of the constant temperature water bath and the two air samples are exhausted from the humidity-measuring chambers by means of a vacuum pump, through tubes passing through the top cover.

The constant temperature water bath, which is of the order of 460 mm diameter by 700 mm high, is equipped with a conical bottom with a valve at the lowest point to permit easy drainage of the water in the tank. The bath is thermally insulated with a 25 mm thick layer of polystyrene insulation.

Once the constant temperature water bath is filled with water and the lid is placed in position, the helical copper coils together with the humidity-measuring chambers

are completely submerged in the water. In view of the adverse effects which the leakage of water from the bath into the copper coils and/or the humidity-measuring chambers could have on the humidity measurements and hence the accuracy of the evaporative heat loss measurement, special precautions were taken during the manufacture of the double circuit heat exchanger to ensure that the coils and humidity-measuring chambers were completely watertight.

A stirrer is provided in order to ensure a reasonably uniform spatial temperature distribution within the bath. Basically the stirrer consists of an impeller which is mounted inside a 60 mm diameter by 600 mm long tube located in the centre of the helical copper coil assembly as shown in Figure 32. The impeller is driven by a motor which is installed on the top cover of the constant temperature water bath. During normal operation, the water is drawn into the top end of the stirrer tube and discharged from the bottom end.

A horizontal deflector plate is installed at a distance of 15 mm from the bottom end of the stirrer tube.

The top of the tube is suspended a short distance (of the order of 300 mm), from the top cover of the constant temperature water bath by means of suitable supporting brackets.

Humidity-measuring chambers

In the case of resistance hygrometers, such as the lithium chloride type, it is important that the air velocity across the sensing element should not be too high; preferably below 3 m/s. (High air velocities are not preferred in view of the erosion of the electrical resistance layer by dust particles that may be present in the air stream).

To achieve relatively low air velocity conditions both humidity-measuring chambers were constructed in the form of cylinders and each humidity-sensing element was mounted in the centre of the particular measuring chamber. The helical copper coils were then connected to the measuring chambers in such a way that the sample air from each coil entered each chamber tangentially near the bottom of the chamber. The air was exhausted from the top ends of the chambers through the cover of the constant temperature tank.

The air thus flowed around the humidity-sensing elements. In this way relatively low air velocities across the elements could be achieved whilst maintaining a satisfactory air flow pattern without any "dead pockets" which could adversely affect the response time of the measuring system.

Humidity-sensing system

The humidity-sensing system is identical to the differential hygrometry system incorporating commercial electrical resistance hygrometers that is described in Section 4.3.4 on page 142. The system is illustrated diagrammatically in Figure 29 on page 182.

The following description of the system is given for the sake of continuity:

Basically the system consists of two Aminco electrical resistance hygrometers and a Kipp Micrograph type BD-597 recorder. Each hygrometer indicating unit contains a built-in Wheatstone bridge network which provides a signal of 0 to 25 millivolts for a change in relative humidity of about 12 per cent. A potential divider is coupled across the output of the bridge network incorporated in each hygrometer (to compensate for small differences in the sensitivities of the two sensors) and the compensated differential output is recorded on the Kipp Micrograph recorder.

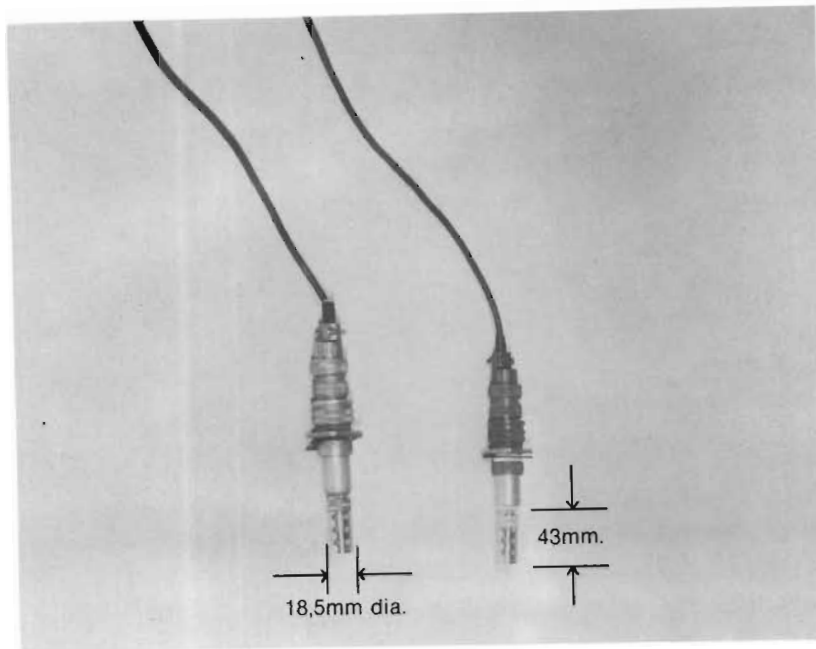
Two narrow range lithium chloride sensors with a range of 12 per cent relative humidity are used as the humidity-sensing elements. (See Figure 34a).

Each sensing element is mounted in the centre of the particular humidity-measuring chamber through a hole in the top cover; the sensors being clamped in position by means of a suitable clamping and locking device which also enables the particular range of sensor to be changed relatively easily. (See Figure 34b). Soft rubber gaskets are provided between the flanges of the humidity-sensing elements and the top cover to act as a seal.

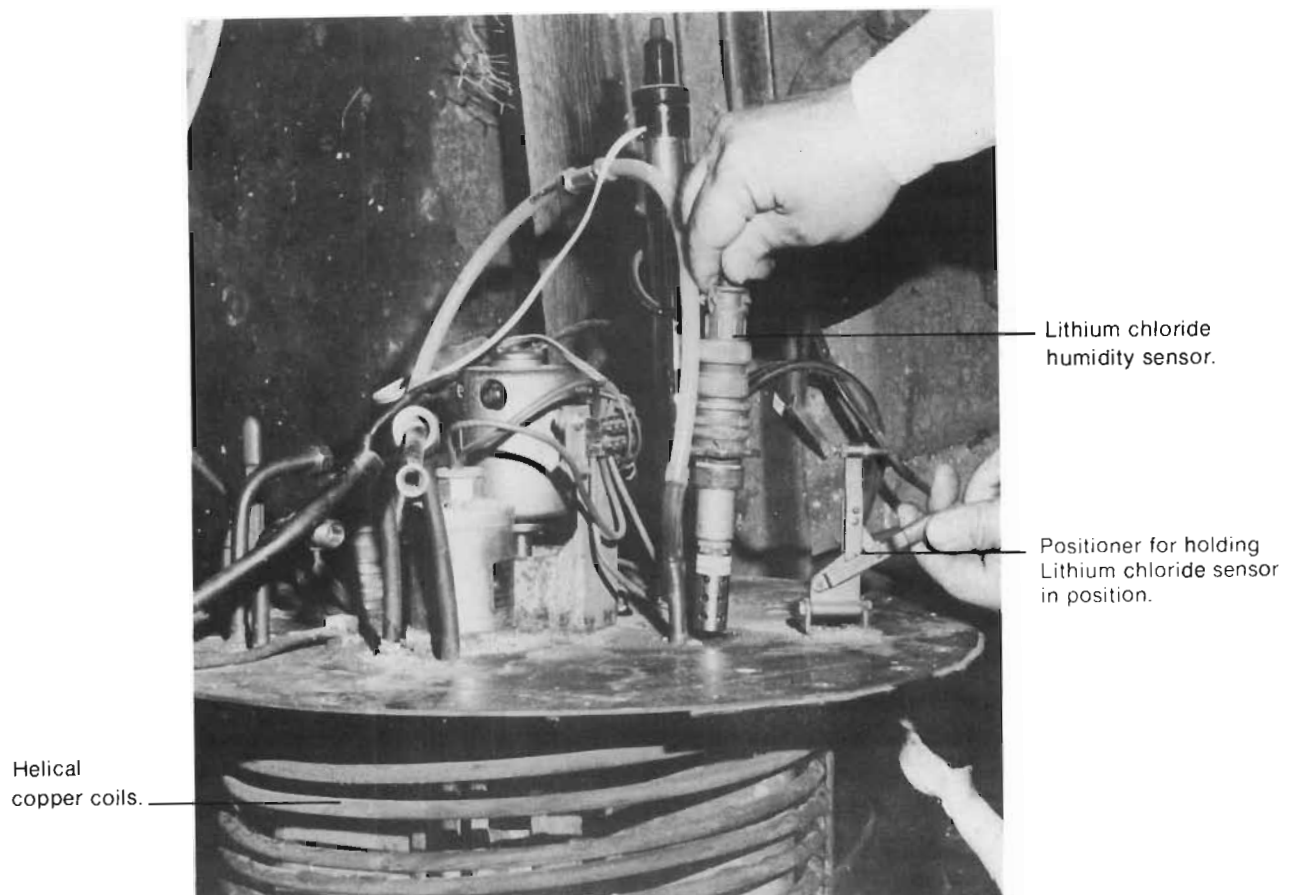
Temperature control system for the constant temperature water bath

Water temperatures within the constant temperature water bath are controlled by means of two electrical heater elements of 1 kW and 2 kW capacity and a 10 mm diameter by 800 mm long cooling coil (see Figures 33 and 35).

The 2 kW heater element is used to bring the tank temperature up to the desired value relatively quickly after a shut down. Thereafter temperatures are controlled by means of the 1 kW heater element and the



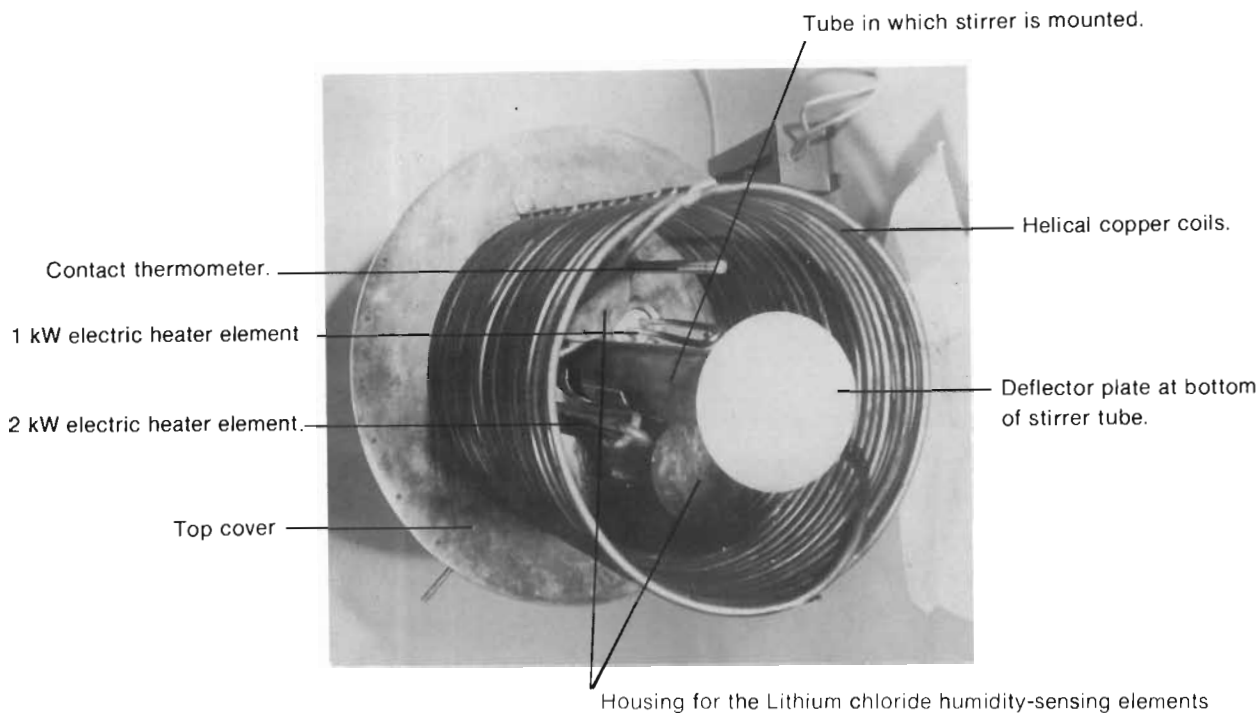
(a) View of the two lithium chloride humidity sensors.



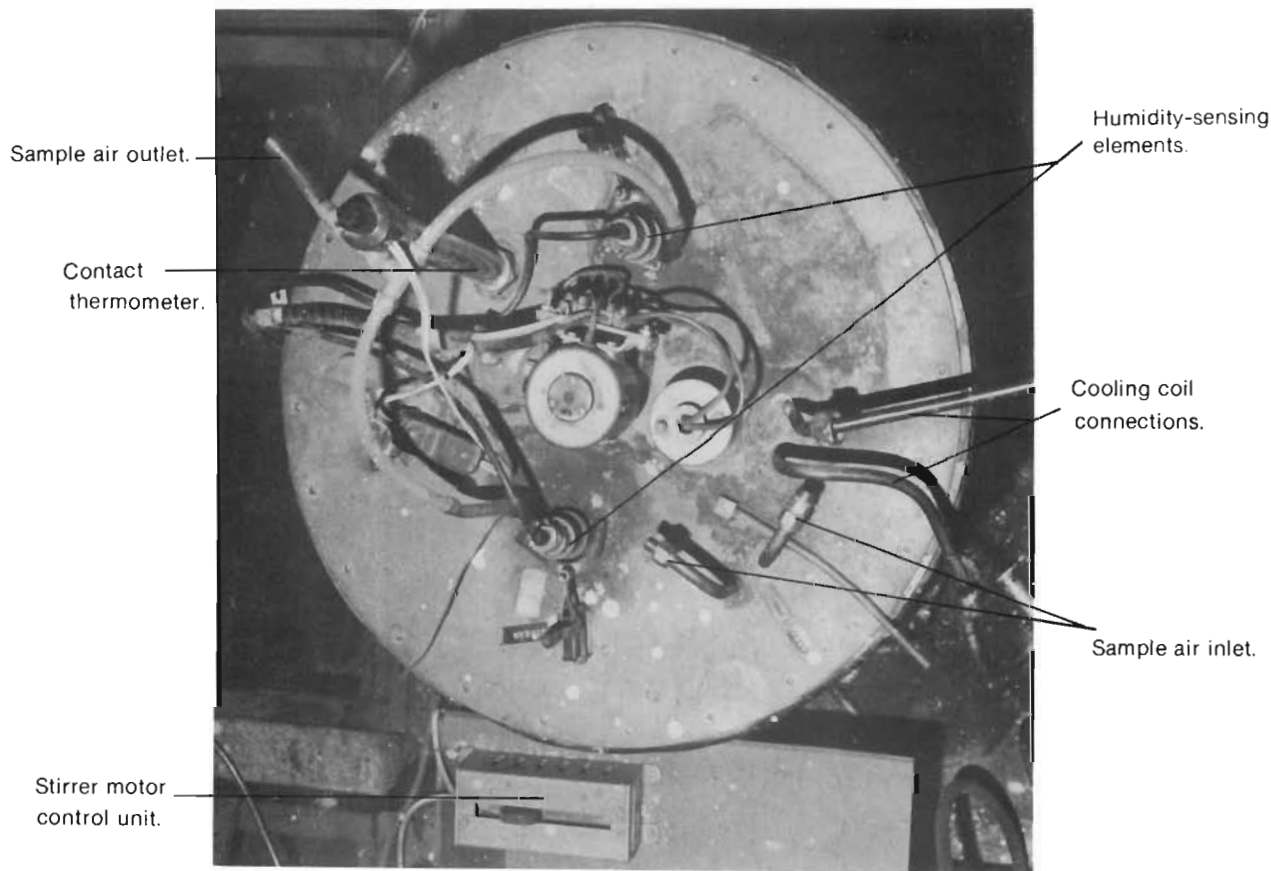
(b) View showing one of the lithium chloride humidity sensors being removed from a humidity-measuring chamber.

FIGURE 34

Differential hygrometer for the measurement of the evaporative heat loss rate from a human body: views of the lithium chloride humidity sensors.



(a) Inverted view.



(b) Top view

FIGURE 35

Differential hygrometer for the measurement of the evaporative heat loss rate from a liquid surface.

cooling coil.

On temperature rise within the tank, the 1 kW electrical heater element is automatically switched off by means of a contact thermometer and relay. On temperature fall within the tank the reverse action takes place. A variac is incorporated in the circuit to enable the voltage across the 1 kW heater element to be adjusted manually for the purpose of minimising the actual amplitude of temperature fluctuations during a control cycle.

Chilled water from the cold tank of the climatic chamber is circulated at a constant flow rate through the chilled water cooling coil incorporated in the constant temperature water bath of the differential hygrometry system in order to dissipate the energy input to the tank by the stirrer motor. (Since the tank is thermally insulated the water temperature would tend to increase continuously due to the latter factor unless some form of cooling is provided).

Water temperatures can be controlled at any value within the range 30°C to 90°C. In view of sensitivity and other requirements, the actual temperature control value is

selected to give a relative humidity condition within each measuring chamber of the order of 20 to 30 per cent. Under these conditions the water temperature would be considerably higher than the dew-point temperature of the air circulating through the double circuit heat exchanger and condensation is avoided.

Installation of the double circuit heat exchanger in the climatic chamber

The double circuit heat exchanger was installed above the horizontal test chamber of the climatic chamber; the helical coils in the heat exchanger being connected to the air-sampling probes in the test section by means of 10 mm diameter copper tubing.

In order to eliminate the possibility of moisture condensation within the tubes (this would occur whenever the temperature of the tubes dropped below the dew-point temperature of the air circulating through the tubes), all tube sections installed outside the climatic chamber were heated by means of heater tapes wound around the tubes.

As mentioned in Section 4.2 on page 119, the increase in the dew-point temperature of the air flowing over the subject is relatively small, of the order of $0,24^{\circ}\text{C}$, even under

high evaporative conditions.

Assuming the increase in the dew-point temperature to be 1°C say, to be on the safe side and the initial dew-point temperature in the climatic chamber to be relatively high, say 53°C (this could be the case under extreme conditions when the dry-bulb temperature is 55°C and the relative humidity is 92 per cent), the dew-point temperature of the air entering the air-sampling probe on the downstream side of the subject would be $1 + 53 = 54^{\circ}\text{C}$.

The inter-connecting tubes between the double circuit heat exchanger and the air-sampling probes must thus be heated to a temperature value above 54°C to prevent condensation under these conditions.

The minimum heat input rate to the heater tape which is wound around the tube to heat the inter-connecting tubes to a sufficiently high temperature, was calculated by means of the following equations:

$$\dot{H}_{ht}'' = h_{c,t,i} \Delta t_{t,i-G} + h_{c,t,o} \Delta t_{t,o-G} \dots (30)$$

and according to McAdams⁶²).

$$h_{c,o} = 0,04 \Delta t_{t,o-G} / D_{t,o}^{0,25} \dots (31)$$

where \dot{H}_{ht}'' = heat input rate by the heater tape per unit area of tube surface, W/m^2

$h_{c,t,i}, h_{c,t,o}$ = inside and outside film coefficients of heat transfer, respectively, $W/m^2 \text{ } ^\circ C$

$\Delta t_{t,i-G}, \Delta t_{t,o-G}$ = respective temperature differences between the tube and the air flowing through the tube and the ambient air, $^\circ C$

$D_{t,o}$ = outside diameter of the tube, $9,5 \times 10^{-3} \text{ m}$

Assuming the inter-connecting tubes to be heated to a temperature of $60^\circ C$, say, the temperature of the air within the tubes to be $55^\circ C$, and the ambient temperature to be $10^\circ C$, $\Delta t_{t,i-G} = 60 - 55 = 5^\circ C$ and

$$\Delta t_{t,o-G} = 60 - 10 = 50^\circ C.$$

Substitution of the latter value for $\Delta t_{t,o-G}$ in equation (31) leads to

$$\begin{aligned} h_{c,t,o} &= 1,3 (50/0,0095)^{0,25} \\ &= 11 \text{ W/m}^2 \text{ } ^\circ C. \end{aligned}$$

For the purpose of the present analysis the value for the inside film coefficient of heat transfer, $h_{c,t,i}$ was

assumed to be equal to $5,48 \text{ W/m}^2 \text{ } ^\circ\text{C}$; the value calculated for the helical copper coils in the double circuit heat exchanger (see Section 1 of Appendix F on page 453).

Substitution of the above-mentioned values for

$h_{c,t,i}$, $h_{c,t,o}$, $\Delta t_{t,i-G}$ and $\Delta t_{t,o-G}$, in equation (30) leads to:

$$\begin{aligned}\dot{H}''_{ht} &= 5,48 \times 5 + 11 \times 50 \\ &= 577,4 \text{ W/m}^2.\end{aligned}$$

This corresponds to a minimum heat input rate per metre length of tubing of

$$\dot{H}'_{ht} = \dot{H}''_{ht} \pi D_{t,o} = 577,4 \times 3,14 \times 0,0095 = 17 \text{ W/m}$$

Suitable heater tapes were selected and wound around the tubes to give a heater capacity of at least 17W per metre length of tubing.

4.6.5 Steam generator

The steam generator is used for introducing a known amount of steam into the wake of the body at a predetermined rate.

Basically the steam generator consists of a flat spiral copper coil constructed from 6 mm copper tubing which is clamped between two electrical heaters. Each heater consists of an electrical heater element of 1 kw capacity

which, in turn, is clamped between two 5 mm thick copper plates.

Water at a predetermined controlled rate is circulated through the heated spiral copper coil; the resultant steam being discharged from the steam generator in a vertical direction.

The method of introducing the steam into the wake of the body is illustrated diagrammatically in Figure 29 on page 182.

The steam generator is installed below the horizontal test chamber of the climatic chamber. The steam produced by the steam generator is discharged into an inverted cone attached to the bottom of a heated 10 mm dia. straight tube which projects through the floor of the climatic chamber. The tube conveys the steam to the wake of the test subject; the outlet end of the tube being positioned at a height of 1 m above the floor of the test chamber and a distance of 300 mm from the subject.

The steam is "pumped" up the heated tube by means of simple compressed air ejector system. Basically, the ejector

consists of a 3 mm diameter compressed air nozzle, which is installed in the inverted cone in such a way that the air is discharged in an upward direction through the neck of the cone and into the heated tube. Apart from pumping the steam up the centre of the tube, the compressed air dilutes the steam with air and in this way minimises the tendency for condensation to occur.

In order to assist with the dispersal of the steam into the wake of the subject an additional small jet of compressed air is provided above the heated tube at a distance of 150 mm from the outlet end of the heated tube. The compressed air jet is directed towards the outlet of the heated tube. This jet of air effectively disperses the steam into the wake and further dilutes the steam with air, thereby eliminating the tendency for steam to condense on the body.

The steam generator was capable of a maximum evaporation rate of 0,25 g/s.

The water flow rate into the generator was controlled by means of a clinical infusion pump (Braun Unita) which was capable of producing a constant flow rate of water at

different flow rates up to 0,25 g/s³⁵⁾.

The rate of water supply to the steam generator was initially checked by means of the mini flow-meter⁶⁰⁾ that was used during the model studies referred to in Section 4.5.2 on page 168.

4.7 Performance tests

4.7.1 Double circuit heat exchanger

Preliminary performance tests were carried out to determine whether the performance of the temperature control system for the double circuit heat exchanger was satisfactory.

For the purpose of these tests Cu-Constantan thermocouples were installed within the constant temperature water bath housing the double circuit heat exchanger and temperature variations with time were measured by means of a potentiometer type recorder.

It was found that water temperatures could generally be controlled within 0,01°C over the temperature range of 40 to 90°C.

In view of the adverse effect which any pressure differences between the two humidity-measuring chambers could have on the accuracy of the humidity measurements, an inclined manometer was installed between the air exhaust lines from each humidity-measuring chamber, relatively close to the humidity-measuring chambers, to enable the absolute pressure in each measuring chamber to be adjusted to the same value.

Since both the upstream and downstream air-sampling lines and probes are similar in construction and layout, pressure conditions in each chamber were found to differ by a small amount. Small adjustments to the respective air flow rates were then made to equalise the absolute pressure in the respective humidity-measuring chambers.

Once the above-mentioned tests had been completed the humidity-measuring probes were installed and performance tests on the differential humidity-measuring system were carried out.

4.7.2 Preliminary full-scale inanimate tests

Certain preliminary full-scale tests were carried out with the view to determining whether the response of the

differential hygrometer was linearly related to the rate of moisture gain by the air flowing through the test section of the climatic chamber. At the same time the performance of the steam injection system was checked.

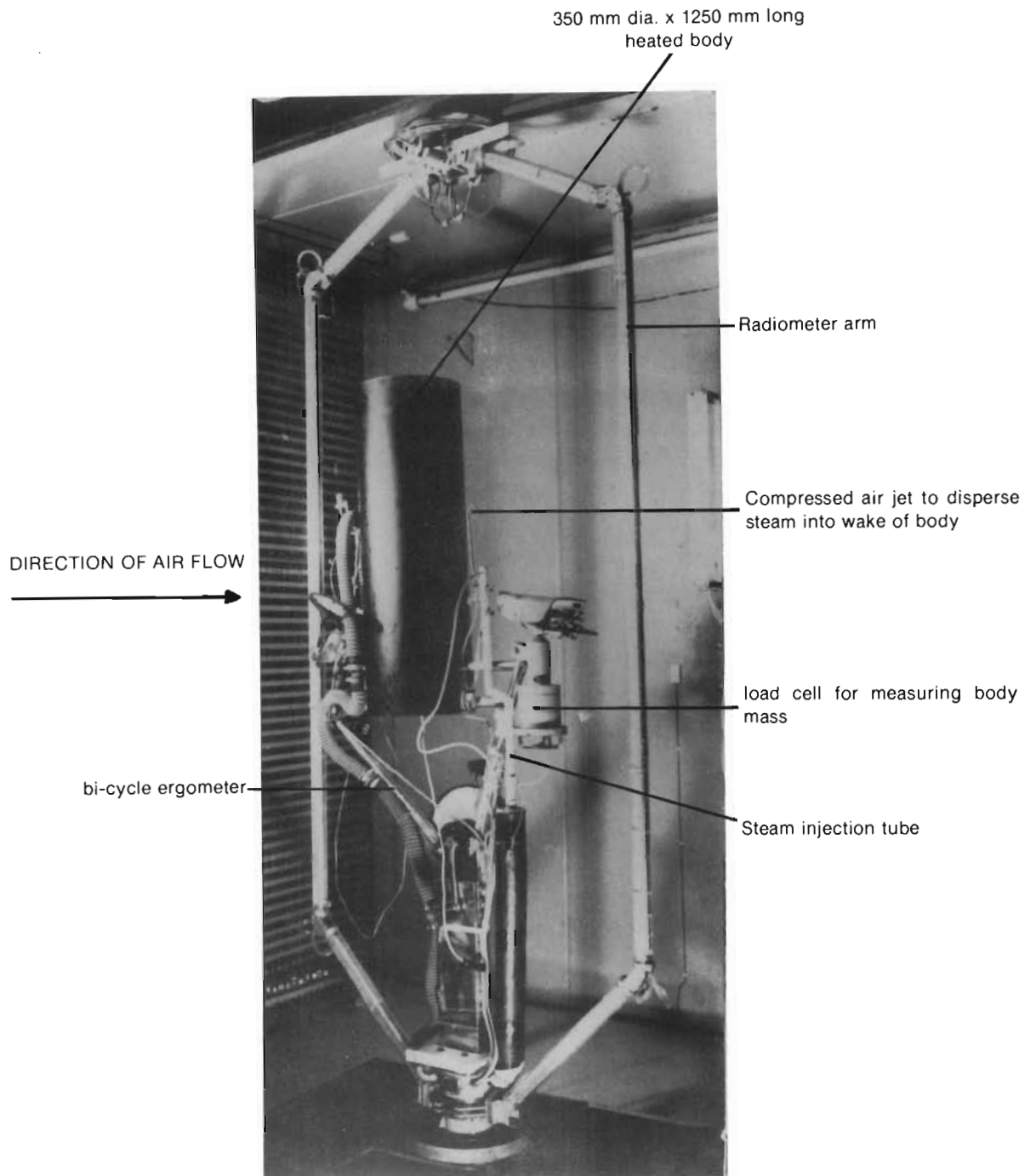
For the purpose of these tests the 350 mm diameter by 1 250 mm long cylinder that is shown in Figure 36 was mounted in the centre of the test chamber to simulate the bluff shape of a human body.

Steam was then injected into the wake of the bluff body at various predetermined mass flow rates and the output of the differential hygrometer as recorded by the Kipp Micrograph type BD-597 recorder was noted for each steam injection rate.

As in the model studies the steam injection rate was controlled by feeding water into the steam generator at a predetermined flow rate; the steam generator being heated to a temperature of at least 350°C immediately prior to the water being fed into the steam generator, in order to ensure complete evaporation of the water.

Test results

As mentioned in Section 4.5 on page 146, linearity of response of the differential hygrometer is a major

**FIGURE 36**

Measurement of the evaporative and radiative heat loss rates from a human body: test rig showing the heated cylinder that was used during preliminary full-scale investigations.

prerequisite for the measurement of the evaporative heat loss from a body by means of the comparative technique of measurement. In this technique the evaporation rate from the body is determined from equation 28 on page 177 which is only valid if the response of the differential hygrometer is linear, namely

$$\dot{m}/\dot{m}_{\text{aux}} = B/A \quad \text{..... (32)}$$

where $\dot{m}, \dot{m}_{\text{aux}}$ = rates of water vapour addition to the wake of the body as a result of the moisture evaporation from the main body and the steam input rate by the steam generator, respectively

and B, A = recorder deflections due to the moisture evaporation rate from the main body and the steam input rate by the steam generator, respectively.

Figure 37 presents typical test data for various steam input rates ranging from 0,06 g/s to 0,17 g/s and an air velocity of 1,0 m/s.

From the test results presented in Figure 37 it is evident that the response of the differential hygrometer is linear.

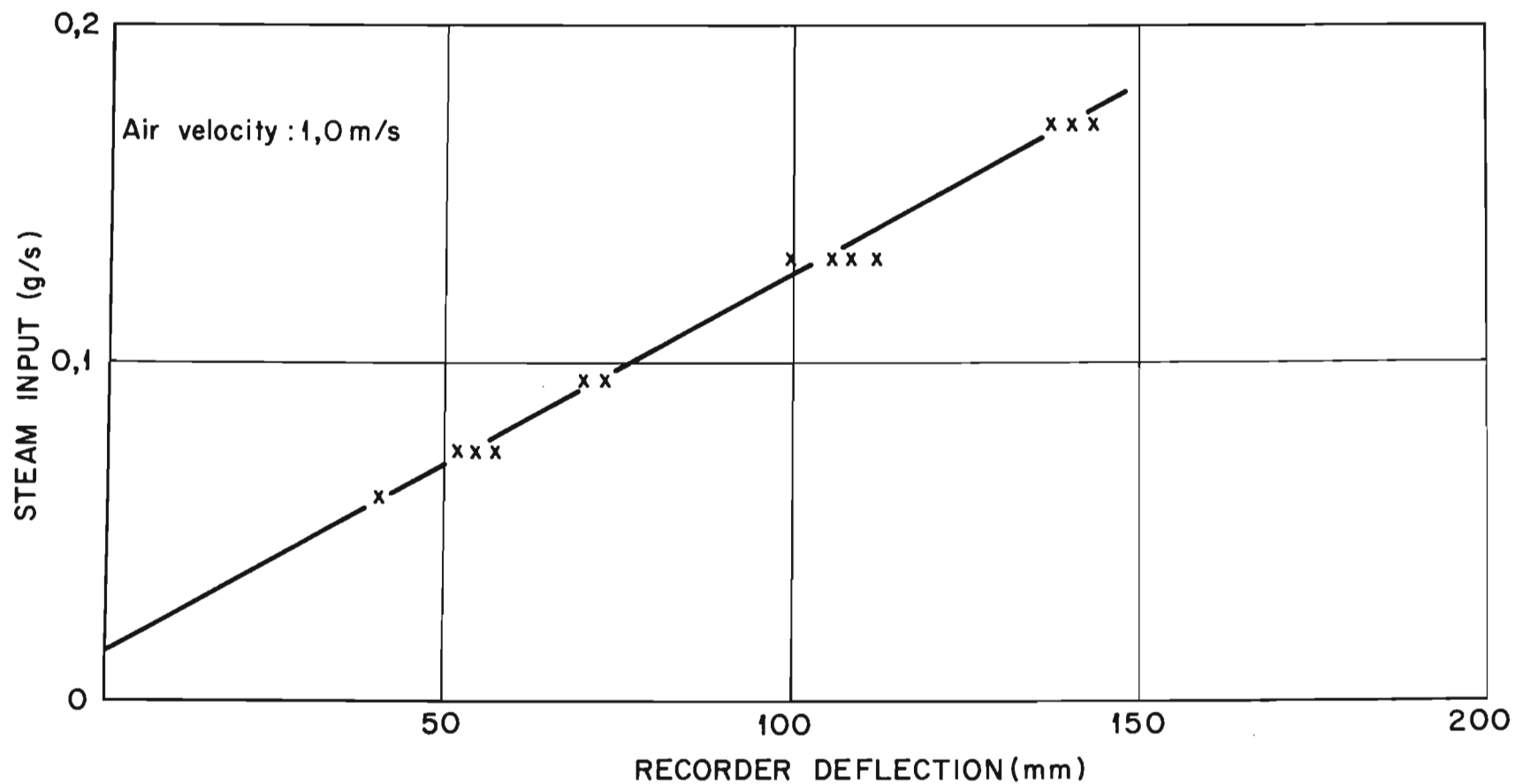


FIGURE 37

*Direct measurement of the evaporative heat loss rate :
full scale tests: recorder deflection as a function of
the steam input rate by the auxiliary steam generator.*

Accuracy

In general, it appeared that the steam input rate could be determined to within 10% from the differential hygrometer reading.

The tests at certain water flow rates were repeated on various days over a test period of one week and it is possible, therefore, that the scatter in the readings in Figure 37 could be due to slight variations in the output of the lithium chloride sensors with time. This was subsequently confirmed to be the case by Mitchell³⁵⁾. Greater accuracies should thus be possible if the hygrometer is calibrated immediately prior to use.

Response time

As in the model studies referred to in Section 4.5.2 on page 171, the response time of the differential hygrometer was determined by injecting steam into the wake of the body at a fixed rate and noting the time taken for the differential hygrometer to give 63.2% of the full-scale deflection.

The response time of the hygrometer was found to be of the order of 30 seconds.

Steam injection system

The steam injection system was found to operate satisfactorily. In particular, the counter flow jet of air above the steam outlet nozzle effectively dispersed the steam into the wake of the body and no condensation of steam was evident on the surface of the body.

General

In general, the performance of the full-scale differential hygrometer appeared to be satisfactory; the test results being generally in accordance with the results obtained during the model studies referred to in Section 4.5.2 on page 171.

In view of the satisfactory operation of the full-scale differential hygrometer it was proposed that the instrument should be used to determine the evaporative heat loss from a human body.

4.7.3 Animate studies

The differential hygrometer was subsequently used by Mitchell³⁵⁾ to determine the moisture evaporation rate and hence the evaporative heat loss rate from test subjects.

(The evaporative heat loss rate is obtained from the moisture

evaporation rate by multiplying the latter value by the corresponding value for the latent heat of evaporation of sweat).

During each test, the subject sat on the saddle of the bicycle ergometer frame, pedalling when it was required by the programme.

In all the tests an attempt was made to prevent the subject developing a water deficit because of the well known effects of water deficit on physiological strain. Thus, whenever the subject was weighed, he was offered a sufficient quantity of water to replace losses due to sweating and urination.

Mitchell³⁵⁾ found that provided the differential hygrometer was calibrated before each test, the sweat rate could be determined to within 0,5 g/m or 8×10^{-6} kg/s.

As mentioned in Section 4.2 on page 119, the evaporative heat loss measuring instrument should be capable of measuring a moisture evaporation rate $0,47 \times 10^{-3}$ kg/s with an accuracy of 15%. The actual accuracy of the differential hygronometry system under these conditions is thus $(8 \times 10^{-6} / 0,47 \times 10^{-3}) \times 100 = 2\%$, which is completely satisfactory.

It is of interest to note that accuracies of better than 15% can be expected whenever the sweat rate exceeds $(8 \times 10^{-6}) \cdot 100/15 = 0,053 \times 10^{-3} \text{ kg/s}$.

In general, Mitchell³⁵⁾ found the evaporative heat loss measuring instrument to be completely acceptable as a direct-measuring instrument for the determination of the evaporative heat loss rate from a human body.

4.8 Discussion of the evaporative heat loss measuring system

The successful development of the evaporative heat loss measuring system referred to in this dissertation, has provided physiologists with a unique facility for determining by direct means the evaporative heat loss rate from a human subject in a normal working mode.

Hitherto such measurements have not been possible.

The moisture evaporation rate and hence the evaporative heat loss rate from subjects in relatively large climatic chambers of adequate size to accommodate the subjects in normal working positions, has in the past, generally been assessed from measurements of the body mass variations with time.

However, the weighing technique is subject to several disadvantages: the mass variations with time of a subject are not only caused by the evaporation of sweat from the skin and numerous corrections are necessary. For example, corrections have to be made for the mass of oxygen absorbed and carbon dioxide eliminated through the lungs of the subject. Care also has to be exercised to differentiate between the total moisture loss (which could include the sweat which drips from the body under high stress conditions), and the moisture which is actually evaporated from the body surface. It is only the latter factor that is active in promoting the loss of heat although the total water loss has certain physiological effects, for example, on the blood. Another disadvantage of the weighing technique is the difficulty of obtaining accurate continuous mass measurements particularly during exercise by this means. As a result the mass variation of the subject is obtained as an average value over a predetermined period of time.

All the major disadvantages of the weighing technique were successfully overcome with the newly developed evaporative heat loss measuring system.

One of the major problems associated with the accurate measurement of the evaporative heat loss rate from a subject in the relatively large horizontal test chamber of the climatic chamber was the relatively small humidity increase of the air flowing over the evaporating body.

The problem of detecting the humidity increase was successfully overcome by means of the unique extremely sensitive differential system of humidity measurement that was developed; the sensitivity of the system being sufficiently high to enable increases in specific humidity in the wake of the evaporating body as small as $0,000004 \text{ kg/kg}$ or $0,007^{\circ}\text{C}$ dew-point temperature to be detected.

The high sensitivity and comparatively short response time, of the order of 30 seconds, of the humidity-detecting system together with the unique calibration procedure which involved the injection of a known amount of steam into the wake of the body, enabled a continuous direct reading of the moisture evaporation rate and hence the evaporative heat loss rate of a working subject in the climatic chamber to be obtained; the system of measurement being sufficiently accurate to enable the evaporation rate of sweat on the surface of the body to be measured to within $8 \times 10^{-6} \text{ kg/s}$ corresponding to a measurement accuracy of 2% for a moisture evaporation rate of $0,47 \times 10^{-3} \text{ kg/s}$.

CHAPTER 5

MEASUREMENT OF THE RADIATIVE HEAT LOSS FROM A HUMAN BODY

In the normal environment the radiant fraction of heat loss amounts to 50 per cent of the thermal output of a living body. For this and other reasons the measurement of the radiative heat loss from a human body is of considerable interest.

Many indices of heat stress and models of the thermoregulatory system of the human body have been proposed, but their confirmation and further development has been seriously limited by a lack of accurate quantitative information on the heat exchange rate between the human body and its environment.

Classic studies of this kind were first performed in the 1930's^{9,63,64}). In these studies the radiant energy exchange was calculated from the measured temperature values of the skin of the human subject and the surrounding surfaces of the booth or calorimeter in which the subject was placed. Attempts were also made by other investigators to separate the convection and radiation components by calculation^{65,66}).

However, this approach is complicated by the irregular and changeable shape of the radiant surface of the body and the non-uniform temperature distribution across the body surface coupled to the difficulty of deter=

mining by the integration of single measurements the average temperature of the human skin. The technique is also entirely unsuitable for the determination of the major components of the heat exchange rate under transient conditions since the procedures are cumbersome and do not lend themselves to continuous recording.

In 1950 Benzinger and Kitzinger⁶⁷⁾ proposed a technique for the direct measurement of the radiant heat loss from a human body. The proposed radiation-measuring system basically consisted of a calorimeter, 800 mm x 800 mm x 2 000 mm in size, which was completely lined with numerous small reflecting and non-reflecting surfaces; each surface being equipped with a thermocouple junction to enable an integrated reading of the temperature difference between the reflecting and non-reflecting surfaces to be obtained. The latter reading was calibrated in terms of the radiant heat loss from a body in the calorimeter.

However, the system of measurement was subject to the major physiological disadvantage of all human calorimeters^{11,12)}; since the human body had to be placed inside a relatively confined space, normal working movement was severely restricted. Furthermore, the emissivity of the surrounding surface could not be altered in any way.

The above-mentioned disadvantages would be eliminated if a direct-measuring technique could be developed for determining the radiative heat loss rate

from a subject in a relatively large climatic chamber in which the subject could perform normal working movements.

5.1 Proposed method of measuring the radiative heat loss rate from a human body

The problem involves the direct measurement of the radiative energy exchange rate between a subject in the horizontal test chamber of the climatic chamber and the surrounding walls.

The main requirement for the radiation measuring instrument is that it should not disturb the normal heat exchanges between the body and environment. Thus, it should not be so bulky as to interfere with the air flow over the body, with consequent influence on the convection and evaporation from the body. Furthermore, it should not be such as to alter the radiation heat exchange conditions, for example, by screening or alteration of the surface properties of walls.

The following methods of measuring the radiative energy exchange rate were considered:

5.1.1 Radiometer layers

In this method the entire surface of the test chamber would be lined with a radiative sensitive layer, similar to the

one used by Benzinger, et al^{46,67)} for their calorimeter.

The main advantage of this method is that it is truly integrating for uniform or symmetrical temperature distributions in the chamber.

However, assymmetrical distributions will introduce "background" readings. Thus, even with no body in the test chamber, readings will be obtained that change with changes in environment. Because the latter condition cannot be precluded, the method offers no particular advantages over other methods in this respect.

The gradient layer will tend to measure the total heat flow through the test chamber walls and in order to differentiate between the convective and radiant heat transfer components the radiometer must be composed of alternatively absorbing and reflecting elements. The emissivity of the walls, therefore, is effected in violation of the requirement referred to in Section 5.1 on page 226.

Further complications would arise with the installation of such measuring elements on the upstream and downstream bar-grid panels of the horizontal test chamber. This

method was, therefore, not pursued.

5.1.2 Spherical integrating grid around the body

This would consist of a spherical lattice framework around the body. Because of its structure, air can flow through the structure and over the body.

The only advantage of this system over the one described in the following section is that it is stationary. Disadvantages include the interference with the air flow and mean radiant temperature of the environment if sufficient radiometer elements are used to give a reasonable integration.

5.1.3 Rotating 4π radiometer

The rotating 4π radiometer* consists of a thin semi-circular hoop rotating around the body as shown in Figure 38. The inside and outside surfaces A and B are lined with radiation-sensing elements, so connected as to measure the net radiation exchange between the subject and the surroundings. The hoop will integrate over the semi-circular

* The basic principle of measurement of the 4π radiometer was proposed by Prof. J. Visser

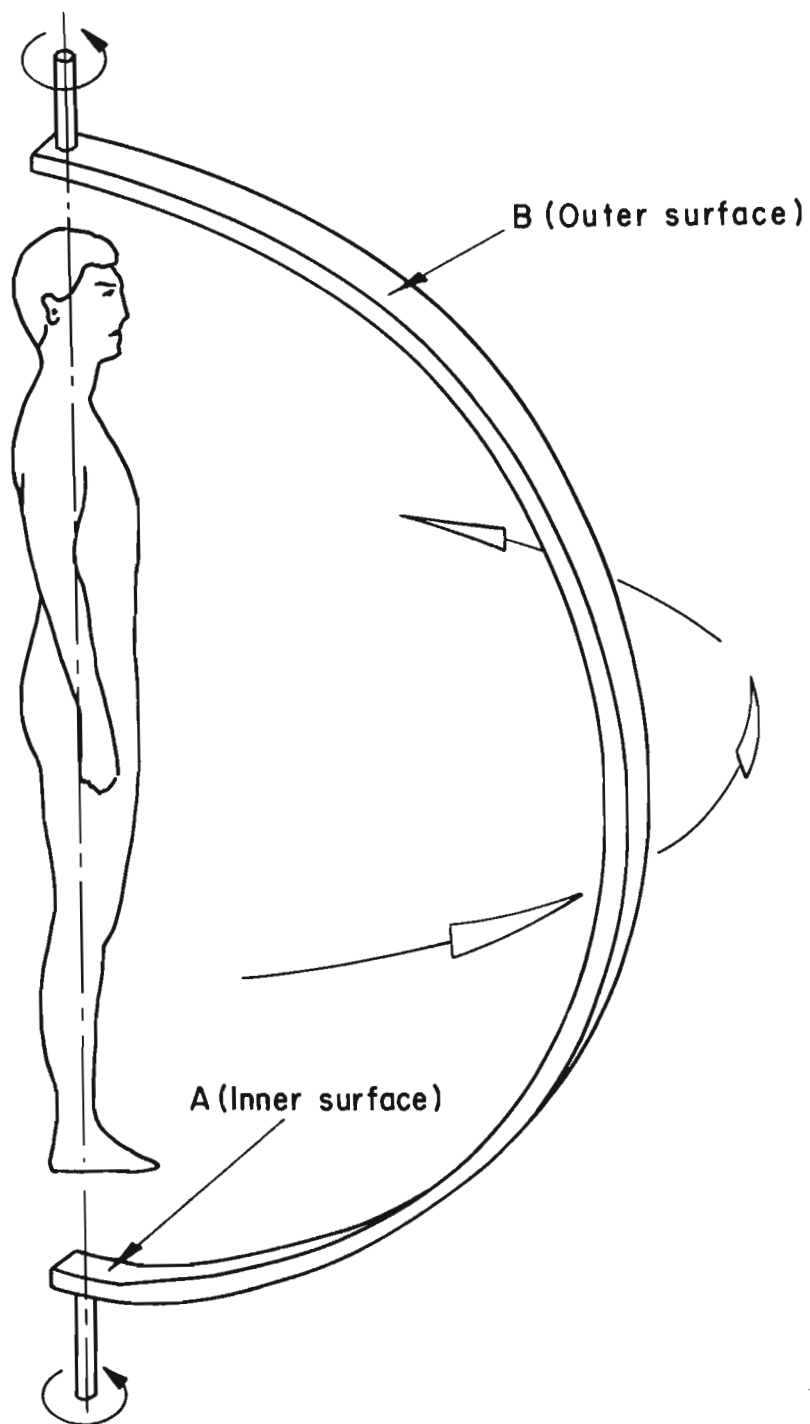


FIGURE 38

Measurement of the radiative heat loss rate from a human body: schematic diagram of the 4π integrating radiometer

strip formed by the elements. Upon rotation through a complete revolution, it will integrate the radiation over the total 4π surface enveloping the subject.

In this method, the interference with the air flow is reduced to a minimum. While the interposition of a surface between the body and its surroundings must of necessity influence the radiation exchange, this method introduces a small surface only.

The strip is interposed between the body and wall for a short while only, so that the general equilibrium of the body-wall system is maintained. The spherical grid in the previous section would upset this equilibrium.

In view of the apparent advantages of the 4π radiometer over other systems of measurement, further consideration was only given to the rotating 4π radiometer as a means of measuring the radiative heat flux from a human body.

5.2 Choice of thermal radiation-sensing elements

All bodies above a temperature of -273°C emit electro-magnetic waves. The selection of a particular type of radiation-sensing

element for the purpose of measuring the thermal radiation of a body largely depends on the intensity of the radiation and the spectrum of wave-lengths involved. The latter factors, in turn, depend on the temperature and surface condition, in particular, the emissivity of the body^{68,69}).

These factors are briefly referred to before discussing the selection of a particular type of radiation-sensing element for the 4π radiometer arm.

Emissivity

In general, the values quoted in the literature for the emissivity of human skin vary between 0,95 and 0,99 at wave-lengths above 3 micron⁷⁰⁻⁷³). At wave-lengths below 3 micron slightly lower values for the emissivity were generally obtained.

Patil⁷⁴) measured the emissivity of skin in vivo as a function of wave-length in the spectral region between 2 micron and 18 micron (by comparing the radiant power emitted by the skin with that emitted by a black body at the same temperature), and found the emissivity to depend on wave-length and to vary between $0,89 \pm 0,02$ and $1,00 \pm 0,02$. Watmough and Olivier^{75,76}) on the other hand, found the emissivity of human skin to vary between 0,98 and 1 in the wave-band between 2 micron and 6 micron.

The relatively high emissivity of human skin was confirmed by Mitchell, Wyndham and Hodgson⁷⁷⁾ who found the total normal emissivity of human skin to be 0,995 irrespective of its visible colour.

In view of the relatively high emissivity of human skin (particularly in the infra-red wave-length region of radiation, above 3 micron), human skin can be regarded as a black body under the radiation conditions encountered in the test chamber of the climatic chamber.

Spectral distribution of radiant intensity

It has been shown by the quantum arguments of Planck⁷⁸⁾ and varified experimentally that the spectral distribution of radiant intensity for a black body is a function of the absolute temperature and wave-length.

Based on ~~the~~ following radiant intensity distribution function by Planck, Figure 39 by Joos⁷⁹⁾ presents the radiant intensity of a black body, as a function of wave-length for various black body temperatures:

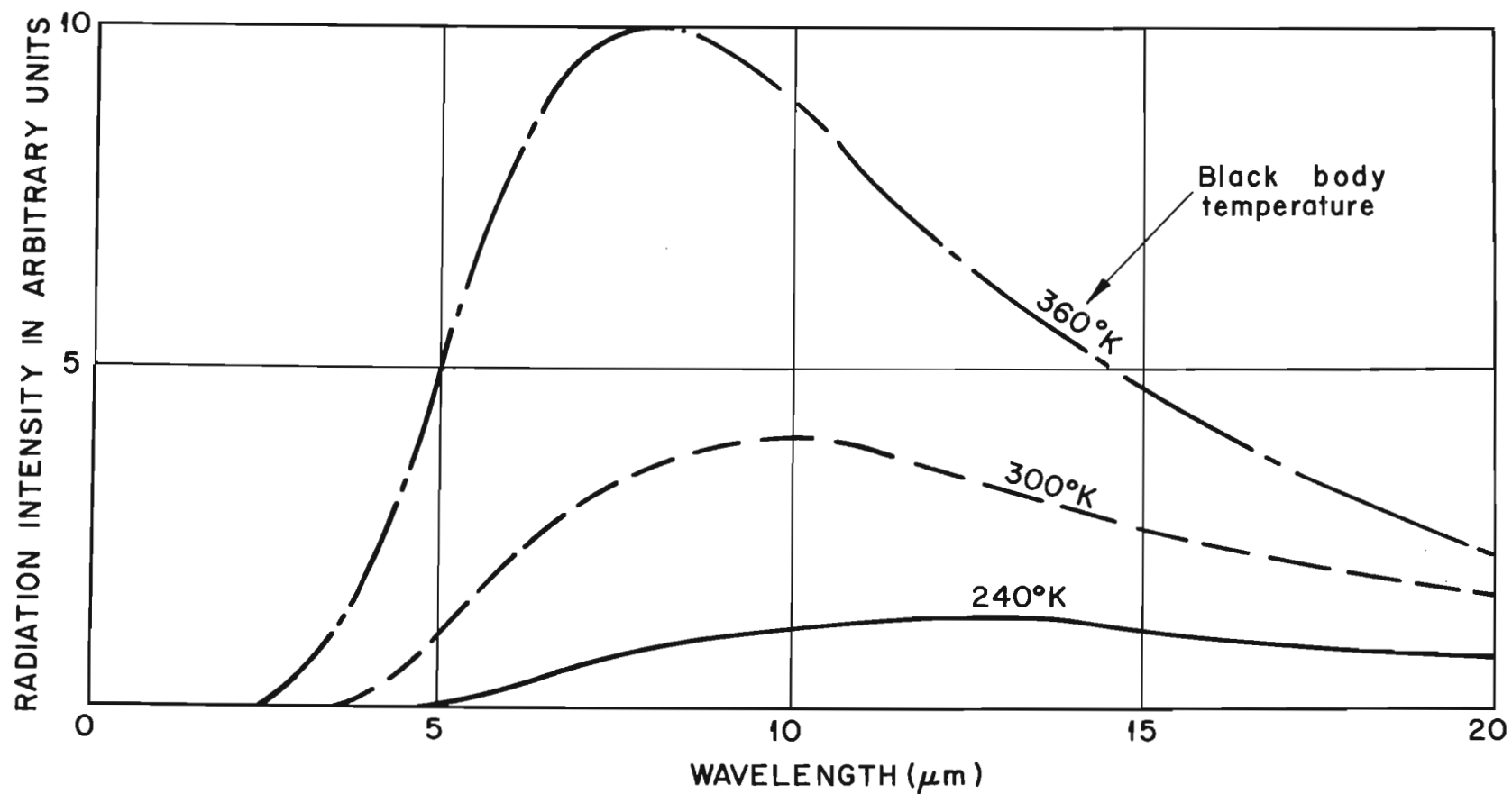


FIGURE 39

Radiation intensity of a black body as a function of wavelength at various black body temperatures.

$$E = \frac{C_1}{\lambda^5} (e^{C_2/\lambda T} - 1) \quad \text{..... (33)}$$

where E = radiant intensity

and λ = wave-length, μm

T = absolute temperature, $^{\circ}\text{K}$

C_1, C_2 = constants.

The value of λ_{max} , the wave-length of the peak radiation intensity in the black body spectrum, may be determined from the Wien displacement law.

$$\lambda_{\text{max}} T = 2897 \mu\text{m } ^{\circ}\text{K} \quad \text{..... (34)}$$

At a black body temperature of 300°K (this corresponds approximately to the surface temperature of a human body), the radiant energy exchange generally takes place at wave-lengths between 3 micron and 40 micron with a peak of 10 micron. Ninety per cent of the thermal radiation energy falls in the 6 to 40 micron wave-band.

The radiation-sensing elements to be incorporated in the proposed radiometer must thus be suitable for the detection of radiation over the above-mentioned spectral range.

In general, thermal radiation detectors can be divided into two main types, namely, thermal detectors and photon-counters.

5.2.1 Thermal detectors

Thermal detectors depend upon the heating effect of the radiant energy being measured for their operation. The most frequently used detectors of this class are the thermopile which is generally constructed from a number of thermocouples connected in series and the bolometer which incorporates electrical resistance elements.

In the case of a thermopile, the "hot" junctions of the thermocouples are generally attached to a blackened low mass receiver which is exposed to the radiation to be measured. The "cold" junctions of the thermocouples are shielded from the radiation.

The bolometer incorporates electrical resistance radiation-sensing elements which are generally connected in the form of a Wheatstone bridge; the resistances in the opposite arms of the bridge network being shielded and the other exposed to the incident radiation.

Another type of thermal detector is the Golay cell which incorporates a small gas cell as detector: when the gas in the cell is heated by incident radiation the resultant expansion causes movement of a flexible wall which is

magnified optically and detected with a photo-cell. However, due to the susceptibility of such detectors to microphonics and vibrations, their application is limited to laboratory use.

In general, thermal detectors are equally sensitive at most wave-lengths and are relatively cheap.

5.2.2 Photon-counter detectors

Photon-counter detectors operate when photons react with electrons, causing a shift of electron orbits. Since photons have appreciable energy only when wave-lengths are short, the use of photon-counter detectors are generally limited to the visible or near infra-red wave-length regions.

Radiometers equipped with photon-counter detectors are relatively expensive; such detectors often require cooling to sub zero temperatures and are wave-length dependant. They are, however, highly sensitive to changes in radiant power.

Figure 40 by Jones⁸⁰⁾ presents the spectral sensitivities of various detectors as a function of wave-length. It is

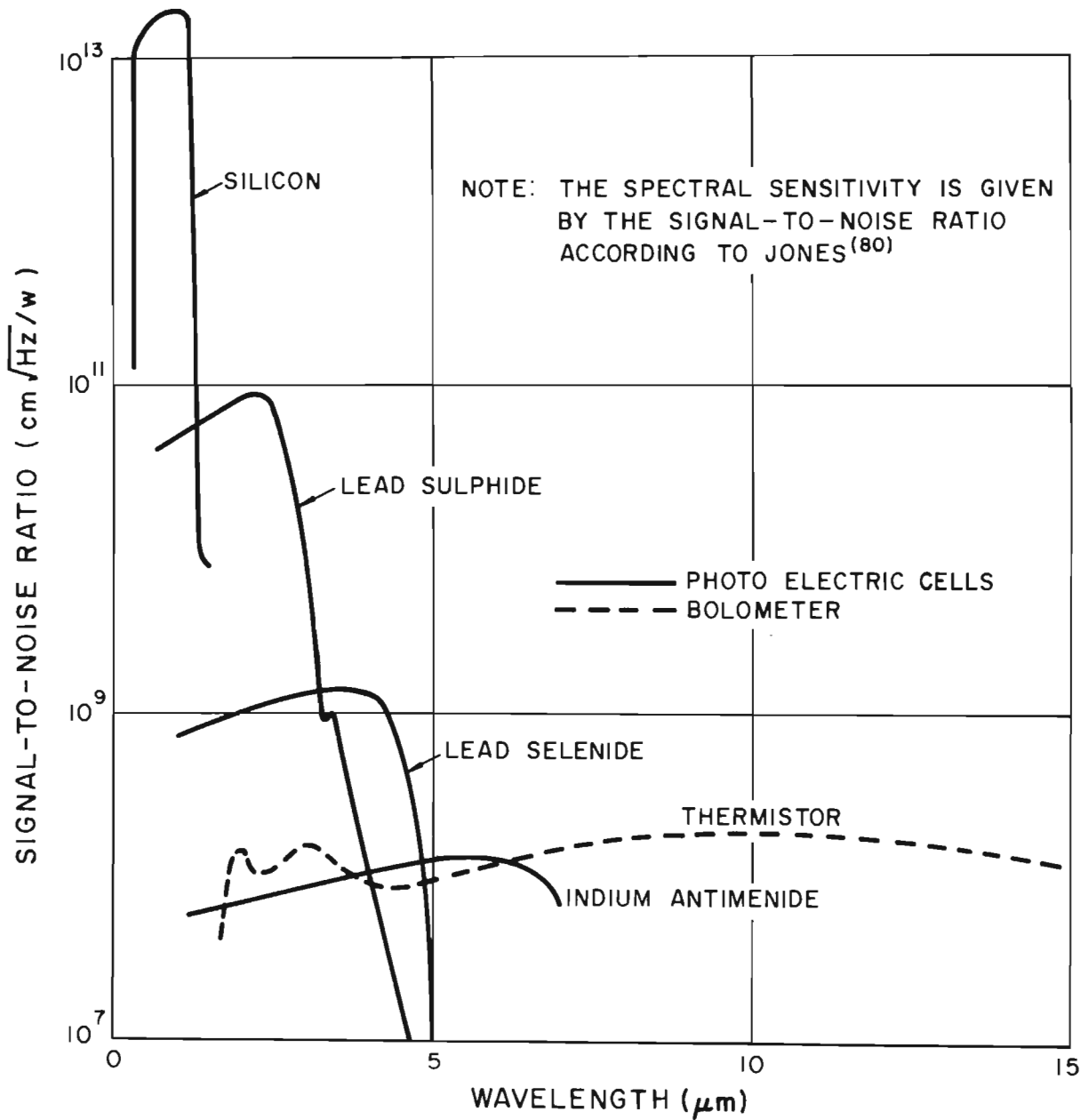


FIGURE 40

The spectral sensitivity of photo-electric cells and thermistor bolometers

seen that, at wave-lengths below 4 micron most photon-counters are more sensitive than the bolometer. According to Vanselow⁸¹⁾, the lead sulphide photocell, when used as a radiometric temperature measuring device, is 1 200 times more sensitive in the wave-band of 2,8 to 3,8 micron compared with a thermal detector such as the bolometer.

5.2.3 Proposed thermal radiation-sensing elements

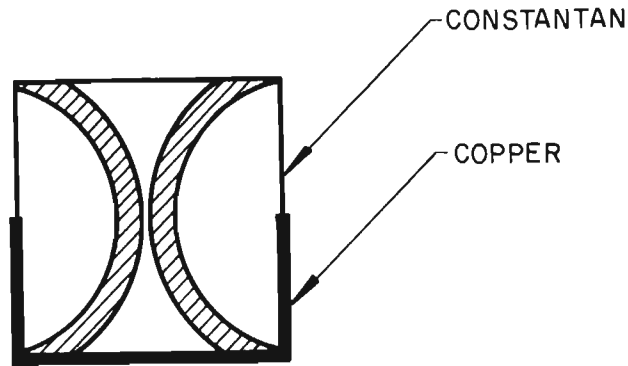
In view of the high sensitivity of photon-counter detectors compared with thermal detectors, photon-counter detectors are often preferred for the measurement of skin temperature. However, it was decided to equip the proposed radiometer with thermal detectors in preference to the photon-counter detectors in view of cost considerations and the relative ease with which the inner and outer surfaces of the radiometer can be "lined" with sensing elements. Furthermore, only thermal detectors are generally suitable as radiation detectors within the 6 to 40 micron wave-band. This type of detector would also be relatively insensitive to radiation at wave-lengths below 2 micron and would thus not be affected by the visible radiation produced by the lights in the test chamber of the climatic chamber.

The initial experimental work was carried out with a model radiometer having a thermopile as sensing element. The radiometer arm was constructed from perspex with a section as shown in Figure 41a. A spiral of 24 SWG constantan wire was wound around the arm over the entire length of the semi-circular hoop. One half of the section was then copper plated, thus forming two rows of thermo-junctions on the inside and outside of the hoop. The wire was painted with a matt black paint. This constituted a thermopile which measured the net radiation exchange between the body and the surroundings.

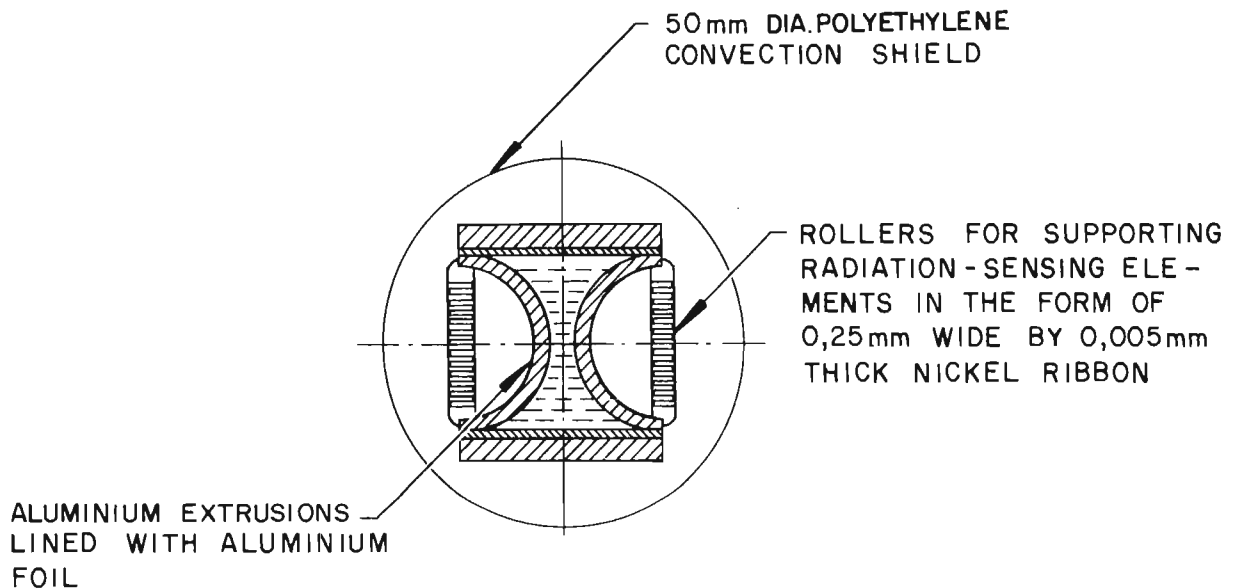
However, during the preliminary experimental studies using a model of the radiometer arm and a 100 mm diameter heated sphere as heat source, the time response of the instrument was found to be unduly long.

Great improvement was obtained by substituting electrical resistance elements in the form of flattened nickel ribbon, 0,25 mm wide by 0,005 mm thick, for the thermocouples. (See Figure 41b).

It was, therefore, decided to investigate the possibility of equipping the prototype radiometer arm with the latter



a) THERMOPILE USED IN THE FIRST PROTOTYPE MODEL OF THE 4π RADIOMETER ARM.



b) ELECTRICAL RESISTANCE THERMAL RADIATION-SENSING ELEMENTS INCORPORATED IN THE PROPOSED 4π RADIOMETER ARM.

FIGURE 41

Sectional views of the thermopile and electrical resistance elements that were investigated as thermal radiation sensors for the 4π radiometer arm.

type of radiation-sensing elements.

5.3 Preliminary performance tests

Preliminary calibration tests were carried out on a 380 mm long portion of the proposed radiometer arm equipped with 0,25 mm wide by 0,005 mm thick flattened nickel ribbon as the radiation-sensing elements with the view to determining the response time of the radiometer.

The test length of the radiometer arm was constructed from aluminium extrusions with a section as shown in Figure 4lb.

The curved surfaces along each side of the arm were lined with aluminium foil to act as reflectors and the radiation-sensing elements, in the form of nickel ribbon, 0,25 mm wide by 0,005 mm thick, were installed in front of the curved surfaces in the following manner:

The nickel ribbon was wound around two sets of perspex rollers located at either end of the test section of the arm. The loops of the wire were spaced relatively close together to form a radiation receiver area of the order of 15 mm wide by 350 mm long; the rollers being suitably mounted to keep the ribbon taut and prevent short circuiting between the individual loops of the wire.

The entire assembly was enclosed in a 50 mm diameter polyethylene wind shield to reduce the influence of air movement on the output of the radiometer.

Provision was also made for circulating water at room temperatures through the test section of the radiometer arm.

The output of the radiometer was measured as follows:

The two radiation-sensing elements (one on either side of the radiometer arm) and two fixed electrical resistances were connected in the form of a Wheatstone bridge; the two radiation-sensing elements formed the opposite arms of the bridge while the two fixed resistances formed the remaining two arms of the bridge. A constant voltage supply was connected across the bridge and the bridge output was measured with a galvanometric type recorder.

The respective magnitudes of the fixed resistances were selected to balance the bridge under zero temperature difference conditions between the two radiation-sensing elements.

5.3.1 Description of the test apparatus

Figure 42 presents a view of the test apparatus that was

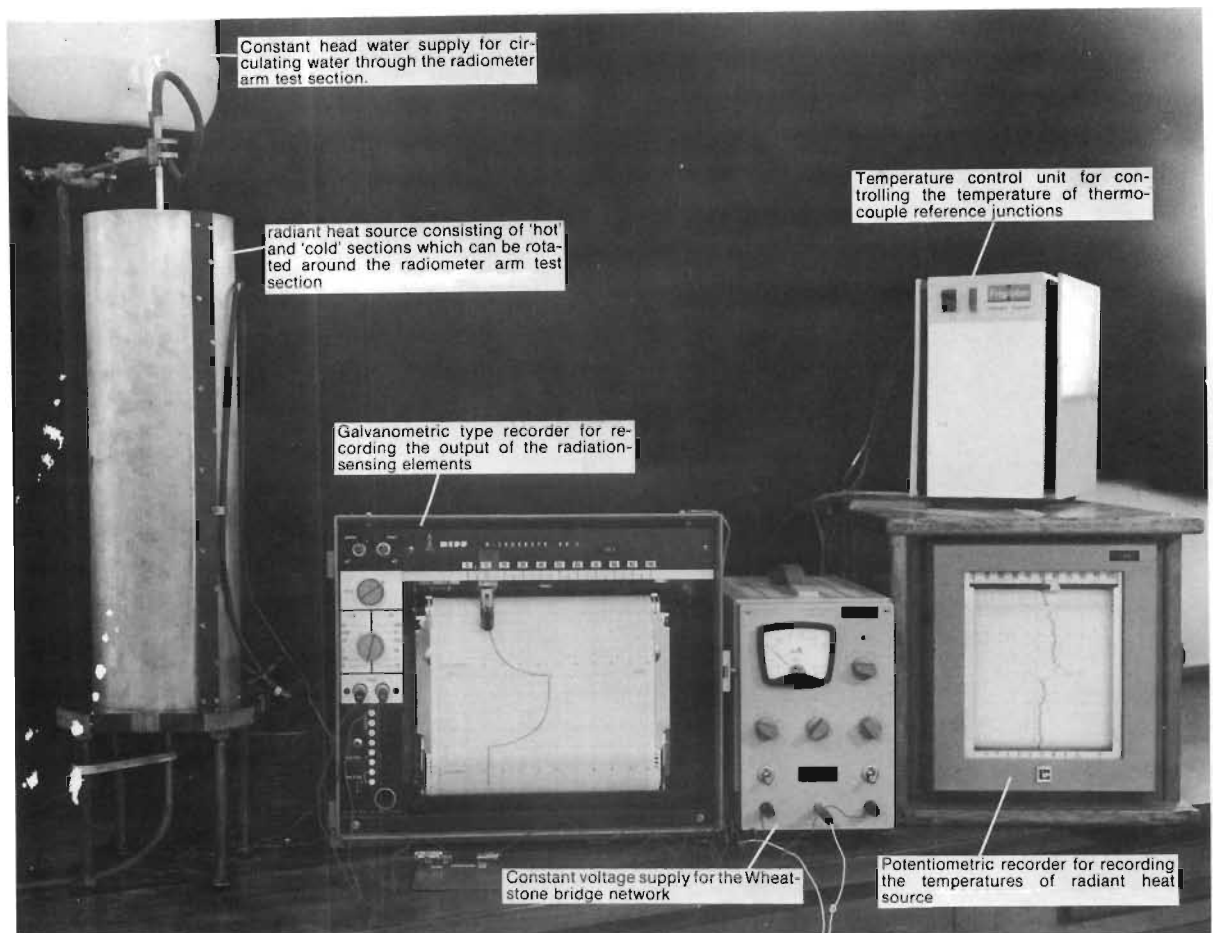


FIGURE 42

Direct measurement of the radiative heat loss rate from a human body: view of the apparatus for determining the response time of the nickel resistance wire thermal radiation-sensing elements of the proposed 4π radiometer arm.

used to determine the response time of the radiometer.

Basically the test apparatus consisted of a cylindrically shaped radiant heat source incorporating an electrically heated section which could be rotated around the test section of the radiometer, as well as thermocouples and a potentiometric type recorder for measuring the temperature difference between the "hot" and "cold" sections of the radiant heat source.

The radiant heat source was constructed from a 520 mm length of 156 mm diameter brass tubing having a wall thickness of 4 mm. The tubing was split longitudinally into two halves and rejoined with strips of bakelite to act as thermal insulation between the two halves.

Provision was made for one half of the radiant heat source to be heated by means of "calrod" type heater elements attached to the surface. The other half of the radiometer was not heated and remained at room temperature.

A variac was incorporated in the electrical supply system to the heater elements to enable the rate of heat input to the heater elements to be varied. This enabled the

temperature difference between the "hot" and "cold" sections of the radiant heat source to be set at predetermined values.

5.3.2 Test procedure

The test length of the radiometer arm was inserted into the radiant heat source as shown in Figure 43 and clamped in a central position. Water at room temperature was then circulated through the radiometer at a relatively slow rate.

The electrical heater elements attached to the radiant heat source were then switched on and the heat input rate to the elements adjusted (by means of the variac) to give a predetermined temperature difference between the "hot" and "cold" sections of the radiant heat source. The radiant heat source was positioned with the "hot" section directly opposite the one set of radiation-sensing elements and the "cold" section opposite the other set of radiation-sensing elements of the test section of the radiation arm.

The power supply to the test section of the radiation arm was then switched on and its output recorded.

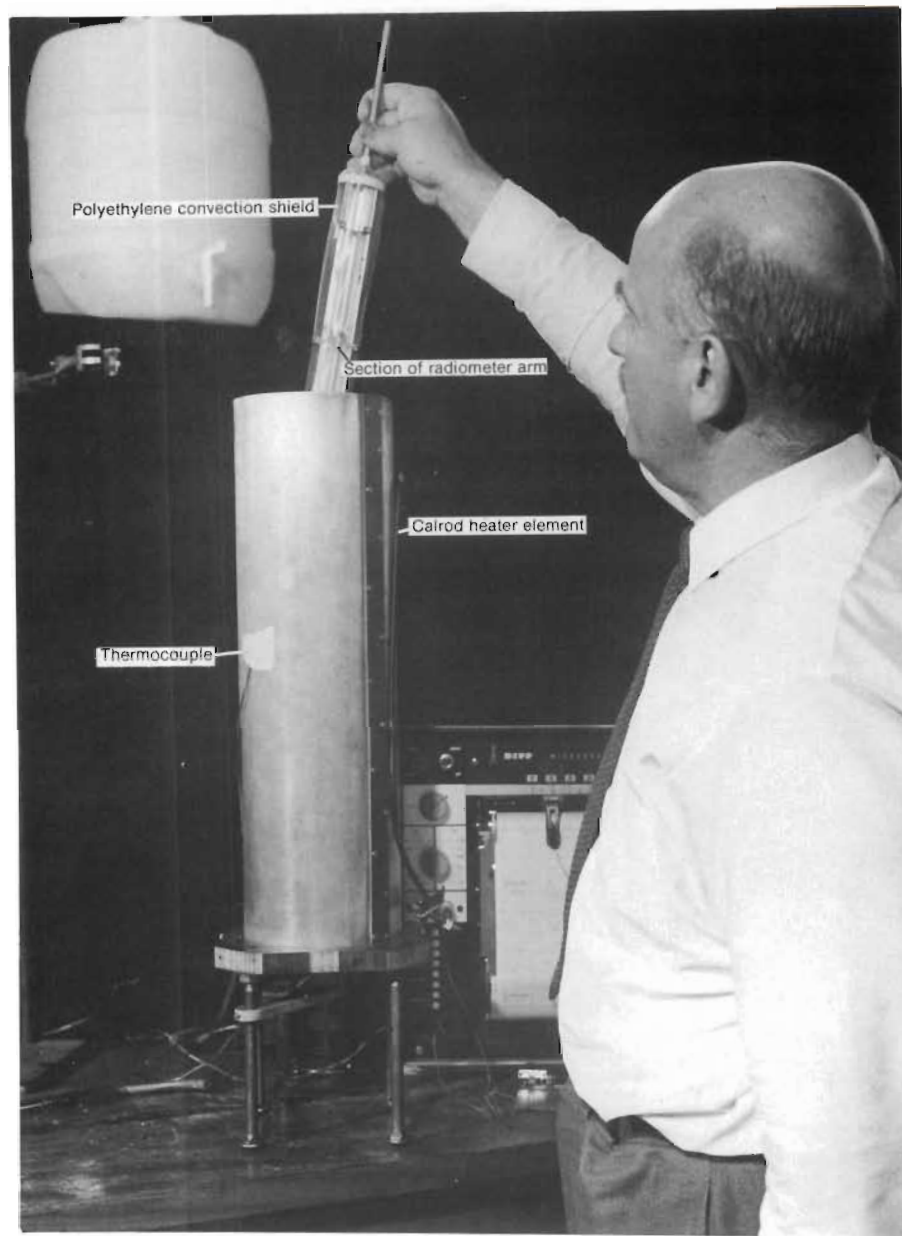


FIGURE 43

Direct measurement of the radiative heat loss rate from a human body: View of a section of the 4π radiometer arm being inserted into the radiant heat source that was used to determine the response time of a test section of the radiometer arm (See Figure 42).

Once the desired temperature difference between the "hot" and "cold" sections of the radiant heat source had been attained, a step change in the radiant heat conditions was created by rotating the radiant heat source through 3 radians (so that the radiation-sensing elements which originally faced the "hot" section now faced the "cold" section of the radiant heat source).

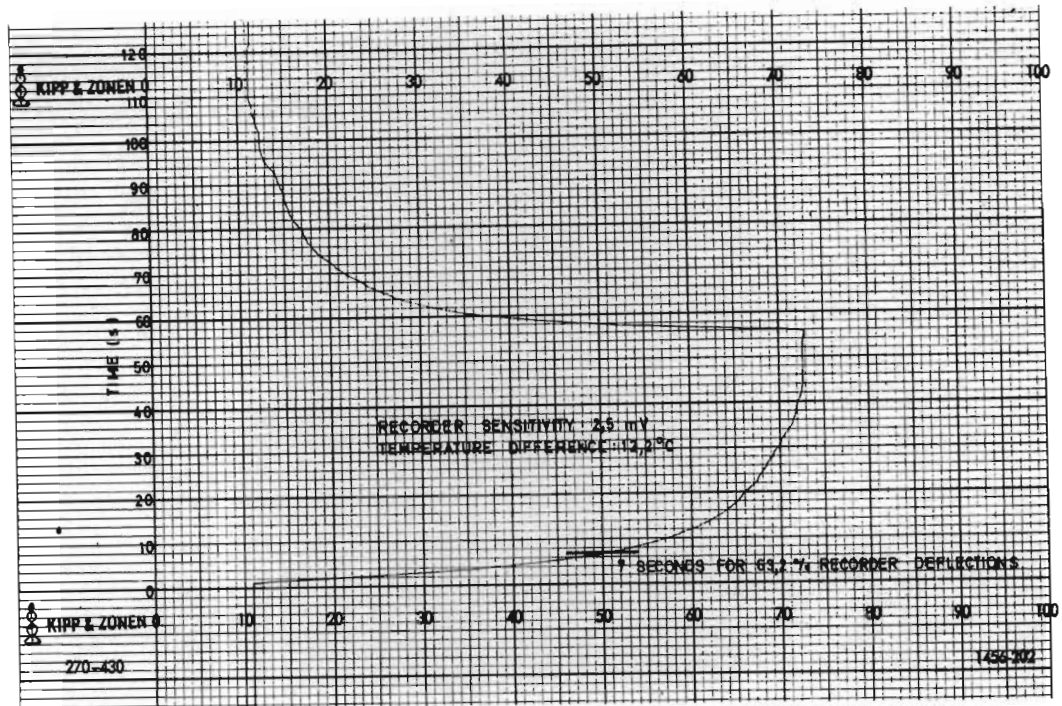
The tests were repeated for variations temperature differences between the "cold" and "hot" sections of the radiant heat source.

5.3.3 Test results

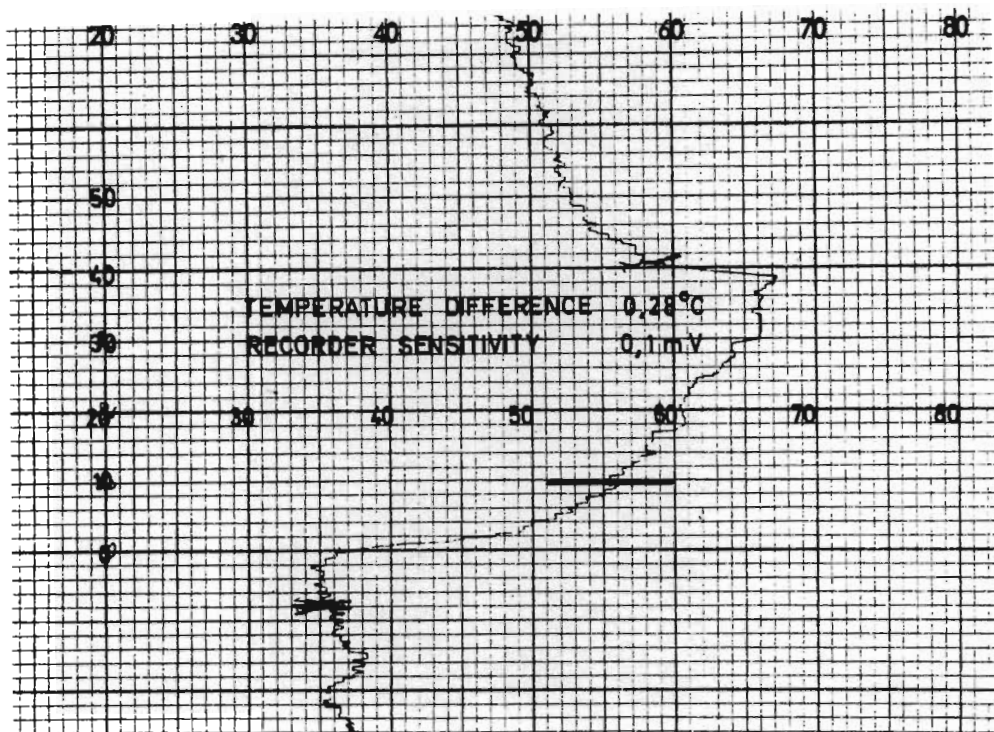
Response time

Typical recordings of the variations in the heat output of the radiometer with time as a result of a step change in the radiant conditions, are presented in Figure 44.

From the results it is seen that the overall response time of the radiometer is of the order of 40 seconds; the response time for a 63,2% variation in the output being of the order of 10 seconds. Since it was proposed that the radiometer arm should rotate around the body at a speed of the order of 0,0167 Hz (corresponding to one revolution



(a)



(b)

FIGURE 44

Direct measurement of the radiative heat loss rate from a human body: variations in the output of a section of the 4π radiometer arm with time, during studies to determine the response time of the 4π radiometer.

every 60 seconds), the response time is satisfactory.

Linearity of response

Figure 45 presents the output of the radiometer test section as a function of the temperature difference between the "hot" and "cold" sections of the radiant heat source. It is seen that the output of the radiometer is linear.

5.3.4 Preliminary performance tests on a full-scale prototype model of the radiometer arm in the form of a semi-circular hoop

Preliminary calibration tests were carried out on a full-scale prototype model of the radiometer arm in the form of a semi-circular hoop using an electrically heated full size articulate model of the human body as heat source. The model was used during the development of the convective heat loss measuring instrument³⁶⁾. (See Figure 46).

In the full-scale model of the radiometer arm, the radiation-sensing elements, in the form of nickel ribbon, 0,25 mm wide by 0,005 mm thick, were installed in the radiometer in such a way that the wires facing the inside of the arm form opposite arms of the bridge while the wires facing the surrounding walls of the test section form the remaining two arms of the bridge.

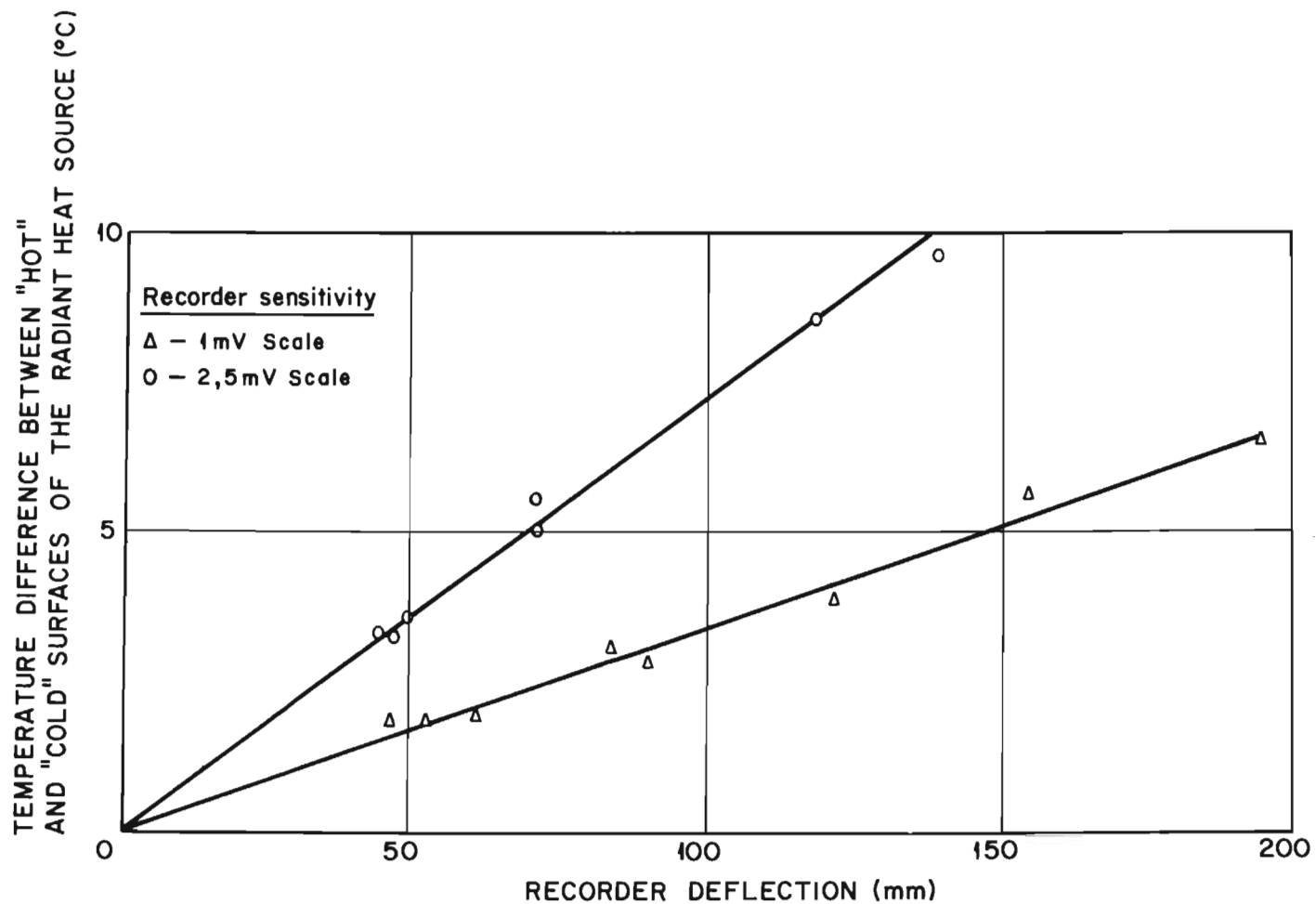


FIGURE 45

*Direct measurement of the radiative heat loss rate from a human body;
Calibration curve for a test section of the prototype radiometer arm
using the test rig shown in figure 42*

**FIGURE 46**

Direct measurement of the radiative heat loss rate from a human body: view of the test rig in the horizontal test chamber of the climatic chamber during preliminary tests on a prototype model of the 4π radiometer arm.

During the calibration tests the output of the radiometer arm was compared with the radiant heat loss rate from the body; the latter being taken as the difference between the total heat input rate to the body (as measured with a watt meter) and the convective heat loss rate (as measured with the convective heat loss measuring instrument³⁶).

It was found that relatively small temperatures between the surrounding temperature-controlled panels of the test chamber of the climatic chamber resulted in comparatively large cyclical variation in the output of the radiometer with time, of a period of 60 seconds (as the radiometer rotated around the body).

The comparatively large effect which the wall temperature had on the output of the radiometer arm was mainly due to the relatively large area of the surrounding walls that is "seen" by the radiometer compared to the comparatively small area which the radiometer "sees" of the body. Close control of the respective temperatures of the surrounding walls is thus desirable.

In order to extract mean values of the radiometer output, the radiometer measurements were integrated electronically

during a predetermined number of rotations of the radiometer arm.

The tests confirmed that the output of the radiometer was linearly related to the radiant heat loss rate from the body. In addition, the effect of the changes in the posture of the articulate body on the calibration curve was found to be negligible.

In view of the satisfactory results that were obtained during the tests on the prototype model of the radiometer arm, it was decided to proceed with the final design of 4π radiometer.

5.4 Constructional details of the 4π radiometer

5.4.1 General description

It was decided to construct the radiometer in the form of a full hoop.

Figure 47 presents a schematic layout of the 4π radiometer arm.

Basically the main framework of the radiometer arm consists of six lengths of hollow aluminium sections which are bolted

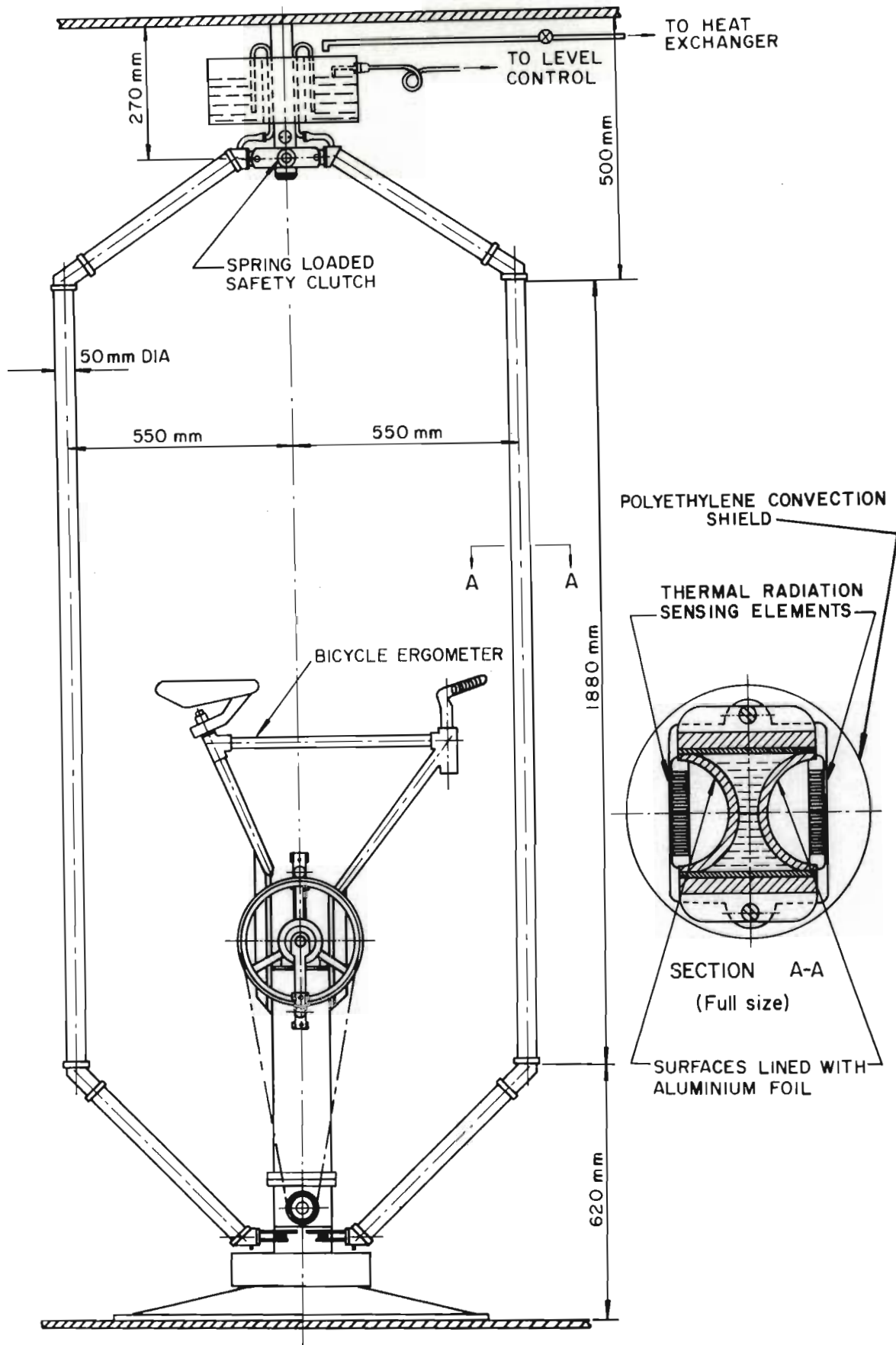


FIGURE 47

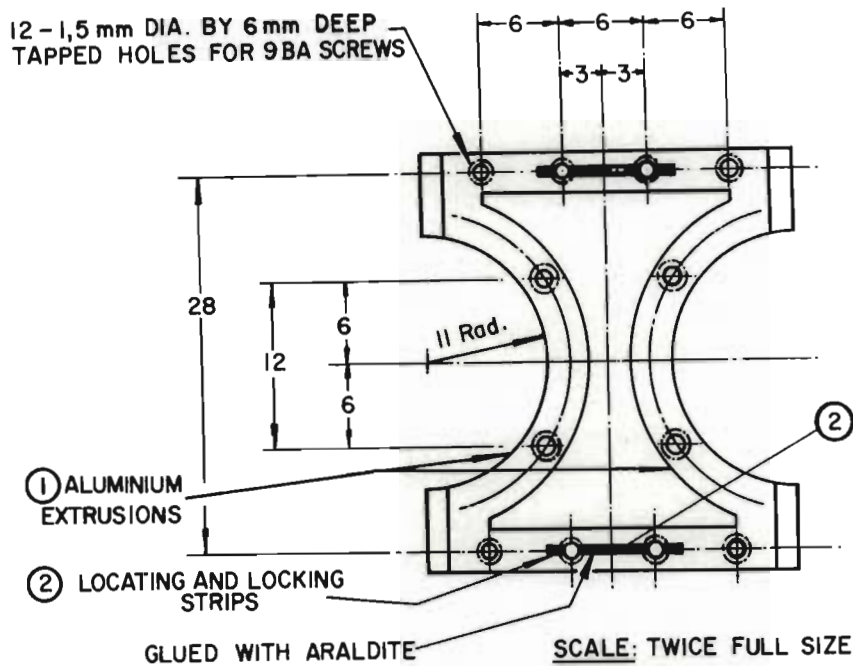
Measurement of the radiative heat loss rate from a human body: schematic layout of the radiometer arm.

together to form a hoop; the whole assembly being installed in the horizontal test chamber of the climatic chamber in such a manner that it can be rotated around the body.

Water at a controlled temperature is circulated through the arm for the purpose of temperature control. The water is supplied to the arm from a constant head container located near roof level. After circulation through the radiometer arm the water is collected in a trough and discharged through the floor of the test chamber.

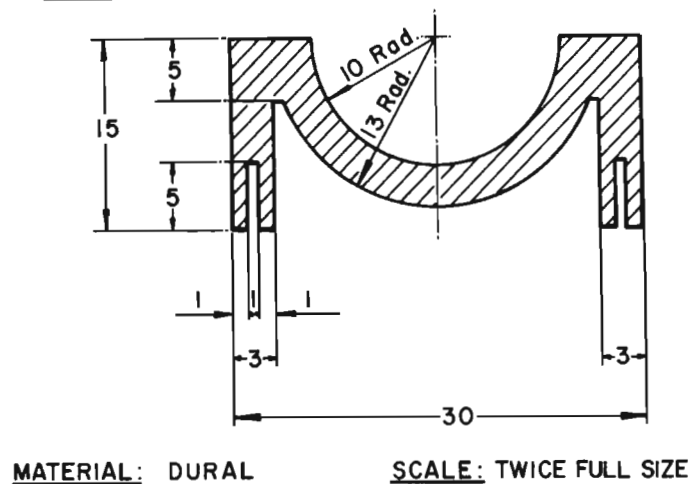
The sections of the radiometer arm are constructed from aluminium extrusions of semi-circular cross-section. As shown in Figure 48, the extrusions are glued back to back with araldite to form the hollow radiometer arm sections. The curved surfaces along the length of each side of the arm are lined with a material of low emissivity; the emissivity being a measure of how well a body can radiate energy compared with a black body.

The main object of lining the curved surfaces of the radiometer arm sections with a material of low emissivity is to (i) reduce the effect of temperature changes of the radiometer arm itself on the output of the radiometer and

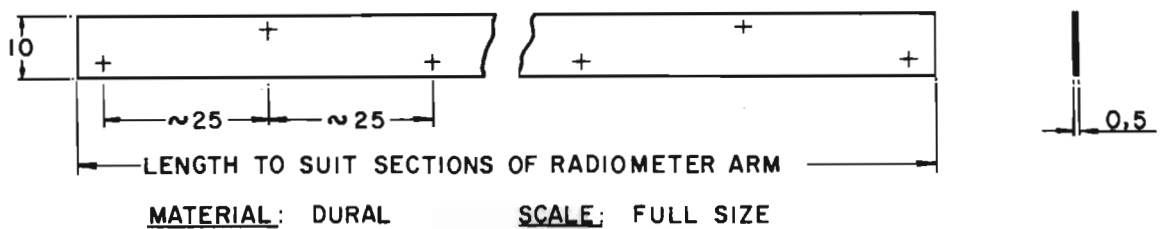


a) END VIEW OF ONE OF THE SECTIONS OF THE RADIOMETER ARM
(WITHOUT THE END FLANGES AND RADIATION SENSING ELEMENTS)

Note: ALL DIMENSIONS IN MILLIMETRES



b) SECTION THROUGH ITEM ①



c) ITEM ②

FIGURE 48

*Measurement of the radiative heat loss rate from a human body:
assembly of the extruded aluminium sections which form the basic
framework of the radiometer arm.*

(ii) to reflect the incoming radiation from the surrounding test chamber walls and/or body onto the radiation-sensing elements.

In Figure 49 the emissivities of various materials are plotted as a function of wave-length. It is seen that polished copper and aluminium have the lowest emissivities at radiation wave-lengths above $1\mu\text{m}$. Due to the ready availability of polished aluminium foil and the fact that the emissivity of aluminium is only slightly higher than that of copper, it was decided to line the curved surfaces along the length of each side of the arm with aluminium foil.

5.4.2 Radiation-sensing elements

The radiation-sensing elements, in the form of fine nickel wire ribbon, 0,25 mm wide by 0,005 mm thick, are located on either side of the radiometer arm as illustrated in Figure 47 on page 254. The wires were painted black with optical matt-black lacquer.

Nickel was chosen as a suitable material for the radiation-sensing elements in view of the following considerations:

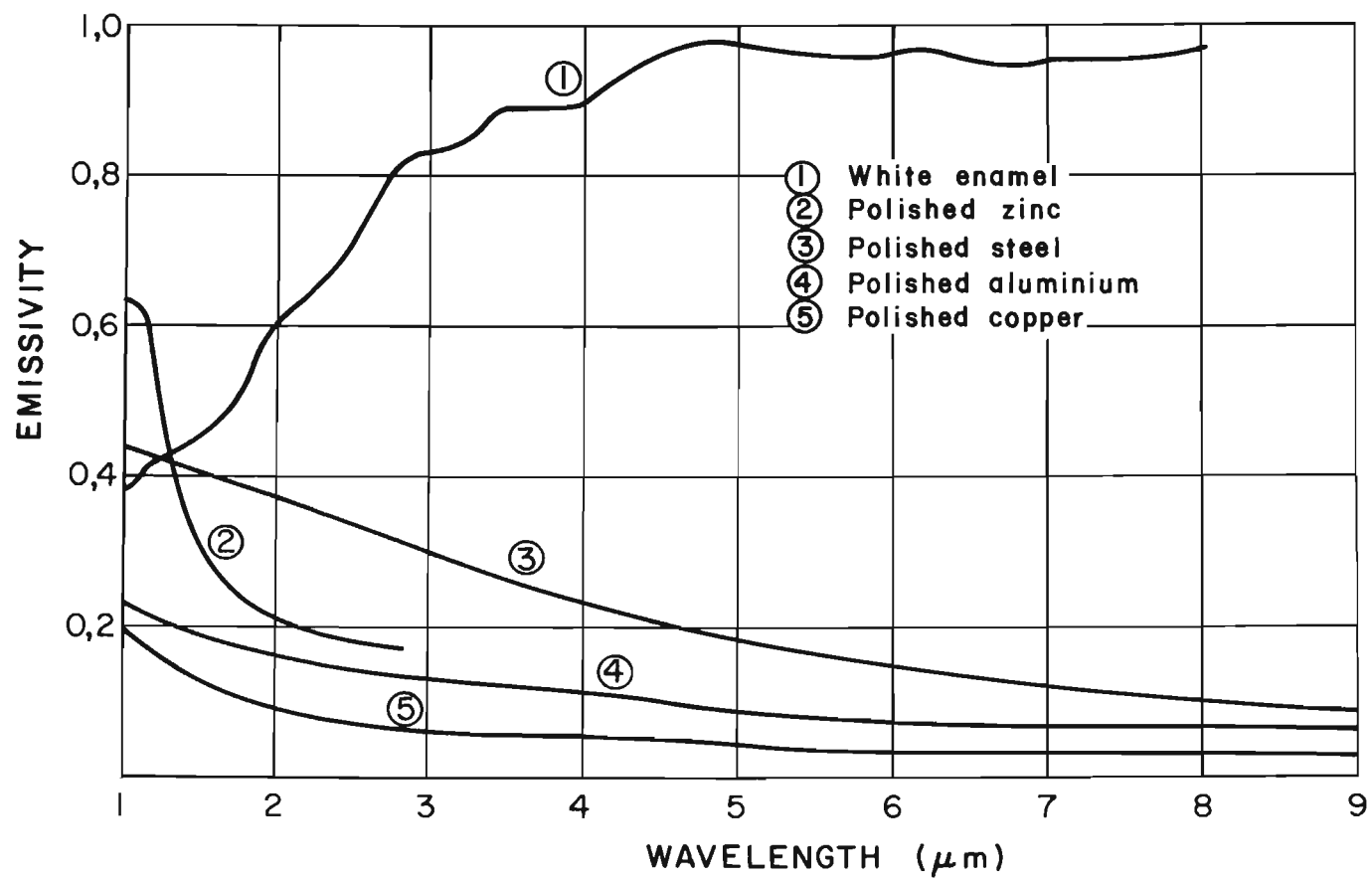


FIGURE 49
Spectral emissivity of different materials

Since the output of the radiometer results from changes in the electrical resistance of the sensing elements which in turn are caused by temperature variations, it is important that for high sensitivities the radiation-sensing elements should be constructed from a material having a relatively high temperature coefficient of electrical resistance.

(The incident radiation causes a temperature rise of the radiation-sensing elements). High purity platinum and nickel have relatively high temperature coefficients of electrical resistance; of the order of 0,004 and 0,006 per °C, respectively. The temperature coefficient of nickel is thus somewhat higher than that of platinum.

Apart from the requirement of a relatively high temperature coefficient of electrical resistance, the sensing element material of resistance thermometers should also be stable. For this reason platinum is often preferred for the accurate measurement of temperature, particularly at high temperatures. However, since the proposed method of measuring the radiative heat loss from a human body involves the "measurement" of a temperature difference between the "thermometers" lining the inner and outer surfaces of the radiometer arm, absolute accuracies are not essential. Furthermore, the radiometer arm will not be required to

operate at abnormally high temperature conditions.

Method of mounting the radiation-sensing elements in the radiometer arm

Since the electrical resistance of most materials is also a function of strain, it is important that the radiation-sensing elements should be mounted in such a manner that the elements are subjected to the minimum stress variations with time.

In order to meet with the foregoing requirements, the following method of mounting the inner and outer radiation-sensing elements in the various sections of the radiometer arm was adopted:

Each sensing element, which is in the form of nickel ribbon, 0,25 mm wide by 0,005 mm thick, was strung in one continuous length between two sets of perspex flanged rollers and spacers located at either end of the particular section of the radiometer arm to form 14 loops of wire. Each set of flanged rollers and spacers were mounted in a sliding bracket which was spring loaded by means of two 3 mm diameter helical coil springs to maintain the wire taut and hence prevent short circuiting between the individual loops of wire. Details of the sliding brackets are pre=

sented in Figure 50.

Figure 51 presents a view of one end of a section of the radiometer arm with the sliding bracket in position.

Additional grooved perspex pins were installed along the length of the radiometer section to support the wires and prevent twisting; the wires being mounted in such a manner that the flat surfaces of the wire face outwards to ensure a maximum radiation surface area.

Figure 52 shows the wire being fitted to one of the vertical sections of the radiometer arm.

5.4.3 Wind-shield for protecting the radiation-sensing elements from forced convective influences due to air movement

A polyethylene wind-shield, which is in the form of a 50 mm diameter tube with a wall thickness of 0,04 mm, completely surrounds the radiation-sensing elements; the main object of the wind-shield being to shield the radiation-sensing elements from forced convective influences due to air movement.

Polyethylene was selected as a suitable material for the wind-shield in view of its comparatively high transmission

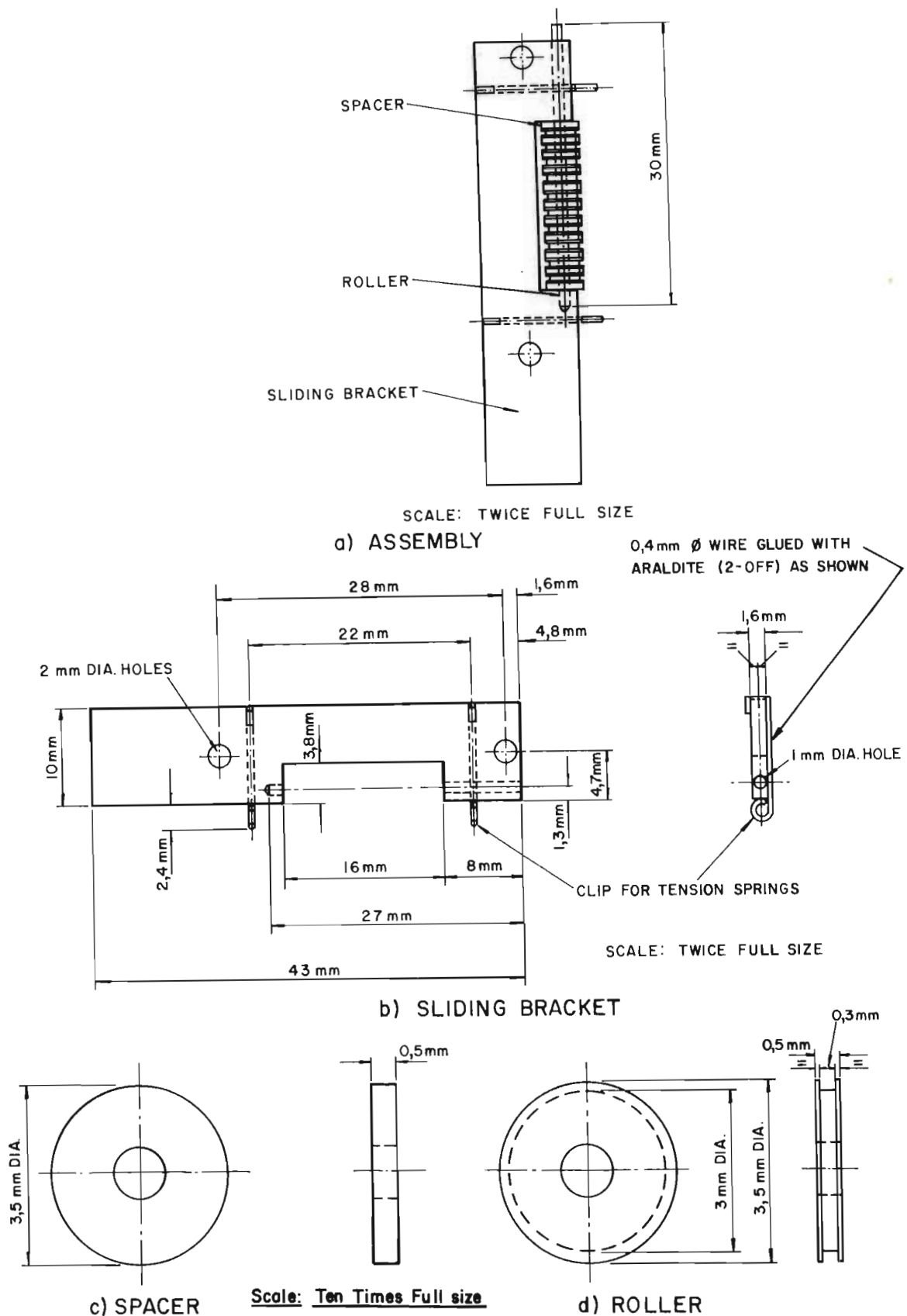
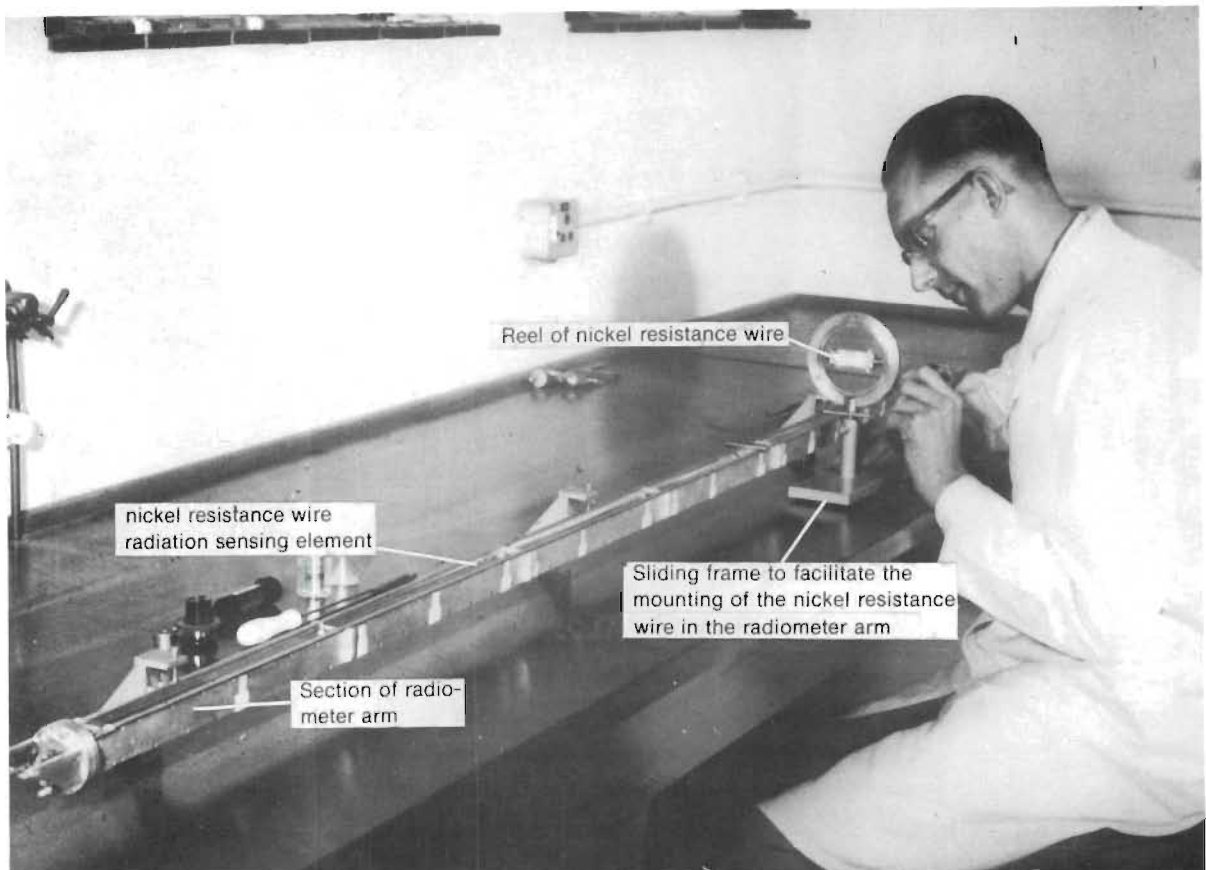


FIGURE 50

Direct measurement of the radiative heat loss rate from a human body: details of the supporting brackets for the radiation-sensing elements of the radiometer arm

**FIGURE 51**

Direct measurement of the radiative heat loss rate from a human body: view of one end of a section of the 4π radiometer arm showing the method of mounting the nickel resistance wire thermal radiation-sensing elements.

**FIGURE 52**

Measurement of the radiative heat loss rate from a human body by means of the 4π radiometer arm: mounting of the thermal radiation-sensing elements in one of the sections of the radiometer arm.

coefficient in the infra-red region.

Figure 53 shows the spectrum of transmission for polyethylene as given by Schulze⁸²⁾ and cited by Funke⁸³⁾.

It is seen that narrow absorption bands around $3,5\mu\text{m}$, $7\mu\text{m}$ and $14\mu\text{m}$, the transmission coefficient of polyethylene is relatively high. Bolle and Fleischer⁸⁴⁾ has shown that the influence of these absorption bands on the accuracy of radiation measurements is relatively small.

It is of interest to note that polyethylene slowly deteriorates through the action of sunlight, as a result of photo oxidization. The effects of this are first noticeable in the infra-red region where new absorption bands appear at $3\mu\text{m}$, $8,5\mu\text{m}$ and $10,65\mu\text{m}$. Later discoloration and increased turbidity occur. Funke⁸³⁾ found the useful life of polyethylene when used as a wind-shield for an outdoor radiometer to be of the order of six months. However, since the wind-shield will not be used outdoors and will only be exposed to ultra violet light from the fluorescent tubes in the test chamber, the effective life of the wind-shield in this case is expected to be considerably longer.

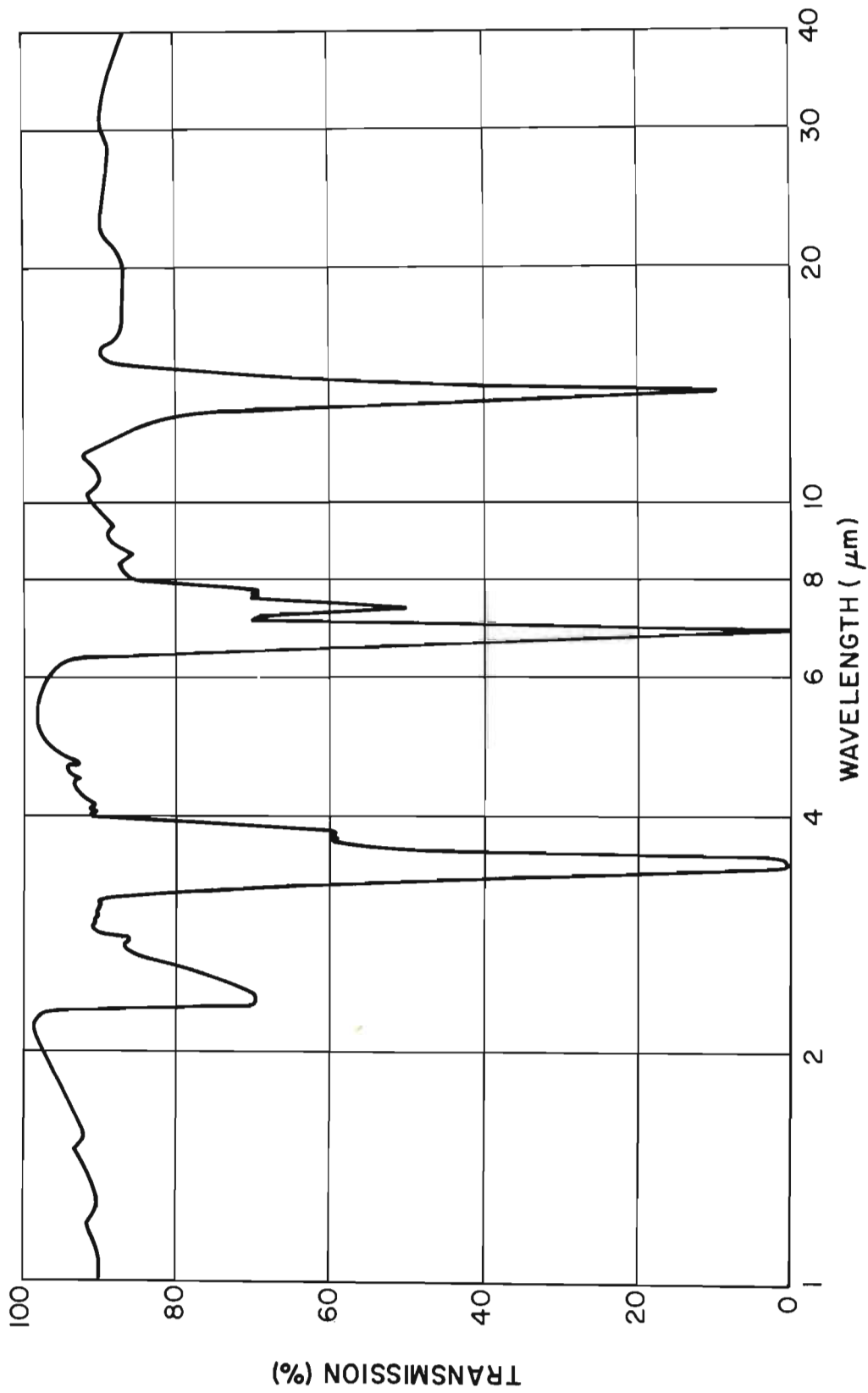


FIGURE 53
*Transmission of polythene (Lupolen-H), 0.1 mm thick
(After Schulze 82)*

Mounting of the wind-shield

Separate polyethylene tubes were provided for each section of the radiometer.

The two ends of each polyethylene tube were clamped between tapered male and female steel rings to form air tight joints.

Since a polyethylene tube of 0,04 mm thickness possesses little rigidity; suitable connections and valves were provided to enable the tubes to be inflated by means of a bicycle pump.

Because of the comparatively high water vapour permeability of polyethylene, and the resultant ingress of moisture into the tube under high humidity conditions, gauze containers containing silica-gel, were mounted inside the wind-shields (at either end of each section of the arm), to maintain low relative humidity conditions within the wind-shields and thus minimise the tendency for moisture to condense onto the inside of the wind-shields and sensing elements. (Alternatively the tubes could be inflated with a gas such as Freon 12. This may be more convenient in view of the inconvenience of having to renew

the silica-gel).

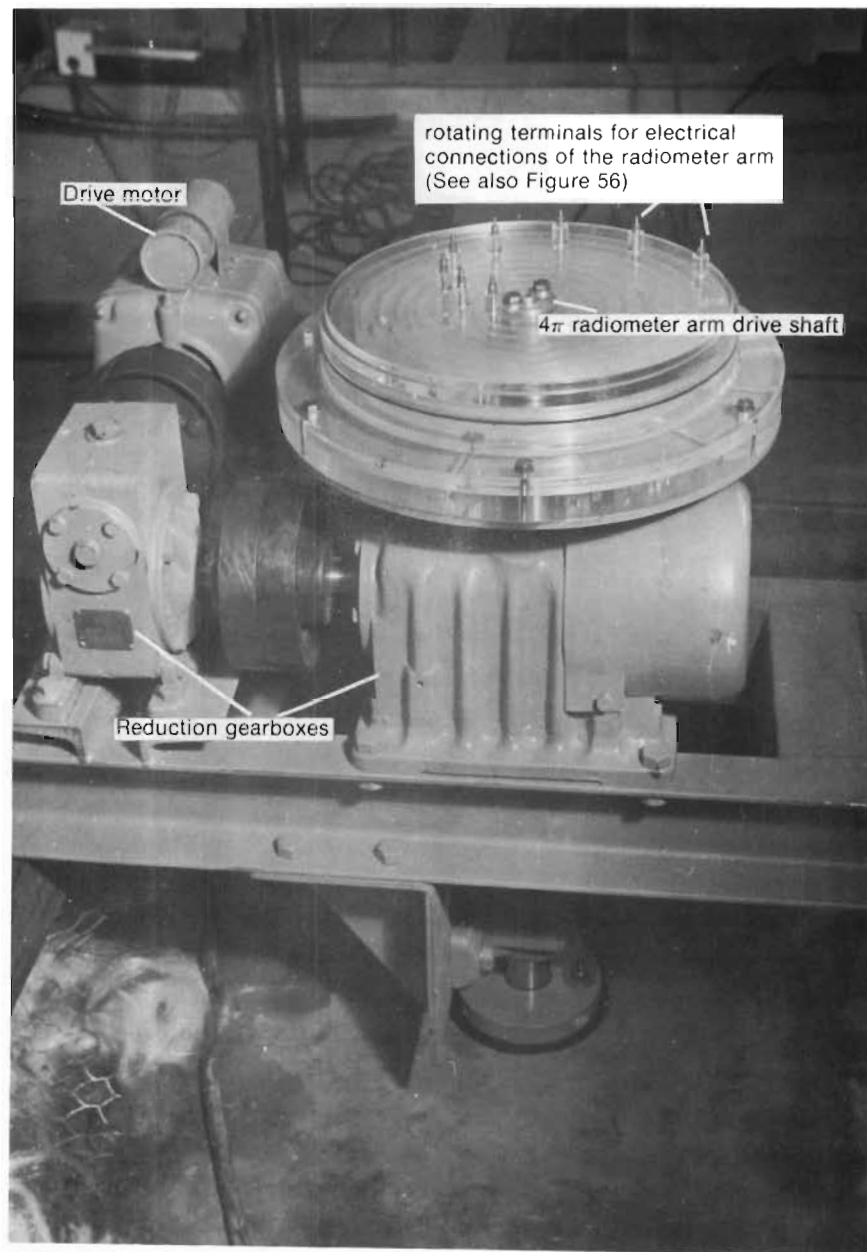
5.4.4 Radiometer arm drive

Figure 54 presents an outside view of the drive unit which is mounted on the roof of the horizontal test chamber of the climatic chamber.

The radiometer arm is driven at a speed of 0,0167 Hz by means of a drive unit which basically consists of a synchronous motor and two reduction gearboxes coupled in series.

The output shaft from the second gearbox extends through the roof panel of the test section.

As shown in Figure 55, the bottom end of the shaft is fitted with a nut and washer for supporting the radiometer arm. The upper sections of the radiometer arm are fitted with a yoke which is clamped around the drive shaft, albeit with a clearance fit and which rests on the supporting washer.

**FIGURE 54**

Direct measurement of radiative heat loss rate from a human body: outside view of the main drive unit for the 4π radiometer arm

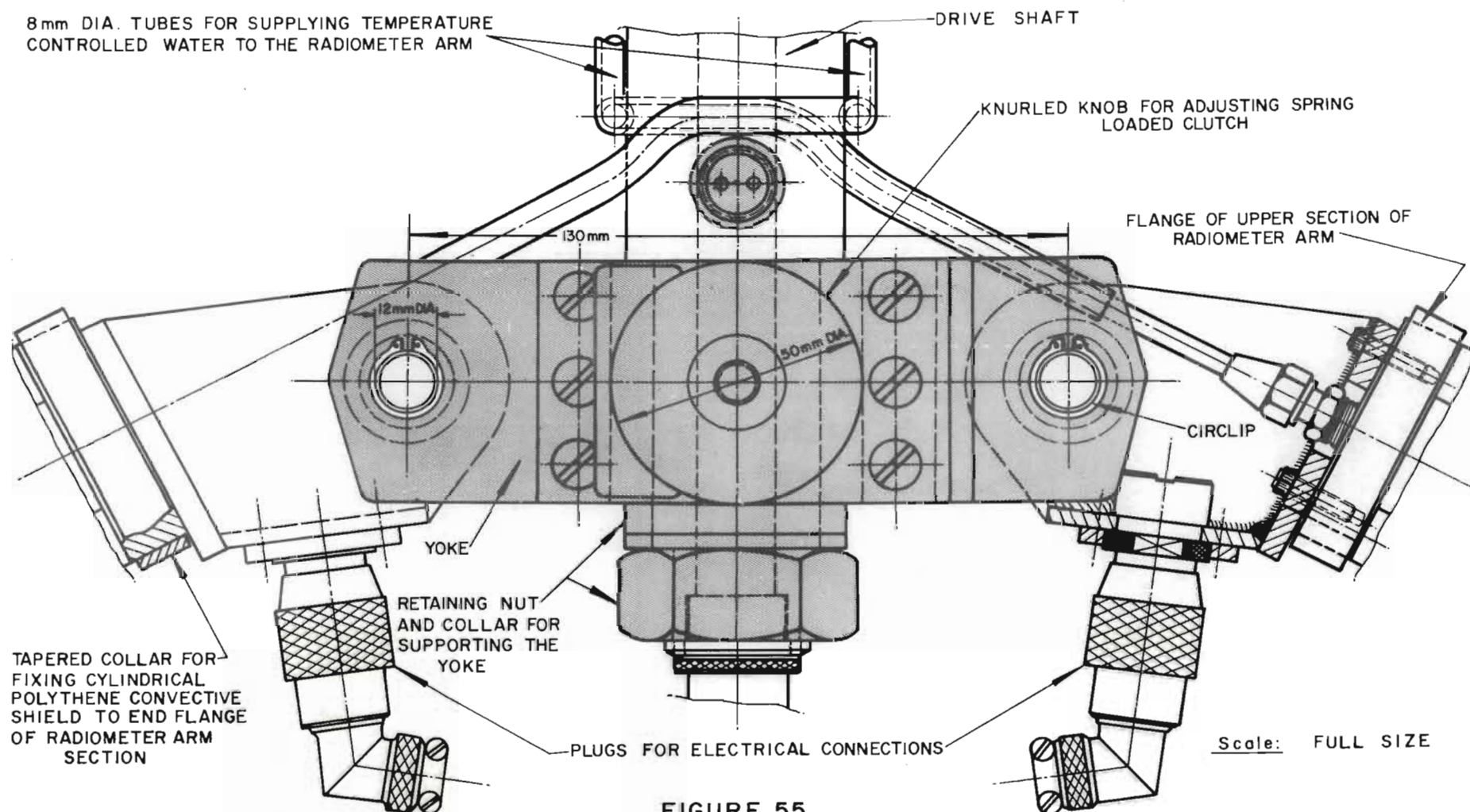


FIGURE 55

*Direct measurement of the radiative heat loss rate from a human body :
outside view of the supporting yoke and clutch assembly of the 4π -radiometer arm.*

Safety clutch

The radiometer arm is driven through a spring loaded safety clutch. The yoke is equipped with two spring loaded 10 mm diameter balls which fit into hardened inserts in the drive shaft. The spring-loaded balls act as a safety clutch which slips if the radiometer arm is obstructed in any way. (In this case the balls slip out of the recesses as the shaft rotated).

Figure 55 presents an outside view of the yoke and clutch assembly.

5.4.5 Electrical connections

Terminal blocks are provided in the positions shown in Figure 51 on page 263, for the electrical connections to each sensing element.

A hole drilled through the radiometer arm drive shaft permits the electrical leads from the radiometer terminal blocks to be taken through the roof of the horizontal test section to terminals which are located in a circular perspex cover plate which rotates with the arm.

The ends of the "moving" terminals are submerged in the stationary channels of mercury, to which the fixed terminals are attached.

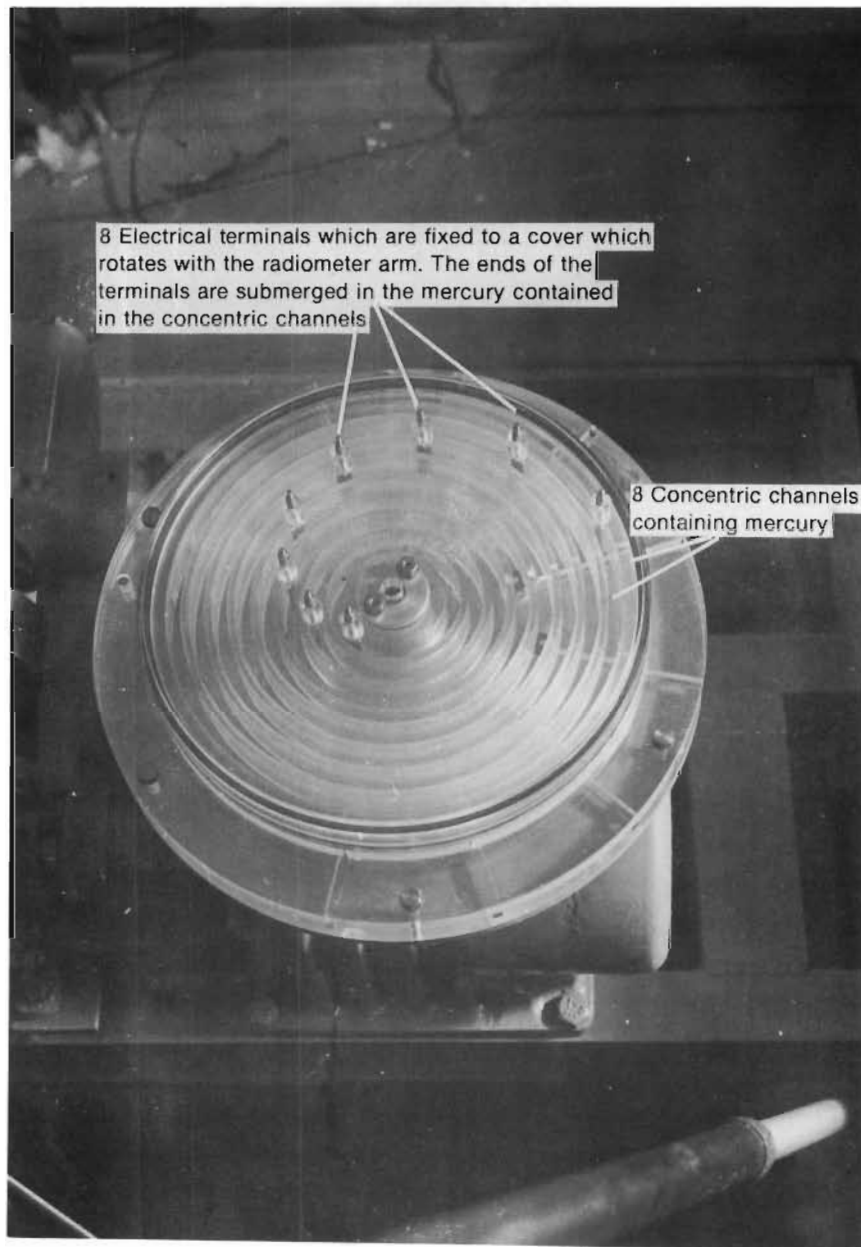
The terminal assembly acts as "slip ring contacts" for the electrical leads from the rotating radiometer arm.

Figure 56 presents an outside view of the whole terminal assembly which, apart from the brass terminals, is constructed from perspex.

5.4.6 Lower support for the radiometer arm

Details of the lower support for the radiometer arm is presented in Figure 57.

Each of the lower sections of the radiometer arm is fitted with two 40 mm diameter x 10 mm wide rollers which rest against a 1 400 mm diameter vertical pillar which is fixed to the floor of the horizontal test chamber of the climatic chamber. The rollers of both the lower sections of the radiometer arm are held in contact with the pillar by means of two 10 mm diameter helical coil springs. As the arm rotates the rollers rotate around the central pillar.

**FIGURE 56**

Direct measurement of the radiative heat loss rate from a human body: 'Slip-ring' contacts for the electrical leads connected to the thermal radiation-sensing elements in the 4π radiometer arm.

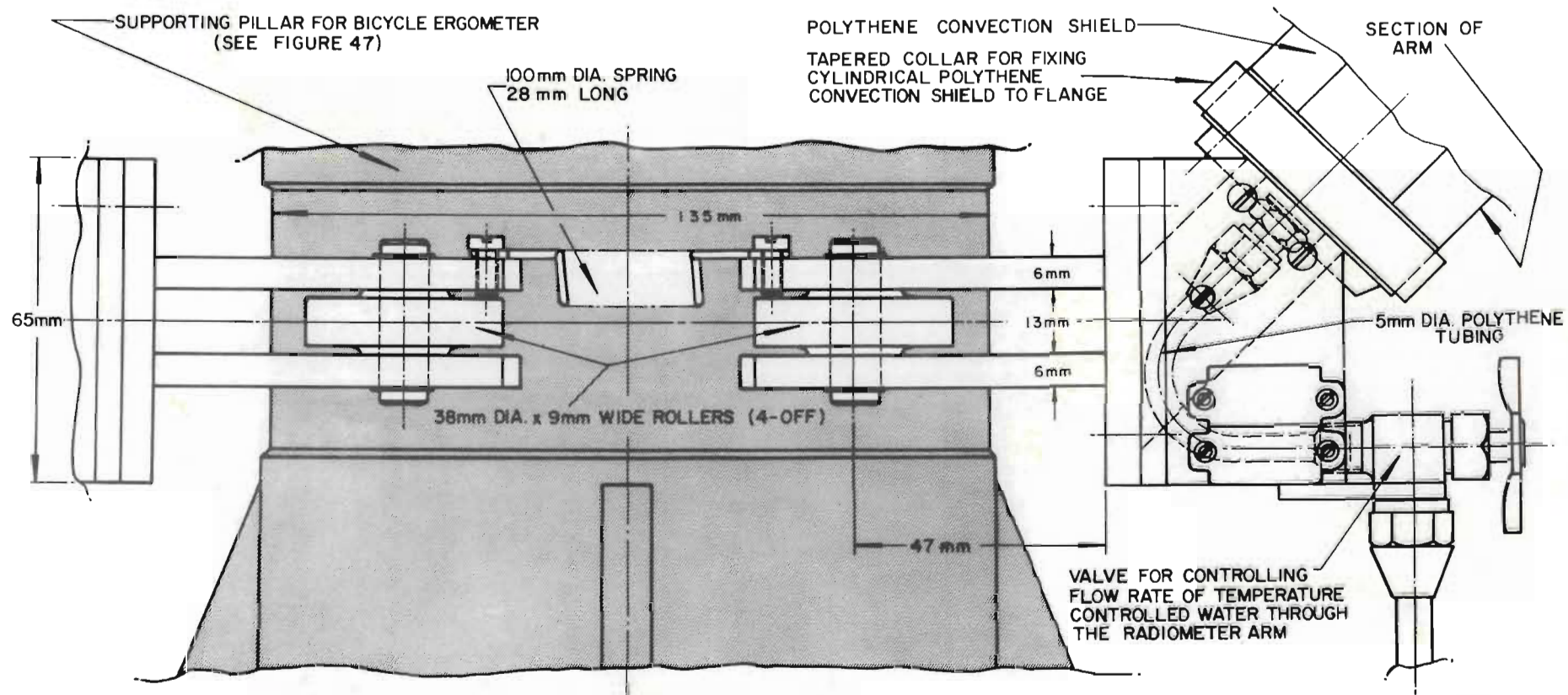


FIGURE 57

*Direct measurement of the radiative heat loss rate from a human body:
 details of the lower roller support for the rotating 4π radiometer arm*

Scale: FULL SIZE

A circular trough is fitted around the pillar for collecting the water which is circulated through the arm.

5.5 Method of recording the radiometer output

A knowledge of the order of magnitude of the temperature difference between the radiation-sensing elements lining the "inner" and "outer" surfaces of the 4π radiometer, under typical radiation conditions, is necessary in order to decide on a suitable method of measuring the radiometer output.

Certain theoretical calculations were, therefore, carried out in order to assess the temperature variations with time of the radiation-sensing elements during a typical revolution of the 4π radiometer arm.

5.5.1 Theoretical considerations

As mentioned in Section 2.1 on page 51, the horizontal test chamber of the climatic chamber is constructed in the form of a cube, 3 m x 3 m x 3 m in size.

Temperature and humidity controlled air enters and leaves the horizontal test chamber through bar-grid panels comprising the opposite walls.

Temperature-controlled fluid is circulated through the bar-grid panels for the purpose of temperature control. Similar facilities are provided for the independent temperature control of the floor, roof and each of the side wall panels of the test chamber.

As the 4π radiometer arm rotates about the body in the test section, the "outer" surface of the radiometer arm "sees" the roof, floor, side wall and bar-grid panels whilst the "inner" surface, in addition, "sees" the body in the centre of the test section.

Under these conditions, the temperature of each radiation-sensing element (which is in the form of fine nickel ribbon), is primarily affected by the rates of radiation heat exchange between the sensing element and the surrounding surfaces and body that are "seen" by the radiation-sensing element and the convective heat exchange between the sensing element and the air contained in the polyethylene tube surrounding the element. In addition, the radiation-sensing element temperature is influenced to some extent by the electrical current which flows through the sensing element and the resultant heating effect, the conduction of heat along the length of the

sensing element to the end terminals and supports as well as the thermal inertia of the sensing element under non-steady state conditions.

The exact magnitude of the electrical heating effect can only be assessed once the method of measuring the radiometer output has been finalised. However, the effect of electrical heating on the temperature of the radiation-sensing element can be minimised by ensuring that the electrical resistance of each element is relatively high and the electrical voltage which is applied across it is sufficiently low. In addition, the effects of electrical heating on the temperature difference between the radiation-sensing elements lining the "inner" and "outer" surfaces of the radiometer and hence the radiometer output will be cancelled out to some extent since both sets of sensing elements will be heated to a similar extent.

Similarly, the effects of heat conduction along the length of each radiation-sensing element on the radiometer output will also be cancelled out to some extent since the sensing elements lining the "inner" and "outer" surfaces of the radiometer arm will be affected to a similar extent. The effects of heat conduction on the temperature of each

radiation-sensing element will in any case be small due to the relatively small cross-sectional area and the comparatively long lengths of fine nickel wire ribbon which form the sensing elements.

Simplifying assumptions

In view of the above-mentioned considerations and the fact that an approximate value of the temperature difference between the radiation-sensing elements lining the "inner" and "outer" surfaces of the 4π radiometer arm was required, the following simplifying assumptions were made in the theoretical analysis to assess the temperature variations with time of the radiation-sensing elements during a typical revolution of the radiometer arm:

- (i) The influence of electrical heating, heat conduction and thermal inertia on the temperature variations with time of the radiation-sensing elements were neglected and the temperature of each sensing element was assumed to be affected principally by radiation and convection,
- (ii) the body was assumed to be in the form of a cylinder; 300 mm dia x 1 500 mm high; located in the centre of the horizontal test chamber of the climatic chamber,

- (iii) the respective emissivities of the surrounding surfaces and body were assumed to be close to unity, and
- (iv) the radiant area of each sensing element was assumed to be equal to half the total surface area of the sensing element.

In addition, the calculations to determine the temperature variations with time of the radiation-sensing elements were confined to the vertical sections of the radiometer arm (see Figure 47 on page 254), it being furthermore assumed that the effects of the roof and floor panels of the horizontal test chamber of the climatic chamber on the temperatures of the sensing elements located in the vertical sections would be comparatively small and could, therefore, be neglected.

Radiation-sensing element lining the "inner" surface of the radiometer

Based on the above-mentioned assumptions, the energy balance equation for the "inner" radiation-sensing element may be written as follows:

$$\begin{array}{c} \text{Heat exchange rate} \\ \text{by radiation} \end{array} \quad \begin{array}{c} \text{Heat exchange rate} \\ \text{by convection} \end{array} \\
 \hline \dot{q}_{\text{rad,ise,so}} + \dot{q}_{\text{rad,ise,bg}} + \dot{q}_{\text{rad,ise,b}} + \dot{q}_{\text{c,ise}} = 0 \dots (35)$$

where $\dot{q}_{\text{rad,ise,so}}, \dot{q}_{\text{rad,ise,bg}}$ = radiation heat exchange rate between the "inner" radiation-sensing element and the solid and bar-grid panels of the horizontal test chamber, respectively, kW

$\dot{q}_{\text{rad,ise,b}}$ = radiation heat exchange rate between the "inner" radiation-sensing element and the body, kW

$\dot{q}_{\text{c,ise}}$ = convective heat exchange rate between the "inner" radiation-sensing element and the surrounding air, kW.

One of the chief mathematical complexities in treating radiative heat transfer between surfaces is accounting for the geometric relations involved in how the surfaces view each other. In the case of the horizontal test section of the climatic chamber, the position is further complicated by the asymmetrical temperature distribution which can occur due to the one wall being at a different temperature to the other.

The mathematical solution of the problem involves the integration of the radiative interchange, over the finite

areas involved in the exchange process. For specific configurations the geometric relations are generally accounted for by a quantity known as the configuration factor.

Based on this concept, equation (35) may be rewritten

as follows:

$$\sigma F_{ise,so} A_{rad} (T_{so}^4 - T_{ise}^4) + \sigma F_{ise,bg} A_{rad} (T_{bg}^4 - T_{ise}^4) + \sigma F_{ise,b} A_{rad} (T_b^4 - T_{ise}^4) + h_{c,ise} A_T (T_G - T_{ise}) = 0 \dots\dots (36)$$

where σ = Stefan-Boltzman constant,

$$56,69 \times 10^{-12} \text{ kW/m}^2 \text{ } ^\circ\text{K}^4$$

$F_{ise,so}, F_{ise,bg}$ = configuration factors between the "inner" radiation-sensing element and the solid and bar-grid panels of the horizontal test chamber, respectively

$F_{ise,b}$ = configuration factor between the body and the "inner" radiation-sensing element

A_{rad}, A_T = radiant and total areas of the inner radiation-sensing element, respectively, m^2 (A_{rad} is assumed to be equal to $0,5 A_T$)

$T_{ise}, T_{so}, T_{bg}, T_b$ = absolute surface temperatures of the "inner" sensing element, the solid and bar-grid panels of the horizontal test chamber and the body, respectively, $^\circ\text{K}$

T_G = absolute temperature of the air
surrounding the radiation-sensing
elements, °K

$h_{c,ise}$ = film coefficient of heat transfer
for the inner radiation-sensing
element, kW/m² °C

Radiation-sensing element lining the "outer" surface of the
radiometer

Similarly, the energy balance equation for the radiation-
sensing element installed along the "outer" surface of the
radiometer can be written as follows:

$$\sigma F_{ose,so} A_{rad} (T_{so}^4 - T_{ose}^4) + \sigma F_{ose,bg} A_{rad} (T_{bg}^4 - T_{ose}^4) + h_{c,ose} A_T (T_G - T_{ose}) = 0 \quad \dots\dots\dots (37)$$

where $F_{ose,so}$, $F_{ose,bg}$ = configuration factors between
the "outer" radiation-sensing
element and the solid and bar-
grid panels of the horizontal
test chamber, respectively

T_{ose}, T_{so}, T_{bg} = absolute surface temperatures of
the "outer" radiation-sensing
element and the solid and
bar-grid panels of the horizontal
test chamber, respectively, °K

T_G = absolute temperature of the air
surrounding the radiation-sensing
element, °C

$h_{c,ose}$ = film coefficient of heat transfer
for the outer radiation-sensing
element, $\text{kW/m}^2 \text{ } ^\circ\text{C}$

For the purpose of calculating the respective temperatures
of the "inner" and "outer" radiation-sensing elements,
equations (36) and (37) can be expressed in the following
form:

Radiation-sensing element lining the "inner" surface of
the radiometer arm

$$h_{\text{rad,ise,so}} A_{\text{rad}} (t_{\text{so}} - t_{\text{ise}}) + h_{\text{rad,ise,bg}} A_{\text{rad}} (t_{\text{bg}} - t_{\text{ise}}) \\ + h_{\text{rad,ise,b}} A_{\text{rad}} (t_{\text{b}} - t_{\text{ise}}) + h_{c,\text{ise}} A_T (t_G - t_{\text{ise}}) = 0 \dots (38)$$

Radiation-sensing element lining the "outer" surface of
the radiometer arm

$$h_{\text{rad,ose,so}} A_{\text{rad}} (t_{\text{so}} - t_{\text{ose}}) + h_{\text{rad,ose,bg}} A_{\text{rad}} (t_{\text{bg}} - t_{\text{ose}}) \\ + h_{c,\text{ose}} A_T (t_G - t_{\text{ose}}) = 0 \dots (39)$$

where $h_{\text{rad,ise,so}}, h_{\text{rad,ise,bg}}$ = radiation heat transfer coefficients
applicable to the radiant heat
exchange rates between the "inner"
radiation-sensing element and the
solid and bar-grid panels,
respectively, $\text{kW/m}^2 \text{ } ^\circ\text{C}$

and $h_{\text{rad,ose,so}}, h_{\text{rad,ose,bg}}$ = radiant heat transfer coefficients applicable to the radiant energy exchange rates between the "outer" radiation-sensing element and the solid and bar-grid panels, respectively, $\text{kW/m}^2 \text{ } ^\circ\text{C}$

$A_{\text{rad}}, A_{\text{T}}$ = radiant and total surface areas of each radiation-sensing element, respectively, m^2

$t_{\text{b}}, t_{\text{so}}, t_{\text{bg}}$ = surface temperatures of the body and solid and bar-grid panels of the horizontal test chamber, respectively, $^\circ\text{C}$

$t_{\text{G}}, t_{\text{ise}}, t_{\text{ose}}$ = air temperature and surface temperatures of the "inner" and "outer" radiation-sensing element, respectively, $^\circ\text{C}$

$h_{\text{c,ise}}, h_{\text{c,ose}}$ = film coefficients of heat transfer for the "inner" and "outer" radiation-sensing elements, respectively, $\text{kW/m}^2 \text{ } ^\circ\text{C}$ ($h_{\text{c,ise}}$ is assumed to be equal to $h_{\text{c,ose}}$).

Film coefficient of heat transfer

According to McAdams⁶²⁾, the film coefficient of heat transfer, h_c , for a vertical surface under still air conditions is given by the following equation:

$$h_c = 1,42 \times 10^{-3} (\Delta t_{s-G}/L)^{0,25} \dots\dots (40)$$

where h_c = film coefficient of heat transfer,
kW/m² °C

Δt_{s-G} = temperature difference between the
surface and the surrounding air, °C

L = length of surface, m.

Substitution of the value of 1,83 m for the length of the sensing elements in the vertical section of the radiometer arm in equation (40) leads to

$$h_c = 1,25 \times 10^{-3} (\Delta t_{se-G})^{0,25} \dots\dots (41)$$

where Δt_{se-G} = temperature difference between the
radiation-sensing element and the
surrounding air, °C.

The film coefficients of heat transfer for the "inner" and "outer" radiation-sensing elements, $h_{c,ise}$ and $h_{c,ose}$, respectively, are assumed to be equal to h_c in equation (41).

Radiation heat transfer coefficient

The radiation heat transfer coefficients in equations (38) and (39) were determined as follows:

The various components of the net radiation energy exchange rate in kilowatts, between the radiation-sensing elements and the surfaces which are "seen" by the sensing elements, were calculated in accordance with the radiation energy terms on the left hand side of equations (36) and (37), assuming certain surface temperature values for the radiation-sensing elements of the radiometer, the surrounding walls of the horizontal test chamber and the body.

The radiation heat transfer coefficients were then obtained by dividing the radiation energy exchange rates by the product of the radiation-sensing element area and the corresponding temperature difference value.

For example, the radiation heat transfer coefficient between the "inner" radiation-sensing element and a solid panel of the test section was obtained by substitution of the relevant data in the following equations and solving for the radiation heat transfer coefficient,

$$h_{\text{rad,ise,so.}}$$

$$\dot{q}_{\text{rad,ise,so}} = \sigma F_{\text{ise,so}} A_{\text{rad}} (T_{\text{so}}^4 - T_{\text{ise}}^4) \dots (42)$$

$$\text{and } h_{\text{rad,ise,so}} = \dot{q}_{\text{rad,ise,so}} / A_{\text{rad}} (t_{\text{so}} - t_{\text{ise}}) \dots (43)$$

where $\dot{q}_{\text{rad,ise,so}}$ = radiation energy exchange rate between the "inner" radiation-sensing element and the solid panel of the horizontal test chamber, kW

σ = Stefan-Boltzman constant,
 $56,69 \times 10^{-12} \text{ kW/m}^2 \text{ } ^\circ\text{K}^4$

$F_{\text{ise,so}}$ = configuration factor between the "inner" sensing element and the solid panel of the horizontal test chamber

A_{rad} = radiant area of the radiation-sensing element, m^2

$T_{\text{so}}, T_{\text{ise}}$ = absolute surface temperatures of the solid panel of the horizontal test chamber and "inner" radiation-sensing element, respectively, $^\circ\text{K}$

$t_{\text{so}}, t_{\text{ise}}$ = surface temperatures of the solid panel of the horizontal test chamber and "inner" radiation-sensing element, respectively, $^\circ\text{C}$.

$h_{\text{rad,ise,so}}$ = radiation heat transfer coefficient applicable to the radiant energy exchange rate between the "inner" radiation-sensing element and the solid panel of the horizontal test chamber, $\text{kW/m}^2 \text{ } ^\circ\text{C}$.

A knowledge of the configuration factors involved is thus a major prerequisite for the determination of the radiation heat transfer coefficients.

The problem of determining the radiation heat transfer coefficients in equations (38) and (39) on page 283, thus resolves to a determination of the configuration factors and hence the corresponding net radiation energy exchange rates under the assumed temperature conditions.

Based on the method of analysis described in Appendix G, configuration factors between the radiation-sensing elements in the vertical section of the 4π radiometer arm and the body and/or the surrounding walls of the horizontal test chamber of the climatic chamber were determined for the radiometer arm positioned in three positions, namely:

with the radiation-sensing elements "facing" (i) the solid panel, (ii) the corner which is formed by the solid and bar-grid panels and (iii) the bar-grid panel.

Figure 58 presents the configuration factors between the radiation-sensing elements, the body and various sections of the surrounding walls for various positions of the 4π radiometer within the horizontal test chamber of the climatic chamber.

Based on the surface temperature values given in Table 9 and the configuration factors that are listed in Figure 58, calculations were carried out to determine the respective net radiation energy exchange rates of the "inner" and "outer" radiation-sensing elements fitted to one of the vertical sections of the radiometer arm.

TABLE 9 : ASSUMED SURFACE TEMPERATURE VALUES FOR THE PURPOSE OF CALCULATING THE NET RADIATION ENERGY EXCHANGE RATES AND HENCE THE RADIATION HEAT TRANSFER COEFFICIENTS FOR THE RADIATION-SENSING ELEMENTS LOCATED IN ONE OF THE VERTICAL SECTIONS OF THE 4π RADIOMETER ARM

	Air Temperature (°C)	SURFACE TEMPERATURE (°C)			
		Radiation-sensing element	Test section walls		Body
			Solid Panels	Bar-grid Panels	
(i)	16	17	15	16	22
(ii)	24	37	35	34	27,3

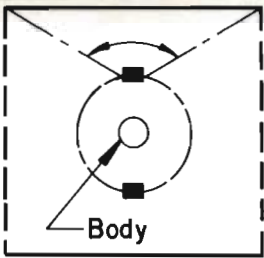
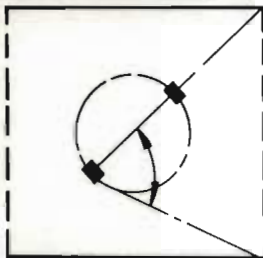
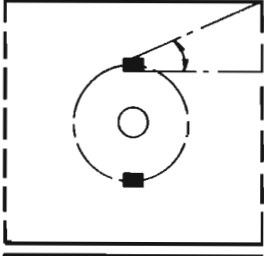
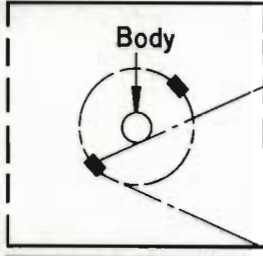
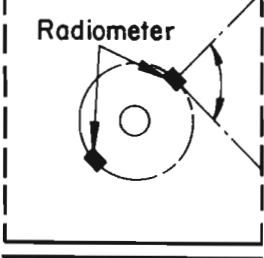
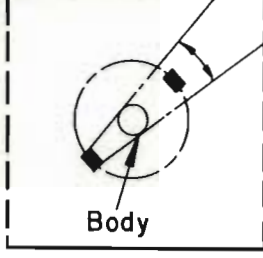
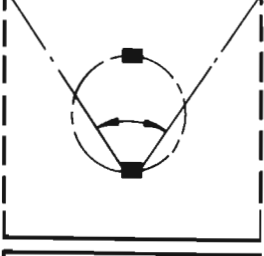
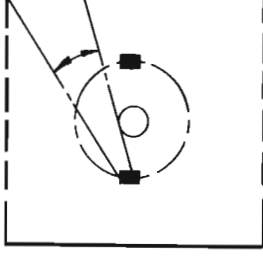
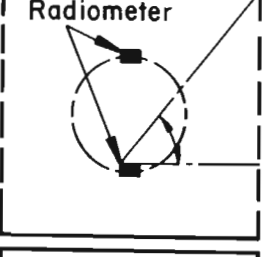
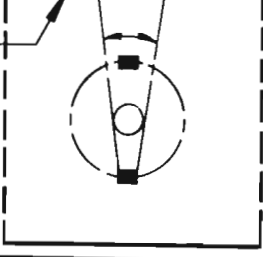
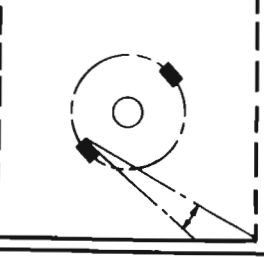
Radiometer position	Configuration factor	Radiometer position	Configuration factor
	0,3718		0,1492
	0,0333		0,1260
	0,2288		0,0557
	0,1864		0,1307
	0,1631		0,0557
	0,0134	Plan views of the test section of the climatic chamber with the vertical arms of the radiometer in various positions	

FIGURE 58

Configuration factors between the radiation-sensing elements located in one of the vertical sections of the 4π radiometer arm, the body and various sections of the surrounding walls of the test section of the climatic chamber, with and without the body in position

The analysis which included the calculations to determine the configuration factors, was carried out with the aid of a digital computer in accordance with the computer flow diagram shown in Figure 59.

The results are presented in Table 10.

Radiation heat transfer coefficients

The radiation heat transfer coefficients referred to in equations (38) and (39) on page 283, were obtained by dividing the radiation energy exchange rate values in Table 10 by the product of the radiation-sensing element area and the corresponding temperature difference values between the sensing element and the surfaces that are "seen" by the radiometer. (See Table 9 on page 289 and equation (43) on page 287).

The calculated values for the radiation heat transfer coefficients are presented in Table 11.

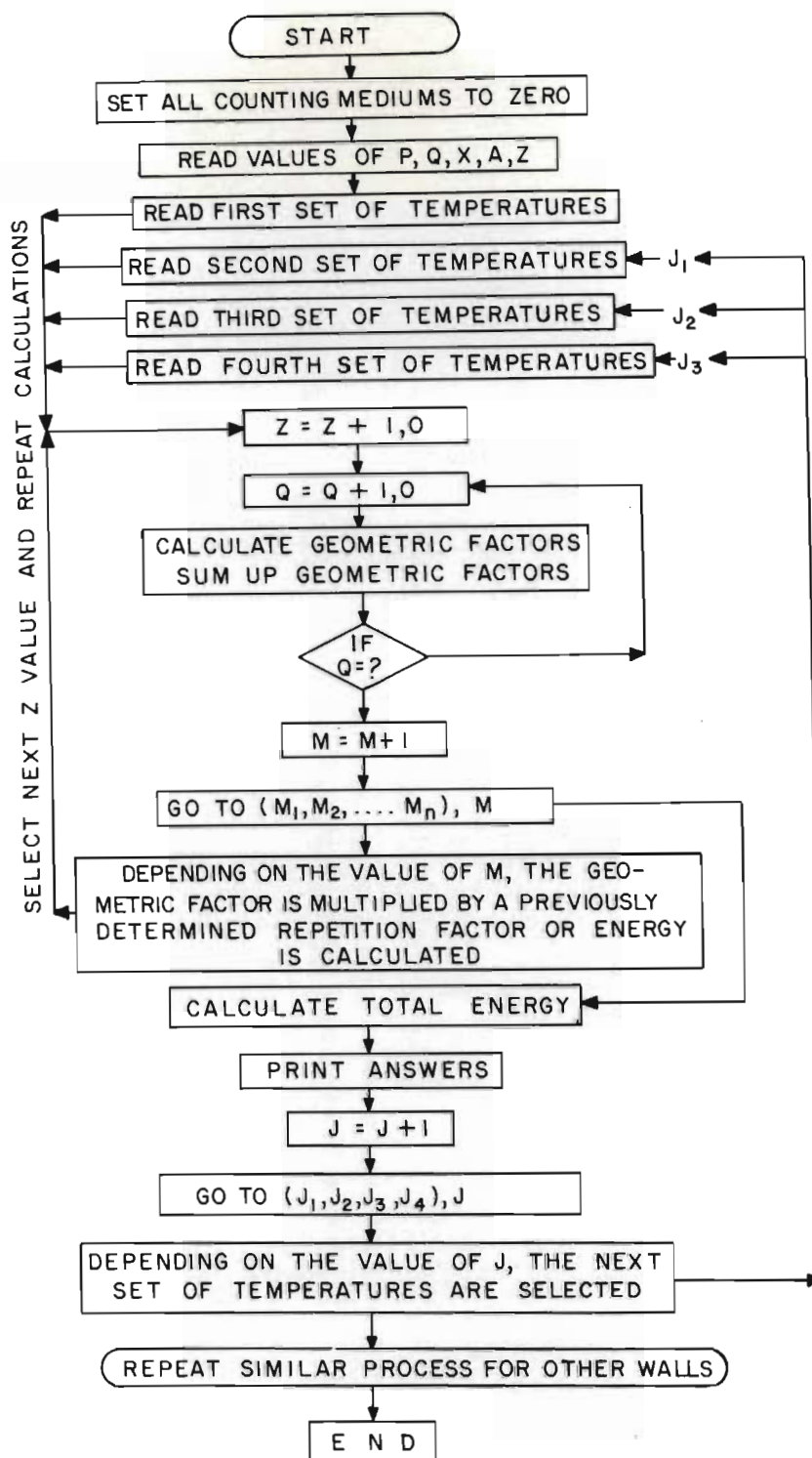


FIGURE 59

Flow diagram of the computer programme for calculating the net radiation energy exchange rate between the radiation-sensing elements in the radiometer arm, the body, and various sections of the surrounding walls of the test chamber.

TABLE 10 : THEORETICAL RADIATION ENERGY EXCHANGE RATES OF THE "INNER" AND "OUTER" RADIATION-SENSING ELEMENTS LOCATED IN ONE OF THE VERTICAL SECTIONS OF THE 4π RADIOMETER, BASED ON THE ASSUMED SURFACE TEMPERATURE VALUES GIVEN IN TABLE 9

Radiation-sensing element under consideration	Position of radiometer : part of the test section which is directly in front of the radiation-sensing element (see Figure 58 on page 290)	Theoretical radiation energy exchange rate between the radiation-sensing element and the particular surface referred to (10^{-6} kW)		
		Solid panel	Bar-grid panel	Body
Conditions : (i) <u>Without</u> body in centre of the horizontal test chamber (ii) Temperature conditions as specified in line (1) of Table 9 on page 289				
Outer	Solid panel	-52,036	- 2,33	-
Outer	Corner	-32,022	-16,011	-
Outer	Bar-grid panel	- 4,66	-26,018	-
Inner	Solid panel	-26,122	-11,427	-
Inner	Corner	-22,762	-11,381	-
Inner	Bar-grid panel	-22,854	-13,061	-
Conditions : (i) <u>With</u> body in centre of the horizontal test chamber (ii) Temperature conditions as specified in line (1) of Table 9 on page 289				
Inner	Solid panel	-18,318	-11,427	39,45
Inner	Corner	-19,570	- 9,785	39,45
Inner	Bar-grid panel	-22,854	- 9,154	39,45

TABLE 10 (Contd)

Radiation-sensing element under consideration	Position of radiometer : part of the test section which is directly in front of the radiation-sensing element (see Figure 58 on page 290)	Theoretical radiation energy exchange rate between the radiation-sensing element and the particular surface referred to (10^{-6} kW)		
		Solid panel	Bar-grid panel	Body
Conditions : (i) <u>Without</u> body in centre of the horizontal test chamber (ii) Temperature conditions as specified in line (2) of Table 9 on page 289				
Outer	Solid panel	-63,276	- 8,502	-
Outer	Corner	-38,860	-58,290	-
Outer	Bar-grid panel	- 5,668	-94,914	-
Inner	Solid panel	-31,722	-41,631	-
Inner	Corner	-27,686	-41,529	-
Inner	Bar-grid panel	-27,754	-47,583	-
Conditions : (i) <u>With</u> body in centre of the horizontal test chamber (ii) Temperature conditions as specified in line (2) of Table 9 on page 289				
Inner	Solid panel	-22,248	-41,631	-69,84
Inner	Corner	-23,736	-35,604	-69,84
Inner	Bar-grid panel	-27,754	-33,372	-69,84

TABLE 11 : RADIATION HEAT TRANSFER COEFFICIENTS OF THE "INNER" AND "OUTER" RADIATION-SENSING ELEMENTS LOCATED IN ONE OF THE VERTICAL SECTIONS OF THE 4π RADIOMETER ARM

Radiation-sensing element under consideration	Part of the test section which is directly in front of the radiation-sensing element (see Figure 58 on page 290)	Radiation heat transfer coefficients, $W/m^2 \text{ } ^\circ C$ (see equation (43) on page 287)		
Conditions : (i) <u>Without</u> body in the centre of the test section (ii) Nominal temperatures of the solid and bar-grid panels of the test section; $15^\circ C$ and $16^\circ C$, respectively				
		$h_{rad,ose,so}$	$h_{rad,ose,bg}$	$h_{rad,ise,b}$
Outer	Solid panel	2,03	0,18	-
Outer	Corner	1,25	1,25	-
Outer	Bar-grid panel	0,18	2,03	-
		$h_{rad,ise,so}$	$h_{rad,ise,bg}$	$h_{rad,ise,b}$
Inner	Solid panel	1,08	0,89	-
Inner	Corner	0,88	0,88	-
Inner	Bar-grid panel	0,89	1,08	-
Conditions : (i) <u>With</u> body in the centre of the test section (ii) Nominal temperatures of the solid and bar-grid panels of the test section and body: $15^\circ C$, $16^\circ C$ and $22^\circ C$, respectively				
		$h_{rad,ise,so}$	$h_{rad,ise,bg}$	$h_{rad,ise,b}$
Inner	Solid panel	0,71	0,89	0,61
Inner	Corner	0,76	0,76	0,61
Inner	Bar-grid panel	0,89	0,71	0,61

TABLE 11 (Contd)

Radiation-sensing element under consideration	Position of the radiometer given by the part of the test section which is directly in front of the radiation-sensing element (see Figure 58 on page 290)	Radiation heat transfer coefficients, $W/m^2 \text{ } ^\circ C$ (see equation (43) on page 287)		
Conditions : (i) <u>Without</u> body in the centre of the test section (ii) Nominal temperatures of solid and bar-grid panels of the test section: $35^\circ C$ and $34^\circ C$, respectively				
		$h_{rad,ose,so}$	$h_{rad,ose,bg}$	$h_{rad,ise,b}$
Outer	Solid panel	2,47	0,22	-
Outer	Corner	1,51	1,51	-
Outer	Bar-grid panel	0,22	2,407	-
		$h_{rad,ise,so}$	$h_{rad,ise,bg}$	$h_{rad,ise,b}$
Inner	Solid panel	1,23	1,08	-
Inner	Corner	1,08	1,08	-
Inner	Bar-grid panel	1,08	1,23	-
Conditions : (i) <u>With</u> body in the test section (ii) Nominal temperatures of the solid and bar-grid panels of the test section and body: $35^\circ C$, $34^\circ C$ and $27,3^\circ C$, respectively				
		$h_{rad,ise,so}$	$h_{rad,ise,bg}$	$h_{rad,ise,b}$
Inner	Solid panel	0,86	1,08	0,56
Inner	Corner	0,92	0,92	0,56
Inner	Bar-grid panel	1,08	0,86	0,56

5.5.2 Temperature variations with time of the radiation-sensing elements incorporated in one of the vertical sections of the radiometer arm

Substitution of the function for the film coefficient of heat transfer, h_c , (see equation (41) on page 285), in equations (38) and (39) leads to:

$$h_{\text{rad,ise,so}} A_{\text{rad}} (t_{\text{so}} - t_{\text{ise}}) + h_{\text{rad,ise,bg}} A_{\text{rad}} (t_{\text{bg}} - t_{\text{ise}}) + h_{\text{rad,ise,b}} A_{\text{rad}} (t_{\text{b}} - t_{\text{ise}}) + 1,25 \times 10^{-3} A_T (t_G - t_{\text{ise}})^{1,25} = 0 \quad \text{..(44)}$$

$$\text{and } h_{\text{rad,ose,so}} A_{\text{rad}} (t_{\text{so}} - t_{\text{ose}}) + h_{\text{rad,ose,bg}} A_{\text{rad}} (t_{\text{bg}} - t_{\text{ose}}) + 1,25 \times 10^{-3} A_T (t_G - t_{\text{ose}})^{1,25} = 0 \quad \text{..(45)}$$

$h_{\text{rad,ise,so}}$ $h_{\text{rad,ise,bg}}$ = radiation heat transfer coefficients applicable to the radiant heat exchange rates between the "inner" radiation-sensing element and the solid and bar-grid panels, respectively, $\text{kW/m}^2 \text{ } ^\circ\text{C}$

$h_{\text{rad,ise,b}}$ = radiation heat transfer coefficient applicable to the radiant heat exchange rate between the "inner" radiation-sensing element and the body, $\text{kW/m}^2 \text{ } ^\circ\text{C}$

$h_{\text{rad,ose,so}}$ $h_{\text{rad,ose,bg}}$ = radiant heat transfer coefficients applicable to the radiant energy exchange rates between the "outer" radiation-sensing element and the solid and bar-grid panels, respectively, $\text{kW/m}^2 \text{ } ^\circ\text{C}$

A_{rad} = radiant surface area of each radiation-sensing element, $12,801 \times 10^{-3} \text{ m}^2$

A_T = total surface area of each radiation-sensing element, $25,602 \times 10^{-3} \text{ m}^2$

t_b, t_{so}, t_{bg} = surface temperatures of the body and solid and bar-grid panels of the test section, respectively, °C

t_G, t_{ise}, t_{ose} = air temperature and surface temperatures of the "inner" and "outer" radiation-sensing elements, respectively, °C.

Substitution of the values for the heat transfer coefficients

$h_{rad,ise,so}, h_{rad,ise,bg}, h_{rad,ise,b}, h_{rad,ose,so}$ and

$h_{rad,ose,bg}$ that are listed in Table 11 and the assumed air

temperature and surface temperature values, t_G, t_b, t_{so}

and t_{bg} , that are presented in Table 9 on page 289 in

equations (44) and (45) enables the respective temperatures

of the "inner" and "outer" radiation-sensing elements,

t_{ise} and t_{ose} , to be determined for various positions of

the radiometer arm within the horizontal test chamber

of the climatic chamber.

For example, assuming the respective temperatures of the

air, solid panel and bar-grid panels to be 16°C, 15°C and 16°C

and the radiometer arm to be positioned in such a way that

the solid panel is directly in front of the radiation-

sensing element, the temperature of the "outer" sensing

element is obtained by substituting the following temperature and heat transfer coefficient values in equation (45) and solving for t_{ose} :

$$\begin{aligned} t_G &= 16^\circ\text{C}, \quad t_{so} = 15^\circ\text{C}, \quad t_{bg} = 16^\circ\text{C} \\ h_{\text{rad},ose,so} &:= 2,03 \text{ kW/m}^2 \text{ }^\circ\text{C} \\ h_{\text{rad},ose,bg} &:= 0,18 \text{ kW/m}^2 \text{ }^\circ\text{C} \\ A_{\text{rad}} &:= 12,801 \times 10^{-3} \text{ m}^2 \\ A_T &:= 25,602 \times 10^{-3} \text{ m}^2 \end{aligned}$$

Substitution of the above-mentioned values in equation (45) leads to:

$$13,3609 - 0,8858 t_{ose} + (16 - t_{ose})^{1,25} = 0$$

Solving for t_{ose} gives $t_{ose} = 15,53^\circ\text{C}$.

In a similar manner, non-linear equations (from which the values for the respective temperatures of the "inner" and "outer" sensing elements, t_{ise} and t_{ose} , could be derived), were obtained for the various temperature conditions and radiometer arm positions listed in Figure 58 on Table 9 on pages 290 and 289, respectively.

The results are presented in Table 12.

TABLE 12 : THEORETICAL TEMPERATURES OF THE "INNER" AND "OUTER" RADIATION-SENSING ELEMENTS INCORPORATED IN THE VERTICAL SECTIONS OF THE 4 π RADIOMETER ARM FOR VARIOUS TEMPERATURE CONDITIONS AND RADIOMETER POSITIONS WITHIN THE HORIZONTAL TEST CHAMBER OF THE CLIMATIC CHAMBER

Radiation-sensing element under consideration	Part of the test section which is directly in front of the radiation-sensing element (see Figure 58 on page 290)	Non-linear equations for determining the "inner" and "outer" radiation-sensing element temperatures, t_{ise} and t_{ose} respectively	Radiation-sensing element temperature, °C	
			Inner, t_{ise}	Outer, t_{ose}
Conditions : (i) Without the body in the centre of the horizontal test chamber (ii) Nominal temperatures of the solid and bar-grid panels of the test section; 15°C and 16°C, respectively				
Outer	Solid panel	$13,3609 - 0,8858 t_{ose} + (16 - t_{ose})^{1,25} = 0$	-	15,53
Outer	Corner	$15,5106 - 1,0016 t_{ose} + (16 - t_{ose})^{1,25} = 0$	-	15,70
Outer	Bar-grid panel	$14,1011 - 0,8858 t_{ose} + (16 - t_{ose})^{1,25} = 0$	-	15,95
Inner	Solid panel	$11,8358 - 0,7652 t_{ise} + (16 - t_{ise})^{1,25} = 0$	15,73	-
Inner	Corner	$11,0253 - 0,7113 t_{ise} + (16 - t_{ise})^{1,25} = 0$	15,75	-
Inner	Bar-grid panel	$11,8945 - 0,7652 t_{ise} + (16 - t_{ise})^{1,25} = 0$	15,76	-

TABLE 12 (Contd)

Radiation-sensing element under consideration	Part of the test section which is directly in front of the radiation-sensing element (see Figure 58 on page 290)	Non-linear equations for determining the "inner" and "outer" radiation-sensing element temperatures, t_{ise} and t_{ose} respectively	Radiation-sensing element temperature °C	
			Inner, t_{ise}	Outer, t_{ose}
Conditions : (i) <u>With</u> the body in the centre of the test section (ii) Nominal temperatures of the solid and bar-grid panels of the horizontal test chamber and body; 15°C, 16°C and 22°C, respectively				
Inner	Solid panel	$15,4311 - 0,8898 t_{ise} - (t_{ise} - 16)^{1,25} = 0$	16,67	-
Inner	Corner	$14,9035 - 0,8581 t_{ise} - (t_{ise} - 16)^{1,25} = 0$	16,67	-
Inner	Bar-grid panel	$15,3600 - 0,8898 t_{ise} - (t_{ise} - 16)^{1,25} = 0$	16,63	-
Conditions : (i) <u>Without</u> the body in the centre of the test section (ii) Nominal temperatures of the solid and bar-grid panels of the horizontal test chamber; 35°C and 34°C, respectively				
Outer	Solid panel	$37,6151 - 1,0772 t_{ose} - (t_{ose} - 34)^{1,25} = 0$	-	34,51
Outer	Corner	$41,8645 - 1,2143 t_{ose} - (t_{ose} - 34)^{1,25} = 0$	-	34,31
Outer	Bar-grid panel	$36,7146 - 1,0772 t_{ose} - (t_{ose} - 34)^{1,25} = 0$	-	34,06
Inner	Solid panel	$32,0922 - 0,9293 t_{ise} - (t_{ise} - 34)^{1,25} = 0$	34,30	-
Inner	Corner	$29,8489 - 0,8652 t_{ise} - (t_{ise} - 34)^{1,25} = 0$	34,27	-
Inner	Bar-grid panel	$32,0303 - 0,9293 t_{ise} - (t_{ise} - 34)^{1,25} = 0$	34,26	-

TABLE 12 (Contd)

Radiation-sensing element under consideration	Part of the test section which is directly in front of the radiation-sensing element (see Figure 58 on page 290)	Non-linear equations for determining the "inner" and "outer" radiation-sensing element temperatures, t_{ise} and t_{ose} , respectively	Radiation-sensing element temperature °C	
			Inner, t_{ise}	Outer, t_{ose}
Conditions : (i) <u>With</u> the body in the centre of the test section (ii) Nominal temperatures of the solid and bar-grid panels of the horizontal test chamber and body; 35°C, 34°C and 27,3°C, respectively				
Inner	Solid panel	$33,0536 - 1,0062 t_{ise} + (34-t_{ise})^{1,25} = 0$	33,39	-
Inner	Corner	$31,7328 - 0,9667 t_{ise} + (34-t_{ise})^{1,25} = 0$	33,39	-
Inner	Bar-grid panel	$33,1397 - 1,0062 t_{ise} + (34-t_{ise})^{1,25} = 0$	33,43	-

As the 4π radiometer rotates about the body in the centre of the test section of the climatic chamber, the radiation-sensing elements in the vertical section of the radiometer "sees" the solid panel, corner, bar-grid panel corner and solid panel in turn during half a revolution of the radiometer arm.

The theoretical temperature variations with time of the radiation-sensing elements during one revolution of the radiometer arm were obtained by plotting the radiation-sensing element temperature values given in Table 12 against time for the above-mentioned positions of the radiometer (the radiometer arm rotates at the speed of 0,0167 Hz). The results are presented in Figures 60 and 61 for cases where the temperature of the body in the centre of the horizontal test chamber is higher and lower than the temperature of the surrounding walls, respectively.

Based on the theoretical results contained in Table 12 for each of the two sets of temperature conditions set out in Table 9 on page 289, the introduction of a body (with an area equivalent to that of a human body), into the centre of the test section, can be expected to change the average temperature of the "inner" radiation-sensing element of the

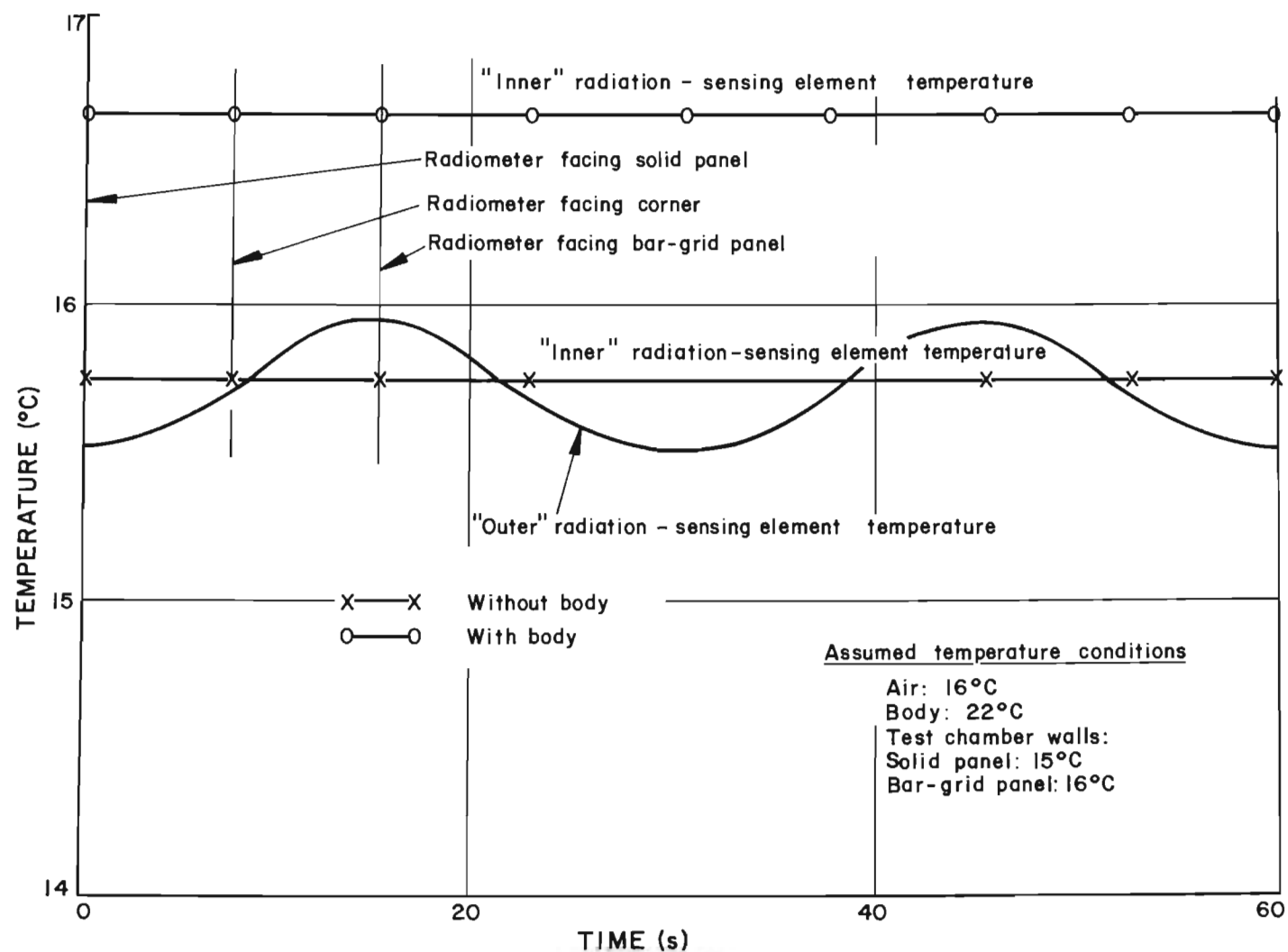


FIGURE 60

Theoretical temperature variations with time of the "inner" and "outer" radiation-sensing elements of the 4π radiometer arm during a typical revolution of the radiometer with the body temperature higher than the surrounding wall temperatures

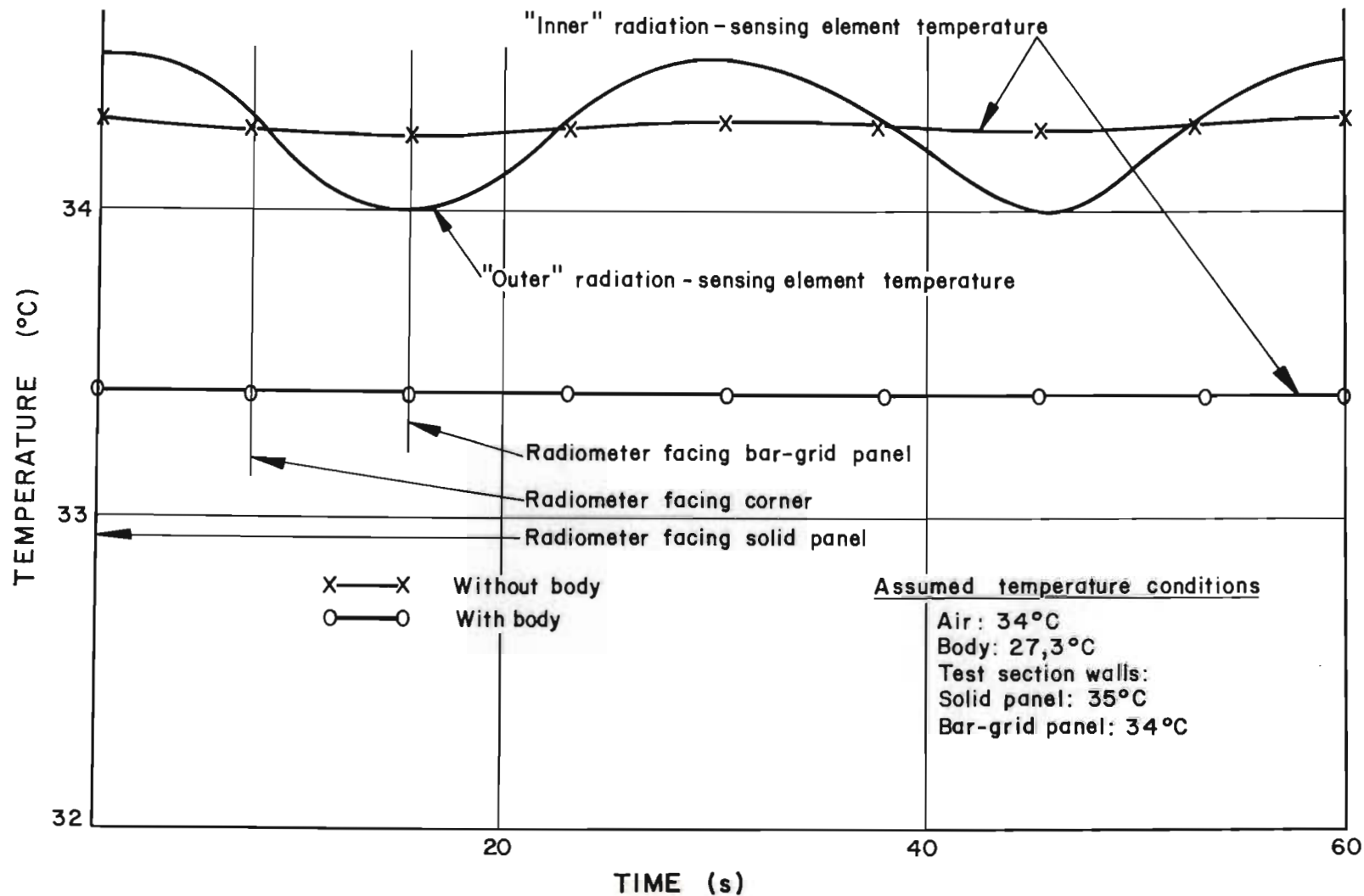


FIGURE 6I

Theoretical temperature variations with time of the "inner" and "outer" radiation-sensing elements of the 4π radiometer arm during a typical revolution of the radiometer with the body temperature lower than the surrounding wall temperatures

radiometer during one revolution of the radiometer arm by the following amounts:

1. Temperatures of the solid and bar-grid panels of the test section and body; 15°C, 16°C and 22°C, respectively

Average temperature of the "inner" radiation-sensing elements (see Table 12 on pages 300 and 301):

$$\begin{aligned} \text{With body in test section : } (16,67 + 16,67 + 16,63)/3 \\ = 16,6^\circ\text{C} \end{aligned}$$

$$\begin{aligned} \text{Without body in test section : } (15,73 + 15,75 + 15,76)/3 \\ = 15,7^\circ\text{C} \end{aligned}$$

Thus, the temperature change of the "inner" radiation-sensing element due to the body is $16,6 - 15,7 = 0,9^\circ\text{C}$.

2. Temperatures of the solid and bar-grid panels of the test section and body; 35°C, 34°C and 27°C, respectively

Average temperature of the "inner" radiation-sensing elements (see Table 12 on pages 301 and 302):

$$\begin{aligned} \text{With body in test section : } (33,39 + 33,39 + 33,43)/3 \\ = 33,4^\circ\text{C} \end{aligned}$$

$$\begin{aligned} \text{Without body in test section : } (34,3 + 34,27 + 34,26)/3 \\ = 34,3^\circ\text{C} \end{aligned}$$

Thus, the temperature change of the "inner" radiation-sensing element due to the body is $33,4 - 34,3 = -0,9^\circ\text{C}$.

Under both the above sets of assumed temperature conditions the introduction of a body in the horizontal test chamber can thus be expected to change the temperature of the "inner" radiation-sensing elements by $0,9^{\circ}\text{C}$ (see also Figures 60 and 61 on pages 304 and 305, respectively).

5.5.3 Required sensitivity of the 4π radiometer

It is required to measure the radiation heat loss rate from a human body under high radiation conditions with an accuracy of 10%.

In the proposed system of measurement, the radiation heat exchange rate between a body located in the centre of the horizontal test chamber of the climatic chamber and the surrounding walls, affects the temperature of the radiation-sensing elements lining the inner surface of the 4π radiometer relative to the radiation-sensing elements lining the outer surface of the radiometer.

It has been shown that, under the assumed temperature conditions set out in Table 9 on page 289, the introduction of a body in the horizontal test chamber can be expected to change the temperature of the "inner" radiation sensing element by $0,9^{\circ}\text{C}$.

Thus, if the radiative heat loss rate from a human body under these conditions is to be determined with an accuracy of 10%, the measuring system of the radiometer should be capable of detecting temperature changes of the "inner" radiation-sensing elements relative to the "outer" radiation-sensing elements incorporated in the radiometer arm, of less than $0,9 \times 0,1 = 0,09^{\circ}\text{C}$.

Various systems of measurement were investigated to determine whether the required sensitivity could be obtained.

5.5.4 Proposed method of measuring the radiometer output

Variations in the temperatures of the "inner" and "outer" radiation-sensing elements of the 4π radiometer arm results in a corresponding change in the electrical resistance values of these elements. The problem of detecting the temperature variations with time of the "inner" radiation-sensing elements, relative to the "outer" radiation-sensing elements thus resolves to detecting changes in the electrical resistances of the one set of radiation-sensing elements relative to the other.

In resistance thermometry, changes in electrical resistances are normally measured potentiometrically or using a

measuring system incorporating a Wheatstone bridge network such as, for example, the Smith resistance bridge⁸⁵⁾.

In the potentiometric method, the resistance of the thermometer is compared with that of a standard resistance. In general, four readings are involved in the application of this method: one of the potential drop across the standard resistance, a similar reading for the thermometer and a repeat of these two readings after the current has been reversed. Consequently, readings are very time consuming and the method is not suitable for continuous recording. However, high accuracies are obtainable by this means.

Measuring systems employing a Wheatstone bridge on the other hand, are ideally suited for continuous recording. In this case the unbalance current of the Wheatstone bridge is used to record a resistance change of one or more arms of the bridge relative to the others; either by direct deflection on a calibrated galvanometer or by amplifying it to actuate some other form of recording mechanism.

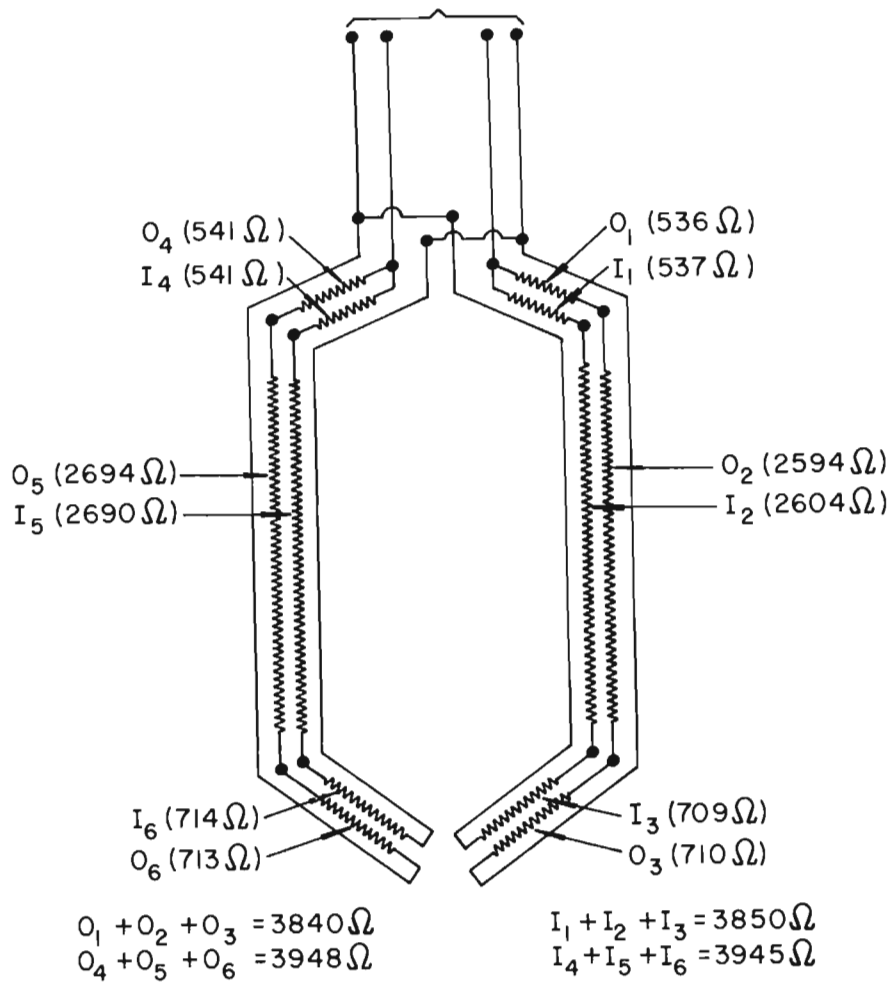
In view of the above-mentioned considerations, the Wheatstone bridge system of measurement was preferred for the 4π radiometer arm.

The radiation-sensing elements in the various sections of the radiometer arm were, therefore, connected in the form of a Wheatstone bridge as shown in Figures 62a and 62b; the resistances being connected in such a way that each of the two radiation-sensing elements lining the inside of the radiometer arm (I_1, I_2, I_3 and I_4, I_5, I_6) formed the opposite arms of the Wheatstone bridge and each of the two radiation-sensing elements lining the outside of the radiometer arm (O_1, O_2, O_3 and O_4, O_5, O_6), formed the remaining two arms of the bridge.

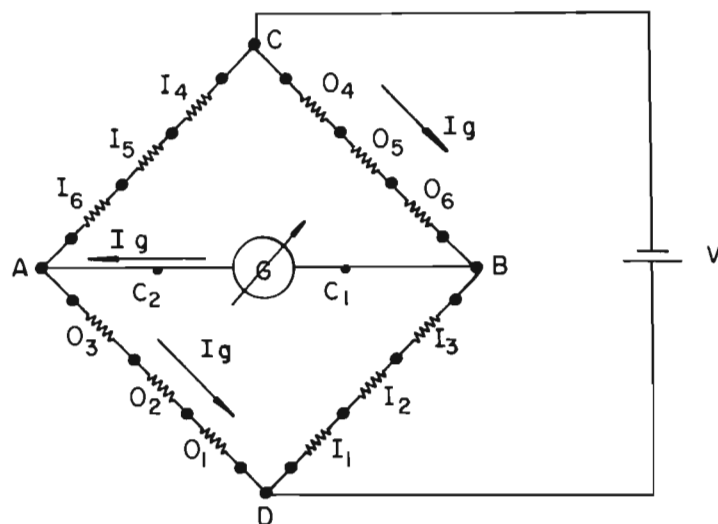
A voltage, V , applied across points C and D of the Wheatstone bridge network shown in Figure 62b, produces an unbalance voltage between points A and B when the temperature and hence the electrical resistance of "inner" radiation-sensing elements (I_1 to I_6) differ from that of the "outer" radiation-sensing elements (O_1 to O_6).

Various measuring instruments were considered for recording the unbalance voltage between points A and B.

PHILLIPS TYPE PR3200P/CO RECORDER



a). LAYOUT OF RESISTANCES IN RADIOMETER ARM



b). WHEATSTONE BRIDGE

FIGURE 62

Direct measurement of the radiative heat loss rate from a human body by means of the 4π radiometer arm: circuit diagram for electrical resistance thermal radiation-sensing elements

From the comparison of various measuring systems presented in Appendix H, it appears that the sensitivities of both the galvanometric type of recorder such as the Kipp Micrograph recorder and a strain gauge recorder are adequate for recording the output of the 4π radiometer.

However, the strain gauge recorder was preferred in view of the following considerations:

The strain gauge recorder is more robust and insensitive to vibrations compared to the galvanometric type of instrument. In addition, the strain gauge recorder has a built-in stable power supply unit specially designed for a Wheatstone bridge. In the case of the galvanometric type of recorder a separate power supply unit would be required.

The type of strain gauge recorder selected, was a Phillips type PR3200 P/00 recorder with the following characteristics:

Amplification : 50 μ strain full-scale deflection for
a full bridge circuit

Accuracy : $\pm 0,25\%$ full-scale value

Maximum sensitivity of amplifier : 2,5 μ V

Balancing time : 1 second
Bridge voltage : 12 volts
Bridge resistance : 600 ohms

Integration of the radiometer output

During the operation of the 4π radiometer within the test section of the climatic chamber, the radiometer output displays a cyclic variation of period 60 seconds; due to the radiometer being rotated at a speed of 0,0167 Hz around the body.

An electronic integrator with a digital display system was thus incorporated in the measuring system to integrate the radiometer output during a predetermined number of revolutions of the radiometer arm.

5.6 Full-scale inanimate tests

Certain preliminary full-scale tests were carried out on the 4π radiometer after the radiometer had been installed in the horizontal test chamber of the climatic chamber, with the view to calibrating the radiometer.

The heat source, for the purpose of the tests, consisted of a 350 mm diameter by 1 250 mm long cylinder which was constructed

from 16 SWG aluminium and equipped with two 500w heater tapes; the heater tapes being suitably clamped to the cylinder to enable the surface of the cylinder to be heated uniformly. The ends of the cylinder were closed with 25 mm thick discs of polystyrene.

The cylinder was suitably mounted in the centre of the test section as shown in Figure 36 on page 215, and painted black with an optical matt black lacquer to simulate the human body and increase the magnitude of the radiation heat loss component. The power input to the heater element, which could be varied by means of a variable auto-transformer, was measured with a watt meter. Surface temperature measurements were carried out by means of 30 SWG copper constantan thermocouples which had been peened into grooves in the cylinder for good thermal contact.

The heat which is supplied to the cylinder, is lost by convection and radiation. Since the heat input rate to the cylinder and the convection heat loss rate were measured by means of a watt meter and convective heat loss measuring instrument that had previously been developed³⁶⁾, respectively, the radiation heat loss rate could be obtained by difference.

5.6.1 Test results

Figure 63 presents typical test data for various air velocity and temperature conditions within the horizontal test chamber of the climatic chamber.

The tests confirmed that the radiometer responds in a linear manner to radiant heat input and that the radiometer output is unaffected by the air temperature and velocity conditions within the test section. In addition, the stability of the instrument was found to be satisfactory.

In general, the radiant energy exchange rate of a body in the centre of the test section could be determined to within 10 per cent by means of the 4π radiometer.

It should be noted, however, that, in view of the fact that the convective heat loss measuring instrument was used for the calibration of the radiometer, the accuracy of the radiometer is affected to some extent by the accuracy of the convective heat loss measuring instrument which was found to be of the order of 5 per cent³⁵⁾.

In view of the satisfactory operation of the 4π radiometer, it was proposed that the instrument should be used to

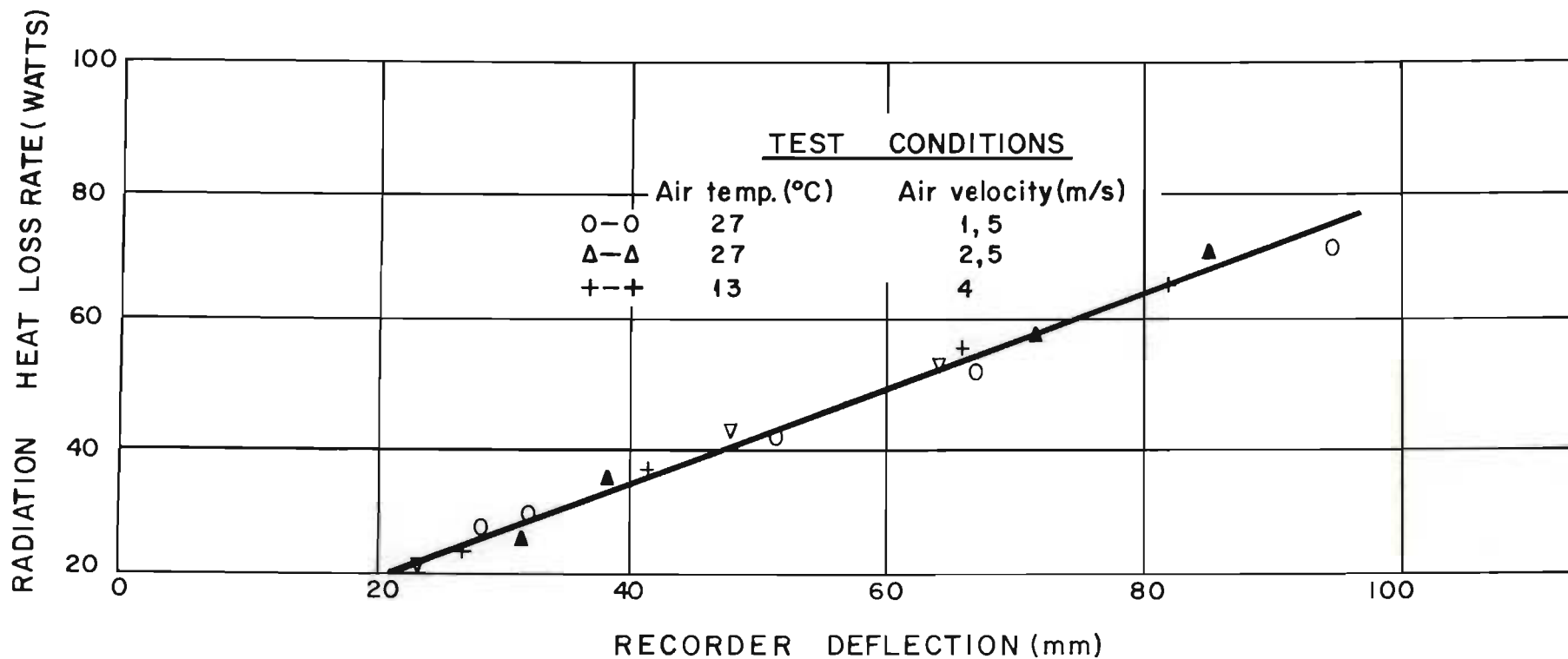


FIGURE 63

Direct measurement of the radiative heat loss rate from a human body: calibration curve for the 4 π radiometer.

determine the radiation heat loss rate from a human body.

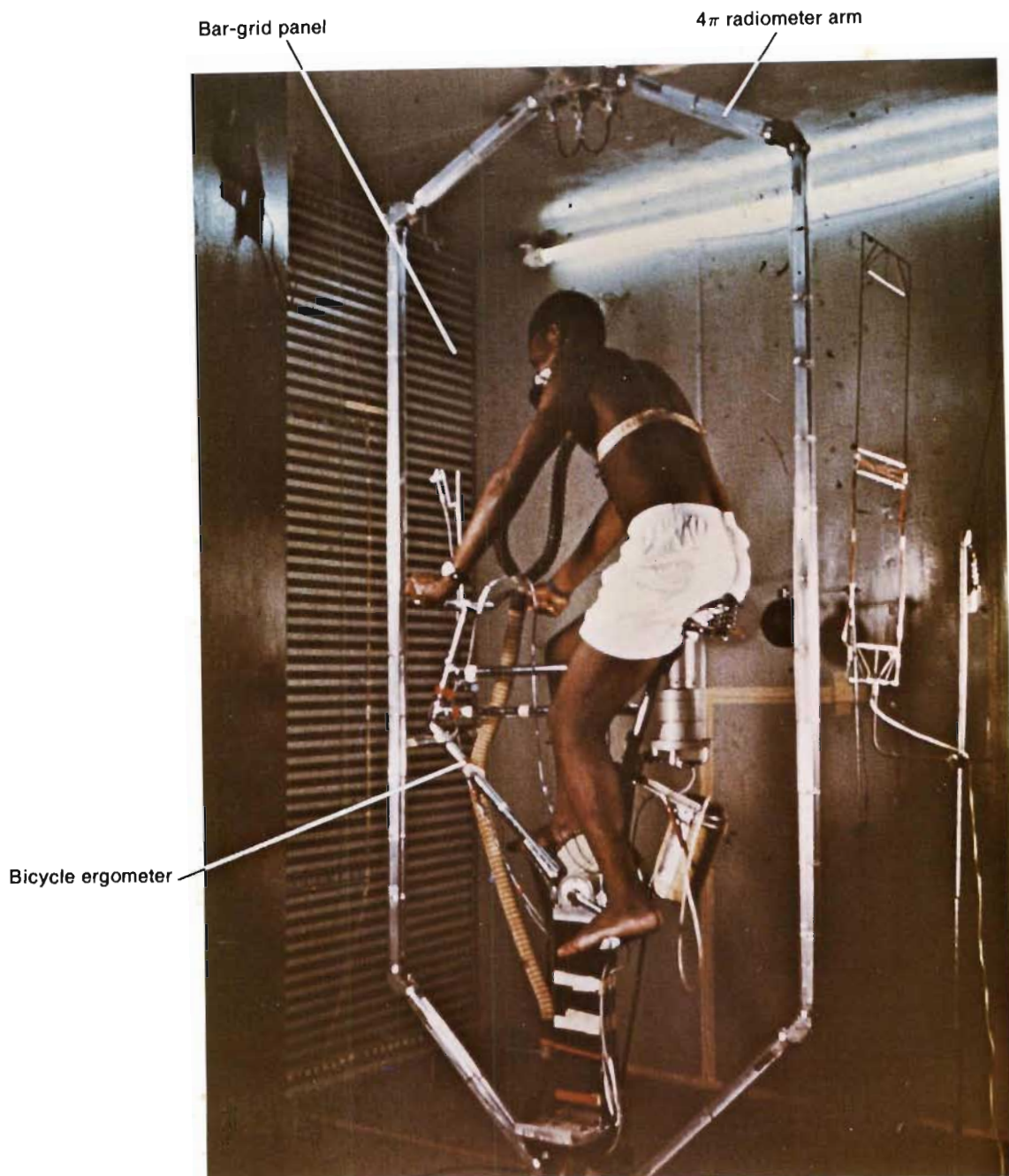
5.7 Animate studies

The 4π radiometer was subsequently used by Mitchell³⁵⁾ to determine the radiation energy exchange rate between human subjects in the horizontal test chamber of the climatic chamber and their surroundings.

During each test the subject sat on the saddle of the bicycle ergometer, for the duration of the experiment, pedalling when it was required by the programme; the bicycle ergometer being so designed that the mechanical power output of the subject could be controlled at a pre-set value. (See Figure 64).

Each test included, inter alia, the direct measurement of the convective, evaporative and radiative energy exchange rates between the subject and his surroundings as well as measurements of the amount of expired air from the subject over a predetermined time interval and his oxygen content to determine the heat production rate by the subject through the metabolic process.

The experiments were carried out on five young healthy men; acclimatized to work in hot environments and trained to use the bicycle ergometer. Body water deficit was prevented throughout all experiments.

**FIGURE 64**

Direct measurement of the heat loss rate from a human body: test rig for animate studies. (Photograph: D. Rabe)

In the first series of experiments two men were exposed at rest for two hours to very dry environments covering a wide range of air temperature and wind speed conditions. In the second series of experiments two men were again exposed to dry environments, at rest for an initial 40 minute period, then at each of three levels of work for two hours. In experiments of the third series, two men were exposed to environments in which the humidity was varied. They rested for 90 minutes, worked at each of two levels for 90 minutes, and then rested for a further 90 minutes. Throughout all the experiments, the men reached thermal equilibrium by the end of each test period, except during exposure at rest to cold environments.

Results of the typical test are presented in Figure 65.

During the tests, Mitchell³⁵⁾ found that the radiation heat exchange rate could be determined to within 9 per cent by means of the 4π radiometer.

In general, Mitchell³⁵⁾ found the 4π radiometer to be completely satisfactory as a direct-measuring instrument for determining the radiation heat exchange rate of a human subject.

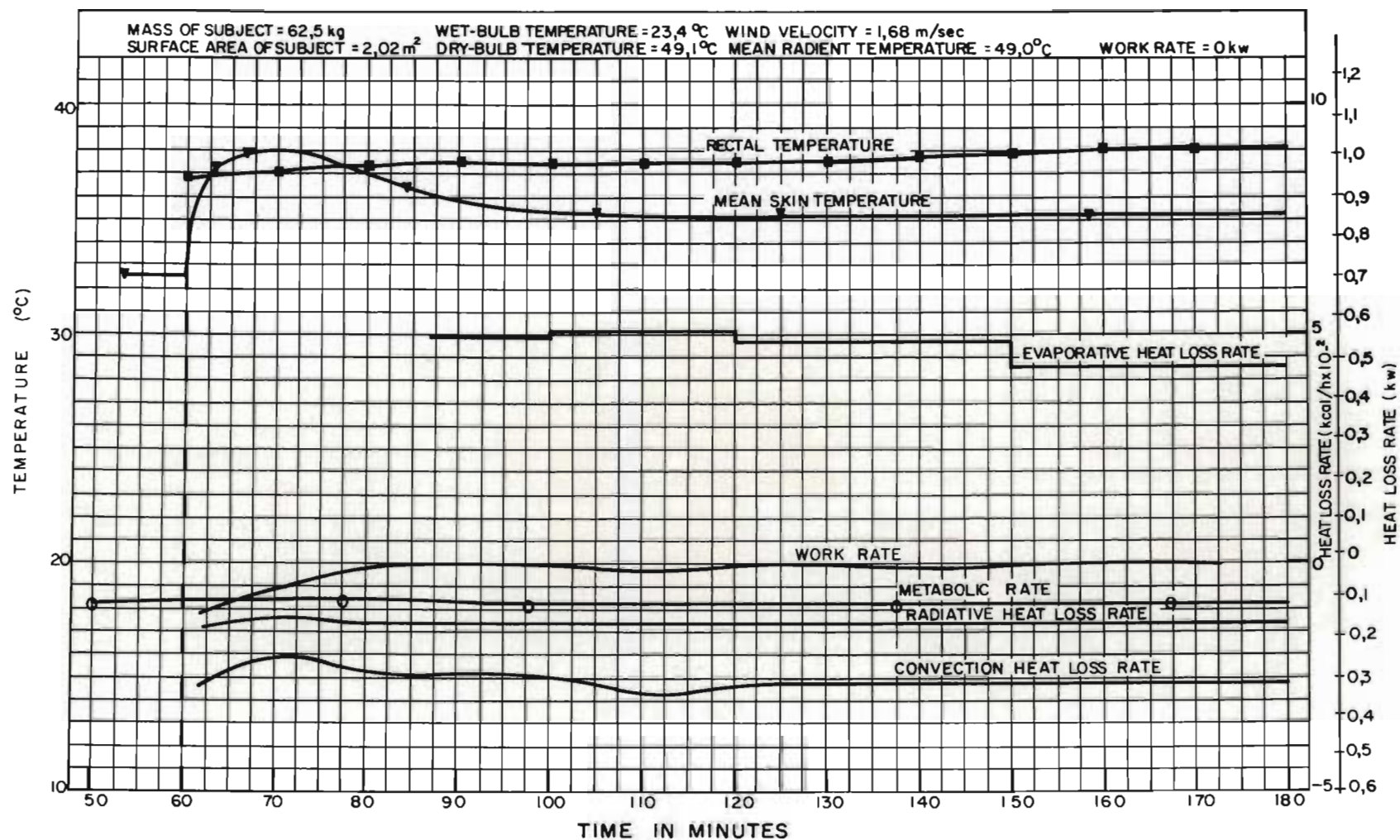


FIGURE 65

Direct measurements of the various components of the heat loss rate from a human body: typical test results showing, inter alia, variations in the radiant heat loss rate with time of a subject in the horizontal test chamber of the climatic chamber of the Human Sciences Laboratory (by Mitchell³⁵)

5.8 Discussion of the 4π radiometer

The 4π radiometer is a unique facility which enables direct measurements of the thermal radiation exchange rate of a human subject in a normal working mode to be carried out in the relatively large horizontal chamber of the climatic chamber.

In the past direct measurements of the radiation exchange rate of a human subject could only be carried out in the specially designed human calorimeter of Benzinger and Kitzinger⁶⁷). However, due to the relatively small size of the calorimeter, the working movement of the subject was severely restricted. Furthermore, the emissivity of the surrounding walls of the calorimeter could not be altered in any way.

In the case of relatively large temperature controlled booths or climatic chambers of adequate size to accommodate a subject in a normal working position, the radiant energy exchange rate was, in the past, calculated from, inter alia, the measured temperature values of the skin of the human subject and the surrounding surfaces of the climatic chamber. However, the approach is complicated by the irregular and changeable shape of the radiant surface of the body during exercise and the non-uniform temperature distribution across the body surface.

The disadvantages of previously developed techniques for determining the thermal radiation energy exchange rate of a subject are eliminated in the newly developed direct-measuring system; the 4π radiometer arm automatically integrates the total radiated heat loss rate over a solid angle of 4π radians in a manner which does not interfere with the radiant environment. As the radiometer rotates, a thin strip is interposed between the body and wall for a short while only so that the general equilibrium of the body wall system is maintained.

Because of the relatively short response time of the 4π radiometer, of the order of 10 seconds, the radiometer could also be used to determine the radiant heat loss rate of a subject under transient conditions.

CHAPTER 6

DEVELOPMENT OF A LOW-COST RADIOMETER FOR SKIN TEMPERATURE
AND EMISSIVITY MEASUREMENTS

The need for accurate techniques for the measurement of human skin temperature and emissivity have long been evident, particularly in the physiology and medical fields.

The value of such measurements is evident from the following considerations:

Skin temperature is a basic parameter in all the heat transfer processes between the human body and its environment. A knowledge of the average skin temperature is thus a major prerequisite for establishing functional relationships capable of describing the heat transfer mechanisms and hence the thermal stress in man in terms of various environmental factors. A knowledge of the skin temperature is also of value in certain types of medical diagnosis, mainly because pathological events often cause local or general skin temperature abnormalities.

The total normal emissivity, usually referred to as the emissivity of a surface, is the ratio of the total radiant power emitted normal to a surface or aperture to that emitted normal to a black body surface at the same temperature.

The emissivity of a surface can be determined indirectly by measuring the transmittance and reflectance at discrete wave-lengths throughout the spectrum of wave-lengths involved, calculating the emissivity by difference and then integrating over the whole wave-band. However, in view of the inherent disadvantages of indirect methods, direct methods of measurement such as those reviewed by Worthing⁸⁶⁾ are often preferred.

In general, the direct methods of measurement involve the comparison of the emittance of the surface and a reference surface at the same temperature. Alternatively, the emissivity can be determined from measurements of the surface temperature and radiation energy exchange rate between the surface and a non-selective radiometer. In all the existing methods of measuring the emissivity of a surface, therefore, a knowledge of the surface temperature is required.

Improvement over existing methods of determining the emissivity of a surface would be possible if the emissivity could be determined without the need for measuring the surface temperature.

6.1 Skin temperature measuring techniques

The first skin temperature measurements are attributed to Davy in 1814⁸⁷⁾. Subsequent to the 1920's the clinical interest in the measurement of human surface temperature increased considerably and numerous studies related to the measurement

of skin temperature were reported in the literature⁸⁸⁻⁹⁰).

In general, skin temperature measuring techniques can be classified into the following two groups:

1. Contact thermometers and
2. Radiometers.

6.1.1 Contact thermometers

Contact thermometers for the purpose of skin temperature measurement, generally incorporate fine wire thermocouples⁹¹) which are pressed against the skin surface by means of specially designed holders to ensure good thermal contact⁹²).

For example, the thermocouple probe which was designed by Atkins⁹³), basically consists of a 36 SWG copper-constantan butt-welded thermocouple which is insulated with a film of epoxy cement and stretched across a bow-shaped holder. The bow, in turn, is attached to a spring-loaded relay tension gauge so that the thermocouple junction can be applied to the skin with a constant thrust (usually 30 g or 50 g). When the bow is applied to the skin the wires on either side of the junction lie along the skin for a distance between

10 mm and 20 mm.

The main advantage of contact thermometers are their simplicity and low cost. Furthermore, temperature measurements can be carried out over a comparatively small area of the surface.

Such systems of measurement can, however, be subject to the following sources of error⁹⁴⁾:

- (i) physical disturbance of the heat exchange between the skin and its surroundings,
- (ii) difficulties in ensuring that the thermocouple junction is at the same temperature as the skin and
- (iii) physiological reactions caused by contact, pressure or irritation.

Considerable differences of opinion exist regarding the magnitude of the errors of contact systems of measurement. Some investigators reported that the errors could be relatively high and that the contact systems were in general less accurate than the radiometric techniques for measuring skin temperature⁹⁵⁻⁹⁹⁾. Others reported that the errors could be relatively small provided certain precautions were taken in the measurement¹⁰⁰⁻¹⁰³⁾.

After an extensive investigation into the use of thermocouple probes for measuring skin temperature, Mitchell³⁵⁾ found that, in warm environments regardless of the humidity, the discrepancy of a thermocouple probe compared to two different types of radiometers was invariably less than $0,5^{\circ}\text{C}$. At ambient temperatures of the order of 35°C , the error averaged less than $0,1^{\circ}\text{C}$.

At skin temperatures below 25°C in cold environments Mitchell³⁵⁾ found that thermocouple probes sometimes indicated a temperature of the order of 1°C too high regardless of wind speed. However, the discrepancy of 1°C between the thermocouple and the radiometric measurements in cold environments decreased when the average temperature over a number of sites was considered; at 15°C the average of the temperatures determined at 15 sites by means of thermocouples was only $0,4 \pm 0,4^{\circ}\text{C}$ higher than the average of the temperature determined at the same sites by means of radiometers.

6.1.2 Radiometric temperature-measuring devices

All bodies above a temperature of -273°C emit electromagnetic waves; the range of wave-lengths and the intensity of the radiation being dependent on the temperature and on the surface condition of the body concerned.

The higher the temperature, the higher are the energy and frequency and the smaller the wave-length of the emitted radiation. (See Section 5.2 and Figure 39 on pages 230 and 233, respectively).

Radiometric temperature-measuring devices generally operate by comparing the amount of radiation emitted by the target with that emitted by a built-in reference black body which is automatically controlled at a predetermined temperature.

Such radiometers generally incorporate optical systems capable of directing the radiation from the target or reference black body on to the radiation detector or receiver.

At least one window is provided in the system to prevent interference by the environment. In certain cases, the incoming radiation is filtered to obtain optimum response to a change in the target temperature.

In view of the inherent stability of AC amplifiers and other considerations, the incoming radiation which is received by the radiometer, is generally chopped by means of a highly reflective multi-bladed disc which is driven

by a synchronous motor; the relative positioning of the chopper, receiver and reference black body within the radiometer being such that the detector receives radiation alternatively from the target and from the reference cavity.

Some of the sophisticated directional radiometers, capable of measuring radiant power very accurately, have been developed for military applications, for satellite meteorology and for other uses associated with space flight¹⁰⁴⁾. In certain cases the radiometers have been adapted for use in human surface thermometry. The suitability of different types of directional radiometers for the measurement of skin temperature have been discussed by Mitchell, Wyndham and Hodgson¹⁰⁵⁾.

Compared with the contact methods of measuring skin temperature, radiometers have the advantage that the body surface need not be touched; the disturbance of existing physiological conditions of the skin is thus minimal. However, radiometers are not completely free of errors. Due to the fact that no material exists which has unit reflectivity, the output of radiometers that are equipped with "choppers" depends to some extent on the "chopper"

temperature; a phenomenon noticed by Buchmiller⁸⁷⁾ and Hardy and Stoll¹⁰⁶⁾.

According to some investigators, the possibility also exists that the radiometer may "see" through the upper layers of the skin (due to thin layers of the epidermus being transparent to infra-red radiation to some extent) and that, because of this, true surface temperatures cannot be measured by this means¹⁰⁷⁾. However, no agreement among the various investigators exists in this regard possibly due, inter alia, to the fact that the information obtained was based partially on investigations of live skin and partially on excised skin from different parts of the body; the position being further complicated by the differences in the performance characteristics of the various radiometers that were used in the investigations¹⁰⁸⁾.

During tests on two sophisticated radiometers incorporating choppers, Mitchell³⁵⁾ found that surface temperatures could generally be measured to within $0,25^{\circ}\text{C}$, by this means, in the ambient temperature range of 15°C to 40°C . When the radiometers were calibrated under carefully controlled conditions against a specially constructed black body, the best of them exhibited an error of $\pm 0,1^{\circ}\text{C}$ in the calibration.

The claims in the literature that radiometers have been used to measure skin temperature with an absolute accuracy of $\pm 0,01^{\circ}\text{C}$ must, therefore, be regarded sceptically.

6.2 Radiometer for human skin temperature and emissivity measurements: design considerations

According to the Stefan-Boltzman law, the rate of radiant energy transfer between a skin target and a non-selective radiometer is given by:

$$\dot{q}_{\text{rad}} = A \epsilon_s \epsilon_{\text{se}} \sigma (T_t^4 - T_{\text{se}}^4) \quad \dots\dots\dots (46)$$

where \dot{q}_{rad} = rate of radiant energy transfer between the skin target and the radiometer

and A = term which depends on the areas and configuration factors involved

σ = Stefan-Boltzman constant

$\epsilon_s, \epsilon_{\text{se}}$ = emissivities of the skin target and radiation detector, respectively

T_t, T_{se} = absolute temperatures of the skin target and radiation detector, respectively.

The term A in equation (46) can be regarded as a constant for a particular radiometer. Thus, the rate of radiant energy transfer between the target and the radiation detector primarily depends on the emissivities and temperatures of the skin target

and radiation detector respectively.

Normally, the radiation detector is controlled at a fixed temperature. In this case a knowledge of, inter alia, the emissivity of the target skin is a major prerequisite for the measurement of the skin temperature by means of a radiometer.

However, if the temperature of the radiation receiver could be varied so that the net radiation energy exchange rate between the skin target and the radiation receiver is zero, the temperature of the radiation receiver would equal that of the skin target, regardless of the emissivities involved.

By measuring the radiation receiver temperature under these conditions, it should be possible to assess the temperature of the skin, without a prior knowledge of its emissivity.

6.2.1 Choice of thermal radiation-sensing elements

One of the major prerequisites for the design of a radiometer for skin temperature and emissivity measurements is the choice of thermal radiation-sensing elements.

The major types of radiation detectors are discussed in some detail in Section 5.2 on page 230. Only a brief

discussion of the detectors is included here for the sake of continuity.

In general, radiation detectors for the purpose of skin temperature measurement can be divided into two main types, namely, thermal detectors and photon-counters.

(a) Thermal detectors

Thermal detectors depend upon the heating effect of the radiant energy being measured for their operation.

The most frequently used detectors of this class are

- (i) the thermopile which is generally constructed from a number of thermocouples connected in series and
- (ii) the bolometer which incorporates electrical resistance elements.

The use of thermal detectors in radiometers is discussed in some detail by Hardy and Stoll¹⁰⁶⁾.

The earlier type of radiometer developed for bio-thermal work generally used thermal detectors; the first relatively accurate bio-thermal radiometer of this type being the one developed by Hardy¹⁰⁹⁾ in 1934.

Thermal detectors have the advantage of being equally sensitive at all wave-lengths. (See Figure 40 on page 237).

(b) Photon-counters

Photon-counter detectors which operate when photons react with electrons and cause a shift of electron orbits, are suitable for radiation measurements in the visible and/or near infra-red regions.

During recent years numerous types of sophisticated radiometers equipped with photon-counters as the radiation-sensing elements, were developed, notably in Europe^{72,87,110-114}).

Radiometers equipped with photon-counter detectors are relatively expensive. The detectors often require cooling to sub zero temperatures and are wave-length dependent.

However, photon-counter detectors are highly sensitive to changes in radiant power due mainly to the following factor:

According to the Stefan-Boltzman law, the emission

power or total rate of radiant energy emission per unit area of a black body or grey body surface is proportional to the fourth power of its absolute temperature. If, however, not all the wave-lengths in the emission spectrum are involved in the radiation heat transfer process but only those in a certain band, the dependence on the fourth power no longer holds.

Based on the work by Dreyfus¹¹⁵⁾, the spectral emittance in a narrow wave-length band per °K change in temperature is proportional to T^n where T = absolute temperature of the black body or grey body surface. Mitchell et al¹⁰⁵⁾ have shown that, in the case of lead sulphide photon-counters which have a cut-off at about 4 micron and which, therefore, respond only to a narrow band centre around 3,5 micron, the corresponding value of n is about 14.

Thus, a small change in the temperature of the skin results in a relatively large change in the radiant energy exchange rate between the skin surface and radiation receiver when using a photon-counter as the radiation detector, compared with the corres=

ponding change in the radiation energy exchange rate applicable to a thermal detector.

The response of photon-counters can also be increased by cooling the detector to temperatures below -200°C . Under these conditions photon-counters respond to wave-lengths greater than 6 micron¹¹⁶⁾.

Factors affecting the choice of a particular type of radiation-sensing element for the purpose of human skin temperature measurements

The choice of a particular type of radiation-sensing element for the measurement of surface temperature largely depends on the intensity of the radiation and the spectrum of wave-lengths involved.

In the case of a human body, the skin temperature generally varies within the range 25 to 40°C ; the exact value being dependent on the environmental conditions with regard to air temperature, humidity and air movement and certain physiological factors. (See also Table 4 on pages 89 to 92).

At black body temperatures of 25° to 40°C , the radiant

energy exchange rate generally takes place at wave-lengths between 3 and 40 microns; 90% of the energy falling in the 6 to 40 micron wave-band. Only thermal detectors are generally suitable as radiation detectors within the latter range; the response of such detectors being independent of the wave-length of the incoming radiation.

In the spectral region where photon-counters are generally suitable for the detection of radiation (at wave-lengths below 4 micron), the rate of radiation energy emission by a black body at temperatures within the range 25 to 40°C is relatively small. According to an analysis by Mitchell et al⁷⁷⁾ which is based on data of Lowan and Blanch¹¹⁷⁾, less than 0,2% of the radiant energy emission takes place at wave-lengths below 4 micron.

However, in view of the considerations set out in paragraph (b) on page 334, photon-counters are relatively sensitive to changes in skin temperature in spite of the radiant exchange rate being relatively small.

Both the thermal and photon-counter type of radiation detectors are thus suitable for the purpose of skin temperature measurement.

However, the thermal type of detector was preferred for the proposed radiometer in view of the requirement that the radiometer should be capable of measuring the total emissivity of the surface over the full spectrum of wave-lengths involved. This, in turn, necessitated the use of a non-selective thermal radiation detector.

6.3 Constructional details of the low-cost radiometer

Figure 66 presents an exploded view of the radiometer.

The instrument is equipped with two commercially available non-selective thermal radiation detectors (Hasian radiation thermocouple, type C manufactured by Pyro-werk GMBH, Hanover). Each radiation-sensing element consists of a single semi-conductor thermocouple in the form of a small rod, a few millimetres in length.

The one end of the rod is fitted with a 3 mm diameter platinum disc of 1 micron thickness which acts as the radiation receiver and which is positioned at the focus of a converging metallic mirror. The other end of the semi-conductor rod, which forms the cold junction of the thermocouple, projects through the mirror. The cold junction is thus located at the back of the mirror.

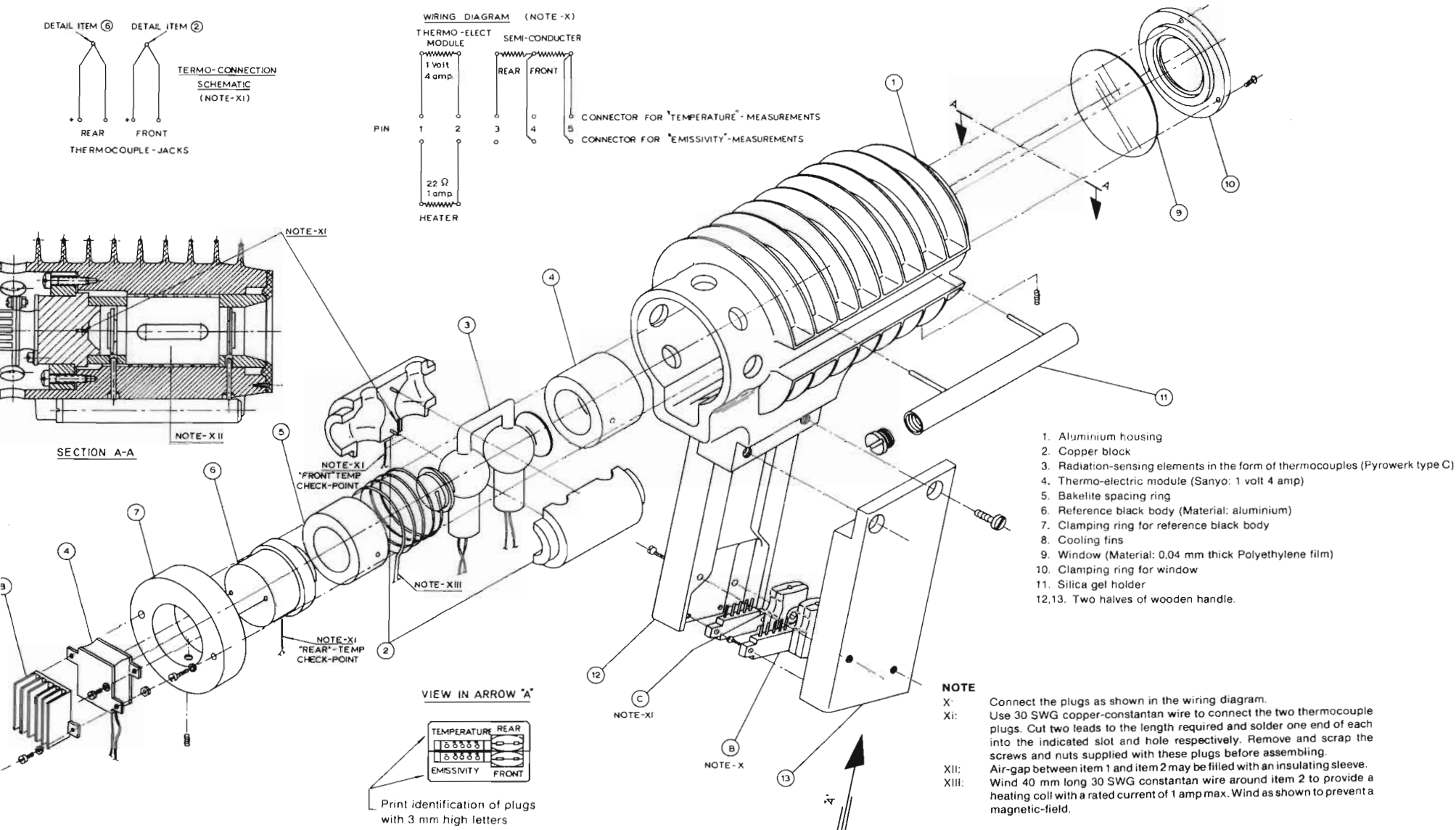


FIGURE 66

Exploded view of the low-cost portable radiometer for surface temperature and emissivity measurements.

To eliminate convection influences around the thermocouple junctions the thermocouple and mirror assembly are enclosed in an evacuated glass capsule fitted with a rock salt window.

Provided that no temperature difference exists between the two junctions of the thermocouple, other than that due to incoming radiation, the detector produces an output voltage directly proportional to the irradiance of the measuring junction.

The two glass capsules containing the radiation-sensing elements were subsequently joined by means of a glass tube to form a complete unit, with the radiation-sensing elements in the two glass capsules positioned back to back to each other.

The two glass capsules are enclosed in a split copper block to form an iso-thermal enclosure; the copper block being equipped with a 20w heater element constructed from 30 SWG constantan wire to enable the temperature of the radiation-sensing elements to be varied. The copper block is equipped with a 30 SWG copper-constantan thermocouple for the purpose of measuring the copper block temperature.

The radiometer is constructed in such a manner that the one radiation-sensing detector faces a built-in reference black body. The other radiation detector is used to detect the incoming radiation from the target.

The reference black body which is constructed from aluminium and painted with optical matt black lacquer, is thermally insulated from the copper block by means of a bakelite spacing ring; the temperature of the reference body being controlled by means of a commercially available thermo-electric module (Sanyo:1V 4A) fitted with cooling fins. A 30 SWG copper-constantan thermocouple is provided in the reference black body to enable its temperature to be measured.

The entire assembly is fitted into an aluminium housing equipped with a wooden handle.

To protect the soluble rock salt windows of the radiation detectors from water vapour, a window of polyethylene film, 37 micron thick, was installed in front of the housing, and the enclosure maintained at a low relative humidity by means of a capsule containing silica gel.

The output of the radiation-sensing elements can either be measured differentially or the output of the radiation-sensing element facing the target can be measured separately.

In the former case, the differential output is detected by means of an electronic galvanometer* which, in turn, controls the polarity of the power supply to the thermo-electric module fitted to the reference black body; if the output of the radiation-sensing element facing the built-in reference black body drops below the output of the radiation-sensing element facing the target, the output of the galvanometer drops below zero and the reference black body is automatically heated by means of the thermo-electric module. On an increase of the galvanometer reading above zero, the polarity of the power supply to the thermo-electric module is automatically reversed and the reference black body is cooled by means of the thermo-electric module. In this manner the temperature of the reference black body is caused to oscillate above and below the target temperature.

* Fluke electronic galvanometer, model 840A

Figure 67 presents a view of the radiometer, power supply unit and the electronic galvanometer.

Details of the electrical circuits for the power supply unit and temperature control systems, are given in Figures 68, 69 and 70.

6.3.1 Spectral response

The spectral wave-band to which the radiometer is sensitive, is determined by the spectral transmittance of the rock salt window.

According to the manufacturers of the radiation detectors, the transmittance of rock salt is 0,9 at wave-lengths between 1 and 15 micron. Between wave-lengths of 15 and 20 micron the transmittance drops, almost linearly to 0,2.

The thin polyethylene film has a uniform transmittance of over 0,85 over this range with comparatively narrow absorption bands around 3,5, 7 and 14 micron of little significance. (See Figure 53 on page 266).

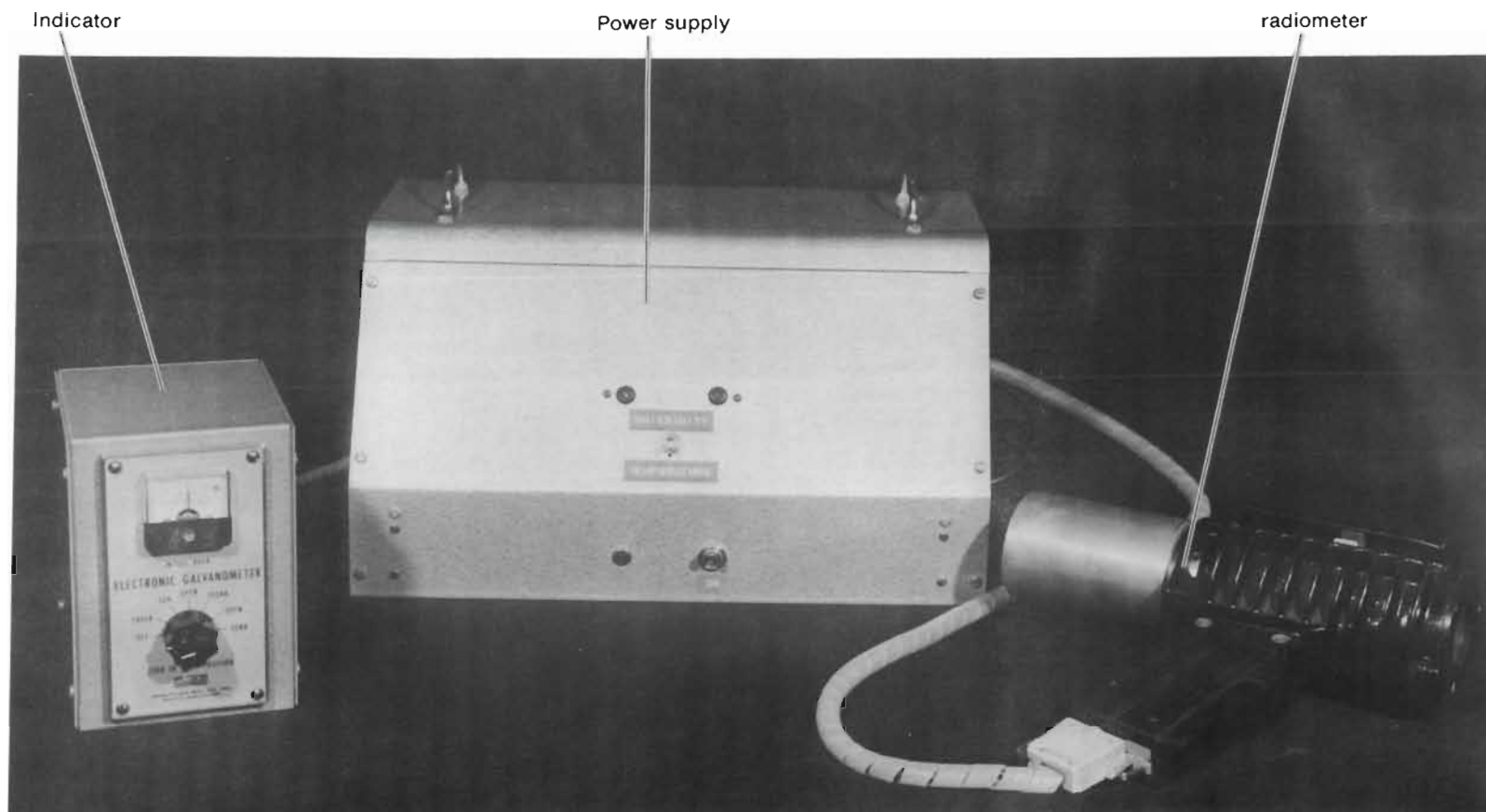


FIGURE 67

View of components of the low-cost portable radiometer for surface temperature and emissivity measurements.

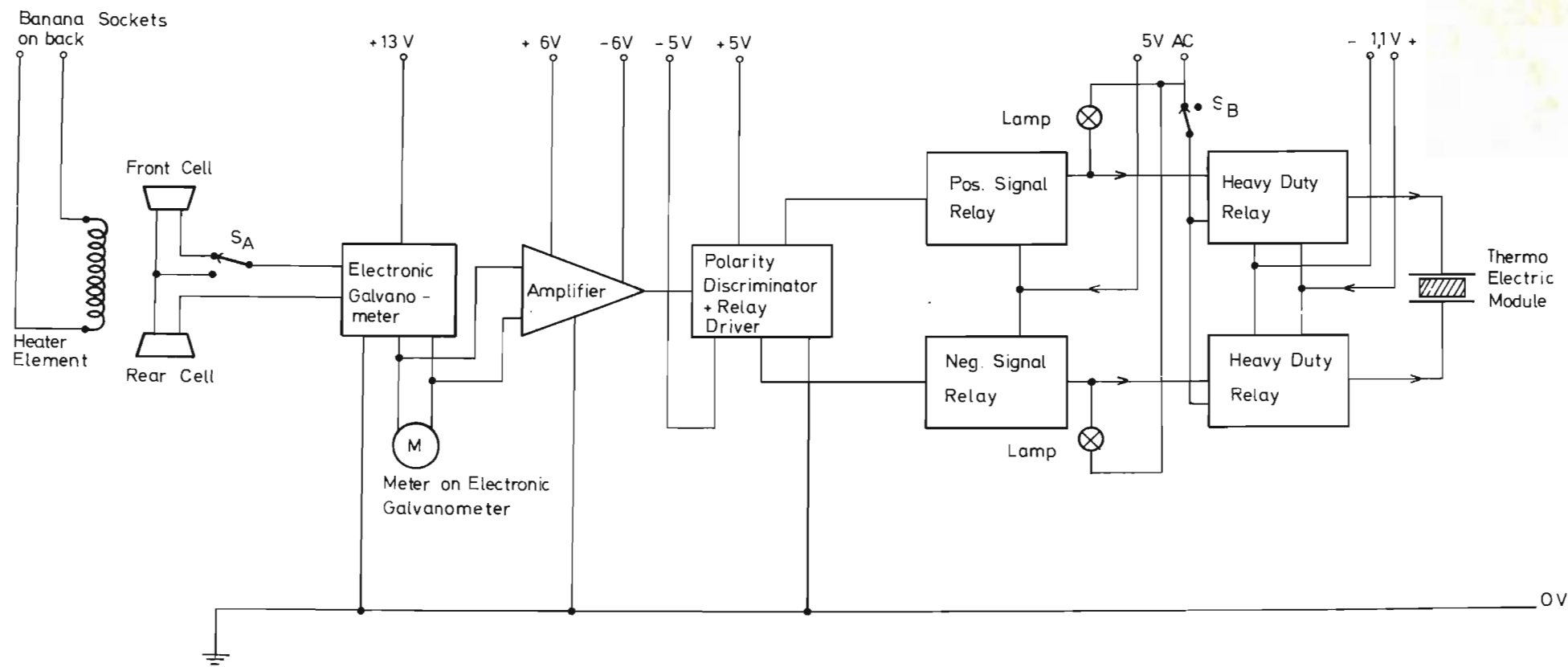


FIGURE 68

Portable low-cost radiometer for surface temperature and emissivity measurements: block diagram and interconnections

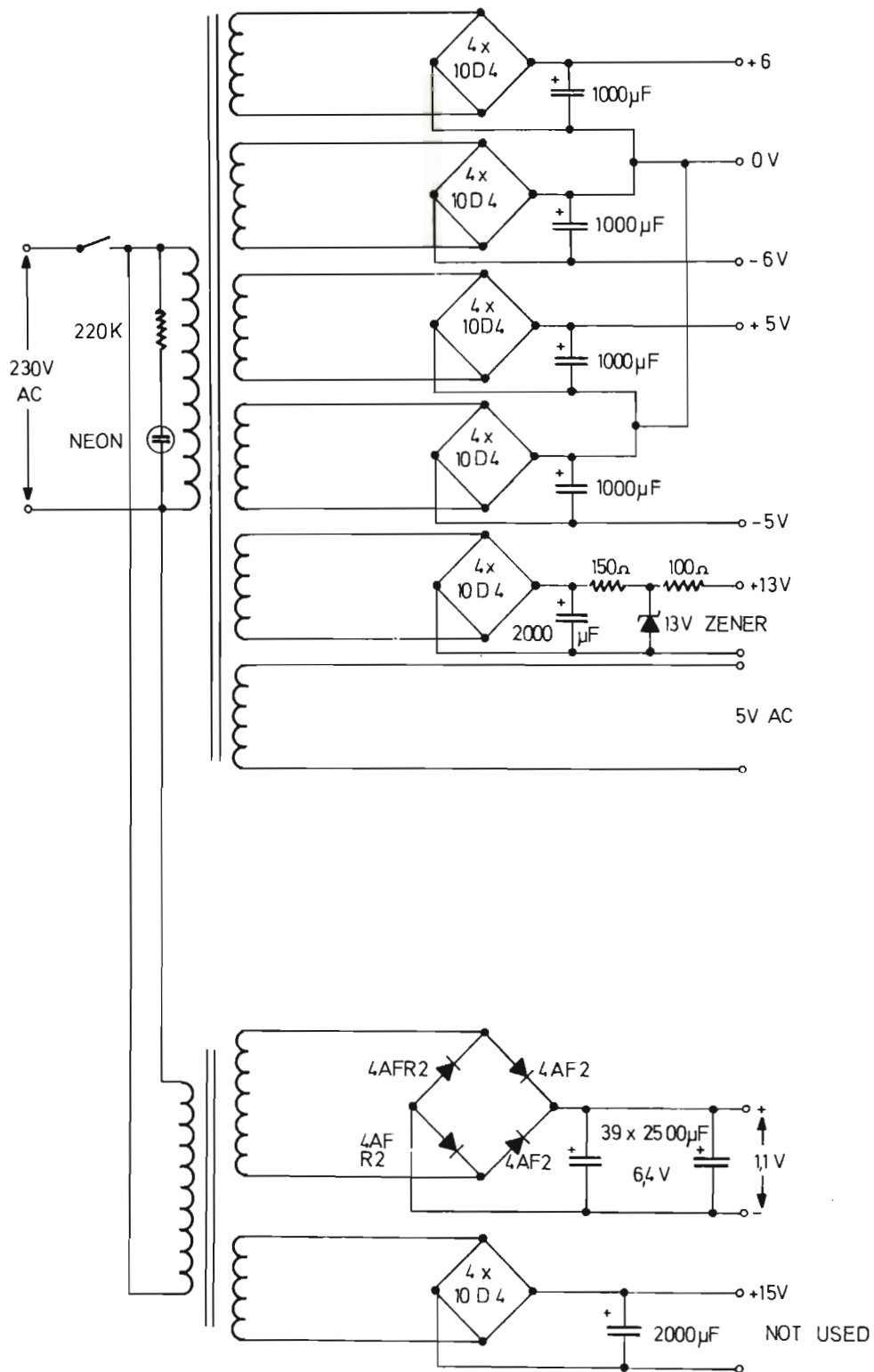
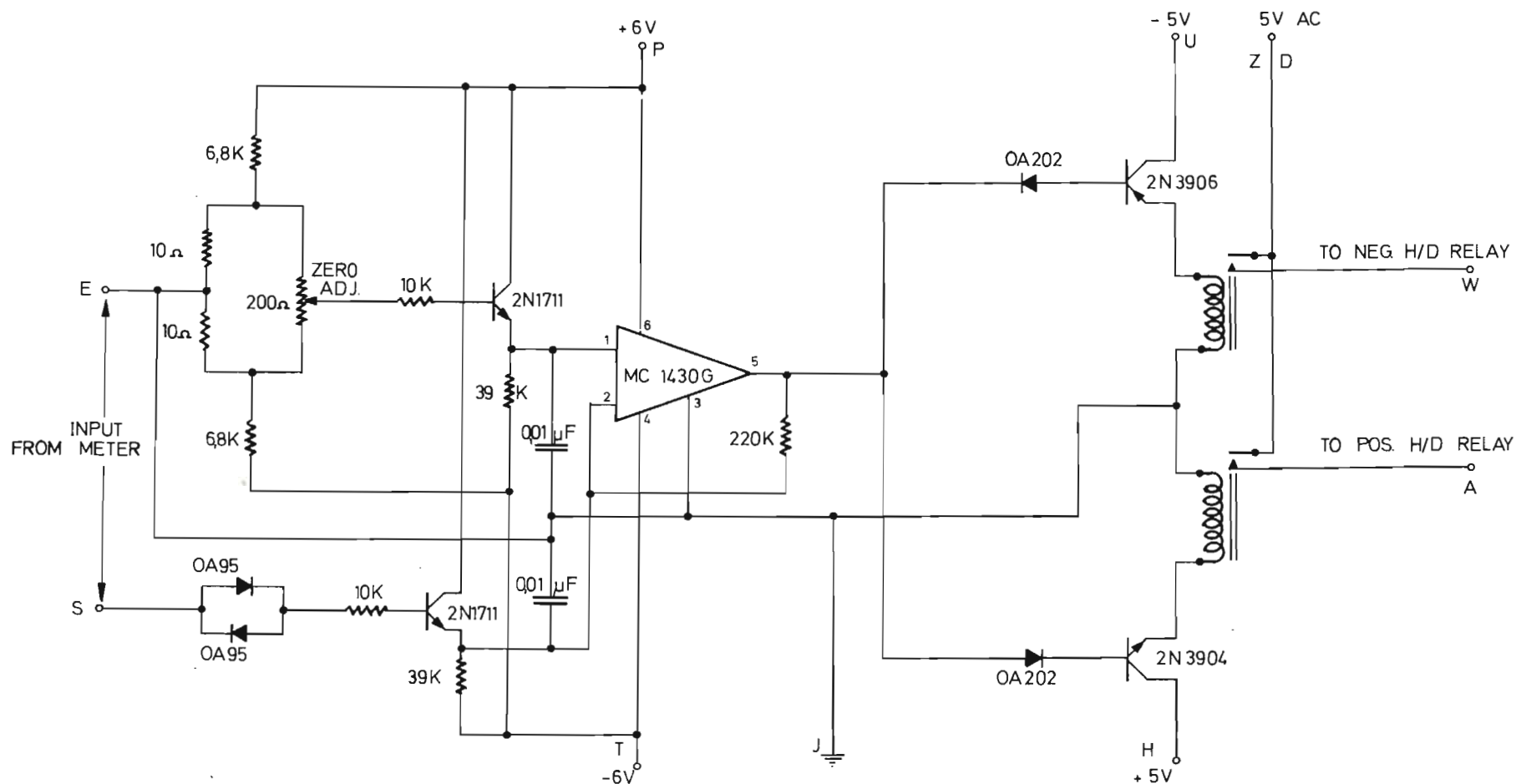


FIGURE 69

Portable low-cost radiometer for surface temperature and emissivity measurements: power supply units



LETTERS REFER TO BORD EDGE CONNECTOR

FIGURE 70

Portable low-cost radiometer for surface temperature and emissivity measurements:
amplifiers, polarity discriminators and relays

6.3.2 View angle

Although the radiometer is not strictly directional in the sense of receiving only rays parallel to the principle axis, it, nevertheless, has a well defined field of view; the included view angle being of the order of 0,4 radians.

The aperture of the radiometer is 30 mm diameter.

6.4 Calibration tests

6.4.1 Temperature measurement

The radiometer was calibrated as a surface temperature measuring device using a conical black body with an emissivity higher than 0,999 as the radiant heat source.

The following method of temperature measurement was investigated: the radiation detectors within the radiometer were connected differentially and the differential output used to control the temperature of the built-in reference black body by means of the system described in Section 6.3 on page 342. The temperature of the built-in reference black body was then noted whenever the differential output of the two radiation detectors was zero.

Test procedure

The conical black body and radiometer were mounted in the vertical test chamber of the climatic chamber with the radiometer positioned directly in front of the aperture of the conical black body.

The power supply unit was switched on and the two radiation detectors incorporated in the radiometer were connected differentially by switching the control switch mounted on the front panel of the power supply unit shown in Figure 67 on page 344 to the position marked "temperature". (This enabled the temperature of the built-in reference black body to be automatically controlled).

Calibration tests were then carried out at various conical black body or target temperatures within the nominal temperature range of 20 to 40°C. During each series of target temperature adjustments, the ambient air temperature was controlled at the nominal values of 15, 25 or 35°C.

The temperature of the built-in reference black body was noted whenever the differential output of the two radiation detectors (as indicated by the electronic

galvanometer) attained a zero value. At the same time temperature measurements of the target and ambient air were carried out.

Test results

The test results are summarised in Table 13.

It was found that the radiometer was sensitive to ambient air temperature variations. To overcome this problem, the following formulae for calculating the target temperature from the ambient air and built-in reference black body temperatures was deduced from a statistical analysis of the test results:

$$t_b = 1 + 0,67 t_t + 0,33 t_G \quad \dots\dots (47)$$

where t_b = temperature indicated by the radiometer (this temperature corresponded to the temperature of the built-in reference black body), °C

and t_t = temperature of the target, °C

t_G = ambient air temperature, °C.

It was found that the target temperature could be determined to within 0,3°C by this means. (See Figure 71).

TABLE 13 : CALIBRATION OF LOW COST RADIOMETER AS A SURFACE
TEMPERATURE-MEASURING INSTRUMENT : TEST RESULTS

TEMPERATURES (°C)			
Ambient air	Built-in reference black body	Target	
		Actual	Calculated
35,0	28,3	22,5	23,5
35,2	30,3	25,9	26,2
35,3	31,2	27,8	27,7
35,4	32,6	30,1	29,7
35,5	33,9	32,0	31,6
35,5	35,0	33,9	32,3
35,5	36,2	35,8	35,1
35,0	38,1	38,4	38,1
35,1	39,1	39,8	39,6
25,2	23,1	20,0	20,6
25,3	24,6	22,3	22,8
25,4	25,7	24,1	24,4
25,5	27,0	26,1	26,2
25,5	28,1	27,9	27,9
25,5	29,4	29,9	29,8
25,5	30,7	31,8	31,6
25,5	32,0	33,7	33,7
25,6	33,0	35,5	35,6
25,6	34,6	37,6	37,5
25,7	36,0	39,4	39,6
25,7	37,2	41,2	41,4
15,4	18,8	19,0	19,0
15,4	20,4	21,7	21,4
15,5	21,9	23,8	23,6
15,6	23,1	25,7	25,3
15,6	24,5	27,6	27,4
15,6	26,1	29,8	29,8
15,6	27,0	31,4	31,1
15,6	28,3	33,4	33,1
15,7	29,6	35,2	35,0
15,7	31,0	37,1	37,0
15,7	32,5	39,0	39,3
15,7	34,0	41,0	41,5

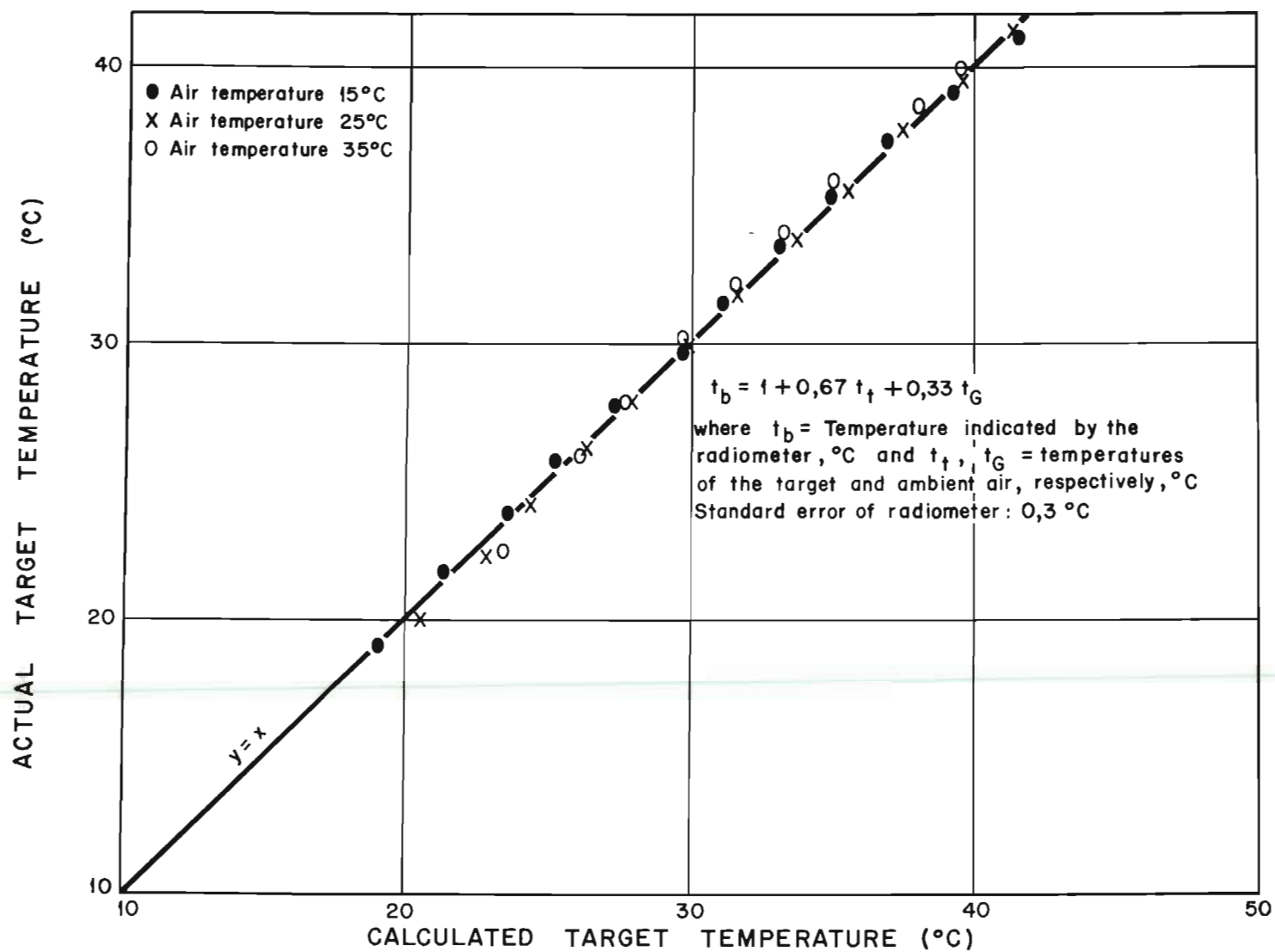


FIGURE 71

Measurement of surface temperature: calibration curve for low-cost radiometer.

6.4.2 Emissivity measurement

The unique facility of being able to vary the temperature of the radiation detector which is used to view the target, enabled a new method of determining the emissivity of a surface to be developed by Mitchell et al¹¹⁸⁾. A brief description of the method is given in the following section for the sake of completeness.

Since the radiometer output is proportional to the radiation energy exchange rate between the target and radiation detector, the relationship between the radiometer output and radiation exchange rate can be expressed in the following form:

$$\alpha = C \dot{q}_{\text{rad}} \quad \text{..... (48)}$$

where α = radiometer output

and C = constant for a particular radiometer

\dot{q}_{rad} = radiation energy exchange rate between the target and the radiation detector.

Substitution of the value for \dot{q}_{rad} , according to equation (46) on page 331 in equation (48) leads to:

$$\alpha = CA\sigma\epsilon_s \epsilon_{se} T_s^4 - CA\sigma\epsilon_s \epsilon_{se} T_{se}^4 \quad \text{..... (49)}$$

where α = radiometer output

and C = constant for a particular radiometer

A = term which depends on the areas and configuration factors involved

σ = Stefan-Boltzman constant

$\epsilon_s, \epsilon_{se}$ = emissivities of the skin target and radiation detector, respectively

T_s, T_{se} = absolute temperatures of the skin target and radiation detector, respectively.

If the skin temperature, T_s , is kept constant, the term $CA\sigma\epsilon_s\epsilon_{se}T_s^4$ would be constant and equal, say to ϕ_0 .

$$\therefore \alpha = \phi_0 - CA\sigma\epsilon_s\epsilon_{se}T_{se}^4 \quad \dots\dots (50)$$

A plot of radiometer output ϕ_0 against T_{se}^4 at constant target temperature would, therefore, yield a straight line of slope $M_s = -CA\sigma\epsilon_s\epsilon_{se}$.

Thus, when a black body surface of emissivity, ϵ_b , and a skin target of emissivity, ϵ_s , are viewed by the radiometer, plots of the radiometer output, α , against T_{se}^4 , at constant black body and skin target temperatures would yield straight lines of slopes $M_b = -CA\sigma\epsilon_b\epsilon_{se}$ and $M_s = -CA\sigma\epsilon_s\epsilon_{se}$ for the black body and skin targets, respectively.

The term $(-CA\sigma\epsilon_{se})$ is naturally the same in both expressions and if the same geometrical configuration is maintained for both the black body and skin target, the term (A) can be kept the same. Thus $M_s/M_b = \epsilon_s/\epsilon_b$.

The above method, which enables the emissivity of the skin target to be determined without a knowledge of the target and black body temperatures, was used by Mitchell¹¹⁹⁾ to determine the emissivity of samples of excised skin controlled at a fixed temperature.

For the purpose of these tests, the electrical power input to the heater element incorporated in the radiometer was varied by means of a Solartron AS757.4 regulated constant voltage supply unit, capable of delivering up to 50 volts in 0.1 volt steps (in order to vary the detector temperature in steps) and the output of the radiation detector after thermal equilibrium conditions were achieved was measured without pre-complication, by means of a Kipp Micrograph BD2 galvanometric recorder.

Accuracy of emissivity measurement

During the investigations to determine the emissivity of excised skin, the sensitivity of the radiometer and the

average standard error of single measurements of emissivity were found to be $1,6 \mu\text{w m}^2 \text{ } ^\circ\text{K}^4/\text{w}$ and 0,01, respectively.

6.5 Discussion

The accuracy with which surface temperatures could be determined by means of the radiometer compared favourably with more sophisticated radiometers. In view of the sensitivity of the radiometer output to ambient temperature variations, however, a knowledge of the ambient temperature is necessary for the determination of surface temperatures by this means.

The fact that the temperature of the radiation detector could be adjusted, is a unique characteristic which enabled a new method of determining the emissivity of a surface to be developed.

Other characteristics which make the radiometer suitable for such measurements are the uniform spectral response of the thermal detector (which is limited only by the cut-off wave-length of the rock-salt window), and the fact that the output of the radiometer is sufficiently high to be measured on a recorder without requiring a chopper-amplifier system.

The radiometer was successfully used for the accurate determination of the emissivities of samples of excised skin. An improvement of the response time of the radiometer would, however, be necessary for the rapid determination of the emissivity of living skin by this means.

CHAPTER 7

DISCUSSION AND CONCLUSIONS

A knowledge of the heat transfer processes between the human body and his environment is one of the major prerequisites for the establishment of functional relationships capable of describing thermal stress in man.

Generally, the heat produced within the human body due to metabolic processes, is dissipated to the surroundings, principally by convection, evaporation and radiation.

The skin is the most important interface in this thermal energy exchange process. Its temperature, apart from being involved to some extent in the thermo-regulatory process of the human body, affects the convection, evaporation and radiation heat loss rates; the latter mode of heat transfer being also influenced by, inter alia, emissivity of the skin.

The low-cost radiometer with its built-in facility to vary the temperature of the radiation detector, enabled the emissivity of excised human skin to be determined with a relatively high degree of accuracy; the average standard error of single measurements of emissivity being of the order of 0,01.

The accuracy with which surface temperatures could be determined by means of the radiometer compared favourably with more sophisticated radiometers.

In the theoretical analysis it was shown that the skin temperature of the human body is affected, within certain limits, by the ratio of the film coefficient of heat transfer to the physiological conductance and thermal radiation. For the purpose of the theoretical analysis the skin was assumed to be completely wet.

Calculation of the skin temperature and relative magnitudes of the convective, evaporative and radiative energy exchange rates is, however, complicated by the lack of information on the degree of "wetness" of the skin under certain environmental conditions, the irregular and changeable shape of the body, particularly during exercise and the non-uniform temperature distribution across the body surface.

The experimental determination of the heat loss rate from a subject in a normal working position has, in the past, been limited by the lack of suitable instrumentation.

The successful development of the evaporative and radiative heat loss measuring systems described in this dissertation, together with the convective heat loss measuring instrument that had previously developed, have provided physiologists with unique facilities for determining by

direct means the convective, evaporative and radiative heat loss rates from a human subject in a normal working mode.

The equipment was specifically designed for installation in the relatively large horizontal test chamber of the Human Sciences Laboratory's climatic chamber; a unique facility in which air temperature, relative humidity and air speed can be closely controlled over a relatively wide range of conditions.

The direct heat loss measuring equipment, together with auxiliary instrumentation for measuring the work rate, metabolic rate, rectal temperature, oesophageal temperature, skin temperature and heart rate of a subject, was subsequently used by the staff of the Human Sciences Laboratory for various animate studies in the climatic chamber.

The studies included systematic investigations into the heat exchanges and thermal reactions of nude, healthy, heat acclimatized young men, resting and working, over a wide range of environmental conditions; the primary object of the experiments being to provide equations for the heat exchange between man and the environment which would be sufficiently accurate for the prediction of heat stress in workers in the gold mining industry. The secondary goal was to elucidate some basic characteristics of the mechanism of temperature regulation in man.

The satisfactory performance of, inter alia, direct heat loss measuring equipment throughout the investigations, enabled reliable equations capable of accurately describing the convective, evaporative and radiative heat loss rates to be established for the first time.

Without the availability of the direct heat loss measuring equipment, this would not have been possible.

8. BIBLIOGRAPHY

1. BRUNT, D. The reaction of the human body to its physical environment. Q. Jl. R. Met. Soc., vol. 69, 1943, pp. 77/114.
2. GRANT, W.L. The design and development of a climatic chamber for the study of human reactions under different environmental conditions. Jl. S. Afr. Instn Mech. Engrs, vol. 4, 1954, pp. 133/206.
3. GRANT, W.L. The constructional and operational aspects of a climatic chamber for the study of human reactions under different environmental conditions. J. Instn Cert. Engrs. S. Afr., vol. 28, 1955, pp. 83/112.
4. GRANT, W.L. The performance characteristics of the climatic chamber of the Chamber of Mines Physiology Laboratory. S. Afr. mech. Engr, vol. 6, 1956, pp. 109/157.
5. VISSER, J. and HODGSON, T. The design of a human calorimeter for the determination of body heat storage. S. Afr. mech. Engr, vol. 9, 1960, pp. 243/269.
6. CARLSON, L.D. Respiratory exchange. In : Methods in medical research, J. Murray Steele, Editor, vol. 6, Chicago, Year Book Publishers, 1954, pp. 60/73.
7. WEIR, J.B. de V. New methods for calculating metabolic rate with special reference to protein metabolism. J. Physiol., vol. 109, 1949, pp. 1/9.

8. BURTON, A.C. and BAZETT, H.C. A study of the average temperature of the tissues of the body, the exchanges of heat and vasometer responses in man by means of a bath calorimeter. Am. J. Physiol., vol. 117, 1936, pp. 36/54.
9. WINSLOW, C.E.A., HERRINGTON, L.P. and GAGGE, A.P. A new method of partitional calorimetry. Am. J. Physiol., vol. 116, 1936, pp. 641/655.
10. BENZINGER, T.H. and KITZINGER, C. Direct calorimetry by the gradient layer principle. Rev. scient. Instrum., vol. 20, 1949, pp. 849/860.
11. NIELSEN, M., HERRINGTON, L.T. and WINSLOW, C.E.A. The effect of posture on peripheral circulation. Am. J. Physiol., vol. 127, 1939, p. 573.
12. RAHN, H., OTIS, A.B., CHADWICK, L.E. and FENN, W.A. The pressure-volume diagram of the thorax and lung. Am. J. Physiol., vol. 146, 1946, p. 161.
13. STITT, J.T. and HARDY, J.D. Thermoregulation in the squirrel monkey (*Saimiri Sciureus*). J. appl. Physiol., vol. 8, 1971, pp. 223/229.
14. ATKINS, A.R. A method of simulating heat flow and control in a nude man with an analogue computer. M.Sc.(Eng) Thesis, University of the Witwatersrand, Johannesburg, 1962.
15. NIELSON, B. Thermoregulation in rest and exercise. Acta physiol. scand., Suppl. 323, 1969, pp. 1/74.
16. PEDERSON, L. The heat regulation of the human body. Acta physiol. scand., vol. 77, 1969, pp. 95/105.

17. COOPER K.E. and KENYON, J.R. A comparison of temperatures measured in the rectum, oesophagus, and on the surface of the aorta during hypothermia in man. Br. J. Surg., vol. 44, 1957, pp. 616/619.
18. NIELSEN, B. and NIELSEN, M. Body temperature during work at different environmental temperatures. Acta physiol. scand., vol. 56, 1962, pp. 120/129.
19. EICHNA, L.W., BERGER, A.R., RADER, B. and BECKER, W.H. Comparison of intracardiac and intravascular temperatures with rectal temperatures in man. J. clin. Invest., vol. 30, 1951, pp. 353/359.
20. MITCHELL, D., WYNDHAM, C.H., ATKINS, A.R., VERMEULEN, A.J., HOFMEYER, H.S., STRYDOM, N.B. and HODGSON, T. Direct measurement of the thermal response of nude resting men in dry environments. Pflügers Arch. ges. Physiol., vol. 303, 1968, pp. 324/343.
21. ROBINSON, S. Circulatory adjustments of men in hot environments. In : Temperature : Its measurement and control in science and industry, C.M. Herzfeld, Editor-in-chief, vol. 3. Biology and medicine, J.D. Hardy, Editor. part 3, New York, Reinhold Publishing Corporation, 1963, pp. 287/297.
22. HATCH, T. Assessment of heat stress. In : Temperature : Its measurement and control in science and industry, C.M. Herzfeld, Editor-in-chief, vol. 3. Biology and medicine, J.D. Hardy, Editor. part 3, New York, Reinhold Publishing Corporation, 1963, pp. 307/318.

23. PHELPS, E.B. and VOLD, A. Studies on ventilation. 1. Skin temperature as related to atmospheric temperature and humidity. Am. J. publ. Hlth, vol. 24, 1934, p. 959/970.
24. WYNDHAM, C.H. Role of skin and of core temperature in man's temperature regulation. J. appl. Physiol., vol. 20, 1965, pp. 31/36.
25. TAYLOR, H.L., YANG WANG, ROWELL, L. and BLOMQUIST, G. The standardization and interpretation of sub-maximal and maximal tests of working capacity. Pediatrics, vol. 30, 1963, pp. 703/722.
26. WILLIAMS, C.G., BREDELL, G.A.G., WYNDHAM, C.H., STRYDOM, N.B., MORRISON, J.F. and PETER, J. Circulatory and metabolic reactions to work in heat. J. appl. Physiol., vol. 17, 1962, pp. 625/638.
27. BELDING, H.S. Resistance to heat in man and other homeothermic animals. In : Thermobiology, A.H. Rose, Editor. London, Academic press, 1967, pp. 479/510.
28. RICHARDSON, H.B. Clinical calorimetry : The effect of the absence of sweat glands on the elimination of water from the skin and lungs. J. biol. Chem., vol. 67, 1926, pp. 397/411.
29. TAYLOR, C.L. and BUETTNER, K. Influence of evaporative forces upon skin temperature dependency of human perspiration. J. appl. Physiol., vol. 6, 1953, pp. 113/123.
30. HERRINGTON, L.P. The biological problem of the human body as a heat exchanger. Trans. Am. Soc. mech. Engrs, Paper No. 57-SA-5, Febr., 1958.

31. WOODCOCK, A.H. and BRECKENRIDGE, J.R. A model description of thermal exchange for the nude man in hot environments. Ergonomics, vol. 8, 1965, p. 223/235.
32. REYNOLDS, O. On the extent and action of the heating surface of steam boilers . Proc. lit. phil. Soc. Lpool, vol. 41, 1874.
33. SPALDING, D.B. Convective mass transfer. London, Edward Arnold Publishers, Ltd., 1963.
34. SHERWOOD, T.K. and AGFORD, R.C. Absorption and Extraction. New York, McGraw-Hill, 1952.
35. MITCHELL, D. Human surface temperature : Its measurement and its significance in thermoregulation. Ph.D. Thesis, University of the Witwatersrand, Johannesburg, 1972.
36. CARROLL, D.F. and VISSER, J. Direct measurement of convective heat loss from a human body. Rev. scient. Instrum., vol. 37, 1966, pp. 1174/1180.
37. HALLIDAY, E.C. and HUGO, T.J. The photodermoplanimeter. J. appl. Physiol., vol. 18, 1963, pp. 1285/1289.
38. VAN GRAAN, C.H. The determination of body surface area. S. Afr. med. J., vol. 43, 1969, pp. 952/959.
39. DU BOIS, D. and DU BOIS, E.F. A formula to estimate the approximate surface area if height and weight be known. Archs int. Med., vol. 17, 1916, pp. 863/871.
40. NEUROTH, G. Die Hauttemperatur im Dienste der Wärmeregulation. Pflügers Arch. ges. Physiol., vol. 250, 1948, pp. 396/413.

41. STOLWIJK, J.A.J. and HARDY, J.H. Partitional calorimetric studies of responses of man to thermal transients. J. appl. Physiol., vol. 21, 1966, pp. 967/977.
42. IAMPIETRO, P.F. Prediction of skin temperature of men in the cold. J. appl. Physiol., vol. 16, 1961, pp. 405/408.
43. LUSK, G. Clinical calorimetry : Respiration calorimeter for the study of disease. Archs int. Méd., vol. 15, 1915, pp. 793/804.
44. RICHE, J.A. and SODERSTROM, G.F. Clinical calorimetry : The respiration calorimeter of the Russel Sage institute of pathology in the Bellvue hospital. Archs int. Méd., vol. 15, 1915, p. 805
45. MURLIN, J.R. and BURTON, A.C. Human Calorimetry. J. Nutr., vol. 9, 1935, pp. 233/300.
46. BENZINGER, R.H., HUEBESHER, R.G., MINARD, D. and KITZINGER, C. Human calorimeter by means of the gradient principle. J. app. Physiol., vol. 12, Suppl. 1 - 24, 1958.
47. SNELLEN, J.W. Mean body temperature and the control of thermal sweating. Acta. physiol. Pharmac. neerl., vol. 14, 1960, pp. 99/174.
48. SNELLEN, J.W., MITCHELL, D. and WYNDHAM, C.H. Heat evaporation of sweat. J. appl. Physiol., vol. 29, 1970, pp. 40/44.
49. NUSSELT, W. Die Verbrennung und die Vergasung der Kohle auf dem Rost. Z. Ver. dt. Ing., vol. 60, 1916, p. 102.

50. RAPP, G.M. Convective mass transfer and the coefficient of evaporative heat loss from human skin. In : Physiological and behavioural temperature regulation, J.D. Hardy, A.P. Gagge and J.A.J. Stolwijk, Editors, Springfield, Thomas, 1970, pp. 55/80.
51. WENTZEL, J.D. Humidity measurement - a critical literature survey. C.S.I.R. Rep. MEG 269, 1964, pp. 1/14.
52. HENDERSON, S.M. Constant-feed all temperature wet-bulb. Agric. Engng, Oct., 1952, p.644.
53. LANNING, J.G. Determination of relative humidities by means of thermocouples. Ind. Engng Chem., vol. 4, 1932, pp. 286/287.
54. LORENZEN, C. Construction and use of a thermo-electric psychrometer. In : Temperature : Its measurement and control in science and industry, Publs Comm.: C.O. Fairchild, J.D. Hardy, R.B. Sosman and H.T. Wensel. Symp. Am. Inst. Phys., Nov., 1939, New York, Reinhold Publishing Corp., 1941, pp. 660/665.
55. FOSKETT, L.W. and FOSTER, N.B. A spectroscopic hygrometer. Bull. Am. met. Soc., vol. 24, 1943, pp. 146/153.
56. FOSTER, N.B. and FOSKETT, L.W. Spectrophotometer for determination of water vapour in a vertical column of atmosphere. J. opt. Soc. Am., vol. 35, 1945, pp. 601/610.
57. FASTIE, W.G. and PFUND, A.H. Selective infra-red gas analyzers. J. opt. Soc. Am., vol. 37, 1947, p. 762.
58. WOOD, R.C. Improved infra-red absorption spectra hygrometer. Rev. scient. Instrum., vol. 29, 1958, pp. 36/42.
59. WYLIE, R.G. A new absolute method of hygrometry. Aust. J. Phys., vol. 10, 1957, pp. 351/365.

60. HEYMAN, S. and HODGSON, T. Theoretical and experimental investigation of absorption refrigerators and their application. C.S.I.R. Rep. Meg 262, 1962.
61. VISSER, J. and CARROLL, D.F. Direct measurement of the heat loss from a human body under different environmental conditions : Convection. C.S.I.R. Rep. N97, 1959.
62. McADAMS, W.H. Heat transmission. 2nd Ed., New York, McGraw-Hill, 1942, pp. 173, 177.
63. HARDY, J.D. and SODERSTROM, G.F. Heat loss from a nude body and peripheral blood flow at temperatures of 22°C to 35°C. J. Nutr., vol. 16, 1938, pp. 493/510.
64. HARDY, J.D. and DU BOIS, E.F. Regulation of heat loss from the human body. Proc. natn. Acad. Sci. U.S.A., vol. 23, 1937, pp. 624/631
65. NELSON, N., EICHNA, L.W., HORVATH, S.M., SHELLEY, W.B. and HATCH, T.F. Thermal exchanges of man at high temperatures. Am. J. Physiol., vol. 151, 1947, pp. 626/652.
66. NIELSON, M. and PEDERSON, L. Studies on the heat loss by radiation and convection from the clothed body. Acta physiol. scand., vol. 27, 1952, pp. 272/294.
67. BENZINGER, T.H. and KITZINGER, C. A 4 π radiometer. Rev. scient. Instrum., vol. 21, 1950, pp. 599/604
68. JAKOB, M. Heat transfer, vol. 11, New York, John Wiley and Sons, 1957.

69. JAKOB, M. and HAWKINS, G.A. Elements of heat transfer. 3rd Ed., New York, John Wiley & Sons, 1957.
70. EIGEL, M. Infra-red radiation of the human body. Elektro-Med., vol. 7, 1962, pp. 13/23.
71. HOLZER, W. Physikalische Medizin in Diagnostik und Therapie. Vienna, W. Maudrich-Verlag, 1940.
72. BUCHMÜLLER, K. Über die ultrarote Emission, Reflexion und Durchlässigkeit der lebenden menschlichen Haut im Spektralbereich $\lambda = 3 - 15 \mu\text{m}$. Pflügers Arch. ges. Physiol., vol. 272, 1961, pp. 360/371.
73. BÜTTNER, K. Über die Wärmestrahlung und die Reflexionseigenschaften der menschlichen. Hte. Strahlentherapie, vol. 58, 1937, p. 345.
74. PATIL, K.D. Infra-red emission from the human skin in vivo between $2,0\mu$ and $18,0\mu$. Physics Med. Biol., vol. 15, 1970, p. 178
75. WATMOUGH, D.J. and OLIVIER, R. Emissivity of human skin in vivo between $2,0\mu$ and $5,4\mu$ measured at normal incidence. Nature, Lond., vol. 218, 1968, pp. 885/886.
76. WATMOUGH, D.J. and OLIVIER, R. Emissivity of human skin in the wave-band between 2μ and 6μ . Nature, Lond., vol. 219, 1968, pp. 622/624.

77. MITCHELL, D., WYNDHAM, C.H. and HODGSON, T. Emissivity and transmittance of excised human skin in its thermal emission wave-band. J. Appl. Physiol., vol. 23, 1967, pp. 390/394.
78. PLANCK, M. Distribution of energy in the spectrum. Annln. Phys., vol. 4, 1901, pp. 553/563.
79. JOOS, G. Lehrbuch der theoretischen Physik. 7th Edition, Leipzig, Akademische Verlagsgesellschaft, Geest & Portig K - G, 1950, p. 544.
80. JONES, R.C. Phenomenological description of the response and detecting ability of radiation detectors. Proc. Instn Radio Engrs, vol. 47, 1959, pp. 1495/1502.
81. VANSELOW, K. Kritische Bemerkungen zur Temperaturmessung über die UR-Strahlung des Menschen. Elektro-Med., vol. 8, 1963, pp. 108/116.
82. SCHULZE, R. Optische durchlässigkeit von Lupolen-H für ultra-violette strahlung, sichtbare und infrarot strahlung. Annln Met., vol. 6, 1953, p. 127.
83. FUNKE, J.P. Improved polyethylene-shielded net radiometer. J. Scient. Instrum., vol. 36, 1959, pp. 267/270.
84. BOLLE, H.S. and FLEISCHER, R. Der einfluss der Lupolen-absorption auf die messung und registrierung der ultrarot-strahlungströme. Annln Met., vol. 6, 1953, p. 380.
85. SMITH, F.E. Resistance measurements of high precision. Phil. Mag., vol. 24, 1912, pp. 541/569.

86. WORTHING, A.G. Temperature radiation emissivities and emittances. J. appl. Physiol., vol. 11, 1940, pp. 421/437.
87. BUCHMÜLLER, K. and FRÜGER, H. Untersuchungen über die Möglichkeiten einer klinischen Ultrarot-emissionsdiagnostik Die Gesundheitswes., vol. 13, 1958, pp. 485/492.
88. BENEDICT, F.G. and PARMENTER, H.S. Human skin temperature as affected by muscular activity, exposure to cold and wind movement. Am. J. Physiol., vol. 87, 1929, pp. 633/653.
89. BEDFORD, T. and WARNER, C.G. On methods of measuring skin temperature. J. Hyg., vol. 34, 1934, pp. 458/473.
90. PFLEIDERER, H. and BUTTNER, K. Die physiologischen und physikalischen Grundlagen der Hautthermometrie. Leipzig, Johan Ambrosius Barth, 1935.
91. ROESER, W.F. Thermoelectric thermometry. J. appl. Physiol., vol. 11, 1940, pp. 388/407.
92. FOSTER, P.C. Thermocouples for the medical laboratory. J. Lab. clin. Med., vol. 22, 1936, pp. 68/81.
93. ATKINS, A.R. Transducers for physiological transducers. In : Symposium on Transducers for the electrical measurement of non-electric quantities. C.S.I.R., Symposia S9, 1964.
94. ELDER, J.S. Thermocouples for temperature measurements on skin surfaces and living tissues. Onderstepoort J. vet. Sci. Anim. Ind., vol. 17, 1941, pp. 141/163.
95. HARDY, J.D. The radiation of heat from the human body. II. A comparison of some methods of measurement. J. clin. Invest., vol. 13, 1934, pp. 605/614.

96. STOLL, A.M. Techniques and uses of skin temperature measurements. Ann. N.Y. Acad. Sci., vol. 121, 1964, pp. 49/56.
97. STOLL, A.M. and HARDY, S.D. Study of thermocouples as skin thermometers. J. appl. Physiol., vol. 2, 1950, pp. 531/534.
98. STILLWELL, G.K., HEMINGWAY, A. and KOTTKE, F.J. Accuracy of thermocouples as surface thermometers. J. appl. Physiol., vol. 8, 1959, pp. 223/229.
99. FREEMAN, H. and LINDER, F.E. Some factors determining the variability of skin temperature. Arch. int. Méd., vol. 54, 1934, pp. 981/987.
100. OGDEN, L.W. and REES, W.H. Measurement of temperature and relative humidity on the skin and clothing of a human subject. J. Text. Inst. Trans., vol. 38, 1947, T 371/T 386.
101. EVANS, J.P. and WILSON, R.E. A comparison of differential measurements of skin temperature using a radiometer, resistance thermometer and thermocouples. J. Lab. clin. Med., vol. 38, 1951, pp. 557/560.
102. WHYTE, H.M. Thermocouples as skin thermometers. Clin. Sci., vol. 10, 1951, pp. 325/332.
103. PALMES, E.D. and PARK, C.R. An improved mounting for thermocouples for the measurement of the surface temperature of the body. J. Lab. clin. Med., vol. 33, 1948, pp. 1044/1046.
104. SUTHERLAND, G.B.B.M., and LEE, E. Developments in the infra-red region of the spectrum. Rep. Prog. Phys., vol. 11, 1946/7, pp. 144/177.

105. MITCHELL, D., WYNDHAM, C.H. and HODGSON, T. The selection of a biothermal radiometer. J. scient. Instrum., vol. 44, pp. 847/851.
106. HARDY, J.D. and STOLL, A.M. Radiometric methods for the measurement of skin temperature. In : Methods in medical research, L.J.M. Steele, Editor. vol. 6, Chicago, Year Book Publishers, 1954, pp. 85/89.
107. GÜRTNER, W. and GÖPFART, H. Topographische Untersuchungen über die Strahlungs-eigenschaften der lebenden menschlichen Haut. Pflügers Arch. ges. Physiol., vol. 280, 1964, pp. 224/225.
108. EIGEL, M. Die Ultrarotstrahlung des menschlichen Körpers. Elektro-Med., vol. 7, pp. 13/23.
109. HARDY, J.D. The radiation of heat from the human body. I. An Instrument for measuring the radiation and surface temperature of the skin. J. clin. Invest., vol. 13, 1934, pp. 593/604.
110. PICK, M. and SCHLEINZER, R. Das ultrarote Strahlungsbild des gesunden und des kranken Menschen Arch. klin. Med., vol. 201, 1954, pp. 286/291.
111. NICOLAI, L. Über die infrarotstrahlung des Menschen : I Über traghertsfreie Registrierung der Infrarotstrahlung von $\lambda = 0,75\mu$ bis $3,6\mu$ besonders der menschlichen Haut. Pflügers Arch. ges. Physiol., vol. 263, 1956, pp. 439/446.
112. KROEBEL, N. and VASENLOW, K. Die Registrierung der Feinstruktur der Wärmestrahlung des menschlichen Körpers. Z. angew. Phys., vol. 11, 1959, pp. 19/27.

113. KAUFMAN, W.C. and PITTMAN, J.C. Quantitative radiometric measurement of skin temperatures. J. appl. Physiol., vol. 21, 1966, pp. 302/314.
114. BARNES, R.B. Determination of body temperature by infra-red emission. J. appl. Physiol., vol. 22, 1967, pp. 1143/1146.
115. DREYFUS, M.G. Spectral radiation of black body radiation. Appl. Opt., vol. 2, 1963, pp. 1113/1115.
116. WOLFE, W.L. Infra-red imaging devices in infra-red medical radiography. Ann. N.Y. Acad. Sci., vol. 121, 1964, pp. 57/70.
117. LOWAN, A.N. and BLANCH, G. Tables of Planck's radiation and photon functions. J. opt. Soc. Am., vol. 30, 1940, pp. 70/81.
118. MITCHELL, D., WYNDHAM, C.H., HODGSON, T. and NABARRO, F.R.N. Measurement of the total normal emissivity of skin without the need for measuring skin temperature. Physics Med. Biol., vol. 12, 1967, pp. 359/366.
119. MITCHELL, D. An investigation of the thermal radiation from excised human skin. M.Sc. Thesis, University of the Witwatersrand, Johannesburg, 1966.
120. DALTON, J. Experimental essays on the construction of mixed gases; on the force of steam or vapour from water and other liquids in different temperatures both in a Torricellian vacuum and in air, on evaporation; and on the expansion of gases by heat. Mem. Proc. Manchr. lit. phil. Soc., vol. 5, 1801, p. 535.
121. MAXWELL, J.C. On the dynamical theory of gases. Phil. Trans. R. Soc., vol. 157, 1867, p. 49.

122. CHAPMAN, S. The kinetic theory of a gas constituted of spherically symmetrical molecules. Phil. Trans. R. Soc., vol. A211, 1912, p. 433.
123. CHAPMAN, S. and COWLING, T.G. The mathematical theory of non-uniform gases. Cambridge, Cambridge University press, 1939.
124. HIRSCHFELDER, J.O., CURTISS, C.F. and BIRD, R.B. The molecular theory of gases and liquids. New York, Wiley, 1956.
125. NERNST, W. Theorie der Reaktionsgeschwindigkeit in heterogenen Systemen. Z. phys. Chem., vol. 47, 1904, p. 52/55.
126. LEWIS, W.K. The evaporation of a liquid into gas. Mech. Engng, vol. 44, 1922, pp. 445/446.
127. WHITMAN, W. A preliminary experimental confirmation of the two-film theory of gas absorption. Chem. Metall. Engng, vol. 29, 1923, p. 146/148.
128. CARRIER, W.H. "The contact-mixture analogy applied to heat transfer mixtures of air and water vapour". Trans. Am. Soc. mech. Engrs, vol. 59, 1937, pp. 49/53.
129. SPALDING, D.B. Combustion of a single droplet and of a fuel spray : Selected Combustion problems. London, Butterworth, 1954.
130. SPALDING, D.B. Berechnung von Massenübertragungsgeschwindigkeiten bei gleichzeitiger chemischer Reaktion und Wärmeübertragung. Chemie-Ingr-Tech., vol. 32, 1960, pp. 91/94.
131. SCHMIDT, E. Verdunstung und Wärmeübergang. Z. Gesundh.-Ingr., vol. 63, 1929, p. 525.

132. NUSSELT, W. Wärmeübergang, Diffusion und Verdunstung.
Z. angew. Math. Mech., vol. 10, 1930, pp. 105/121.
133. MOLLIER, R. Ein neues Diagramm für Dampfluftgemische.
Z. Ver. dt. Ing., vol. 73, 1929, pp. 1009/1013.
134. MERKEL, F. Verdunstungskühlung. ForschArb. Geb. IngWes,
No. 275, 1925.
135. ECKERT, E.R.G. and LIEBLEIN, V. Berechnung des Stoffüberganges
an einer ebenen längsangeströmten Ober Fläche bei grossen
Teildruckgefälle. ForschArb. Geb. IngWes, vol. 16, 1949.
136. WHILLIER, A. The calculation of heat exchange between air and wet
surfaces. Jl. S. Afr. Inst. Min. Metall., vol. 67, 1967, pp. 396/402.
137. DEISSLER, R.G. Analysis of turbulent heat transfer, mass
transfer and friction in smooth tubes at high Prandtl and
Schmidt numbers. NACA Rep., 1210, 1955.
138. EVANS, H.L. "Mass transfer through laminar boundary layers - 7.
Further similar solutions to the b-equation for the case $B = 0$ ".
Int. J. Heat Mass Transfer, vol. 5, 1962, pp. 35/37.
139. MURLIN, J.R. Skin temperature, its measurement and significance
for energy metabolism. Ergebn. Physiol., vol. 42, 1939,
pp. 153/227.
140. BREBNER, D.F., KEESLAKE, D. McK. and WADDELL, J.L. The
relationship between the coefficients for heat exchange by
convection and by evaporation in man. J. Physiol., Lond.,
vol. 141, 1958, pp. 164/168.

141. SIBBONS, J.L.H. Assessment of thermal stress from energy balance considerations. J. appl. Physiol., vol. 21, 1966, pp. 1207/1217.
142. NISHI, Y. and GAGGE, A.P. Direct evaluation of convective heat transfer coefficient by naphthalene sublimation. J. appl. Physiol., vol. 29, 1970, pp. 830/838.
143. CARLSON, L.D. and HSIEH, A.C.L. Control of energy exchange. New York, MacMillan, 1970.
144. GOODMAN, W. Air-conditioning analysis. New York, The MacMillan Company, 1944.
145. SIEGEL, R and HOWELL, J.R. Thermal radiation heat transfer. New York, McGraw - Hill book company, 1972.
146. SPENCER-GREGORY, H. and ROURKE, E. Hygrometry, London, Crosby Lockwood and Son, Ltd., 1957.
147. BEHAR, M.F. Industrial humidity instruments. Instruments, vol. 3, 1930, pp. 605/659.
148. GRIFFITHS, E. Some modified forms of hygrometers. Proc. phys. Soc. Lond., Suppl., vol. 35, 1921, pp. 8/49.
149. MOSS, E.B. An apparatus for the determination of dew-point. Proc. phys. Soc. Lond., vol. 46, 1934, pp. 450/458.
150. STEVENSON, R. and BABOR, J.A. Determination of the volatility of gasoline. Ind. Engng Chem., vol. 19, 1927, pp. 1361/1366.
151. WALKER, R.C. Photo-electric dew-point hygrometer. Electronics, vol. 24, 1951, pp. 136/138.

152. REGNAULT, V. Etudes sur l'Hygrométrie. Annls. Chim. Phys., vol. 3, 1845, p. 129
153. ARNOLD, J.H. The theory of the psychrometer. Physics, vol. 4, 1933, pp. 255/261.
154. BARENBRUG, A.W.T. Psychrometry and psychrometric charts. S. Afr. J. Chem. Soc., vol. 47, 1948, pp. 393/417.
155. AUGUST, E.F. Über die Verdunstungskalte under deren Anwendung auf Hygometrie. Annls Chim. Phys., col. 335, 1825, p. 69.
156. CARRIER, W.H. and MACKEY, C.O. A review of existing psychrometric data in relation to practical engineering problems. Trans. Am. Soc. mech. Engrs, vol. 59, 1937, pp. 33/47, 528/529.
157. WYLIE, R.G. Tech. Pap. C.S.I.R.O. Aust., PA-4, 1949.
158. MIDDLETON, W.E.K. and SPILHAUS, A.F. Meteorological instruments. Toronto, Canada University Press, 1953.
159. DOWLING, J.J. A vapour pressure hygrometer. J. scient. Instrum., vol. 13, 1936, p. 214.
160. HARKNESS, H.W. Study of ideal absorption hygrometer. Rev. scient. Instrum., vol. 10, 1939, pp. 237/241.
161. MAYO, H.G. and TYNDALL, A.M. Tilting hygrometer : a new form of absorption hygrometer. Proc. phys. Soc. Lond., vol. 34, 1921, pp. 67/71.
162. OKADO, H.G. and TAMURA, M. Studies with the condensation hygrometer. Proc. imp. Acad. Japan, vol. 16, 1940, pp. 141 and 208.
163. SHAW, A.N. Improved methods of hygrometry. Trans. R. Soc. Can., Series 3, vol. 10, 1916, p. 85.
164. AWBERRY, J.H. Water content of saturated air at temperatures up to 100°C. Proc. phys. Soc. Lond., vol. 44, 1932, pp. 143/150.

165. SHAW, W.N. Report on hygrometric methods. Phil. Trans. R. Soc., vol. 179, 1888, p. 73.
166. SWARTZ, A. Colour changes in hygroscopic salts and their use for humidity measurements. Messtechnik, vol. 9, 1933, p. 87.
167. BIRNBAUM, G. A recording micro-wave refractometer. Rev. scient. Instrum., vol. 21, 1950, pp. 169/176.
168. GREGORY, H.S. and ROURKE, E. A theoretical basis for the diffusion hygrometer. Phil. Mag., vol. 38, 1947, pp. 573/580.
169. WHIPPLE, F.J.W. The theory of the hair hygrometer. Proc. phys. Soc. Lond., vol. 34, 1921, pp. 50/55.
170. APTHORPE, W.H. and MARSH, M.C. A simplified humidity control. J. scient. Instrum., vol. 8, 1931, pp. 152/154.
171. GLUKAUF, E. Calculation of the relative humidity from hair hygrometer readings during balloon ascents. Jl. R. met. Soc., vol. 70, 1944, pp. 293/301.
172. ILES, W.G. and WORSNOP, K. The behaviour of a single hair hygrometer under varying conditions of temperature and humidity. Proc. phys. Soc. Lond., vol. 48, 1936, pp. 358/371.
173. PALMES, E.D. An apparatus and method for the continuous measurement of evaporative heat loss from human subjects. Rev. scient. Instrum., vol. 19, 1948, pp. 711/717.
174. SCHMIDT, E. Messung der Gesamtschrahlung des Wasserdampfes bei Temperaturen bis 1000°C. ForschArb. Geb. IngWes., vol. 3, 1932, p. 57.

175. WEXLER, A. Electric hygrometers. Natn. Bur. Stand. Circular No. 586, 1957.
176. WEAVER, E.R. Electrical measurement of water vapour with a hygroscopic film. Analyt. Chem., vol. 23, 1951, p. 1076.
177. WEAVER, E.R. and RILEY, R. Measurement of water in gases by electrical conduction in a film of hygroscopic material and the use of pressure changes in the calibration. J. Res. natn. Bur. Stand., vol. 40, 1948, pp. 169/213.
178. DUNMORE, F.W. An electrical hygrometer and its application to radio meteorography. J. Res. natn. Bur. Stand., vol. 20, 1938, pp. 723/744.
179. LARACH, S. Humidity-sensing device. U.S. Pat. No. 2 609 688. Sept. 9, 1952.
180. GREGORY H.S. and ROURKE, E. Modern aspects of hygrometry. Trans. Soc. Instrum. Technol., vol. 4, 1952, No. 3, p. 125.
181. FIRESAH, A.M. An electrolytic hygrometer. Proc. math. phys. Soc. Egypt, vol. 2, 1942, p. 3.
182. WHITE, W.C. A new electrolytic hygrometer. Electl. Engng, vol. 73, 1954, pp. 1084/1087.
183. EDLEFSEN, N.E. A glass wool cell for measuring aqueous vapour pressure. Rev. scient. Instrum., vol. 4, 1933, p. 345.
184. SMAIL, BROOKSBANK and THORNTON. The electrical resistance of moisture films on glazed surfaces. J. Instn elect. Engrs, vol. 69, 1931, pp. 427/438.

185. WEXLER, A. et al. A fast responding electric hygrometer.
J. Res. natn Bur. Stand., vol. 55, 1955 p. 71.
186. JASON, A.C. and WOOD, J.L. Some electrical effects of the
adsorption of water vapour by anodized aluminium. Proc. phys.
Soc. Lond., Series B, vol. 68, 1955, pp. 1105-1116.
187. UNDERWOOD, C.R. and HOUSLIP, R.C. The behaviour of humidity
sensitive capacitors at room temperatures. J. scient. Instrum.,
vol. 32, 1955, pp. 432/436.
188. KUNIN, R. and MYERS R.J. Ion exchange resins. New York,
John Wiley and Sons, Inc., 1950.
189. POPE, M. Electric hygrometer. U.S. Pat. No. 2 728 831, Dec. 27.
1955.
190. LICHTGARN, F. New method of measuring relative humidity.
Instruments, vol. 20, 1947, p. 336.
191. MARSH, M.C. and KARP, K. The electrical resistance of wood
fibres. Trans. Faraday Soc., vol. 29, 1933, p. 173.
192. SLATER, F.P. A sensitive method for observing changes of
electrical conductivity in single hygroscopic fibres. Proc. R.
Soc., Series B, vol. 96, 1924, p. 181.
193. SMITH, W.K. and HOEFLICH, N.J. The carbon film electric hygrometer
element. Bull. Am. met. Soc., vol. 35, 1954, p. 60.
194. WELCO, L.A. Humidity resistance relations in carbon coated
hygroscopic materials. Nature, Lond., vol. 134, 1934, p. 936.
195. HICKS, W.F. Humidity measurement by a new system. Refriger.
Engng, vol. 54, 1947, p. 351.

196. HAWKINS, J.C. Dewcell. Refrig. Engng., vol. 62, No. 3, March, 1954, pp. 68/71 and 100/102.
197. SCHLICHTING, H. Boundary layer theory. 6th Ed., New York, McGraw-Hill, 1968.
198. JAKOB, M. Heat Transfer, vol. 1, New York, John Wiley & Sons, 1949, p. 544.
199. HOLMAN, J.P. Heat Transfer, 2nd Ed., New York, McGraw-Hill, 1968, p. 177.
200. KAYS, W.M. and LONDON, A.L. Compact Heat Exchangers, New York, McGraw-Hill, 1964, pp. 14/19.
201. de HEER, T. and ERKENLENS, H.J. Heat transmission by radiation : a new method of calculating the local and total effects. Heat. Vent. Engr., vol. 30, Jan. 1963, pp. 357/372.
202. KNOWLTON, A.E. Standard handbook for electrical engineers. New York, McGraw-Hill book company, 1957, pp. 35, 135.
203. HODGSON, T. and VERMEULEN, A.J. Boundary layer control in the climatic chamber. C.S.I.R. Rep. Meg. 304, 1964.
204. BOLTZMANN, L. Ableitung des Stefan'schen Gesetzes, betreffend die Abhängigkeit der Wärmestrahlung von der Temperatur aus der electromagnetischen Licht-theorie. Annln Phys., ser. 2, vol. 22, 1884, pp. 291/294.
205. WIEN, W. Temperatur and Entropie der Strahlung. Annln Phys., ser. 2, vol. 52, 1894, pp. 132/165.

206. WIEN, W. Über die Energievertheilung im Emissions-spectrum eines schwarzen Körpers. Annln Phys., ser. 3, vol. 58, 1896, pp. 662/669.
207. LORD RAYLEIGH. The law of complete radiation. Phil. Mag., vol. 49, 1900, pp. 539/540.
208. JEANS, J. On the partition of energy between matter and ether. Phil. Mag., vol. 10, 1905, pp. 91/97.
209. SUMPNER, W.E. The diffusion of light. Proc. phys. Soc., vol. 94, 1894, pp. 10/29.
210. BUCKLEY, H. Radiation from the interior of a reflecting cylinder. Phil. Mag., vol. 4, 1927, pp. 753/762.
211. FANGER, P.O. Thermal comfort, Copenhagen, Danish Technical Press, 1970.
212. IMBATHO, K. and NISHI, Y. Thermal sensation analysis and its application to air conditioning. Bull. Fac. Engng, Hokkaido Univ., vol. 46, 1968, pp. 73/121.

APPENDIX A

METHOD OF CALCULATING THE MOISTURE EVAPORATION RATE FROM
A HEATED SURFACE SUCH AS THE HUMAN BODY1. HISTORICAL DEVELOPMENT OF THE MASS TRANSFER THEORY

Dalton's¹²⁰⁾ discovery in 1801 that the rate of vaporation of a liquid into gas depends on the difference which exists between the equilibrium partial pressure of the saturated vapour and its partial pressure in the bulk of the gas, may be regarded as the dawn of the science of mass transfer.

Subsequent investigations by Maxwell¹²¹⁾ in 1867 and Chapman¹²²⁾, Chapman and Cowling¹²³⁾ and Hirschfelder et al¹²⁴⁾ during the early part of the twentieth century led to a fairly complete theory of diffusion in gases.

The work, however, was mainly related to stagnant gases and did not apply to the experimental results obtained from heat and mass studies in more complex situations such as, for example, the turbulent flow of fluids in pipes. Such problems were investigated by Reynolds³²⁾ who conceived the model transport process and Nernst¹²⁵⁾, who possibly originated the idea of a "stagnant film".

The latter idea was taken up by chemical engineers such as Lewis¹²⁶⁾

and Whitman¹²⁷⁾ and is the origin of the mass-transfer formulae to be found in most current chemical engineering text books such as Sherwood and Agford³⁴⁾. Carrier¹²⁸⁾ made use of a similar model proposed by Reynolds which he called the "contact-mixture analogy" in developing the theory of vapourisation or condensation of water. Spalding^{129,130)} extended the model to cover homogeneous chemical reactions.

German engineers followed a different course. On the one hand Schmidt¹³¹⁾ and Nusselt¹³²⁾ used partial differential equations for determining diffusion rates in a moving medium. Mollier¹³³⁾ and Merkel¹³⁴⁾ who dealt with the processes of simultaneous heat and mass transfer, drew attention to the importance of the enthalpy of the gas stream rather than its temperature. The equations developed, were mainly for problems where the mass transfer rate was relatively low. In this case the equations for heat transfer could be assumed to be equally valid for mass transfer. The problem of high mass transfer rates, where this assumption may not be valid, was subsequently investigated by Eckert and Lieblein¹³⁵⁾.

2. DETERMINATION OF THE MOISTURE EVAPORATION RATE FROM A HUMAN BODY : THEORETICAL CONSIDERATIONS

Use is made of the hypothetical model originally proposed by Reynolds³²⁾ for determining the mass transfer flux or moisture

evaporation rate from a human body.

2.1 Mass driving force

In the Reynolds model, the so-called Reynolds flux, represents the amount of stream material, in this case air and water vapour, that is brought to the condition of the film of sweat on the body by contact with its surface*.

The general relationship between the Reynolds flux and the mass transfer rate is given by the equation:

$$\dot{m}'' = gB \quad \text{..... (1)}$$

where \dot{m}'' = mass transfer rate across unit area of the interface into the air stream, $\text{kg/m}^2 \text{ s}$

g = Reynolds flux per unit area, $\text{kg/m}^2 \text{ s}$

B = mass driving force, dimensionless.

The mass driving force is deduced from a consideration of the Reynolds flow model illustrated in Figure A1.

Since no chemical reaction occurs, the amount of water and vapour

* The older literature on engineering heat transfer contains many references to the so-called "scrubbing action" of the fluid stream on the interface. The Reynolds flux, g , can be regarded as a quantitative measure of the rate of scrubbing.

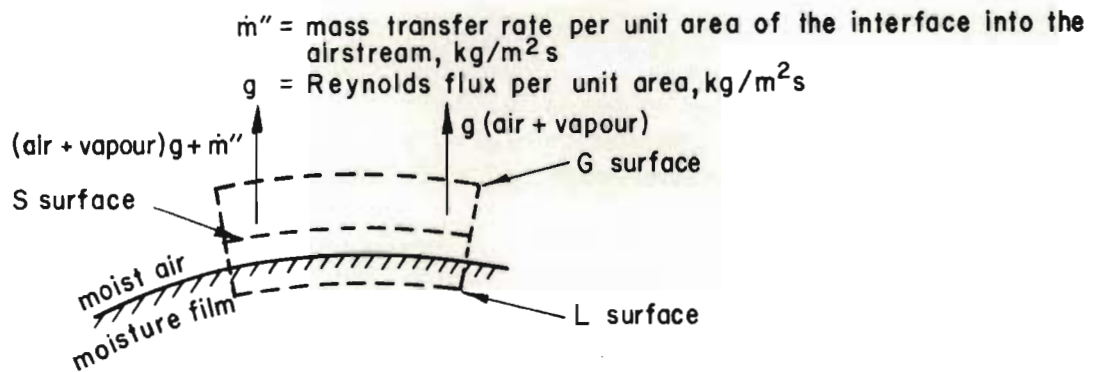


FIGURE A1

Reynolds flow in the air and water vapour mixture adjacent to an interface.

\dot{q}_L'' , \dot{q}_S'' = heat transfer rates per unit area through the L and S-surfaces, respectively, kW/m^2

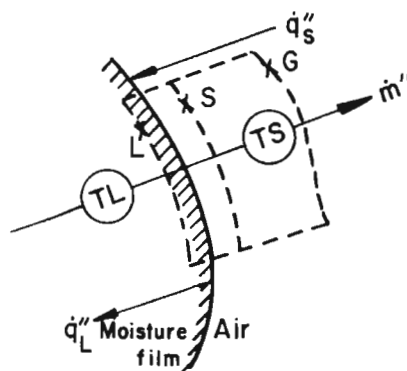


FIGURE A2

Mass transfer and heat fluxes across an interface.

which enters the control volume bounded by the G- and S-surfaces, adjacent to the skin must, in the steady state, be equal to the amount which leaves that control volume in unit time.

$$\text{Thus } \frac{\text{entry rate}}{f_G g + \dot{m}''} = \frac{\text{leaving rate}}{f_S (g + \dot{m}'')} \quad \dots\dots\dots (2)$$

where f_G, f_S = respective mass concentrations of moisture in the air stream and adjacent to the interface on the air side, respectively

Rearrangement of equation (2) gives:

$$\dot{m}''/g = (f_G - f_S)/(f_S - 1) \quad \dots\dots\dots (3)$$

In this case, where the Reynolds flux is based on the mass concentration values in a mixture, the Reynolds flux will be referred to as g_f . Thus, equation (3) becomes:

$$\dot{m}''/g_f = (f_G - f_S)/(f_S - 1) \quad \dots\dots\dots (4)$$

Since $\dot{m}''/g = B$ from equation (1), equation (3) may be rewritten as:

$$B = (f_G - f_S)/(f_S - 1) \quad \dots\dots\dots (5)$$

A similar expression for the driving force, B, can be deduced on the basis of enthalpy. According to the first law of

thermo-dynamics the inflow of enthalpy into the control volume bounded by the G and S surfaces shown in Figure A2 minus the outflow of enthalpy is equal to the negative of the net heat flow into the control volume.

$$\text{Thus } \frac{\text{inflow}}{gH_G + \dot{m}''H_{TS}} - \frac{\text{outflow}}{(g + \dot{m}'')H_S} = \frac{\text{heat flux}}{\dot{q}''_s} \quad \dots\dots\dots (6)$$

where H_G, H_S = respective specific enthalpies of the air in the main air stream and the air adjacent to the interface, respectively, kJ/kg

h_{TS} = enthalpy of the water as it crosses into the air stream, kJ/kg

and \dot{q}''_s = heat transfer rate through the S surface per unit area, kW/m²

Rearrangement of equation (6) leads to:

$$\dot{m}''/g = \frac{h_G - h_S}{h_S - h_{TS} + \dot{q}''_s/\dot{m}''} \quad \dots\dots\dots (7)$$

Since the Reynolds flux in this case is based on enthalpies, it will be referred to as g_h . Equation (7) becomes:

$$\dot{m}''/g_h = \frac{h_G - h_S}{h_S - h_{TS} + \dot{q}''_s/\dot{m}''} \quad \dots\dots\dots (8)$$

or

$$B = \frac{h_G - h_S}{h_S - h_{TS} + \dot{q}''_s/\dot{m}''} \quad \dots\dots\dots (9)$$

Since the transferred material, namely the water, undergoes no chemical change and since it has a temperature, t_s , prevailing at the S surface, $h_{TS} = h_s$.

Thus, equation (9) reduces to:

$$B = \dot{m}''/g_h = \frac{h_G - h_s}{\dot{q}''_S/\dot{m}''} \quad \text{..... (10)}$$

$$h_G - h_s = c_G(t_G - t_s) \quad \text{..... (11)}$$

where h_G, h_s = respective enthalpies of the air in the main air stream and the air adjacent to the interface, respectively, kJ/kg

and c_G = specific heat at constant pressure of the air in the main air stream, kJ/kg °C

t_G, t_s = the temperatures of the air stream and the air adjacent to the interface, respectively, °C.

Substitution of $h_G - h_s$ according to equation (11) in equation (10) leads to:

$$B = \dot{m}''/g_h = \frac{c_G(t_G - t_s)}{\dot{q}''_S/\dot{m}''} \quad \text{..... (12)}$$

The driving force, B, may also be obtained by applying the first law of thermo-dynamics to the control volume bounded by the LS surfaces. (See Figure A2).

$$\text{In this case } \frac{\text{inflow}}{\dot{m}''h_{TL}} - \frac{\text{outflow}}{\dot{m}''h_{TS}} = \frac{\text{heat flux}}{\dot{q}''_L - \dot{q}''_S} \quad \text{..... (13)}$$

where \dot{m}'' = mass transfer rate across unit area of the interface into the air stream, $\text{kg/m}^2 \text{ s}$

h_{TL}, h_{TS} = respective specific enthalpies of the water crossing the L and S surfaces, respectively, kJ/kg

\dot{q}''_L, \dot{q}''_S = heat transfer rate per unit area through the L and S surfaces, respectively, kW/m^2 .

Rearranging equation (13) yields:

$$\dot{q}''_S = \dot{q}''_L - \dot{m}''(h_{TL} - h_{TS}) \quad \text{..... (14)}$$

Substitution of \dot{q}''_S in equation (12) leads to:

$$B = \frac{c_G(t_G - t_S)}{h_{TS} - h_{TL} + \dot{q}''_L/\dot{m}''} \quad \text{..... (15)}$$

Since the specific enthalpy difference, $h_{TS} - h_{TL}$, is equal to the latent heat of phase change of the water, ℓ , as it evaporates into the air stream, equation (15) may be rewritten as:

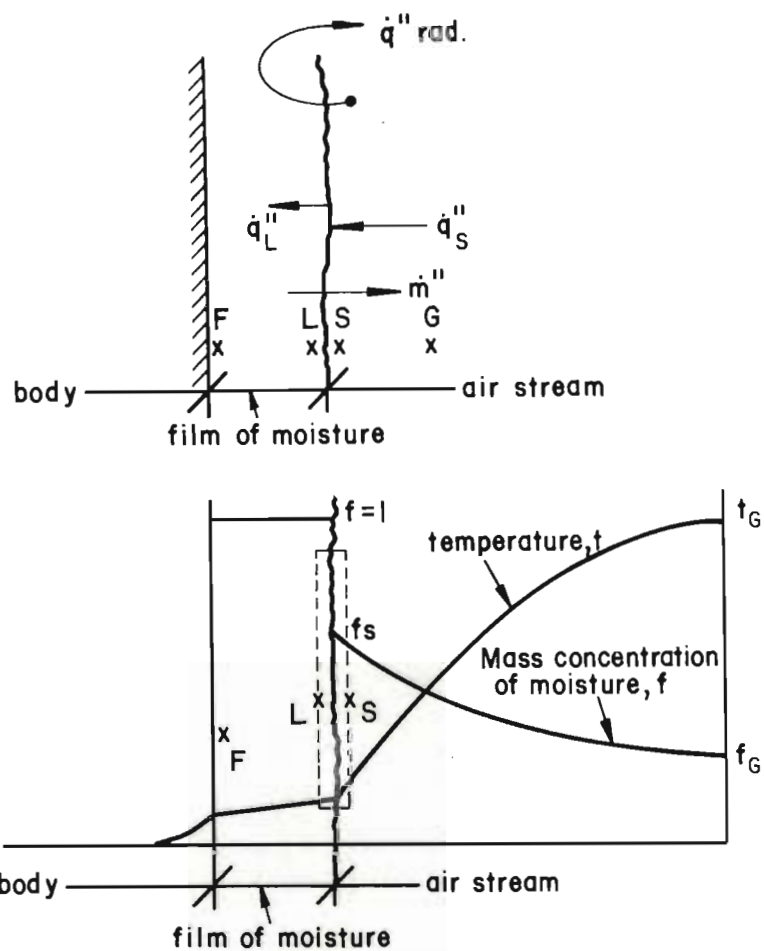
$$B = \frac{c_G(t_G - t_S)}{\ell + \dot{q}''_L/\dot{m}''} \quad \text{..... (16)}$$

2.2 Influence of the conductance, radiative flux and the film coefficient of heat transfer on the mass transfer rate

Figure A3 illustrates an interface element lying between an air-water vapour mixture and a film of water covering a body.

\dot{q}_L'' , \dot{q}_S'' = heat transfer rates per unit area through the L- and S-surfaces, respectively, kW/m²

\dot{q}_{rad}'' = radiative flux which is the algebraic sum of the emitted radiation, and of the absorbed radiation per unit area of body surface, kW/m²



TEMPERATURE AND MASS CONCENTRATION GRADIENTS

FIGURE A3

An illustration of the processes which occur adjacent to the interface of a "sweating" body exposed to relatively dry air

The heat transfer between the liquid-gas interface and the core of the body can be characterised by the conductance, K'' , such that:

$$\dot{q}''_L - \dot{q}''_{\text{rad}} - \dot{m}'' c_f (t_s - t_f) = K'' (t_s - t_r) \quad \dots\dots\dots (17)$$

where \dot{q}''_L = heat transfer rate, per unit area, kW/m^2

\dot{q}''_{rad} = radiative heat flux which is the algebraic sum of emitted radiation and of the absorbed radiation per unit area of body surface, kW/m^2

\dot{m}'' = mass transfer rate across unit area of the interface into the air stream, per unit area of body surface, $\text{kg/m}^2 \text{ s}$

c_f = specific heat at constant pressure of water on the surface, $\text{kJ/kg } ^\circ\text{C}$

t_s, t_f = respective temperatures of the human skin and water film surface, $^\circ\text{C}$

t_r = core temperature of the body, $^\circ\text{C}$

K'' = conductance between the core of the body and the water-air interface, per unit area of body surface, $\text{kW/m}^2 \text{ } ^\circ\text{C}$.

In the case of the human body, K'' can be assumed to be equal to the physiological conductance.

The left hand side of equation (17) indicates what is left from \dot{q}''_L when the radiative heat flux and the enthalpy increment

of the vapourising water are deducted. (The heat flow rate is considered to be positive when the heat flows towards the core of the body).

Substitution of \dot{m}''/g_h for B (see equation (1) on page 387), in equation (16) and rearranging leads to:

$$\dot{m}''\ell = g_h c_G(t_G - t_s) - \dot{q}''_L \quad \text{..... (18)}$$

Substitution of \dot{q}''_L obtained from equation (17) in equation (18) gives:

$$\dot{m}''\ell = g_h c_G(t_G - t_s) - \{\dot{q}''_{\text{rad}} + \dot{m}''c_f(t_s - t_f) + K''(t_s - t_r)\}$$

rearranging leads to:

$$\dot{m}''\ell + \dot{m}''c_f(t_s - t_f) = g_h c_G(t_G - t_s) - \{K''(t_s - t_r) + \dot{q}''_{\text{rad}}\}$$

$$\text{or } \dot{m}'' = g_h \left[\frac{c_G(t_G - t_s) - \{K''(t_s - t_r) + \dot{q}''_{\text{rad}}\}/g_h}{\ell + c_f(t_s - t_f)} \right] \quad \text{..... (19)}$$

dividing both sides of the equation (19) by g_f yields:

$$\begin{aligned} \dot{m}''/g_f &= g_h/g_f \left[\frac{c_G(t_G - t_s) - \{K''(t_s - t_r) + \dot{q}''_{\text{rad}}\}/g_h}{\ell + c_f(t_s - t_f)} \right] \\ &= (f_G - f_s)/(f_s - 1) \quad (\text{See equation (4) on page 389}) \quad (20) \end{aligned}$$

Equation (20) may also be rewritten in the form:

$$\begin{aligned} \dot{m}''/g_f &= g_h/g_f \left\{ \frac{c_G \left[\{t_G - (K''/g_h c_G) t_r\} - t_s \{1 + (K''/g_h c_G)\} - \dot{q}''_{\text{rad}}/g_h c_G \right]}{\ell + c_f(t_s - t_f)} \right\} \\ &= (f_G - f_s)/(f_s - 1) \quad \text{..... (21)} \end{aligned}$$

where \dot{m}'' = mass transfer rate across unit area of the interface into the air stream, $\text{kg/m}^2 \text{ s}$

$g_f = \dot{m}''(f_s - 1)/(f_G - f_s)$ = Reynolds flux based on mass concentration values of a mixture per unit area of body surface, $\text{kg/m}^2 \text{ s}$

c_G, c_f = specific heats at constant pressure of the air and the water film on the surface of the body, respectively, $\text{kJ/kg } ^\circ\text{C}$

t_r, t_G, t_s, t_f = temperature of the core of the body, air temperature, body surface temperature, and water film surface temperature, respectively, $^\circ\text{C}$

K'' = conductance per unit area of body surface, $\text{kW/m}^2 \text{ } ^\circ\text{C}$

\dot{q}''_{rad} = net radiant heat flux per unit area of body surface, kW/m^2

ℓ = latent heat of change of phase of water, kJ/kg .
(In the case of the human body ℓ can be assumed to be equal to the latent heat of change of phase of sweat)

g_h = Reynolds flux, based on enthalpy values per unit area of body surface, $\text{kg/m}^2 \text{ s}$. The value for g_h is deduced from the convective film coefficient of heat transfer, h_c , by means of the following relation:

$$g_h = h_c / c_G \quad \dots\dots\dots (22)$$

Determination of the ratio g_h/g_f in equation (21)

The ratio g_h/g_f is determined as follows:

Use is made of the analogy between heat and mass transfer¹³⁶⁾ to determine the ratio g_h/g_f .

The existence of the analogy between heat and mass transfer was first made explicit by Nusselt⁴⁹⁾ (who postulated the existence of a Reynolds flow in a theoretical study of carbon combustion), and later by Lewis¹²⁶⁾. Deissler¹³⁷⁾ confirmed the analogy between heat and mass transfer during his survey of most of the data on the mass-transfer conductance in turbulent pipe flow which could be found in the English literature at that date. He presented the mass transfer data in the form of logarithmic plots of Stanton number versus Schmidt number for a fixed Reynolds number and the heat transfer data as Stanton number versus Prandtl number and found that the heat transfer and mass transfer data fell on identical curves.

$$N_{St,h} = g_h/\dot{G}'' = A(N_{Re})^a (N_{Pr})^{-b} \quad \dots\dots (23)$$

$$\text{and } N_{St,f} = g_f/\dot{G}'' = (A(N_{Re})^a (N_{Sc})^{-b}) \quad \dots\dots (24)$$

where $N_{St,h}, N_{St,f}$ = Stanton number for heat and mass transfer, respectively

$$\text{and } N_{Re} = \dot{G}''D/\mu = \text{Reynolds number}$$

$$N_{Pr} = c_G \mu / k = \text{Prandtl number}$$

$$N_{Sc} = \mu / \rho D_i = \text{Schmidt number}$$

$$A, a, b = \text{constants}$$

$$\dot{G} = \text{mass velocity of bulk of stream of fluid, kg/m}^2 \text{ s}$$

$$D = \text{diameter or other dimension of body, m}$$

$$\mu = \text{dynamic viscosity of fluid, kg/m s}$$

$$k = \text{thermal conductivity of fluid, kW/m } ^\circ\text{C}$$

$$c_G = \text{specific heat at constant pressure of fluid,} \\ \text{kJ/}^\circ\text{C kg}$$

$$\rho = \text{fluid density, kg/m}^3$$

$$D_i = \text{diffusion coefficient of mixture component, i.}$$

Division of equation (23) by (24) leads to:

$$g_h/g_f = (N_{Sc}/N_{Pr})^b \quad \dots\dots\dots (25)$$

The ratio N_{Pr}/N_{Sc} is known as the Lewis number, N_{Le} .

For air with moderate concentrations of water vapour, the Schmidt number, $N_{Sc} = 0,60$ and the Prandtl number, $N_{Pr} = 0,70$.

$$\text{Thus, } N_{Le} = 0,70/0,60 \\ = 1,167$$

Evans^{13e)} found b in equation (25) equal to 0,67 for values of

$$N_{Pr}/N_{Sc} \text{ greater than } 0,5.$$

Since N_{Pr}/N_{Sc} in this case is greater than 0,5, b is assumed to be equal to 0,67.

Thus, equation (25) can be rewritten as:

$$\begin{aligned} g_h/g_f &= (1/1,167)^{0,67} \\ &= 1/1,11 \\ &= 0,901. \end{aligned}$$

The value for g_h/g_f was based on the assumption that a fixed relationship exists between the convective and evaporative heat loss rates.

There are conflicting opinions, however, with regard to the validity of this assumption for the human body. Whereas Murlin¹³⁹⁾, Brebner et al¹⁴⁰⁾, Woodcock and Breckenridge³¹⁾, Rapp⁵⁰⁾, Sibbons¹⁴¹⁾ and Nishi and Gagge¹⁴²⁾ accept that an analogy between heat and mass transfer from a human body exists, other physiologists such as Carlson and Hsieh¹⁴³⁾ don't. For this reason further experimental studies to establish the exact relationship between heat and mass transfer may be necessary.

The ratio $K''/g_h c_G$ in equation (21) on page 395

The dimensionless expression, $K''/g_h c_G$ which appears in equation (21) measures the ratio of the conductance of the body per unit area of body surface to the conductance on the air side of the body interface. If $K''/g_h c_G$ is to be very much larger

than unity, the air velocity must be small or the physiological conductance must be high. When the air velocity and hence $g_h c_G$ becomes very large, $K''/g_h c_G$ tends to zero.

Solution of equation (21) on page 395

The second and third terms in equation (21) are plotted against the body surface temperature, t_s . Their intersection has the required t_s as abscissa and the required mass transfer driving force, $(f_G - f_s)/(f_s - 1)$, as ordinate.

Since the temperature difference, $t_s - t_f$, appearing in the denominator of the middle term in equation (21) is very small and the latent heat, ℓ , can be assumed to be constant; the denominator of the middle term can be taken as constant without introducing an appreciable error. With this approximation the family of curves with the middle term of equation (21) as parameter reduces to a family of straight lines; all of which pass through the point with abscissa t_r and ordinate $(g_h/g_f)(c_G/\ell)(t_G - t_r - \dot{q}''_{\text{rad}}/g_h c_G)$. (See figure 4 on page 83).

Neglecting radiation the ordinate is $(g_h/g_f)(c_G/\ell)(t_G - t_r)$.

As a first step in the calculations to determine the mass transfer rate, the mass transfer driving force, $B = \dot{m}''/g_f$ (see equation (1) on page 387), was calculated from equation (21)

The following procedure was adopted for determining the mass transfer driving force:

The term $(f_G - f_s)/(f_s - 1)$ in equation (21) was calculated for various body surface temperature conditions (f_G and f_s are the respective mass concentrations of moisture in the air stream and adjacent to the body, respectively*).

Graphs of $(f_G - f_s)/(f_s - 1)$ versus the body surface temperature, t_s , were then plotted for the various assumed environmental conditions with regard to air temperature and humidity.

The family of straight lines representing the middle term of equation (21) were plotted on the same graphs for various assumed values for the ratio $K''/g_h c_G$ where

K'' = physiological conductance per unit area of body surface, kW/m^2 , and

$g_h c_G$ = h_c , the film coefficient of heat transfer, $\text{kW/m}^2 \text{ } ^\circ\text{C}$.

(See equation (22) on page 396).

* Values for f_G and f_s were obtained from Table 6 in reference (144) for an atmospheric pressure of 837 kPa

The intersections of the $(f_G - f_s)/(f_s - 1)$ curve with the various straight lines give the values of the driving force, \dot{m}''/g_f and skin temperature, t_s , for the various assumed values of $K''/c_G g_h$. (See figure 4 on page 83).

The moisture evaporation rate or mass transfer rate from the wetted surface was determined as follows:

The value of $\dot{m}'' c_G / K''$ was calculated from

$$\dot{m}'' c_G / K'' = (\dot{m}'' / g_f) (g_f / g_h) (g_h c_G / K'') \quad \text{..... (26)}$$

where \dot{m}'' = mass transfer rate across unit area of the interface into the air stream, $\text{kg/m}^2 \text{ s}$

c_G = specific heat at constant pressure of air,
1,01 kJ/kg °C

K'' = conductance per unit area of body surface,
 $\text{kW/m}^2 \text{ °C}$

g_f / g_h = 1/0,901 (See page 399)

$g_h c_G / K''$ = ratio of the film coefficient of heat transfer to the physiological conductance, dimensionless.

The values of \dot{m}''/g_f and $g_h c_G / K''$ in equation (26) are obtained from the intersection points of the $(f_G - f_s)/(f_s - 1)$ curve with the family of straight lines representing the middle term in equation (21).

Graphs of the surface temperature, t_s , and the ratio $\dot{m}'' c_G / K''$ versus the ratio $g_h c_G / K''$ permit the mass transfer rate to be obtained for various values of the conductance, K'' , and the film coefficient of heat transfer, $h_c = g_h c_G$. (See figure 6 on page 85).

APPENDIX B

NET THERMAL RADIATIVE FLUX BETWEEN A HUMAN SUBJECT IN THE
HORIZONTAL TEST CHAMBER OF THE CLIMATIC CHAMBER AND THE
SURROUNDING TEST CHAMBER WALLS

All substances continuously emit electromagnetic radiation by virtue of the molecular and atomic agitation associated with the internal energy of the material; the type of radiation being classified according to its wave-length. In the case of the thermal radiation energy exchange between the human body and its surroundings, the region of interest lies in the infra-red region which extends from $0,7 \mu\text{m}$ to $1\ 000 \mu\text{m}$.

1. THERMAL RADIATION EXCHANGE RATE BETWEEN A BODY AND ENCLOSURE

Generally the system of body and enclosure may be represented as in Figure B1.

For the purpose of calculating the net radiation energy exchange between the body and the enclosure, it is assumed that the space between the surfaces is perfectly transparent and thus does not participate in the radiative interchange. It is known, of course, that the horizontal test chamber will, in fact, contain limited amounts of radiation gases such as water vapour and carbon dioxide. However, since the respective concentrations of these gases in the air stream and the radiant path lengths involved will be small, the resultant influence on the radiation interchange between the body and the enclosure will

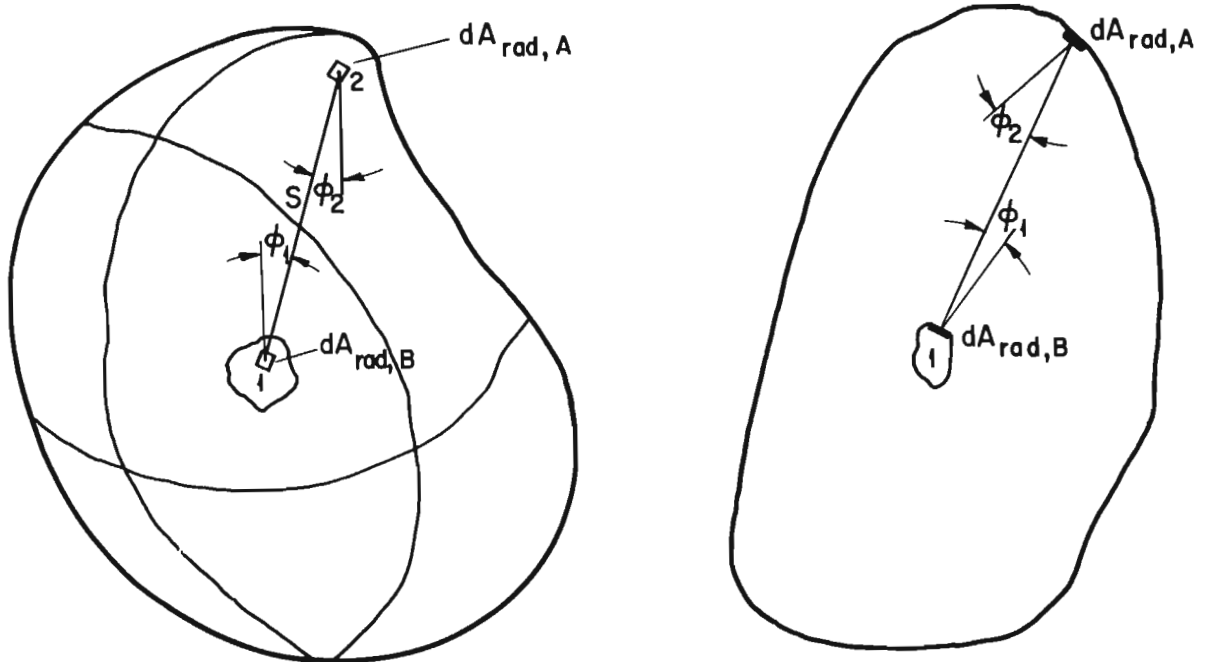


FIGURE B1

*Geometrical data referring to thermal radiation from
a body in an enclosure.*

also be small.

For the initial analysis the further assumption is made that the enclosed and enclosing bodies behave as black bodies.

Consider two points 1 and 2 on the enclosed and enclosing bodies with respective areas $dA_{\text{rad},B}$ and $dA_{\text{rad},A}$ as shown in Figure B1. The elements $dA_{\text{rad},B}$ and $dA_{\text{rad},A}$ which are isothermal at temperatures T_B and T_A , respectively, have their normal at angles of ϕ_1 and ϕ_2 to the line of length S joining them.

The total energy per unit time leaving $dA_{\text{rad},B}$ and incident on $dA_{\text{rad},A}$ is

$$d^2\dot{q}_{\text{rad},B-A} = E_{b,B} dA_{\text{rad},B} \cos\phi_1 d\omega_1 \quad \text{..... (1)}$$

where $d^2\dot{q}_{\text{rad},B-A}$ = total radiant energy per unit time leaving $dA_{\text{rad},B}$ and incident upon $dA_{\text{rad},A}$

$E_{b,B}$ = total radiation intensity of black surface, $dA_{\text{rad},B}$

and $d\omega_1$ = solid angle subtended by $dA_{\text{rad},A}$ when viewed from $dA_{\text{rad},B}$.

The solid angle $d\omega_1$ is related to the projected area of $dA_{\text{rad},A}$ and the distance between the differential elements by the relation

$$d\omega_1 = dA_{\text{rad},A} \cos\phi_2 / S^2 \quad \text{..... (2)}$$

Substituting this relation into equation (1) gives the following equation for the total energy per unit time leaving $dA_{\text{rad},B}$ that is incident upon $dA_{\text{rad},A}$:

$$d^2\dot{q}_{\text{rad},B-A} = E_{b,B} dA_{\text{rad},B} \cos\phi_1 dA_{\text{rad},A} \cos\phi_2 / S^2 \dots\dots (3)$$

An analogous derivation for the radiation leaving $dA_{\text{rad},A}$ that arrives at $dA_{\text{rad},B}$ results in

$$d^2\dot{q}_{\text{rad},A-B} = E_{b,A} dA_{\text{rad},A} \cos\phi_2 dA_{\text{rad},B} \cos\phi_1 / S^2 \dots\dots (4)$$

where $E_{b,A}$ = total radiation intensity of black surface,
 $dA_{\text{rad},A}$.

The net energy per unit time, $d^2\dot{q}_{\text{rad}}$ exchanged between the black elements $dA_{\text{rad},B}$ and $dA_{\text{rad},A}$ along path S is then the difference of $d^2\dot{q}_{\text{rad},A-B}$ and $d^2\dot{q}_{\text{rad},B-A}$ given by equations (3) and (4), respectively.

$$\text{Thus, } d^2\dot{q}_{\text{rad}} = (E_{b,A} - E_{b,B}) \frac{\cos\phi_1 \cos\phi_2}{S^2} dA_{\text{rad},B} dA_{\text{rad},A} \dots (5)$$

The black body total intensity is related to the black body total hemispherical emissive power by

$$E_b = e_b / \pi = \sigma T_b^4 / \pi \dots\dots\dots (6)$$

where E_b = black body total radiation intensity

e_b = emissive power of black body

T_b = absolute temperature of black body

σ = Stefan-Boltzman constant

Equation (5) can thus be rewritten as

$$d^2 \dot{q}_{\text{rad}} = \sigma (T_A^4 - T_B^4) \frac{\cos \phi_1 \cos \phi_2}{\pi S^2} dA_{\text{rad},B} dA_{\text{rad},A} \dots (7)$$

where $d^2 \dot{q}_{\text{rad}}$ = net energy exchange rate between the elements with areas $dA_{\text{rad},B}$ and $dA_{\text{rad},A}$

and T_B, T_A = respective absolute temperatures of the elements $dA_{\text{rad},B}$ and $dA_{\text{rad},A}$

ϕ_1, ϕ_2 = respective angles of the normals of the elements $dA_{\text{rad},B}$ and $dA_{\text{rad},A}$ to the line joining them

S = distance between the elements $dA_{\text{rad},B}$ and $dA_{\text{rad},A}$

σ = Stefan-Boltzman constant

The total net radiation \dot{q}_{rad} is obtained by integrating equation (7)

over the respective areas of the enclosed and enclosing bodies.

This presents considerable difficulties, particularly in the case of the human body.

For the case of a convex body in a concave enclosure, the following assumptions may be made:

- (a) the temperature across each surface is uniform,
- (b) the surfaces are grey, that is, the spectral emissivity and absorptivity are independent of the wave-length and direction, and
- (c) all energy is emitted and reflected diffusely, that is, Lambert's cosine law applies and the emitted radiation intensity

is uniform over all directions as in the case of a black body.

For concentric spheres where the differential configuration factors are invariable equation (7) reduces to¹⁴⁵⁾:

$$\dot{q}_{\text{rad}} = \frac{A_{\text{rad},B}(T_A^4 - T_B^4)}{1/\epsilon_B + (A_{\text{rad},B}/A_{\text{rad},A})(1/\epsilon_A - 1)} \dots\dots (8)$$

$$\text{or } \dot{q}_{\text{rad}} = \frac{A_{\text{rad},B}/A_{T,B}(T_A^4 - T_B^4)}{1/\epsilon_B + (A_{\text{rad},B}/A_{\text{rad},A})(1/\epsilon_A - 1)} \dots\dots (9)$$

where \dot{q}_{rad} = radiative energy exchange rate per unit time,
kW

\dot{q}_{rad} = radiative heat flux per unit area of body
surface, kW/m²

σ = Stefan-Boltzman constant, $56,69 \times 10^{-12}$ kW/m² °K⁴*

T_B, T_A = absolute temperature of the enclosed and
enclosing bodies, respectively, °K = °C + 273,2

$A_{\text{rad},B}, A_{\text{rad},A}, A_{T,B}$ = respective radiant surface areas of the
enclosed and enclosing bodies and the total
surface area of the enclosed body, respectively

ϵ_B, ϵ_A = respective emissivities of the enclosed and
enclosing bodies.

Equation (9) can be simplified when applied to a human subject in the
horizontal test chamber of the climatic chamber. Since the surface

* Calculated value from reference (145), p.738.

area of the test chamber is much larger than the radiant area of the subject, $A_{\text{rad},B}/A_{\text{rad},A} \ll 1$. Furthermore, the emissivity of the test chamber walls is close to unity. Thus $1/\epsilon_{\text{rad},A} - 1 \ll 1$.

Neglecting second order small quantities equation (9) thus becomes:

$$\dot{q}''_{\text{rad}} = \sigma A_{\text{rad},B}/A_{T,B} \epsilon_B (T_A^4 - T_B^4) \quad \dots\dots\dots (10)$$

1.1 Radiation heat transfer coefficient

It may be more convenient to represent the net effect of the radiation in the same form employed in convection, namely,

$$\dot{q}''_{\text{rad}} = h_{\text{rad}} A_{\text{rad},B}/A_{T,B} (t_A - t_B) \quad \dots\dots\dots (11)$$

where t_B, t_A = the respective surface temperatures of the body and enclosure or test chamber walls, °C

and h_{rad} = fictitious film coefficient representing the rate at which radiant energy is exchanged between the body and the test chamber walls, kW/m² °C

An approximate value for h_r can be derived from equation (11) based on the assumption that $T_A - T_B \ll T_A + T_B$.

In this case the equation

$$T_A^4 - T_B^4 = \frac{1}{2}(T_A - T_B)(T_B + T_A) \{(T_B + T_A)^2 + (T_A - T_B)^2\}$$

can be written as

$$T_A^4 - T_B^4 \approx \frac{1}{2}(T_B + T_A)^3 (T_B - T_A) \quad \dots\dots\dots (12)$$

since $(T_A - T_B)^2$ is negligible compared with $(T_B + T_A)^2$.

Substituting the value for $T_A^4 - T_B^4$ according to equation (12), in equation (10) leads to

$$\dot{q}''_{\text{rad}} \approx \frac{1}{2} \sigma A_{\text{rad},B} / A_{T,B} \epsilon_B (T_B + T_A)^3 (T_A - T_B) \quad \dots\dots\dots (13)$$

From equations (11) and (13)

$$h_{\text{rad}} \approx \frac{1}{2} \sigma \epsilon_B (T_B + T_A)^3 \quad \dots\dots\dots (14)$$

It is of interest to note that h_r varies by a comparatively small amount over the temperature range of T_B and T_A that would normally occur in the horizontal test chamber of the climatic chamber.

For example,

for t_B and t_A of 15°C and 35°C, respectively,

$$h_r \approx 6,0 \text{ } \epsilon_B \times 10^{-3} \text{ kW/m}^2 \text{ } ^\circ\text{C} \text{ and}$$

for t_B and t_A of 34°C and 35°C, respectively,

$$h_r \approx 6,6 \text{ } \epsilon_B \times 10^{-3} \text{ kW/m}^2 \text{ } ^\circ\text{C}.$$

The average value for h_{rad} is thus $6,3 \text{ } \epsilon_B \times 10^{-3} \text{ kW/m}^2 \text{ } ^\circ\text{C}$.

1.2 Net radiative flux between a human subject in the test chamber of the climatic chamber and the surrounding test chamber walls

Substitution of the expression for the radiation heat transfer

coefficient, h_{rad} , given by equation (14) in equation (11) leads to:

$$\dot{q}''_{\text{rad}} = 6,3 \epsilon_B \times 10^{-3} A_{\text{rad},B}/A_{T,B} (t_A - t_B) \dots\dots (15)$$

where \dot{q}_{rad} = radiative heat flux per unit area of body surface, kW/m²

$A_{\text{rad},B}, A_{T,B}$ = radiant surface area and total surface area of the enclosed body, respectively, m²

t_A, t_B = surface temperatures of the enclosing and enclosed bodies, respectively, °C.

In the case of the human body, the emissivity, ϵ_B , is high; of the order of 0,997¹¹⁹⁾.

Substitution of this value for the emissivity in equation (15) leads to the following equation for the radiative flux between a human subject in the test chamber of the climatic chamber and the surrounding walls:

$$\dot{q}''_{\text{rad}} = 6,28 \times 10^{-3} A_{\text{rad},B}/A_{T,B} (t_A - T_B) \dots\dots\dots (16).$$

APPENDIX C

METHODS OF MEASURING HUMIDITY

In general, the humidity measuring devices can be divided into the following two main groups:

- (a) absolute instruments which measure:
 - (i) the thermodynamic dew-point temperature
 - (ii) the thermodynamic wet-bulb temperature
 - (iii) the vapour pressure, or
 - (iv) the humidity ratio, and
- (b) indirect measuring instruments which include:
 - (i) diffusion hygrometers
 - (ii) refractometers
 - (iii) chemical techniques
 - (iv) mechanical hygrometers such as the hair hygrometer
 - (v) spectroscopic instruments, and
 - (vi) electrical resistance hygrometers.

1. DEW-POINT HYGROMETER

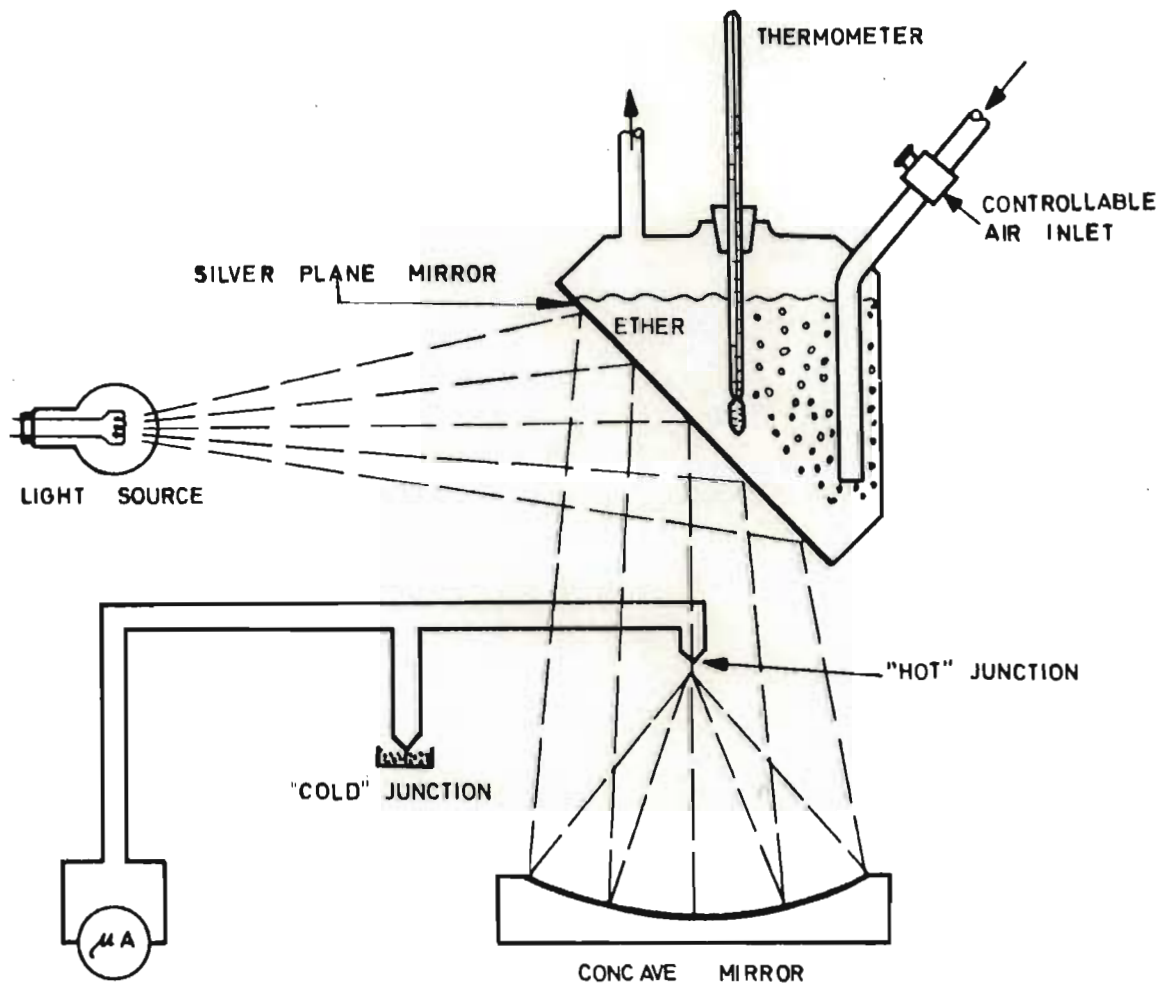
Dew-point hygrometers¹⁴⁶⁻¹⁵¹⁾ generally operate on the principle established by Renault in 1845¹⁵²⁾, namely, that when a volume of moist air is slowly and uniformly cooled under conditions of constant total pressure, the pressure of the air and vapour components remain constant throughout the cooling process until finally a temperature

is attained at which the vapour component becomes saturated. The latter temperature is known as the dew-point temperature.

Basically, a dew-point hygrometer consists of a polished metal or glass surface which can be temperature controlled, either manually or automatically. The surface element is slowly cooled down along with the air immediately adjacent to it until the first traces of dew form on the surface. (In the original Reynault hygrometer shown in Figure C1, the surface element was cooled by bubbling compressed air through a bath of ether). The surface temperature is then raised until the dew disappears. For convenience, the dew-point temperature is defined as the mean of the temperatures at which the mist or dew on the surface appears and disappears.

To eliminate human error, optical techniques may be used. In this case, a light source and a photo-electric detector are incorporated in the instrument to detect the dew; the light beam is directed onto the temperature controlled surface and the reflected light is concentrated on the photo-electric detector.

Any droplets of dew which may form on the surface scatters the light rays and hence reduces the output of the photo-electric detector which is coupled to a suitable indicating meter or recorder.

**FIGURE C1**

Schematic layout of manually-operated dewpoint hygrometer

Manually operated dew-point hygrometers have practical limitations and precision of measurement depends on the skill and patience of the operator. These problems may be overcome to some extent if the hygrometer is arranged to operate automatically.

The system may be converted to automatic operation by incorporating a suitable temperature control system that can be operated by the output signal of the light detection unit or photo-electric cell in the hygrometer; as the output of the photo-electric cell is reduced (thereby indicating the formation of dew), the temperature of the surface is automatically increased. The reverse action takes place when the output of the photo-electric cell is increased. The temperature of the surface, which can be recorded, is thus automatically maintained close to the dew-point temperature and the mean of the temperature readings during a typical control cycle can be taken as the dew-point temperature.

The main advantage of the dew-point hygrometer is that the dew-point temperature is independent of dry-bulb temperature and the specific humidity, in kilogram of water vapour per kilogram of dry air, say, can be determined directly from the dew-point temperature reading. No additional temperature measurements are thus necessary.

One of the major problems associated with this technique, however, is the close control of the temperature of the surface on which the dew is formed, particularly when comparatively small changes in specific humidity have to be detected. An accuracy of within 2 per cent of the specific humidity is about the best that can be expected with dew-point practice.

Thus, at a dew-point temperature of 10°C, specific humidities could possibly be measured to within 0,000185 kg/kg of dry air by this means.

2. WET- AND DRY-BULB PSYCHROMETER

Basically the wet- and dry-bulb psychrometer⁵²⁻⁵⁴⁾ comprises two thermometers one of which, the wet-bulb, is covered with a cotton sheath which is maintained moist.

To determine the water vapour pressure of an air sample from ventilated wet- and dry-bulb measurements, the following psychrometric equation is generally used:

$$p_{wv,G} = p_{wv,wb} - A p (t_G - t_{wb}) \quad \text{..... (1)}$$

where $p_{wv,G}, p_{wv,wb}$ = partial vapour pressure and saturated partial vapour pressure at the wet-bulb temperature, respectively, kPa

and A = psychrometric constant. (A , as well as depending on the Reynolds number, is slightly dependent on t_{wb} and to a lesser extent on t_G).

P = total atmospheric pressure, kPa

t_G, t_{wb} = dry- and wet-bulb temperatures, respectively, °C

Considerable theoretical^{153,154)} and experimental work¹⁵⁵⁻¹⁵⁶⁾ have been done on the theory of the wet- and dry-bulb psychrometer.

The customary procedure to determine the moisture content of the air from wet- and dry-bulb readings is to employ tables or charts^{144,154)} which give, inter alia, specific humidity in terms of the wet- and dry-bulb temperature readings.

Factors influencing the accuracy of the psychrometric method have been described in the literature¹⁴⁷⁾. Thermal radiation from the surrounding walls is one of the factors that can adversely affect the wet-bulb reading. To minimise radiative influences the wet-bulb must be suitably screened and the air velocity across the wet-bulb must be sufficiently high. The critical air speed for round elements up to 10 mm was found to be 3 m/s by Wylie¹⁵⁷⁾.

The Sling psychrometer¹⁵⁸⁾ and Assman psychrometer¹⁴⁷⁾ (which is of the aspirated type), are the most common forms of wet- and dry-bulb instruments.

Under normal conditions, it should be possible with a well designed psychrometer to determine the prevailing vapour pressure within 5 per cent by this means. At a dew-point temperature of 10°C , the corresponding accuracy in terms of specific humidity and dew-point temperature would thus be $0,000460 \text{ kg/kg}$ of dry air and $0,75^{\circ}\text{C}$, respectively.

3. VAPOUR PRESSURE HYGROMETER

Vapour pressure hygrometers generally incorporate a pressure measuring device which measures the change in pressure at constant volume of an air sample before and after the water vapour in the air sample has been absorbed by a suitable chemical¹⁵⁹⁻¹⁶³). In view of the problem of accurately measuring small pressure changes, the hygrometer is most suited for measurements at high specific humidity values where the pressure change during the absorption of the water vapour, is relatively high.

Vapour pressure hygrometers are not available commercially and have only been developed for specific applications. The laboratory type of instruments, however, require patience and skill to operate. For this reason, this type of instrument was considered to be unsuitable for the direct measurement of the evaporative heat loss rate from a human body.

4. GRAVIMETRIC HYGROMETERS

In the case of the gravimetric type of hygrometer, the specific humidity of a measured quantity of air is deduced from the overall mass change of chemicals which are used to absorb the moisture contained in the air sample^{164,165}).

High accuracies have been claimed for gravimetric hygrometers and, as a result, the gravimetric technique has been accepted as a standard of reference against which humidity measuring devices are calibrated. However, the measurements have to be carried out over a comparatively long period of time. When the specific humidity value of the air sample thus changes with time (this may happen when the specific humidity measurements are carried out in the wake of a human body), an average reading of the humidity over the period of measurement is obtained.

The gravimetric hygrometer is thus not a direct measuring instrument and for this reason, this type of hygrometer was considered to be unsuitable for the measurement of the humidity increase in the wake of a human body.

5. CHEMICAL METHODS OF MEASURING HUMIDITY

In this type of measurement use is generally made of chemical compounds which are colour sensitive to changes in relative humidity.

A colour scale employed in conjunction with a suitable indicating material, gives a rough indication of relative humidity.¹⁶⁶⁾

6. REFRACTOMETER FOR MEASURING HUMIDITY

In this system of humidity measurement the microwave technique is employed; in particular, the increment of refractive index due to the presence of water vapour in an air sample, is measured. The main advantage of such a system is the high rate of response. Due to the short response time, the system can be incorporated in a fast moving projectile to measure the moisture content of the air through which the projectile is passing¹⁶⁷⁾.

7. DIFFUSION HYGROMETERS

The principle of operation of the diffusion hygrometer¹⁶⁸⁾ is based on the difference in the respective rates of diffusion of water vapour and of air through a semi-permeable membrane, for example, a porous clay plate.

8. MECHANICAL HYGROMETERS

The most commonly used type of mechanical hygrometer is the so-called hair hygrometer. This hygrometer is based on the principle that animal hairs which have been carefully cleaned and freed from grease, change their length when they absorb or part with moisture. In particular, the length generally increases as the moisture content

of the surrounding gas increases.

The theory of the hair hygrometer is discussed by Whipple¹⁶⁹⁾.

In 1783 de Saussure¹⁴⁶⁾ constructed a hygrometer working on this principle. Although the defects of this type of hygrometer have subsequently been severely criticised, the hygrometer still remains from a simplicity and ease of operation points of view, one of the most convenient and widely used hygrometers at the present time. It lends itself readily to use at ordinary temperatures and is eminently suitable for recording purposes.

The accuracy of recording hair hygrometers for determining the relative humidity at room temperatures is of the order of 4 per cent^{158,170-172)}. At an air temperature of 35°C and a dew-point temperature of 10°C, the corresponding accuracy in terms of specific humidity is of the order of 0,0017 kg/kg of dry air or 2,53°C.

Previous attempts by von Willibrande (1902), Schwenkenbecher (1905), Moog et al (1921) and Schlueter (1925) to measure the increase in vapour pressure of air passing over a subject in a calorimeter, by means of hair hygrometers, were reported by Palmes¹⁷³⁾.

However, preliminary investigations into the use of a specially constructed differential hair hygrometer for the measurement of the humidity increase in the wake of a human body in the test chamber of the climatic chamber indicated that, because of a marked hysteresis effect, this method of measurement would be unsuitable in this particular case.

9. SPECTROSCOPIC HYGROMETERS

The basic design of the spectroscopic hygrometer is based on the attenuation of infra red radiation by water vapour⁵⁵⁻⁵⁸⁾.

Figure C2 presents the absorption spectrum of water vapour as a function of radiation wave-length¹⁷⁴⁾. From Figure C2 it is seen that the wave-length range of 0,8 micron to 4 micron, a fairly strong absorption band is centred around the wave-length range of 2,56 micron to 2,85 micron.

As the output of the infra red hygrometer is a function of the total amount of water molecules in the optical path, the method is thus ideally suited to the determination of humidity in the outer atmosphere where long path lengths and hence relatively large signals can be obtained.

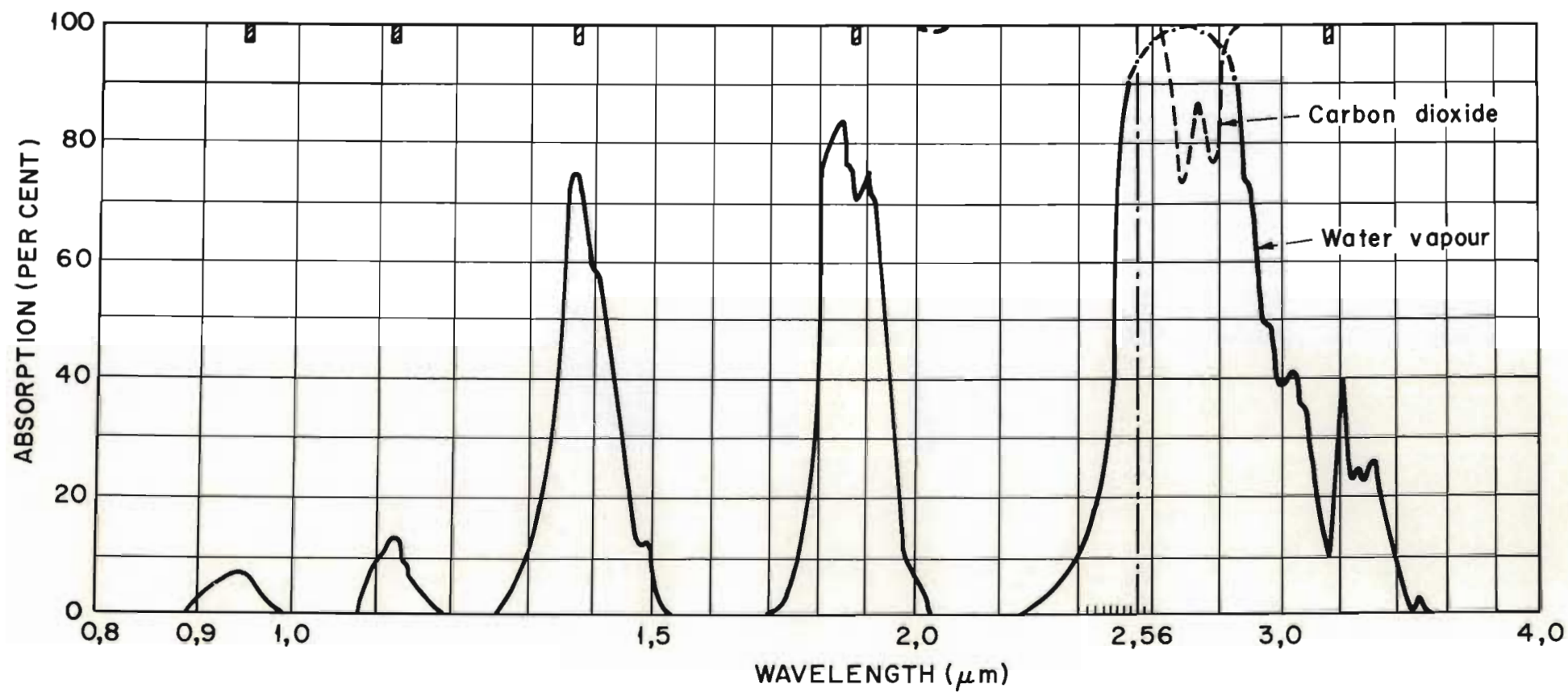


FIGURE C2
*Monochromatic absorptivity for water vapour and
carbon dioxide.*

The infra-red hygrometer that was constructed by Wood⁵⁸⁾ is shown diagrammatically in Figure C3. Basically, the instrument consists of a radiation source, a sector disc filter, a 300 mm long tube which forms the sensing path, a closed-loop balancing system and a standardizing system for drift correction.

A beam of light from a tungsten lamp is brought into collimation by means of a plano-convex lens. The resultant parallel beam of light is then transmitted through two glass wedges and the sector disc filter in turn. The sector disc which rotates at 30 herz is made up of two absorption (2,60 micron) and two reference (2,45 micron) band-pass filters. The light beam is then reflected along the sensing path and focussed on a glass diffusing plate by means of a plano-convex lens. A lead sulphide photo-counter is located behind the diffusing plate.

Since the sector disc interposes alternate filter sectors at a frequency of $2 \times 30 = 60$ herz, the photo-counter signal consists of two 60 herz components, each at a different wave-length. One band, centred near the wave-length of 2,60 micron, is subject to attenuation by water vapour, the other located near the wave-length of 2,45 micron, is not. Thus, the ratio of transmitted band energies is sensitive only to the concentration of water vapour in the path. The ratio is effectively maintained at unity through the use of the servo-operated glass wedge which moves to compensate for any energy

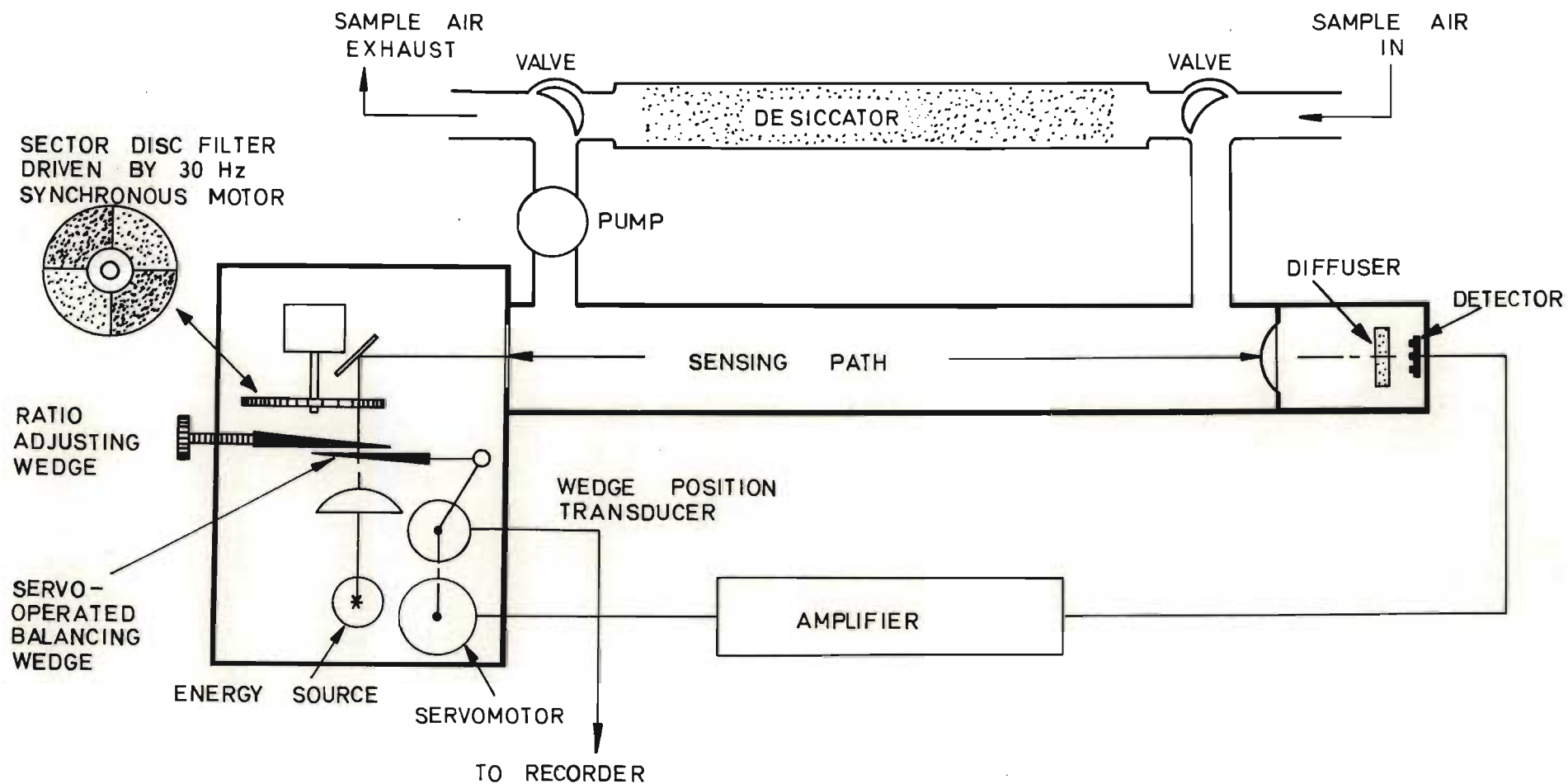


FIGURE C3
Schematic layout of infra-red hygrometer by Wood 58)

unbalance which may tend to occur whenever the concentration of the absorbing vapour changes; the resultant beam modulation causes an error signal to appear at the output of the photo-cell which, through a suitable amplifier and phase sensitive servo-mechanism, adjusts the glass wedge to enable the system to be restored to a fully balanced condition.

The degree of radiant transmission through the glass wedge is a function of the wedge thickness. Thus, a departure from an energy ratio of unity due to a variation of water vapour, is automatically compensated for by an appropriate change in position and hence thickness of the glass wedge. The position of the wedge is, therefore, an index of the amount of water vapour in the path.

Included in the design is a dry-gas purge standardisation system whereby periodic checks of the zero point enable compensation for drift factors.

The main advantages of spectroscopic hygrometers are:

- (i) short time response,
- (ii) the method in no way alters the humidity content of the air sample, and
- (iii) since the sensing element is a beam of radiation, an integrated reading of humidity in the radiation path is obtained.

In view of the above-mentioned factors, the method appeared to be ideally suited for carrying out humidity measurements in the wake of a human body.

In this case, a filtered light beam of selected wave-length could be split in two, such that one half of the light beam traverses the front or upstream of the body and the other the downstream side. By incorporating a rotating sector disc, which alternately cuts off the beams on the upstream and downstream side of the body, the ratio of the respective transmitted energies of each of the two light beams would be proportional to the humidity increase in the wake of the body. (See Figure 13 on page 128).

The major problem experienced with the infra-red technique was the lack of sensitivity due mainly to insufficient active path length to provide sufficient absorption. Problems were also experienced in producing parallel rays of light which would be of sufficient intensity at the end of the path length to activate the photo detector at its most efficient level; it appeared that a radiant path length of at least 6,5 m would be required to achieve a sensitivity of 0,000022 kg/kg of dry air, specific humidity.

10. ELECTRICAL RESISTANCE HYGROMETERS

The humidity-sensing elements incorporated in electrical resistance hygrometers generally consist of hygroscopic materials which change in moisture content and hence electrical resistance whenever the relative humidity of the surrounding air changes.

In general, electrical resistance hygrometers are very sensitive to small changes of humidity and have a rapid response.

In the past, the chief defect of electrical resistance hygrometers has been the instability of calibration but this problem seems to have been overcome in certain commercial models of the instrument.

The following classification of the various types of electrical hygrometers is given by Wexler¹⁷⁵):

1. Hygrometers which incorporate an aqueous electrolytic solution as the humidity-sensing element. In such hygrometers conductivity variations of the aqueous electrolytic solution is taken as a measure of humidity.
 - (a) Electrolytic solutions on impervious insulating surfaces:
 - (i) Weaver water vapour indicator^{176,177})
 - (ii) Dunmore hygrometer¹⁷⁸)
 - (iii) Larach hygrometer¹⁷⁹)
 - (iv) Gregory hygrometer¹⁸⁰)

- (b) Electrolytic solutions in fibre and fabrics¹⁸¹⁾
- (c) Electrolytic solutions in porous ceramics¹⁸²⁾.

2. Hygrometers which detect humidity as a change in the resistivity of impervious solids^{183,184)} or alternatively a film of salt¹⁸⁵⁾. In the latter case the change in electrical resistance due to the ionizing of salt molecules in a layer of adsorbed moisture is taken as a measure of humidity.
3. Hygrometers incorporating an oxide film as the humidity-sensing element^{186,187)}. The oxide film on an aluminium plate is generally employed.
4. Hygrometers which detect humidity as a change in the electrical resistance of ion-exchange resins^{188,189)}. Such resins, which can be produced from high polymetric cross-linked plastics by treatment with various reagents, are hydrophilic and in the presence of water are capable of electrolytic conduction.
5. Hygrometers which depend on the volume resistivity of porous materials for their operation¹⁹⁰⁻¹⁹²⁾.
6. Resistance hygrometers which make use of the property of some materials to undergo dimensional changes whenever the humidity changes^{193,194)}. In this case the material is coated or impregnated with a conductive substance. The change in electrical resistance of the conductive substance as the humidity sensitive material expands or contracts is then taken as a

measure of humidity.

7. Hygrometers incorporating temperature-control systems which automatically control the concentration of saturated salt solutions at preset values^{59,195,196}). In this case the temperature of the salt solution becomes a measure of the ambient vapour pressure or humidity.

The operation of the Wylie⁵⁹) and the Dewcel¹⁹⁶) hygrometers, are based on this principle.

Consideration was given to the use of various types of electrical resistance hygrometers for the measurement of the evaporative heat loss from a human body in the test chamber of the climatic chamber. In particular, the use of the Wylie⁵⁹) hygrometer and other humidity-measuring systems which depend on the change in electrical resistance of a salt film for their operation, were investigated.

10.1 Wylie electrolytic condensation hygrometer

The principle of operation of the Wylie⁵⁹) hygrometer is derived from the fact that water vapour is taken up by the surface of a water soluble crystal if the water vapour pressure is greater than the vapour pressure of a saturated solution of the crystalline substance at the temperature of the crystal surface.

The temperature of the crystal is determined at which a thin layer of the saturated solution, formed on the surface of the crystal and observed by virtue of its electrical properties, is in equilibrium with the gas which is the subject of measurement. The conducting layer of saturated solution is maintained in thermal equilibrium with the gas by controlling the crystal temperature; a temperature which, according to Wylie, was related to the dew-point temperature of the gas.

The Wylie hygrometer is shown in diagrammatic form in Figure C4. The practical form of the hygrometer is a small cylindrically shaped "isothermal" metal enclosure, in which a suitable water soluble ionic crystal such as potassium chloride is mounted between two chemically inert electrodes. The crystal is housed in a central cavity within the metal enclosure; both the crystal and enclosure being assumed to be equal in temperature.

The incoming gas, the humidity of which is to be measured, is brought to the temperature of the metal enclosure, before entering the central cavity through eight holes drilled in the cylinder wall, parallel to the cylindrical axis.

A constant supply of expanded carbon dioxide gas flows through the enclosure for cooling. On the outer surface of the

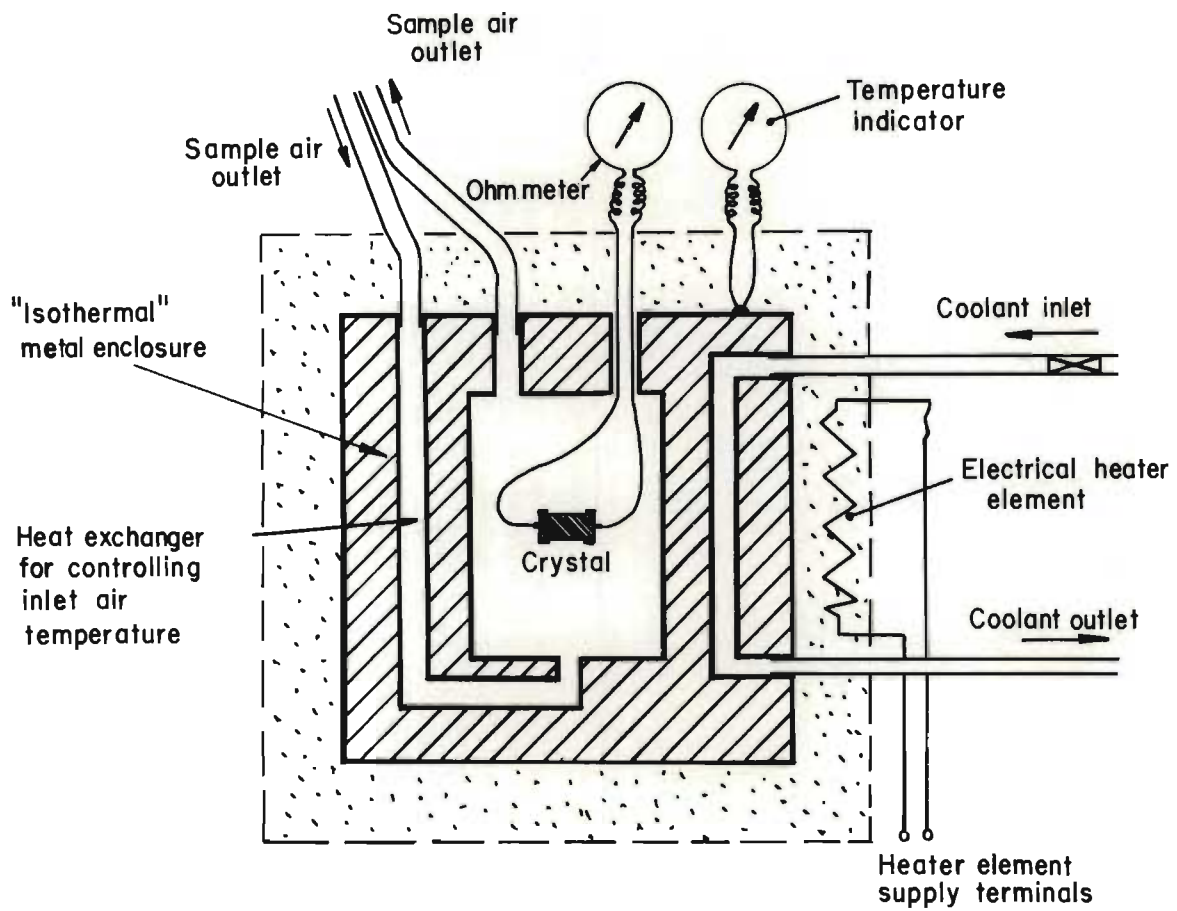


FIGURE C4

Schematic diagram of the Wylie electrolytic condensation hygrometer

cylinder are two bifilar windings of insulated copper wire which serve as the electrical heater element and resistance thermometer. The latter measures the temperature of the crystal enclosure and the heater controls the temperature of the enclosure and crystal. The temperature of the enclosure is controlled in such a way that the crystal resistance remains constant at a predetermined value, regardless of humidity. The equilibrium temperature is thus a function of the specific humidity or dew-point temperature of the air flowing through the enclosure.

The instrument is usually operated automatically. For automatic operation, the temperature of the metal enclosure is controlled by the electrical resistance of the crystal through an electronic controller and the temperature of the enclosure, corresponding to the equilibrium temperature at which the crystal moisture is constant at a predetermined value, is continuously recorded.

According to Wylie, the hygrometer is capable of measuring the absolute dew-point temperature to within $0,01^{\circ}\text{C}$. At a dew-point temperature of 10°C , this corresponds to a specific humidity value of $0,000006 \text{ kg/kg}$ of dry air.

In view of the high degree of accuracy claimed by Wylie, the use of the Wylie hygrometer was investigated for measuring the humidity increase in the wake of a human body.

Figures 14 and 15 on pages 134 and 135, present cross-sectional and exploded views of the prototype model of an electrolytic condensation hygrometer that was tested.

Initial calibration studies indicated that the proposed system of humidity measurement would be capable of measuring the humidity increase in the wake of the human body to within a dew-point temperature of $0,04^{\circ}\text{C}$ or a specific humidity of $0,000024 \text{ kg/kg}$ of dry air. The limited degree of accuracy attainable with the system was mainly due to the problem of controlling the temperature of the air circulating through the enclosure and hence the crystal temperature to within sufficiently close limits.

10.2 Electric grid hygrometer

In this method, a long length of platinum cotton covered wire was twisted together and impregnated with a lithium chloride solution. The twisted wire was mounted on an insulated frame to form a grid.

Two similar grids were constructed to investigate the possibility of measuring the integrated humidity rise in the wake of the body; the two grids being connected in a Wheatstone bridge with two other fixed resistances. The difference in

resistance was measured by means of a strain gauge recorder.

Tests with this type of hygrometer were disappointing in view of certain uncontrolled changes in the resistance of the salt that took place resulting in a zero shift. In addition, the desired sensitivity could not be attained.

10.3 Use of commercially available electrical resistance hygrometers

Investigations were carried out to determine the suitability or otherwise of a commercially available electrical resistance hygrometer for measuring the humidity increase in the wake of the body.

It was found that commercial lithium chloride sensors, the resistance of which is a function of the relative humidity of the surrounding air, were comparatively stable and extremely sensitive to variations in relative humidity. The absolute accuracy to which these elements can be calibrated is of the order of 0,1% relative humidity.

At dry-bulb and dew-point temperatures of 35°C and 10°C, respectively, this corresponds to a specific humidity difference of 0,00004 kg/kg of dry air or a dew-point temperature change of 0,065°C.

APPENDIX D

TESTS ON AN ELECTROLYTIC CONDENSATION HYGROMETER

Performance tests were carried out on the prototype electrolytic condensation hygrometer described in section 4.3.4 on page 132 with the view to determining (a) whether certain assumptions underlying the principle of operation of the Wylie hygrometer⁵⁹⁾ were correct, (b) the pressure drop of the sample of air which is drawn through the hygrometer, (c) the time response of the instrument and (d) the accuracy of the hygrometer.

Figures 14 and 15 on pages 134 and 135, present cross-sectional and exploded views of the hygrometer components, respectively.

(a) Changes in the electrical conductivity of a KCl crystal with changes in the relative humidity of the surrounding air

According to Wylie the point at which the crystal starts absorbing water vapour is well defined by a sudden increase in the electrical conductivity of the crystal.

It should be noted, however, that, although the absorption of water vapour only takes place when the vapour pressure of the air sample surrounding the crystal is higher than the saturation vapour pressure of the saturated salt solution, adsorption of water molecules to the

surface of the salt crystal takes place even when the vapour pressure of the surrounding air sample is less than the saturation vapour pressure of the saturated solution of the salt crystal.

The number of molecular layers of water adsorped on to the surface of the crystal increases as the relative humidity of the surrounding air sample increases. Since the adsorped layers of water molecules are subject to relatively large physical forces, free ions are formed which may increase the surface conductivity of the crystal considerably.

The influence of adsorption is known to be a function of temperature, kind of crystal involved and the surface characteristics of the crystal, but is less clearly understood than the process of absorption.

Tests were conducted to determine whether a sudden change in the electrical conductivity of a salt crystal occurred as soon as the absorption of water commences.

An air sample with fixed dew-point temperature was drawn over one of the crystals and the temperature of the air sample at which the resistance of the crystal was in equilibrium with a known resistance, (which could be varied from 0,02 to 40 megohm), was measured.

In curve (a) in Figure D1, the equilibrium resistance of a NaCl crystal is shown as a function of the relative humidity of the air sample flowing over the crystal.

A marked change in the crystal resistance at relative humidities below 70 per cent is evident. Since an alternating current was used in the measurement of the crystal resistance, it was realised that this change could be due to the di-electric breakdown of the leads, which were about 2 m long between the controller and the crystal enclosure.

When the length of the leads between the controller and the crystal was reduced to about 150 mm, this sudden change in the measured crystal resistance disappeared (see curve (b) in Figure D1). At the higher crystal resistances a capacitance effect between the two leads could, however, still be detected.

Special high insulation leads, about 150 mm long, were then installed between the controller and the crystal. The relative humidity at which the crystal resistance reached equilibrium with the preselected fixed resistances, is shown in curve C in Figure D1. Apart from a small capacitance effect at crystal resistances above 1 megohm, the short high insulation leads had no significant influence on the shape of the resistance versus the relative humidity curve.

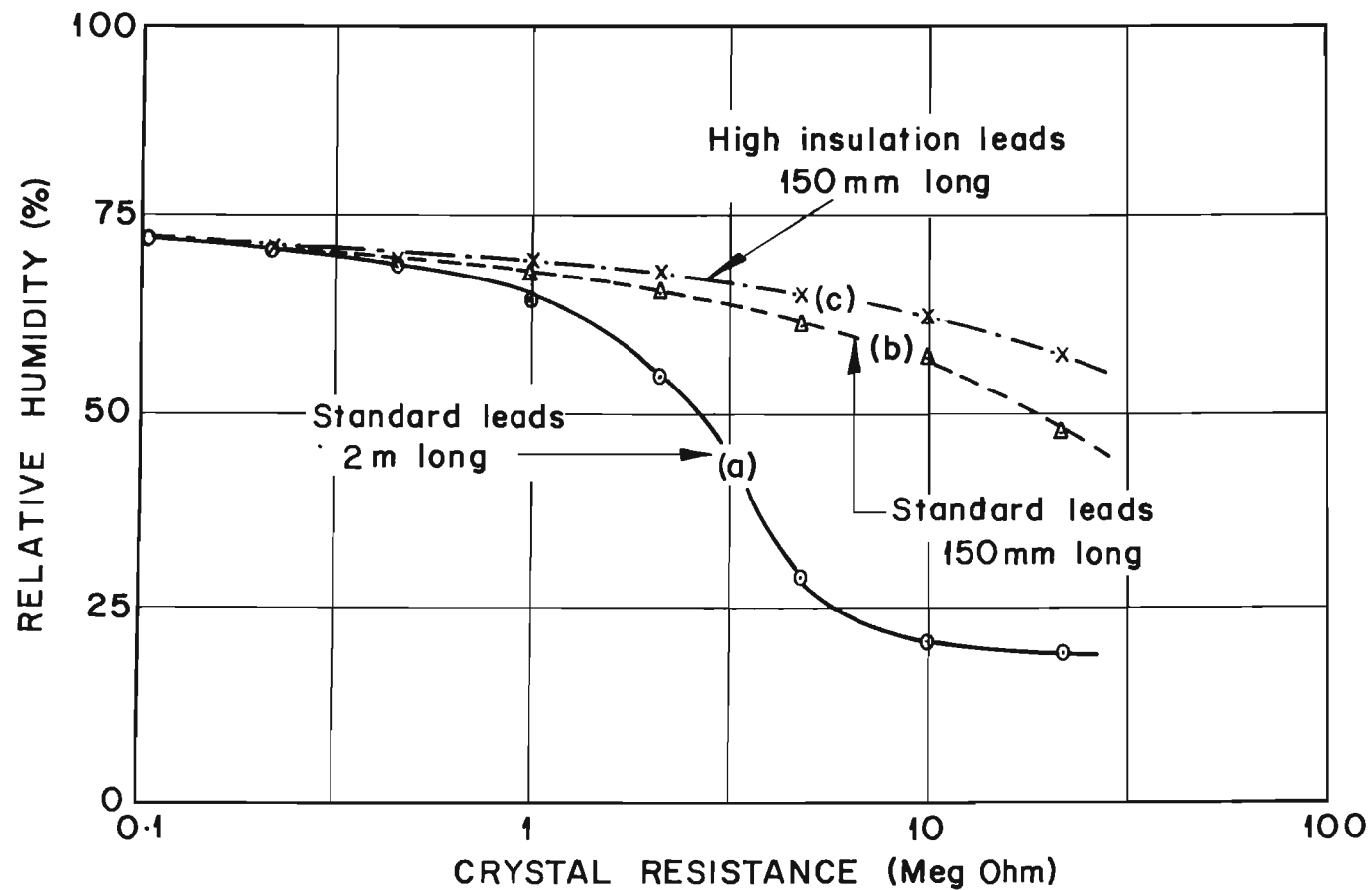


FIGURE D1

The measured equilibrium resistance of a Na Cl crystal in the electrolytic hygrometer as a function of the relative humidity of the surrounding air.

In order to ensure that the electrical system for measuring the crystal resistance in fact measures the crystal resistance and not the impedance of some of the component parts of the circuit, relatively low crystal resistances should preferably be selected when using a salt crystal as the humidity-sensing element.

Using short high insulation leads, a KCL crystal was subsequently exposed to atmospheres of known relative humidity whilst the electrical resistance of the crystal was recorded. Typical test results are presented in Figure D2.

It follows from Figure D2 that, within the range of the measuring equipment, the logarithm of the crystal resistance is a linear function of the relative humidity of the controlled atmosphere. No sudden change in the resistance of the crystal was evident. Calibration of the instrument is thus essential.

The repeatability of the observations indicates that a high degree of precision was achieved: a change of only 10% in the relative humidity of the controlled atmosphere caused a change in the electrical resistance of the crystal of approximately 100 megohm.

(b) Pressure drop of the sample air which is drawn through the hygrometer

In Figure D3 the ventilation rates through the crystal enclosure and heat exchanger are shown as a function of the corresponding pressure

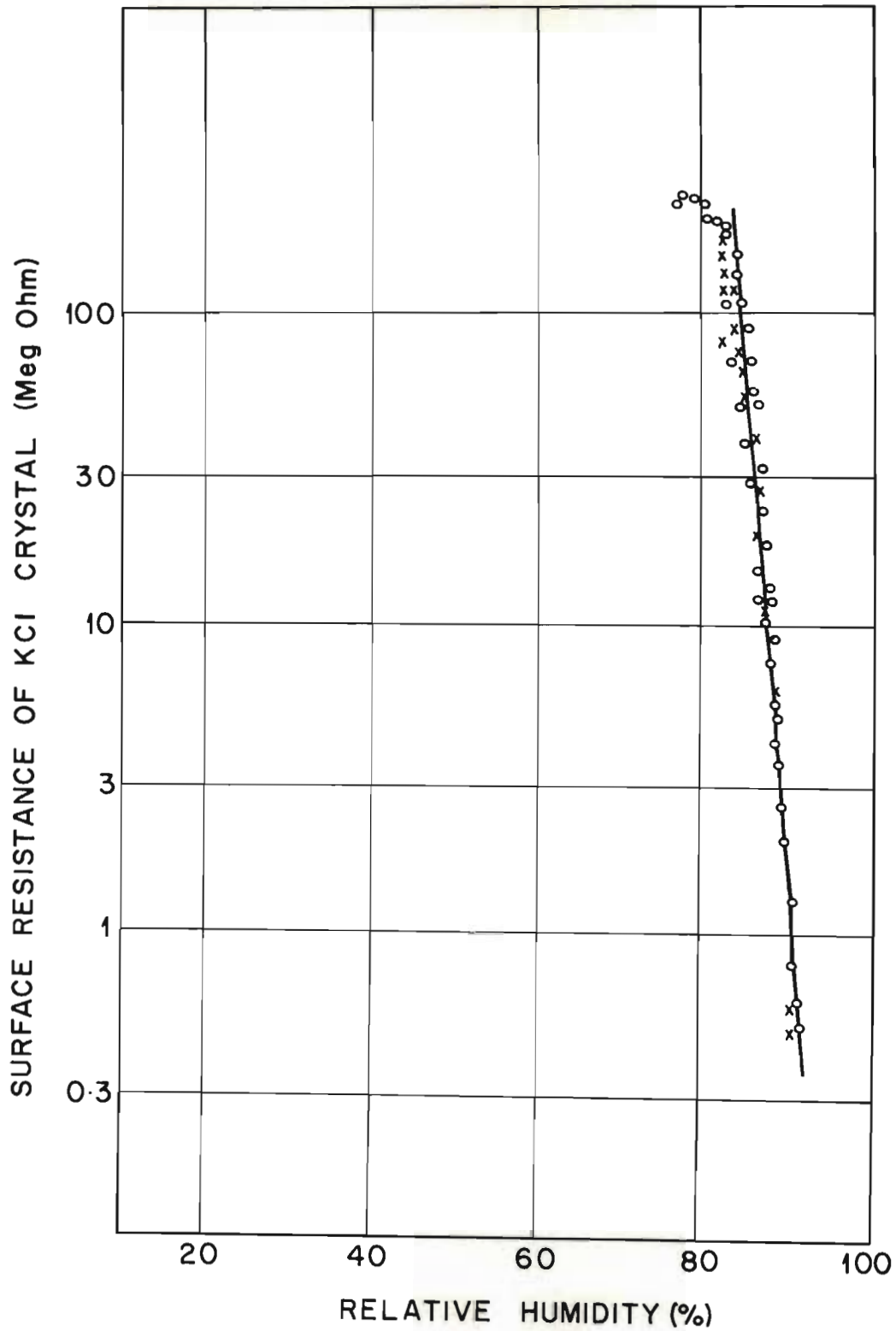


FIGURE D2

The surface resistance of a KCl crystal as a function of the relative humidity of the surrounding air.

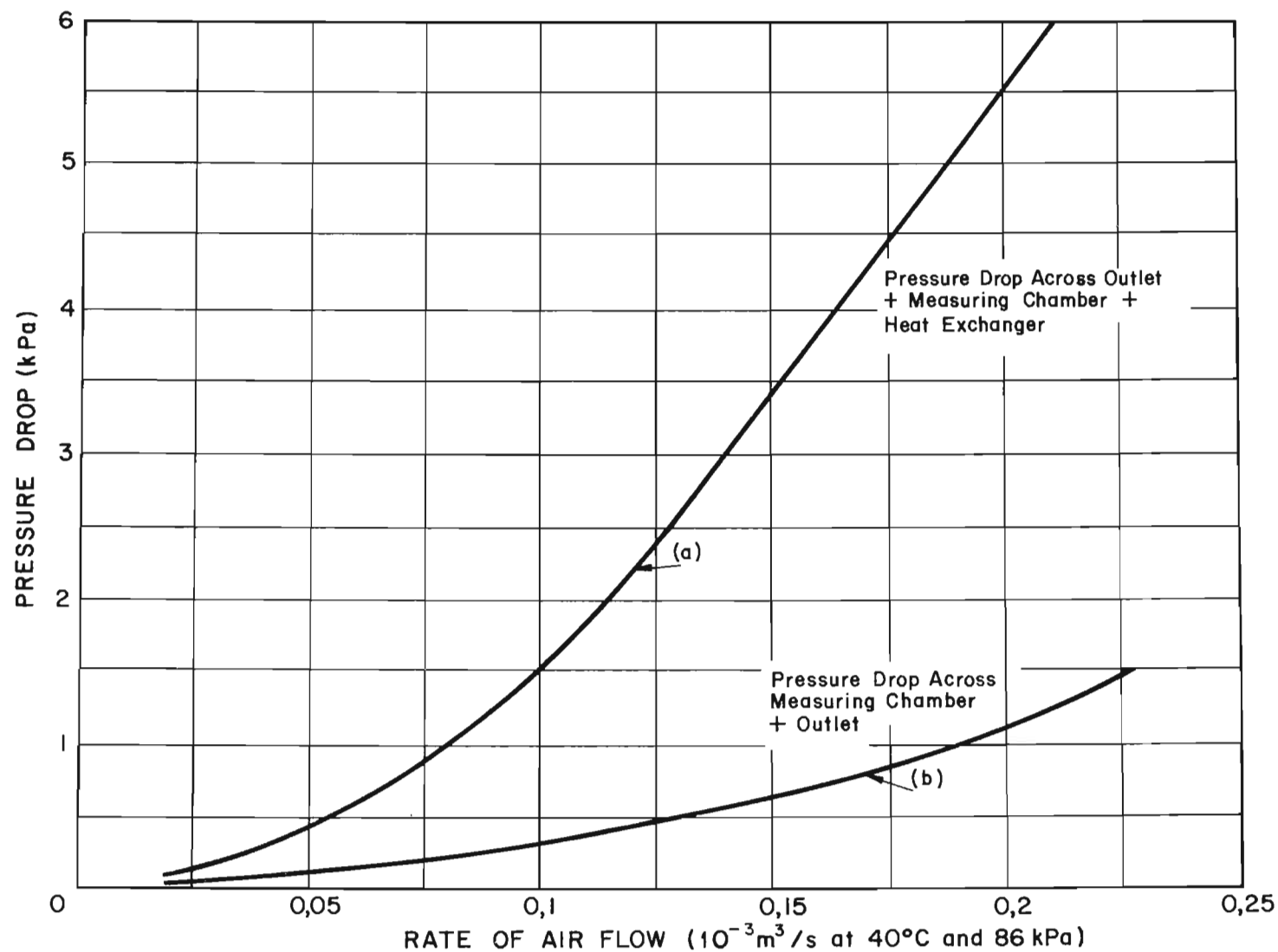


FIGURE D3

Ventilation rate through the component parts of the modified Wylie hygrometer as a function of the pressure drop across the instrument. (See Figure 15)

drop.

Due to the pressure drop across the hygrometer, the total pressure of the air sample flowing across the crystal is lower than atmosphere. This results in a change in the relative humidity of the air sample; the change in the relative humidity of the air sample being proportional to the change in the total pressure.

$$\text{Thus, } \frac{\text{Rel. hum.}_{\text{crystal}}}{\text{Rel. hum.}_{\text{atm.}}} = \frac{\text{Total press.}_{\text{crystal}}}{\text{Total press.}_{\text{atm.}}}$$

In the proposed system of measurement in which two hygrometers are coupled differentially to give a direct reading of the humidity increase in the wake of the human body, therefore, the respective pressure drops from atmosphere to the crystal of each hygrometer should be maintained equal, in order to minimize errors. (See section 4.3.4 on page 132).

(c) The influence of ventilation rates through the crystal enclosure on the response time of the electrolytic condensation hygrometer

Air at a constant temperature and flow rate was drawn through the crystal enclosure until equilibrium conditions were attained. A step-change in the air temperature was then introduced, and the time taken to indicate 66% and 90% of the change in temperature noted.

In Figure D4 the time response as a function of the pressure drop across the crystal enclosure is illustrated graphically.

(d) Calibration tests

Initial calibration studies indicated that the proposed system of humidity measurement would be capable of measuring the humidity increase in the wake of the human body to within a dew-point temperature of $0,04^{\circ}\text{C}$ or a specific humidity of $0,000024 \text{ kg/kg}$ of dry air.

The limited degree of accuracy attainable with the system was mainly due to the problem of controlling the temperature of the air circulating through the enclosure and hence the crystal temperature to within sufficiently close limits.

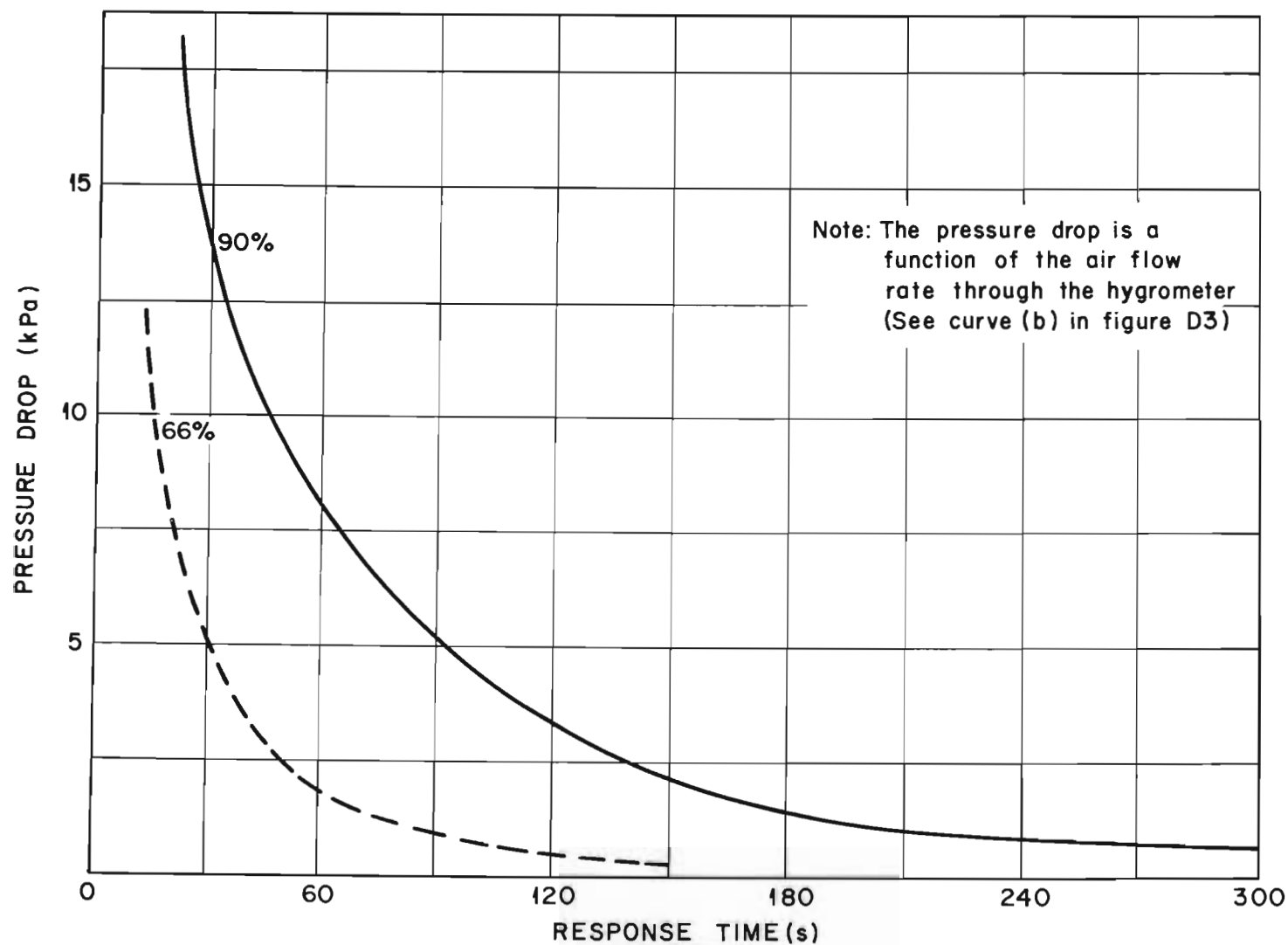


FIGURE D4

The modified Wylie electrolytic condensation hygrometer: time taken to indicate 66 and 90% of a step change in temperature for various pressure drop values across the instrument.

APPENDIX E

CALCULATIONS TO DETERMINE THE MAXIMUM DIFFERENCE BETWEEN THE
RESPECTIVE AIR FLOW RATES THROUGH THE VARIOUS SAMPLING HOLES
IN THE DOWNSTREAM AIR-SAMPLING PROBE OF THE EVAPORATIVE HEAT
LOSS MEASURING INSTRUMENT

Basically the evaporative heat loss measuring system consists of two air-sampling probes, for sampling the air on the upstream and downstream sides of the body, a double circuit heat exchanger and a differential humidity-measuring system for measuring the difference in specific humidity difference between the two air samples.

Figure 30 on page 187 presents a view of the downstream air-sampling probe. The probe was constructed from 13,5 mm diameter brass tubing in the form of a cross, with a tip to tip length of 1,87 m. One hundred and sixty eight 0,343 mm diameter holes were drilled in each arm of the probe for the purpose of sampling the air.

The following calculations were carried out to determine to what extent the air flow rate through each sampling hole can be expected to vary from each other:

Consider the air flow rate through the first and the 168th air-sampling hole, namely \dot{Q}_1 , and \dot{Q}_{168} , respectively, of one of the arms of the air-sampling probe.

Since the pressure drop across an orifice is proportional to the

square of the air flow rate through the orifice

$$\begin{aligned}\dot{Q}_{G,1}/\dot{Q}_{G,168} &= \sqrt{\Delta p_1/\Delta p_{168}} \\ &= \sqrt{\Delta p_1/(\Delta p_1 - \Delta p_t)} \quad \dots\dots (1)\end{aligned}$$

where $\dot{Q}_{G,1}, \dot{Q}_{G,168}$ = air flow rates through the 1st and 168th air-sampling hole of each sampling arm, respectively, m^3/s

and $\Delta p_1, \Delta p_{168}$ = pressure drops across the 1st and 168th air-sampling hole, respectively, Pa

Δp_t = pressure drop along the length of the tube (between the 1st and 168th air-sampling hole).

First assumption

As a first assumption it was assumed that the respective air flow rates through all the holes are the same; that is, the air velocity in each hole is 3,24 m/s (see Section 4.6.3 on page 188).

The pressure drop across each orifice is given by the equation:

$$\Delta p_{or} = \dot{v}_{G,or}^2 \rho_G / k^2 2g \quad \dots\dots (2)$$

where Δp_{or} = pressure drop across the orifice, Pa

$\dot{v}_{G,or}$ = air velocity through the orifice, m/s

ρ_G = air density, 1 kg/m^3

k = coefficient of discharge, 0,7

g = acceleration due to gravity, $9,8 \text{ m/s}^2$

$$\begin{aligned}\text{Thus } \Delta p_1 &= 3,24^2 \times 1/0,7^2 \times 2 \times 9,8 \\ &= 1,093 \text{ Pa.}\end{aligned}$$

Second assumption

In order to obtain a conservative estimate of the pressure drop across the length of the sampling tube, Δp_t , it was assumed that the total air flow rate of $0,2 \times 10^{-3}/4 = 0,05 \times 10^{-3} \text{ m}^3/\text{s}^*$ would flow along the entire length of the tube. (In actual fact, of course, the air flow rate in the tube would gradually increase from a flow rate of $0,05 \times 10^{-3}/168 = 0,3 \times 10^{-6} \text{ m}^3/\text{s}$ near the tip of the tube, at the 168th hole, to $0,05 \times 10^{-3} \text{ m}^3/\text{s}$ adjacent to the central boss.

The corresponding air velocity in the tube is given by the equation:

$$\dot{v}_{G,t} = \dot{Q}_{G,t}/A_t \quad \dots\dots\dots (3)$$

where $\dot{v}_{G,t}$ = air velocity in the tube, m/s

and $\dot{Q}_{G,t}$ = air flow rate in the tube, $0,05 \times 10^{-3} \text{ m}^3/\text{s}$

A_t = cross-sectional area of the tube

$$= \pi(0,0135)^2/4 = 143 \times 10^{-6} \text{ m}^2$$

$$\text{Thus } \dot{v}_{G,t} = 0,05 \times 10^{-3}/143 \times 10^{-6} = 0,35 \text{ m/s.}$$

The corresponding Reynolds number, N_{Re} , is given by the following equations:

$$N_{Re} = \frac{\dot{G}''_{G,t} D_t}{\mu} \quad \dots\dots\dots (4)$$

$$\text{and } \dot{G}''_t = \dot{v}_t \rho \quad \dots\dots\dots (5)$$

* See Section 4.6.3 on page 185

where N_{Re} = Reynolds number, dimensionless

and D_t = tube diameter, 0,0135 m

μ = dynamic viscosity of the air, 18×10^{-6} kg/ms

$\dot{G}_{G,t}$ = mass flow rate of the air in the tube, $\text{kg/m}^2 \text{s}$

$\dot{v}_{G,t}$ = air velocity in the tube, 0,35 m/s

ρ_G = density of the air, 1 kg/m^3

From equations (4) and (5)

$$\begin{aligned} N_{Re} &= 0,35 \times 1 \times 0,0135 / 18 \times 10^{-6} \\ &= 262. \end{aligned}$$

The flow is thus laminar and the friction factor, f , according to the theory by Hagen and Poiseville which is cited in reference (197), is $64/262 = 0,244$.

The corresponding pressure drop along the length of the tube is given by the following equation:

$$\Delta p_t = f L \dot{v}_{G,t}^2 \rho_G / D_t^5 \quad \text{..... (6)}$$

where Δp_t = pressure drop along the length of the tube, Pa

and f = friction factor, 0,244

$\dot{v}_{G,t}$ = air velocity in the tube, 0,35 m/s

ρ = density of the air, 1 kg/m^3

D_t = tube diameter, 0,0135 m

g = acceleration due to gravity, $9,8 \text{ m/s}^2$

L_t = tube length, $0,915 \text{ m}$ (see Figure 30 on page 187)

$$\begin{aligned}\text{Thus, } \Delta p_t &= 0,244 \times 0,915 \times (0,35)^2 \times 1/(0,0135 \times 2 \times 9,8) \\ &= 0,1 \text{ Pa.}\end{aligned}$$

From equation (1) on page 448,

$$\begin{aligned}\dot{Q}_1/\dot{Q}_{168} &= \sqrt{\Delta p_1/(\Delta p_1 - \Delta p_t)} \\ &= \sqrt{1,093/(1,093 - 0,1)} \\ &= 1,049.\end{aligned}$$

Thus, under the assumed conditions of air flow, the air flow rate through the 168th air-sampling hole, \dot{Q}_{168} , will be 4,9% less than the air flow rate through the first hole, \dot{Q}_1 . Actually, the variation in air flow rate through the air-sampling holes along the length of the tube will be less than 4,9% since the first and second assumptions that were made in the theoretical analysis tend to over estimate Δp_t and hence the ratio, \dot{Q}_1/\dot{Q}_{168} . Variations in the air flow rate of less than 5% are considered to be acceptable.

APPENDIX F

CALCULATIONS TO DETERMINE THE EFFECTIVENESS OF THE DOUBLE
CIRCUIT HEAT EXCHANGER INCORPORATED IN THE EVAPORATIVE
HEAT LOSS MEASURING SYSTEM

The major function of the double circuit heat exchanger is to equalise the respective dry-bulb temperature of the two air samples which are drawn through the air-sampling probes on the upstream and downstream side of the body, to within 0,0005°C. (See Section 4.6.1 on page 185).

Basically the double circuit heat exchanger consists of two helical copper coils mounted in a constant temperature water bath; the one coil being connected to the air-sampling probe on the downstream side of the body and the other to the probe on the upstream side of the body.

Based on a preliminary analysis of the problem the constructional details and certain performance characteristics of the heat exchanger were assumed to be as follows:

(i) Coil data

material	:	copper
tube diameter	:	9,52 mm outside
	:	7,5 mm inside
mean coil diameter	:	355 mm
number of coils	:	14

- (ii) Velocity of water across the coils : 0,5 m/s
- (iii) Air flow rate through each helical copper coil : 0,2 m/s
- (iv) Temperature difference between the two air streams
entering the two helical copper coils : 2°C*
- (v) Water temperature in the constant temperature bath : 40°C

1. OVERALL COEFFICIENT OF HEAT TRANSFER

(a) Air side coefficient

The Reynolds number N_{Re} , is obtained from the following equations:

$$N_{Re,G} = \dot{G}_{G,t} D_{t,i} / \mu_G \quad \dots\dots\dots (1)$$

$$\text{and } \dot{G}_{G,t} = \dot{Q} \rho_G / A_{t,i} = \dot{v}_{G,t} \rho_G \quad \dots\dots\dots (2)$$

where $N_{Re,G}$ = Reynolds number, dimensionless

and $D_{t,i}$ = internal diameter of tube, $7,5 \times 10^{-3}$ m

μ_G = dynamic viscosity of the air, 18×10^{-6} kg/ms

$\dot{G}_{G,t}$ = mass flow rate of the air in the tube, kg/m² s

$\dot{v}_{G,t}$ = air velocity in the tube, m/s

ρ_G = density of the air at 40°C, 0,974 kg/m³

\dot{Q} = air flow rate, $0,2 \times 10^{-3}$ m³/s

$A_{t,i}$ = cross-sectional area of the inside of the tube
 $= \pi \times (0,0075)^2 / 4 = 44,1 \times 10^{-6}$ m²

* See section 4.6.4 on page 194

From equations (1) and (2)

$$\begin{aligned} N_{Re,G} &= 0,2 \times 10^{-3} \times 0,974 \times 7,5 \times 10^{-3} / (18 \times 10^{-6} \times 44,1 \times 10^{-6}) \\ &= 1\,850. \end{aligned}$$

The following equations give the inside film coefficient of heat transfer for a straight tube at a Reynolds number, $N_{Re} = 1850^{198}$:

$$N_{Nu,G} = 1,86(N_{Re,G} N_{Pr,G} D_{t,i}/L_t)^{0,33} (\mu_G/\mu_{G,f})^{0,14} \dots (3)$$

$$L = \pi D_c n_c \dots (4)$$

$$\text{and } h_{c,i} = k_G N_{Nu,G} / D_{t,i} \dots (5)$$

where $N_{Nu,G}$ = Nusselt number, dimensionless

and $N_{Re,G}$ = Reynolds number, dimensionless

$N_{Pr,G}$ = Prandtl number, 0,71 for air, dimensionless

$D_{t,i}$ = internal diameter of tube, $7,5 \times 10^{-3}$ m

D_c = mean coil diameter, 0,355 m

n_c = number of coils, 14

L_t = tube length = $\pi \times 0,355 \times 14 = 15,6$ m

$h_{c,i}$ = inside film coefficient of heat transfer for straight tube, $W/m^2 \text{ } ^\circ C$

k_G = thermal conductivity of air, 0,0256 $W/m \text{ } ^\circ C$

$\mu_G/\mu_{G,f}$ = ratio of dynamic viscosities at the temperature of the bulk fluid and the temperature of the fluid adjacent to the tube walls, respectively.

The ratio $\mu_G/\mu_{G,f}$ is assumed to be equal to 1.

Substitution of the above-mentioned values in equation (3) leads to:

$$\begin{aligned} N_{Nu,G} &= 1,86 (1\,850 \times 0,71 \times 0,0075/15,6)^{0,33} \times 1 \\ &= 1,605 \end{aligned}$$

From equation (5)

$$\begin{aligned} h_{c,i} &= 0,0256 \times 1,605/0,0075 \\ &= 5,48 \text{ W/m}^2 \text{ } ^\circ\text{C}. \end{aligned}$$

The above-mentioned film coefficient of heat transfer applies to a straight tube. In the case of a spiral tube the film coefficient of heat transfer will be somewhat higher and can be estimated from the following equation⁶²⁾:

$$h_{c,i,sp} = h_{c,i} (1 + 3,5 D_{t,i}/D_c) \quad \dots\dots\dots (6)$$

where $h_{c,i,sp}$ = inside film coefficient of heat transfer for a spiral tube, $\text{W/m}^2 \text{ } ^\circ\text{C}$

$h_{c,i}$ = inside film coefficient of heat transfer for the straight tube, $5,48 \text{ W/m}^2 \text{ } ^\circ\text{C}$

$D_{t,i}$ = inside diameter of the tube, $0,0075 \text{ m}$

D_c = mean coil diameter, $0,355 \text{ m}$.

Substitution of the above-mentioned values in equation (6) leads to:

$$\begin{aligned} h_{c,i,sp} &= 5,48 (1 + 3,5 \times 0,0075/0,355) \\ &= 5,88 \text{ W/m}^2 \text{ } ^\circ\text{C} \end{aligned}$$

The air side film coefficient of heat transfer referred to the outside of the tube, is given by the following equation:

$$h_{c,o} = h_{c,i,sp} D_{t,i}/D_{t,o} \quad \text{..... (7)}$$

where $h_{c,o}$ = air side film coefficient of heat transfer referred to the outside of the tube, $W/m^2 \text{ } ^\circ C$

and $h_{c,i,sp}$ = inside film coefficient of heat transfer for the spiral tube, $5,88 W/m^2 \text{ } ^\circ C$

$D_{t,i}$ = inside diameter of the tube, 0,0075 m

$D_{t,o}$ = outside diameter of the tube, 0,0095 m

Substitution of the above-mentioned values in equation (7) leads to:

$$h_{c,o} = 5,88 \times 0,0075/0,0095 = 4,32 W/m^2 \text{ } ^\circ C.$$

(b) Water side film coefficient of heat transfer

The water side film coefficient of heat transfer is calculated from the following equations¹⁹⁹⁾:

$$N_{Nu,w} = 0,193(N_{Pr,w})^{0,33} (N_{Re,w})^n \quad \text{..... (8)}$$

$$N_{Pr,w} = c_{p,w} \mu_w/k_w \quad \text{..... (9)}$$

$$N_{Re,w} = \dot{G}_w'' D_o/\mu_w \quad \text{..... (10)}$$

$$\dot{G}_w'' = \dot{v}_w/\rho_w \quad \text{..... (11)}$$

$$\text{and } h_{c,o,w} = k_w N_{Nu,w}/D_o \quad \text{..... (12)}$$

where $N_{Nu,w}$ = Nusselt number, dimensionless

and $N_{Pr,w}$ = Prandtl number, dimensionless

$N_{Re,w}$ = Reynolds number, dimensionless

n = constant, 0,618

$c_{p,w}$ = specific heat of water at constant pressure,
4 190 J/kg °C

μ_w = dynamic viscosity of water at 40°C,
0,654 x 10⁻³ kg/ms

k_w = thermal conductivity of water at 40°C, 0,635 W/m °C

\dot{G}_w = mass velocity of water across the tubes, kg/m² s

\dot{v}_w = velocity of water, 0,5 m/s, say

ρ_w = density of water at 40°C, 990 kg/m³

$h_{c,o,w}$ = film coefficient of heat transfer on the water
side, W/m² °C

D_o = outside diameter of tube, 0,0095 m.

$$\begin{aligned} \text{From equation (9), } N_{Pr,w} &= 4\,190 \times 0,654 \times 10^{-3} / 0,635 \\ &= 4,3 \end{aligned}$$

$$\begin{aligned} \text{From equation (10), } N_{Re,w} &= 495 \times 0,0095 / 0,654 \times 10^{-3} \\ &= 7\,200 \end{aligned}$$

$$\text{From equation (11), } \dot{G}_w = 0,5 \times 990 = 495 \text{ kg/m}^2 \text{ s}$$

Substitution of the above-mentioned values in equation (8) leads to:

$$\begin{aligned} N_{Nu,w} &= 0,193 \times 4,3^{0,33} \times 7200^{0,618} \\ &= 75,4. \end{aligned}$$

Substitution of the values for k_w , $N_{Nu,w}$ and D_o in equation (12) leads to:

$$\begin{aligned} h_{c,o,w} &= 0,635 \times 75,4 / 0,00952 \\ &= 5020 \text{ W/m}^2 \text{ } ^\circ\text{C}. \end{aligned}$$

(c) Overall coefficient of heat transfer, U

Neglecting the resistance to heat flow of the copper tube itself, the overall coefficient of heat transfer, U, is given by the following equation:

$$U = h_{c,o} \times h_{c,o,w} / (h_{c,o} + h_{c,o,w}) \quad \dots\dots (13)$$

where U = overall coefficient of heat transfer, $\text{W/m}^2 \text{ } ^\circ\text{C}$

and $h_{c,o}$, $h_{c,o,w}$ = air and water side film coefficients of heat transfer; $4,32 \text{ W/m}^2 \text{ } ^\circ\text{C}$ and $5020 \text{ W/m}^2 \text{ } ^\circ\text{C}$, respectively.

$$\begin{aligned} \text{Thus, } U &= 4,32 \times 5020 / (4,32 + 5020) \\ &= 4,31 \text{ W/m}^2 \text{ } ^\circ\text{C}. \end{aligned}$$

2. EFFECTIVENESS OF THE DOUBLE CIRCUIT HEAT EXCHANGER

The method proposed by Kays and London²⁰⁰⁾ was used to determine the effectiveness of the heat exchanger.

As a first step the number of so-called heat exchanger transfer units,

N_{tu} , is calculated from the following equations:

$$N_{tu} = A_{t,o} U / C_{air} \quad \dots\dots (14)$$

$$C_{air} = \rho_G \dot{Q} c_{p,G} \quad \dots\dots (15)$$

$$A_{t,o} = \pi D_o L_t \quad \dots\dots (16)$$

where N_{tu} = number of heat exchanger transfer units, dimensionless

$A_{t,o}$ = outside surface area of tube, m^2

U = overall coefficient of heat transfer, $4,31 \text{ W/m}^2 \text{ } ^\circ\text{C}$

C_{air} = air capacity rate, $\text{W}/^\circ\text{C}$

ρ = density of the air, $0,974 \text{ kg/m}^3$

Q = air flow rate, $0,2 \text{ m}^3/\text{s}$

$c_{p,G}$ = specific heat of the air at constant pressure,
 $1\,010 \text{ J/kg } ^\circ\text{C}$

D_o = outside diameter of tube, $0,0095 \text{ m}$

L_t = length of tube, $15,6 \text{ m}$

$$\begin{aligned} \text{From equation (16) } A_{t,o} &= \pi \times 0,0095 \times 10^{-3} \times 15,6 \\ &= 0,466 \text{ m}^2. \end{aligned}$$

$$\begin{aligned} \text{From equation (15) } C_{air} &= 0,974 \times 0,2 \times 1\,010 \\ &= 0,1967 \text{ W}/^\circ\text{C}. \end{aligned}$$

Substitution of the values for $A_{t,o}$, U and C_{air} in equation (14) leads to:

$$\begin{aligned} N_{tu} &= 0,466 \times 4,31 / 0,1967 \\ &= 10,25. \end{aligned}$$

The heat exchanger effectiveness, E , is given by the following equation:

$$E = 1 - e^{-N_{tu}} \quad \text{..... (17)}$$

$$\begin{aligned} \text{Thus } E &= 1 - e^{-10,25} \\ &= 0,9999457. \end{aligned}$$

Knowing the effectiveness of the heat exchanger, the temperature at which the air leaves each heat exchanger coil can be expressed as a function of the entering air temperature by means of the following equations:

$$t_{l,1} - t_{e,1} = E(t_w - t_{e,1}) \quad \text{..... (18)}$$

$$\text{and } t_{l,2} - t_{e,2} = E(t_w - t_{e,2}) \quad \text{..... (19)}$$

where $t_{l,1}, t_{e,1}$ = leaving and entering air temperature of the first coil, respectively, °C

$t_{l,2}, t_{e,2}$ = leaving and entering air temperature of the second coil, respectively, °C

E = heat exchanger effectiveness, 0,9999457

t_w = water temperature, 40°C.

From equations (18) and (19)

$$t_{l,2} - t_{l,1} = (t_{e,2} - t_{e,1})(1 - E) \quad \text{..... (20)}$$

Substitution of the value of E in equation (20) leads to:

$$t_{l,2} - t_{l,1} = 0,0000543 (t_{e,2} - t_{e,1}) \quad \text{..... (21)}$$

The temperature differences, $(t_{e,2} - t_{e,1})$ and $(t_{l,2} - t_{l,1})$ represent the initial temperature difference between two air samples entering the double circuit heat exchanger and the value to which the temperature difference between the two air samples is ultimately reduced as the air samples circulate through the double circuit heat exchanger.

The maximum temperature increase in the wake of a human body in the horizontal test chamber of the climatic chamber is of the order of $2^{\circ}\text{C}^{(61)}$.

Substitution of the value of 2°C for $(t_{e,2} - t_{e,1})$ in equation (21) leads to:

$$t_{l,2} - t_{l,1} = 0,0000543 \times 2 = 0,0001086^{\circ}\text{C}$$

Thus, the double circuit heat exchanger would be capable of reducing an initial temperature difference between the two air samples of 2°C to $0,0001086^{\circ}\text{C}$ which is well below the required value of $0,0005^{\circ}\text{C}$.

The heat exchanger is thus highly effective and the effect of initial temperature differences between the two air samples on the upstream and downstream side of the body on the accuracy of the evaporative heat loss measuring instrument can be expected to be extremely small.

APPENDIX G

DETERMINATION OF THE CONFIGURATION FACTORS BETWEEN THE
RADIATION-SENSING ELEMENTS, THE BODY AND VARIOUS SECTIONS
OF THE SURROUNDING WALLS OF THE HORIZONTAL TEST CHAMBER
OF THE CLIMATIC CHAMBER

The method proposed by de Heer and Erkenlen²⁰¹⁾ was used to determine the configuration factors between the radiation-sensing elements, the body and various sections of the surrounding walls for various positions of the 4π radiometer within the horizontal test chamber of the climatic chamber.

The method involves the division of the surfaces between which the radiation heat transfer takes place into a number of small squares of equal size. A factor referred to by de Heer and Erkenlen as the geometric factor is then calculated for each small area and the various factors summed up to derive the geometric factor for the entire surface under consideration.

The configuration factor is then determined from a consideration of the radiant energy transfer equations involved. The method of determining the geometric and hence the configuration factors is illustrated in the following example:

Consider two parallel surfaces, B; 120 mm wide by 280 mm long and A; 40 mm wide by 160 mm long, located at a distance of 1 000 mm from each

other as shown in Figure G1. The temperature distribution across each surface is assumed to be uniform.

Let each surface be divided into squares of side $A = 40 \text{ mm}$ long; each elemental area of the small and large surfaces being referred to as A_1, A_2, \dots, A_n and B_1, B_2, \dots, B_n , respectively.

Let the vertical axis be Z and the horizontal axis Y , (see Figure G1). The Z axis is referenced with respect to each individual area A_n . Thus, for example, the areas B_7, B_8 and B_9 lie on the $Z = 0$ axis for the area A_1 , and the areas B_{16}, B_{17} and B_{18} lie on the axis $Z = 0$ for the area A_4 and on the axis $Z = 3$ for the area A_1 . Since the radiation between A_1 and B_4 is the same as that between A_1 and B_{10} , the Z co-ordinate for each is unity with no change in sign.

The range of Z co-ordinates for the areas A_1 and A_4 are given in Table G1.

TABLE G1 : RADIATION ENERGY EXCHANGE : CALCULATION OF THE CONFIGURATION FACTOR BETWEEN THE SURFACES DEPICTED IN FIGURE G1 : RANGE OF Z CO-ORDINATES FOR THE ELEMENTAL AREAS OF SURFACE A

ELEMENTAL AREA OF SURFACE A	RANGE OF Z CO-ORDINATES
A_1	2 ——— 0 ——— 4
A_2	3 ——— 0 ——— 3
A_3	4 ——— 0 ——— 2
A_4	5 ——— 0 ——— 1

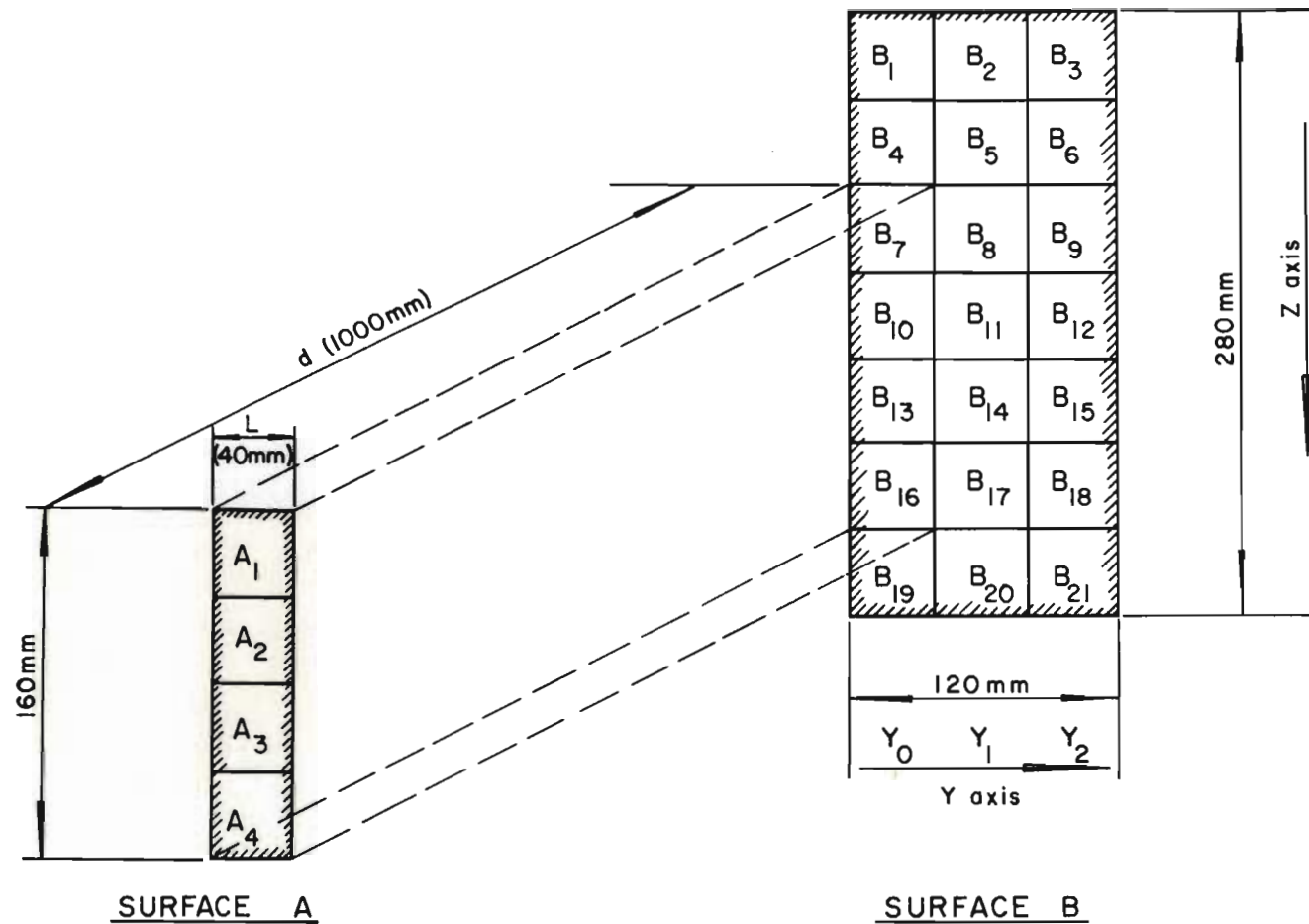


FIGURE G1

Radiation energy exchange: isometric view showing the layout of surfaces referred to in an example to demonstrate the method of calculating the configuration factor between surfaces.

The numbers of Z co-ordinates which are equal to each other are referred to as symmetry repetition coefficients. For example, there are four Z co-ordinates equal to zero. Thus, for the $Z = 0$ co-ordinate the symmetry repetition coefficient is 4.

Based on the information contained in Table G1, Table G2 gives the symmetry repetition coefficients for the various Z co-ordinates:

TABLE G2 : RADIATION ENERGY EXCHANGE : CALCULATION OF THE CONFIGURATION FACTOR BETWEEN THE SURFACES DEPICTED IN FIGURE G1 : SYMMETRY REPETITION COEFFICIENTS FOR THE VARIOUS Z CO-ORDINATES

SYMMETRY REPETITION COEFFICIENTS	Z CO-ORDINATES
4	0
8	1
6	2
5	3
3	4
1	5

1. GEOMETRIC FACTOR

The geometric factor, S_{AB} , is obtained from the summation of the geometric factors for each elemental area.

$$\text{Thus, } S_{AB} = \sum_Y \sum_Z S_{YZ}^X \quad \dots\dots\dots (1)$$

where S_{AB} = geometric factor for the surfaces A and B

$$\text{and } S_{YZ}^X = X^2 / (X^2 + Y^2 + Z^2) \quad \dots\dots\dots (2)$$

In the case of surfaces which are parallel to each other

$$X = d/L \quad \dots\dots\dots (3)$$

where d = distance between the surfaces, 1 000 mm

and L = length of one of the sides of the small squares, 40 mm

$$\text{Thus, } X = 1\,000/40 = 25$$

Substitution of the various Y and Z co-ordinates in equation (2) leads to the following:

For $Y = 0, 1, 2$ and $Z = 0$

$$S_{0,0}^{25} = 25^2 / (25^2 + 0^2 + 0^2) = 0,00160$$

$$S_{1,0}^{25} = 25^2 / (25^2 + 1^2 + 0^2) = 0,00159$$

$$S_{2,0}^{25} = 25^2 / (25^2 + 2^2 + 0^2) = 0,00158$$

Due to the symmetry involved, the values for the geometric factors for $Z = 0$ must be multiplied by the symmetry repetition coefficient number n , for $Z = 0$, which is '4 (see Table G2 on page 465).

Thus, the geometric factor for the elemental areas having a Z co-ordinate equal to zero, say, is as follows:

$$\begin{aligned}
 \sum_{Z=0} n_0 s_{YZ}^X &= 4(s_{0,0}^{25} + s_{1,0}^{25} + s_{2,0}^{25}) \\
 &= 4(0,00477) \\
 &= 0,0191.
 \end{aligned}$$

Similarly, the values of the geometric factors for elemental areas having various other Z co-ordinates, were calculated. The results are summarised in Table G3.

TABLE G3 : RADIATION ENERGY EXCHANGE : CALCULATION OF THE CONFIGURATION FACTOR BETWEEN THE SURFACES DEPICTED IN FIGURE G1: GEOMETRIC FACTORS FOR THE ELEMENTAL AREAS HAVING SIMILAR Z CO-ORDINATES

SYMMETRY REPETITION FACTOR	Z CO-ORDINATE	GEOMETRIC FACTOR
4	0	0,0191
8	1	0,0381
6	2	0,0283
5	3	0,0232
3	4	0,0135
1	5	0,0044
Total geometric factor		0,1226

The total geometric factor for the surfaces A and B is thus

$$S_{AB} = 0,1266.$$

2. CONFIGURATION FACTOR

The corresponding configuration factor between the surfaces A and B in Figure G1 is determined from a consideration of the following equations which express the radiant energy exchange rate:

$$\dot{q}_{\text{rad}} = \sigma S_{AB} L^2 (T_A^4 - T_B^4) \text{ by de Heer and Erckenlen}^{201) \dots (4)$$

$$\text{and } \dot{q}_{\text{rad}} = \sigma F_{AB} A_A (T_A^4 - T_B^4) \dots\dots\dots (5)$$

where \dot{q}_{rad} = radiation energy exchange rate, kW

and σ = Stefan-Boltzman constant, kW/m² K⁴

S_{AB} = geometric factor for the surfaces, A and B, dimensionless

L = length of one of the sides of the small squares on the surfaces, A and B, m

T_A, T_B = absolute surface temperatures of the surfaces A and B, respectively, °K

F_{AB} = configuration factor between the surfaces, A and B, dimensionless

A_A = surface area of the surface A, m².

Consideration of equations (4) and (5) leads to:

$$F_{AB} = S_{AB} L^2 / A_A \dots\dots\dots (6)$$

The configuration factor may thus be obtained by multiplying the geometric factor by the ratio of one of the small elemental areas to the total surface area of the surface A.

By substituting the values for $S_{AB} L^2$ and A_A , in equation (6) the

value for F_{AB} , the configuration factor between the surfaces shown in Figure G1 is obtained.

$$\begin{aligned}\text{Thus, } F_{AB} &= 0,1266 (40 \times 40 / 160 \times 40) \\ &= 0,0316.\end{aligned}$$

Based on the above-mentioned method of analysis, configuration factors between the radiation-sensing elements in the vertical section of the 4π radiometer arm and the body and/or the surrounding walls of the horizontal test chamber of the climatic chamber were determined for the radiometer arm positioned in three positions; with the radiation-sensing elements "facing" (i) the solid panel, (ii) the corner which is formed by the solid and bar-grid panels and (iii) the bar-grid panel.

In the case of the corner position the geometric factors S_{PQ}^Z were determined by means of the following equation (instead of equation (2) on page 466) which applies only to surfaces that are parallel to each other):

$$S_{PQ}^Z = pq \sin^2 \phi / (p^2 + q^2 + z^2 - pq \cos \phi)^2$$

where ϕ = the angle subtended between the two surfaces and

p, q, z = the co-ordinates of the small squares on the surfaces.

Figure 58 on page 290 presents the configuration factors between the radiation-sensing elements, the body and various sections of the surrounding walls for various positions of the 4π radiometer within the horizontal test chamber of the climatic chamber.

APPENDIX H

COMPARISON OF ALTERNATIVE SYSTEMS OF MEASURING
THE OUTPUT OF THE 4π RADIOMETERSENSITIVITY OF ALTERNATIVE SYSTEMS OF MEASUREMENT

Various methods of recording the output of the 4π radiometer arm were considered with the view to determining the most suitable system of measurement.

In order to assess the relative sensitivity of various measuring instruments, a knowledge of the magnitude of the unbalance current of the Wheatstone bridge network of resistance elements incorporated in the radiometer is required. (See Figure 62 on page 311).

In the case of the 4π radiometer arm, the two radiation-sensing elements lining the inner surface of the radiometer "sees" the body in the test section and for this reason can be regarded as the two active arms of the Wheatstone bridge.

Assuming each of the four arms of the Wheatstone bridge to have an initial nominal resistance of R , say, and the internal resistance of the power supply system to be negligibly small, Ohm's law and Kirchhoff's laws may be used to determine the following relationship between the unbalance current in the galvanometer circuit, I_g , the voltage applied across the bridge, V ,

and the various resistances which form the bridge network if the resistances in the two opposite arms of the bridge were to change to $R + \Delta R$, say²⁰²):

$$I_g = V\Delta R / (2R + \Delta R) + R_g(2R + \Delta R) \quad \dots\dots\dots (1)$$

Since $\Delta R \ll R$ and $R + \Delta R \approx R$ equation (1) may be rewritten as follows:

$$I_g \approx V\Delta R / 2R(R + R_g) \quad \dots\dots\dots (2)$$

where I_g = unbalance current through the galvanometer, A

and V = voltage applied across the Wheatstone bridge, V

R = initial resistance values of each of the four arms of the
Wheatstone bridge, ohms

ΔR = change in the resistance of the two active arms in the
Wheatstone bridge, ohms

R_g = resistance of the galvanometer circuit, ohms.

Since the change in resistance, ΔR , of the two active arms of the Wheatstone bridge is caused by the temperature change of these two elements, the following relationship exists:

$$\Delta R / R = C \Delta t \quad \dots\dots\dots (3)$$

where C = temperature coefficient of resistance of the radiation-sensing elements, 0,006 per °C (see Section 5.4.2 on page 259)

and Δt = temperature change of the two resistance elements in the opposite arms of the Wheatstone bridge, °C.

Substitution of the value for $\Delta R/R$ according to equation (3), in equation (2) leads to:

$$I_g \approx VC\Delta t/2(R + R_g) \quad \dots\dots\dots (4)$$

The following assumptions were made regarding the parameters contained in equation (3) in order to compare various methods of recording the output of the 4π radiometer arm:

- (i) Voltage across the Wheatstone bridge, $V : 12$ volts
- (ii) Electrical resistance of each arm of the bridge under identical temperature conditions, $R : 4\ 000$ ohms (see Figure 62 on page 311)
- (iii) Two arms of the bridge are active and
- (iv) The temperature change of each of the two active arms, Δt , is $0,09^\circ\text{C}$, say (see Section 5.5.3 on page 308).

Substitution of the above-mentioned values in equation (4) leads to:

$$\begin{aligned} I_g &= (12 \times 0,006 \times 0,09)/2 (4\ 000 + R_g) \\ &= 0,00648/2 (4\ 000 + R_g) \quad \dots\dots\dots (5) \end{aligned}$$

where I_g = unbalance current through the galvanometer

and R_g = galvanometer resistance.

1. ALTERNATIVE INSTRUMENTS FOR MEASURING THE OUTPUT OF THE 4π RADIOMETER

1.1 "Pye" galvanometer

Assume the unbalance current is to be measured by means of a "Pye" galvanometer with an internal resistance, R_g , of 400 ohms and a sensitivity of 90 mm deflection per μA .

Substitution of the value of $R_g = 400$ ohms in equation (5) leads to:

$$I_g = 0,00648/2 (4\ 000 + 400) = 0,73\ \mu\text{A}.$$

The deflection of the galvanometer, D , is thus:

$$d = 0,73 \times 90 = 65\ \text{mm}.$$

1.2 Galvanometric type recorder

Assume the unbalance current is to be measured by means of a Kipp micrograph galvanometric type recorder with an internal resistance, R_g , of 0,25 ohms and a sensitivity of 250 mm deflection per μA .

Substitution of the value of $R_g = 0,25$ in equation (5) leads to:

$$I_g = 0,00648/2 (4\ 000,25) = 0,81\ \mu\text{A}.$$

The deflection of the recorder, d , is thus:

$$d = 0,81 \times 250 = 202\ \text{mm}.$$

1.3 Strain gauge recorder

Normally, strain gauge recorders such as the Phillips strain gauge recorder, are used to measure the output of a Wheatstone bridge network incorporating strain gauges; the primary object of such measurements being to determine the mechanical strain in a component to which the strain gauges are attached.

Since the strain gauge recorder basically detects changes in the electrical resistance values between the strain gauges, this type of recorder can also be used for detecting variations in the relative electrical resistance values of the radiation-sensing elements of the 4π radiometer arm.

Assume the output of the radiometer is to be measured with a strain gauge recorder having a sensitivity of 50 μ strain or 50×10^{-6} strain for full-scale deflection when all four arms of the Wheatstone bridge are active.

Since the resistances of only two arms of the Wheatstone bridge network are active, the value of $\Delta R/R$ would have to be $2 \times 50 \times 10^{-6} = 100 \times 10^{-6}$ in order to produce full-scale deflection of the recorder.

Substitution of the values of 0,006 and 0,09°C, the temperature

coefficient of resistance of the radiation-sensing elements, C , and the estimated temperature change of the two "inner" radiation-sensing elements of the 4π radiometer arm, Δt , respectively, in equation (3) on page 472 gives:

$$\begin{aligned}\Delta R/R &= 0,006 \times 0,09 \\ &= 540 \times 10^{-6}\end{aligned}$$

Assuming a recorder scale length of 300 mm, say, the above value for $\Delta R/R$ would result in a recorder deflection of $300 (540 \times 10^{-6} / 100 \times 10^{-6}) = 1\,620$ mm.

The sensitivity can be expected to be reduced to some extent if the Wheatstone bridge resistance exceeds the value for which the recorder was designed.

The sensitivities of both the galvanometric type of recorder and the strain gauge recorder appear to be adequate for measuring the output of the 4π radiometer.